This is to certify that the

dissertation entitled

MICROWAVE ASSISTED PLASMA CVD OF DIAMOND FILMS
USING A THERMAL-LIKE PLASMA DISCHARGE

presented by

Kuo-Ping Kuo

has been accepted towards fulfillment
of the requirements for

Ph.D. degree in Electrical Eng

Major professor

Date 8/20/87

MICROWAVE ASSISTED PLASMA CVD OF DIAMOND FILMS USING THERMAL-LIKE PLASMA DISCHARGE

By

Kuo-Ping Kuo

A DISSERTATION

Submitted to

Michigan State University

in partial fulfillment of the requirements

for the degree of

DOCTOR OF PHILOSOPHY

Department of Electrical Engineering

1997

ABSTRACT

Microwave Assisted Plasma CVD of Diamond Films Using A Thermal-like Plasma Discharge

By

Kuo-Ping Kuo

Two new microwave plasma reactor configurations have been developed to improve the deposition efficiency and controllability of microwave plasma reactors. The first concept extends the conventional microwave plasma reactor from a 20-80 Torr, nonequilibrium discharge regime to the higher pressure 80-150 Torr, thermal-like discharge operating regime. This new reactor configuration includes a water cooling stage and an improved input feed gas flow configurations. A thermal-like discharge is created and uniform diamond films are deposited over 2″ diameter substrates with average growth rates of 5-6 μm/h(45-50 mg/h). Growth energy efficiencies of 70 kW-h/g (~ 20 kW-h/ct) and carbon conversion efficiencies of 7-10% are comparable to the best performance reported in the literature. This reactor concept opens up the possibility of applying microwave plasma assisted CVD of diamond to thick film deposition applications.

The second of these prototype reactors, i.e., microwave plasma jet reactor, is operated at pressure between 10 to 45 Torr. It utilizes an unique force-flow concept to create a microwave plasma discharge in a region where the electromagnetic field strength is low. The force flow feature reduces gas bypassing and forces the excited species and radicals onto irregular and complex shaped conducting substrates. Mixtures of CO, CH_4, and H_2 source gases together with this force-flow concept are utilized to enhance the diamond film growth on thirty six 1/8" diameter tungsten carbide round tools and thousands of 5-7 μm diameter carbon fibers.

To my parents

Fonro-Yisi and Miko

ACKNOWLEDGEMENTS

The author wishes to express his sincere appreciation to Professor Dr. Jes Asmussen, Jr. for his guidance, encouragement, and support for this thesis research. Thanks are also due the other members of the author's quidance committee: Professor Dr. Donnie Reinhard, Professor Dr. Timothy Grotjohn and Professor Dr. Brad Golding. In addition, the author owes a debt of gratitude to Dr. Jie Zhang, Dr. Saeid Khatami, Dr. Jorge Mossbrucker, Dr. PengUn Mak, Uwe Kahler, and Wen-shin Huang for providing me with their knowledge. The author have to thank Roxanne Peacock and Brian Wright for their technical support. Last, the author would like to thank Professor Dr. Stanley L. Flegler for training me SEM and Professor Dr. John McGrath for providing thermal conductivity information on the CVD diamond films.

Sincere appreciation is also extended to Dr. Chow Ling Chang and Brian Cline at Norton Diamond Film Corp. and the Michigan Research Excellence Fund for the financial assistance which made this thesis research possible.

TABLE OF CONTENT

LIST OF TABLES xviii

LIST OF FIGURES xiv

CHAPTER ONE
Introduction

1.1 Introduction 1
1.2 Research Objectives 4
1.3 Dissertation Outline 4

CHAPTER TWO
Literature Review of
Diamond Film Deposition Reactors

2.1 Introduction 6
2.2 A General Description of Chemical Vapor Deposition (CVD) of Diamond Films 6
2.3 The Multivariable Diamond Film Deposition Reactor 9
2.3.1 Experimental Variables of a Diamond Film Deposition Reactor 9
2.3.2 "Figures of Merit" of Reactor Performance 11
2.4 Diamond Thin Film CVD Reactor Technologies 12
2.4.1 Notes on Literature Review. 12
2.4.2 Hot Filament CVD (HFCVD) Reactors 14
2.4.2.1 Conventional HFCVD Reactor 14
2.4.2.2 Electron-assisted HFCVD Reactor. 17
2.4.3 Direct Current(DC) Plasma CVD Reactors 20
2.4.3.1 Conventional DC plasma CVD Reactor 20
2.4.3.2 Enclosed DC Arc Jet CVD Reactor 23
2.4.4 Combustion Flames 29
2.4.4.1 Atmospheric Pressure Combustion Flame. 29
2.4.4.2 Enclosed Flat Combustion Flame 32
2.4.5 RF Plasma CVD Reactors 35

2.4.5.1 Conventional RF Plasma CVD Reactor 35
2.4.5.2 RF Thermal Plasma CVD Torch 37
2.5 Microwave Plasma CVD Reactors 40
2.5.1 Magneto-microwave Plasma CVD Reactors 40
2.5.2 Tubular Microwave Plasma Reactors 44
2.5.3 Microwave Plasma Jet Reactors 47
2.5.4 Bell Jar Microwave Plasma CVD Reactors 50
2.5.4.1 Astex Bell Jar Microwave Plasma CVD Reactor 50
2.5.4.2 UC-Berkeley Bell Jar Microwave Plasma CVD Reactor 53
2.5.4.3 MSU Bell Jar Microwave Plasma CVD Reactor 56
2.5.5 Surface-wave Microwave Plasma CVD Reactors 59
2.6 Summary 62

CHAPTER THREE
High-Pressure Microwave Cavity Plasma Reactor: Experimental Systems, Experimental Procedures, Experimental Parameter Space, Measurement Methodologies, and Reactor Configuration

3.1 Introduction 67
3.2 Experimental Systems 68
3.2.1 Introduction 68
3.2.2 Microwave Power Supply and Waveguide/ Transmission system 68
3.2.3 Flow Control and Vacuum Pump System 71
3.2.4 Computer Monitoring System 74
3.3 Common Experimental Procedures 76
3.3.1 Seeding Procedure 76
3.3.2 Start-up and Shut-down Procedures 77
3.4 Experimental Parameter Space 78
3.4.1 Introduction 78
3.4.2 Independent Experimental Input Variables 80
3.4.3 Dependent Experimental Internal Variables 82
3.4.4 External Experimental Output Variables 82
3.5 Measurement of Experimental Output Variables 83
3.5.1 Measurement of Film Characteristics 83
3.5.1.1 Measurement of Film Uniformity 83
3.5.1.2 Measurement of Film Structural Quality 83
3.5.1.3 Measurement of Film Texture 84
3.5.1.4 Measurement of Film Morphology 85
3.5.2 Calculation of Reactor Performance 87
3.5.2.1 Measurement of Film Growth Rate 87
3.5.2.2 Measurement of Specific Yield 87
3.5.2.3 Measurement of Gas Efficiency 88
3.5.2.4 Measurement of Carbon Conversion Efficiency 88

3.6 Design of High-Pressure MCPR 89
3.6.1 Introduction. 89
3.6.2 Operation of Moderate-Pressure MCPR. 91
3.6.2.1 Operation of Microwave Cavity Excitation and Tuning 91
3.6.2.2 Operation of Air Cooling System 91
3.6.2.3 Operation of Thermally Floating Substrate Holder Setup 93
3.6.3 Substrate Cooling Stage - The First Design 94
3.6.3.1 Introduction 94
3.6.3.2 The Change in The Air Cooling System 94
3.6.3.3 Substrate Cooling Stage - The First Design 96
3.6.3.4 Drawbacks of The First Design 98
3.6.3.5 Final Substrate Cooling Stage Design 100
3.7 Summary 104

CHAPTER FOUR
Reactor Experimental Output Performance -
Reactor Performance (Y_1)

4.1 Introduction 105
4.2 Reactor Performance (Y_1)- Linear Growth Rate 110
4.2.1 Linear Growth Rate=f (c, f_t,T_s,t) 110
4.2.2 Linear Growth Rate=f (P_t-p) 119
4.3 Reactor Performance (Y_1)- Specific Yield 124
4.3.1 Specific Yield=f (c, f_t, T_s, t) 124
4.3.2 Specific Yield=f (P_t-p) 127
4.4 Reactor Performance (Y_1)- Carbon Conversion Efficiency 128
4.4.1 Carbon Conversion Efficiency=f (c, f_t, T_s, t) 128
4.4.2 Carbon Conversion Efficiency=f (P_t-p) 132
4.5 The Growth of Thick Free Standing Diamond Films 133
4.6 Summary 133

CHAPTER FIVE
Reactor Experimental Output Performance-
Film Characteristics (Y_2)

5.1 Introduction 136
5.2 Effect of Methane Concentration (c) 139
5.2.1 Introduction 139
5.2.2 Experimental Variables 139
5.2.3 Growth Rate=f(c) 140
5.2.4 Film Morphology=f(c) 143
5.2.5 Film Texture=f(c) 146
5.2.6 Film Structural Quality=f(c) 149
5.3 Effect of Total Flow Rate (f_t) 152
5.3.1 Introduction 152
5.3.2 Experimental Variables 152
5.3.3 Growth Rate=f(f_t) 153
5.3.4 Film Morphology=f(f_t) 154
5.3.5 Film Texture=f(f_t) 158
5.3.6 Film Structural Quality=f(f_t) 161
5.4 Effect of Substrate Temperature (T_s) 164
5.4.1 Introduction 164
5.4.2 Experimental Variables 164
5.4.3 Growth Rate=f(T_s) 165
5.4.4 Film Morphology=f(T_s) 167
5.4.5 Film Texture=f(T_s) 170
5.4.6 Film Structural Quality=f(T_s) 173
5.5 Effect of Deposition Time(t) 175
5.5.1 Introduction 175
5.5.2 Experimental Variables 175
5.5.3 Growth Rate=f(t) 176
5.5.4 Film Morphology=f(t) 177
5.5.5 Film Texture=f(t) 180
5.5.6 Film Structural Quality=f(t) 183
5.6 Summary 185

CHAPTER SIX
Development and Optimization of the
Microwave Plasma Jet Reactor

6.1 Introduction 187
6.2 Development of the MPJR 188
6.2.1 Experimental Systems 188
6.2.2 Early Version of MPJR 189
6.2.3 Basic Configuration of the MPJR for Diamond Film Deposi-

tion on Round Tools 192
6.3 Optimization of the MPJR for Diamond Film Deposition on Round Tools 194
6.3.1 Introduction 194
6.3.2 Optimization 194
6.3.3 Operation of the Final MPJR 201
6.4 Summary 203

CHAPTER SEVEN
The Experimental Performance of the Microwave Plasma Jet Reactor

7.1 Introduction 205
7.2 Experimental Input/Output Variable Space 205
7.3 Experimental Procedures 209
7.3.1 Substrate Pretreatment Procedure 209
7.3.2 Start-up and Shut-down Procedures 210
7.3.3 Measurement of Substrate Temperature 210
7.3.4 Measurement of Reactor Output Variables (**Y**) 210
7.3.4.1 Measurement of Reactor Performance Variable ($\mathbf{Y_1}$) 211
7.3.4.2 Measurement of Film Characteristic Variables ($\mathbf{Y_2}$) 211
7.4 Diamond Film Deposition on WC-6%Co Round Tools 211
7.4.1 Reactor Configuration 212
7.4.2 Experimental Controllable Input Variables (**U**) and Internal Input Variables (**X**) 212
7.4.3 Reactor Performance ($\mathbf{Y_1}$) - Linear Growth Rate 214
7.4.4 Film Characteristic ($\mathbf{Y_2}$) 215
7.4.4.1 Film Uniformity 215
7.4.4.2 Film Morphology 217
7.4.4.3 Film Structural Quality 222
7.5 Diamond Film Deposition on Carbon Fibers 224
7.5.1 Reactor Configuration 224
7.5.2 Experimental Controllable Input Variables (**U**) and Internal Input Variables (**X**) 226
7.5.3 Film Characteristic ($\mathbf{Y_2}$) 227
7.6 Summary 231

CHAPTER EIGHT
Conclusions

8.1 Introduction 232
8.2 Operational Characteristics of the High-Pressure MPCR 234
8.2.1 Introduction 234

8.2.2 Diamond Film Deposition on 2″ Silicon Wafers 235
8.3 Operational Characteristics of the MPJR 239
8.3.1 Diamond Film Deposition on 1/8″ diameter WC-Co Round Tools 239
8.3.2 Diamond Film Deposition on 5-7 μm diameter Carbon Fibers 239
8.4 Recommendations for Future Research 240
8.4.1 High-Pressure MPCR 240
8.4.2 MPJRs 241

APPENDIX A 243

LIST OF REFERENCES 248

LIST OF TABLES

Table 2.1 Summary of "figures of merit". 64

Table 3.1 Definition of the experimental variables for the high-pressure MCPR. 81

Table 3.2 Location of XRD peaks and their relative intensity in a powder pattern. 85

Table 4.1 The Ranges of reactor variables investigated in this chapter. 110

Table 7.1 Reactor input/internal/output variables investigated in this and next chapters. 209

Table A.1 Experimental conditions of the diamond films presented described in Chapter 3 and 4. 243

LIST OF FIGURES

Figure 2.1 A general process for diamond film growth by chemical vapor deposition[3]. 3

Figure 2.2 Multivariables of a diamond film deposition reactor. 10

Figure 2.3 Schematic diagram of a conventional HFCVD reactor [18],[19]. 15

Figure 2.4 Schematic diagram of an Electron-assisted HFCVD reactor[22]. 18

Figure 2.5 Schematic diagram of the DC plasma CVD reactor[23]. . . . 21

Figure 2.6 Schematic diagram of a DC plasma jet CVD reactor[26]. . . . 24

Figure 2.7 Schematic illustration of an atmospheric pressure DC arc jet CVD reactor and its substrate biasing system[27]. 27

Figure 2.8 Schematic diagram of an atmospheric-pressure oxygen-acetylene combustion flame[29]. 30

Figure 2.9 Schematic of an enclosed flat flame[32]. 33

Figure 2.10 A schematic diagram of a conventional RF plasma CVD reactor[35]. 36

Figure 2.11 A schematic diagram of a RF thermal plasma torch[36][37]. 38

Figure 2.12 The schematic drawing of a magneto-microwave plasma CVD reactor[38],[39]. 41

Figure 2.13 Schematic diagram of a tubular microwave plasma-assisted CVD reactor[1]. 45

Figure 2.14 Schematic drawing of a microwave plasma jet torch[41]. 48

Figure 2.15 Schematic drawing of the Astex bell jar microwave PACVD reactor[43]-[46]. 51

Figure 2.16 Schematic of the 4″ UC-Berkeley bell jar PACVD system[47]-[50]. 54

Figure 2.17 Schematic diagram of the moderate-pressure microwave cavity plasma reactor (MCPR)[9],[51]. 57

Figure 2.18 Schematic illustration of a surface-wave microwave PACVD apparatus[52]-[54]. 60

Figure 2.19 Summary of linear growth rate vs. area power density for diamond film deposition reactors. 65

Figure 2.20 Summary of linear growth rate vs. pressure for diamond film deposition reactors. 66

Figure 3.1 Microwave power supply and microwave waveguide/transmission system for high-pressure MCPR and MJPR. 70

Figure 3.2 Flow control and vacuum system for high-pressure MCPR and MPJR. 73

Figure 3.3 Flow chart of Computer monitor program[9]. 75

Figure 3.4 Multivariables for the high-presure MCPR a diamond film deposition reactor. 79

Figure 3.5 A typical SEM photo from JEOL 6400 at MSU. 86

Figure 3.6 Reactor operating field map under thermally floating configuration for 5″ quartz dome/ 3″ substrate reactor configuration[51] 90

Figure 3.7 The cross sectional view of the thermally floating MCPR system. 92

Figure 3.8 The cross sectional view of the high-pressure MCPR system. 95

Figure 3.9 Typical substrate holder setup used in high-pressure MCPR for diamond film deposition: (a) 2″ silicon wafer, (b) 2″ graphite substrate holder, (c) boron nitride ring, (d) insulation discs, (e) graphite flow regula-

tor, (f) water coolling stage. 97

Figure 3.10 Can Body of the 3″ Water Cooling Stage[107] 99

Figure 3.11 Bottom Body of the 3″ Water Cooling Stage[107]. 99

Figure 3.12 Typical substrate holder setup used in high-pressure MCPR for diamond film deposition: (a) 2″ silicon wafer, (b) 2″ molybdnrum substrate holder, (c) boron nitride ring, (d) insulation discs, (e) graphite flow regulator, (f) water coolling stage. 101

Figure 3.13 Can Body of the 3″ Water Cooling Stage[107]. 102

Figure 3.14 Bottom Body of the 3″ Water Cooling Stage[107]. 102

Figure 4.1 High-pressure MCPR block diagram for the experiments described in this chapter. 109

Figure 4.2 Summary of growth rate vs. methane/hydrogen concentration in high-pressure MCPR. 114

Figure 4.3 Summary of growth rate vs. total flow rate in HPMCPR. 114

Figure 4.4 Summary of linear growth rate vs. substrate temperature. 115

Figure 4.5 Summary of linear growth rate vs. deposition time. 115

Figure 4.6 Summary of growth rate vs. methane/hydrogen concentraion and substrate temperature in the high-pressure MCPR. 116

Figure 4.7 Locations of different methane concentrations for the experiments that were investigated in this thesis. The solid curve represents the diamond growth region for the moderate pressure MCPR[9],[51] and the dash curve represents the growth region for the high pressure MCPR discribed in this thesis. 117

Figure 4.8 Location of diamond zones vs. c, f_t, and T_s for higg pressure and moderater pressure[51] MCPRs. 118

Figure 4.9 Summary of growth rate vs. pressure for the high pressure MCPR. 119

Figure 4.10 Summary of film growth rate vs. absorbed power. 120

Figure 4.11 The effect of $\%CH_4/H_2$ on the specific yield in high-pressure MCPR. 125

Figure 4.12 Summary of specific yield vs. total flow rate in the high-pressure MCPR. 125

Figure 4.13 Summary of specific yield vs. T_s in high pressure MCPR. 126

Figure 4.14 Summary of specific yield vs. deposition time in high-pressure MCPR. 126

Figure 4.15 Summary of specific yield vs. absorbed micorwave power in HPMCPR. 127

Figure 4.16 Summary of carbon conversion efficiency vs. $\%CH_4/H_2$ 128

Figure 4.17 Summary of carbon conversion efficiency vs. total flow rate. 129

Figure 4.18 Summary of carbon conversion efficiency vs. T_s 130

Figure 4.19 Summary of carbon conversion efficiency vs. deposition time. 131

Figure 4.20 Summary of carbon conversion efficiency vs. absorbed microwave power in the high pressure MCPR. 132

Figure 5.1 Linear growth rates (weight gain) versus methane concentrations. The experimental conditions are shown in Section 5.2.2 142

Figure 5.2(a)-(h) Surface morphology vs. $\%CH_4/H_2$ varied from 1% to 8%. 145

Figure 5.3 The X-ray diffraction spectra as a function of methane concentrations of (a) 2%, (b) 3%, (c) 4%, (d) 5%, (e) 6%, (f) 7% and (g) 8%. Maximum ratio of I(220)/I(111) was observed at c=4% and 5%. They are summarized in Figure 5.4. 147

Figure 5.4 The ratio of the XRD peak height of (220) to (111) versus the methane concentration. The experimental conditions are shown in Section 5.2.2. 148

Figure 5.5 Raman spectra of various methane concentrations.The

Experimental conditions are shown in Section 5.2.2. 150

Figure 5.6 FWHM of Raman spectra as a function of CH_4/H_2 concentration. The experimental conditions are shown in Section 5.2.2.1 151

Figure 5.7 Linear growth rate as a function of total flow rate at fixed methane/hydrogen concenctration(3%). 154

Figure 5.8(a)-(f) Film morphologies vs. total flow rates. The experimental conditions are shown in Section 5.3.2. 157

Figure 5.9 XRD spectra of diamond films synthesized by CH_4/H_2 flow rates of (a)12/400 sccm, (b)18/600 sccm, (c) 24/800 sccm, (d) 30/1000 sccm, (e) 36/1200 sccm and (f) 42/1400 sccm, using the experimental conditions described in Section 5.3.2.. 159

Figure 5.10 The XRD height of (220) relative to that of (111) as function of total flow rate in microwave plasma cavity system. The experimental conditions for these experiments are described in Section 5.3.2. 160

Figure 5.11 The effect of total flow rate on Raman spectrum. The experimental conditions are listed in Section 5.3.2.. 162

Figure 5.12 The effect of total flow rate on FWHM of Raman spectrum. The experimental conditions are shown in Section 5.3.2. 163

Figure 5.13 The effect of T_s on the film growth rate.. 166

Figure 5.14(a)-(f) Film morphologies vs. substrate temperatures. The experimental conditions are described in Section 5.4.2. 169

Figure 5.15 X-ray diffraction spectra of diamond films synthesized for (a) 950C, (b) 1025C, (c) 1050C, (d) 1075C, (e) 1100C and (f) 1125C. Maximum ratio of I(220)/I(111) was observed at (e) 1100C. They are summarized in Figure 5.16. 171

Figure 5.16 The XRD peak height of (220) relative to that of (111) as a function of substrate temperature. The experimental conditions for these experiments are shown in Section 5.4.2.. 172

Figure 5.17 The effect of substrate temperatures on FWHM of diamond peak lines from Raman spectra. Their Raman spectra are shown in Figure 5.18. 173

Figure 5.18 The effect of substrate temperature on Raman spectra. The experimental conditions are listed in Section 5.4.2.. 174

Figure 5.19 Linear growth rate as a function of deposition time. The experimental conditions are described in Section 5.5.2. 177

Figure 5.20 (a)-(f) Film morphology vs. deposition time. The experimental conditions are shown in Section 5.5.2. 179

Figure 5.21 X-ray diffraction spectra of diamond films synthesized for (a) 5 h, (b) 10 h, (c) 20 h, (d) 30 h, (e) 55 h and (f) 100 h, using the experimental conditions described in Section 5.5.2. 181

Figure 5.22 The XRD height of (220) relative to that of (111) as a function of deposition time in high pressure MCPR. 182

Figure 5.23 FWHM of the diamond peak lines vs. deposition times. Their Raman spectra are shown in Figure 5.24. 183

Figure 5.24 The effect of deposition time on Raman spectrum. The experimental conditions are listed in Section 5.5.2. 184

Figure 6.1 Cross sectional view of the early version of MPJR for high rate diamond film deposition on flat substrates[9]. 191

Figure 6.2 The cross sectional view of the basic version of MPJR for diamond film coating on two WC-6%Co round tools[110]. 193

Figure 6.3 The cross sectional view of the first variation of MPJR for diamond film coating on six WC-6%Co round tools. 196

Figure 6.4 The cross sectional view of the first variation of MPJR for diamond film coating on eighteen and thirty six WC-6%Co round tools. 198

Figure 6.5 The cross sectional view of the thirdth variation of MPJR for diamond film coating on many carbon fibers. 200

Figure 6.6 The cross sectional view of the final optimized configuration of MPJR which was used for diamond film coating on eighteen and thirty six WC-6%Co round tools. 202

Figure 7.1 MPJR block diagram for diamond thin film deposition on the benchmark substrates. 208

Figure 7.2 Thickness measurements of 36 WC-6%Co round tools. . . 215

Figure 7.3 Film Uniformity of diamond films for thirty six WC-6%CO round tools. 216

Figure 7.4 SEM photo of the pre-deposited WC-6%Co round tool surface. 218

Figure 7.5 SEM photo of a diamond film deposited WC-6%Co surface. The deposition time is 0.5 h. 218

Figure 7.6 SEM photo of a diamond film deposited WC-6%Co surface. The deposition time is 1 h. 219

Figure 7.7 SEM photo of a diamond film deposited WC-6%Co surface. The deposition time is 2 h. 219

Figure 7.8 SEM photo of a diamond film deposited WC-6%Co surface. The deposition time is 3 h. 220

Figure 7.9 SEM photo of a diamond film deposited WC-6%Co surface. The deposition time is 4 h. 220

Figure 7.10 SEM photo of a diamond film deposited WC-6%Co surface. The deposition time is 5 h. 221

Figure 7.11 SEM photo of a diamond film deposited WC-6%Co surface. The deposition time is 6 h. 221

Figure 7.12 SEM photo of a diamond film deposited WC-6%Co surface. The deposition time is 8 h. 222

Figure 7.13 Raman spectrum of the diamond film that was deposited on a WC-6%Co round tool surface. 223

Figure 7.14 The cross sectional view of the microwave plasma jet reactor for diamond thin film coating on carbon fibers[14]. 225

Figure 7.15 The SEM picture of a diamond film coated carbon fiber. The experimental conditions are shown in Section 7.3.2. 228

]Figure 7.16 The SEM picture of the diamond film on carbon fibers. This figure is an enlarge of Figure 7.15 that contains more carbon fibers.. 229

Figure 7.17 Raman spectrum of the diamond film on the carbon fibers. 230

CHAPTER ONE

Introduction

1.1 Introduction

Microwave discharges were utilized in many of the first experimental demonstrations of plasma assisted CVD deposition of diamond thin films[1]-[8]. These early experiments made use of a 3-4 cm diameter tubular microwave reactor to create a 2.45 GHz excited discharge. Using CH_4/H_2 feed gases polycrystalline diamond films were deposited on substrates that were placed adjacent to or into the microwave discharge. Since these early experiments many other types of plasma sources have also demonstrated plasma assisted diamond thin film deposition. Some of these plasma sources are (1) RF thermal discharges, (2) DC arc discharges, (3)DC glow discharges, etc. These plasma sources, especially the higher pressure thermal-like discharges, have demonstrated linear deposition rates exceeding 100 μm/h.

In addition to a number of plasma assisted deposition processes diamond films can also be synthesized by hot filament and combustion reactors. However, microwave plasma assisted deposition still remains one of the most common laboratory methods used in scientific deposition

investigations. Microwave discharges have a number of intrinsic advantages. They are a relatively simple technology, are easy to operate and can deposit films on small substrate areas over a 10-70 Torr operating pressure range. While deposition rates are usually a modest 0.5-3 μm/h, the film quality is high and repeatable. The modest deposition rates together with the electrodeless nature of the discharge produce films of good quality and experiments that are repeatable from run to run. Thus microwave discharges have developed an excellent reputation as a plasma source in which to investigate the fundamental science of diamond deposition.

The research described in this dissertation is concerned with improving microwave plasma assisted CVD diamond film deposition technology. Of particular importance are the objectives of increasing the deposition rate and the deposition area of microwave plasma reactors. In addition, methods of depositing films on irregular shaped substrates and especially the deposition of films on objects with sharp edges and points are investigated. This thesis is part of a long-term research effort at Michigan State University where microwave plasma technology was invented, developed and evaluated in specific applications. Thus this thesis builds upon earlier research by J. Zhang (see Ph.D Thesis[9]) and U.S. Patent Number 5,311,103[107]) where an improved 12.5 cm diameter plasma reactor, identified as microwave cavity plasma reactor(MCPR), was developed and applied to diamond thin film deposition in the 20-70 Torr pressure regime. It also makes use of a new microwave reactor concept,

identified as the microwave jet reactor (see J. Zhang's Ph.D Thesis [9] and U.S Patent Number 5,571,577[108]) to deposit films on irregular shaped objects.

This dissertation summarizes the experimental development and investigation that lead to a successful demonstration of a high pressure microwave cavity plasma reactor (HPMCPR) and a microwave plasma jet reactor (MPJR). Some of this work has been published in part in scientific journals[10],[11] and has been presented at international conferences[12],[13] and a patent disclosure has been submitted to MSU[14].

The research in this thesis utilizes the moderate-pressure MCPR reactor design[9] and modifies its design to extend its operation to higher pressures. The research activities involved the addition of a substrate cooling assembly to the MCPR and then exploring how to operate the reactor under the higher pressure (80-150 Torr) and higher power (2-4.5 kW) regime. A part of the experimental work in this thesis is also concerned with applying the microwave jet reactor concept[108] to diamond film deposition on irregular shaped objects. A series of experiments are described that demonstrate the usefulness of this technology to deposit films on round tools, and even very small, fragile objects such as carbon fibers.

The research described in this thesis was carried by the author over a period of four years from 1993 to 1997 at Michigan State University under the guidance of Dr. Jes Asmussen. Research funding in this period

was provided by Norton Diamond Film Corp., Michigan State Research Excellent Fund, and NSF MRSEC/Center for Sensor Materials

1.2 Research Objectives

The research described in this thesis has three objectives. The first objective was to develop and test a high pressure MCPR for the synthesis of large area and uniform diamond films with high deposition rates (3-7 μm/h). The second objective was to experimentally characterize the high pressure microwave cavity plasma reactor for CVD diamond processes by evaluating the reactor performance over a wide range of reactor experimental variables. The third objective was to apply and optimize the microwave plasma jet reactor concept for the important application of depositing uniform and adherent diamond thin films on cemented carbide cutting tools and carbon fibers.

1.3 Dissertation Outline

This dissertation is divided into three parts: (1) literature review (Chapter 2), (2) description, development, and characterization of the high pressure microwave plasma reactors (Chapter 3, 4, 5), and (3) description and application of the microwave plasma jet reactor (Chapter 6,7).

Chapter 2 is a two-part review of the literature. The first section describes and compares the nonmicrowave plasma-assisted CVD reactors. A brief review of the "figure of merits" of the microwave plasma-

assisted CVD reactors is presented. Chapter 3 has three sections. First section describes the experimental systems and the redesigned high pressure MCPR and second section describes the experimental procedures that were used in the experiments reported in this thesis research. The last section describes the methods of the measurement of the output variables. Chapter 4 presents an overview of the reactor performance ($\mathbf{Y_1}$) of the high-pressure MCPR vs. five independent input variables, i.e., pressure, absorbed power, flow rate, substrate temperature, gas chemistry, and deposition time. Chapter 5 describes the deposited film properties ($\mathbf{Y_2}$) versus the multidimensional input variable space. The experimental details and results of CVD diamond deposition films vs. each single input variable are highlighted. The first part of Chapter 6 describes the microwave plasma jet reactor. The state of the art performance of this microwave plasma jet reactor is presented and the method of measurement of the output variables ($\mathbf{Y}$) for diamond film deposition on cemented carbide cutting tools and carbon fibers is reported in third section of Chapter 6. Chapter 7 presents the growth and characterization of microwave plasma CVD diamond films on WC-Co cutting tools and carbon fibers. Experimental details, results and analysis of the experimental evaluation of CVD diamond films in terms of tool packing capacity, film uniformity, film growth rate, film quality, film morphology are presented. Chapter 8 summarizes the research that was investigated in this thesis.

CHAPTER 2

Literature Review of Diamond Film Deposition Reactors

2.1 Introduction

This chapter reviews a number of diamond film chemical vapor deposition (CVD) technologies. These technologies include hot filament CVD, direct current (DC) CVD, combustion flame, radio frequency (RF) and microwave plasma assisted CVD. The experimental performance of these different reactors is compared by computing a number of reactor performance measures. These reactor output measures are (1) film growth rate, (2) film weight gain, (3) specific yield, (4) gas efficiency, and (5) carbon conversion efficiency. Since the major focus of this dissertation is concerned with microwave plasma assisted diamond film CVD, microwave plasma reactors are reviewed and discussed in detail in Section 2.5.

2.2 A General Description of the Chemical Vapor Deposition of Diamond Films

A general process for diamond film growth by chemical vapor deposition is demonstrated by the diagram shown in Figure 2.1[3]. The gas input is a mixture of hydrogen (H_2) and hydrocarbon (CH_4, C_2H_2, etc.) gases. The energy input is supplied by electrical (DC, Radio Frequency, or Microwave) energy and chemical energy. With sufficient energy input, the input gas mixtures are dissociated and chemically react with each other. A mixture of activated hydrocarbon and atomic hydrogen species are generated and diffuse onto substrate surface. During the surface reconstruction, clusters of diamond, amorphous carbon (a-C), amorphous hydrocarbon (a-C:H), and graphite are formed. As shown in Figure 2.1, the atomic hydrogen facilitates the diamond formation with only sp^3 bonds and suppresses the graphitic carbon clusters. The role of atomic hydrogen was first noted by Angus *et al.*[15], who reported on the preferential etching of graphite compared to diamond by atomic hydrogen.

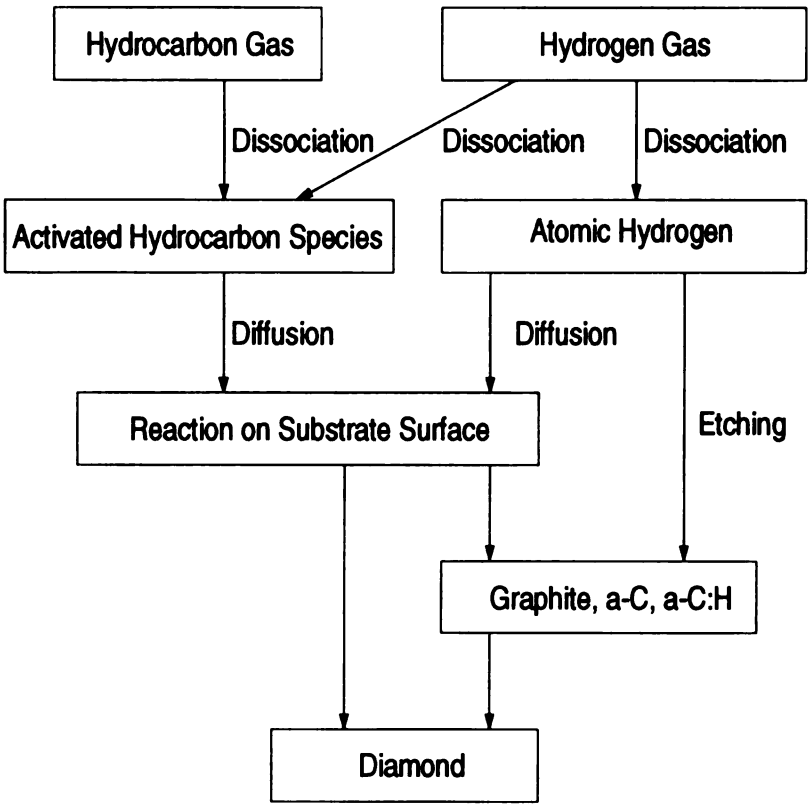

Figure 2.1 A general process for diamond film growth by chemical vapor deposition[3].

2.3 The Multivariable Diamond Film Deposition Reactor

2.3.1 Experimental Variables of a Diamond Film Deposition Reactor

The many experimental variables of a typical diamond film deposition reactor are identified in Figure 2.2. As shown, controllable input variables ($\mathbf{U_1}$) are defined as the variables which can be independently controlled during an experiment such as input power, gas chemistry, gas flow rate, deposition pressure, etc. Reactor design variables ($\mathbf{U_2}$) are identified as the variables which can be prechosen by the reactor designer such as reactor configuration and reactor wall materials, etc. Deposition process variables ($\mathbf{U_3}$) include the variables concerned with substrate process procedures and substrate preparation such as substrate biasing/cooling/heating, substrate seeding procedure, start-up and shut-down procedures, deposition time, etc. Internal variables are concerned with the variables related to internal discharge states such as discharge volume, species densities and temperatures, electron density and temperature, substrate temperature, etc. Output variables are identified as output performance or "figures of merit" of a diamond film deposition reactor such as linear growth rate, total growth rate, specific yield, gas flow efficiency, carbon conversion efficiency, etc., or film characteristics such as film uniformity, film Raman Spectrum, film morphology, etc.

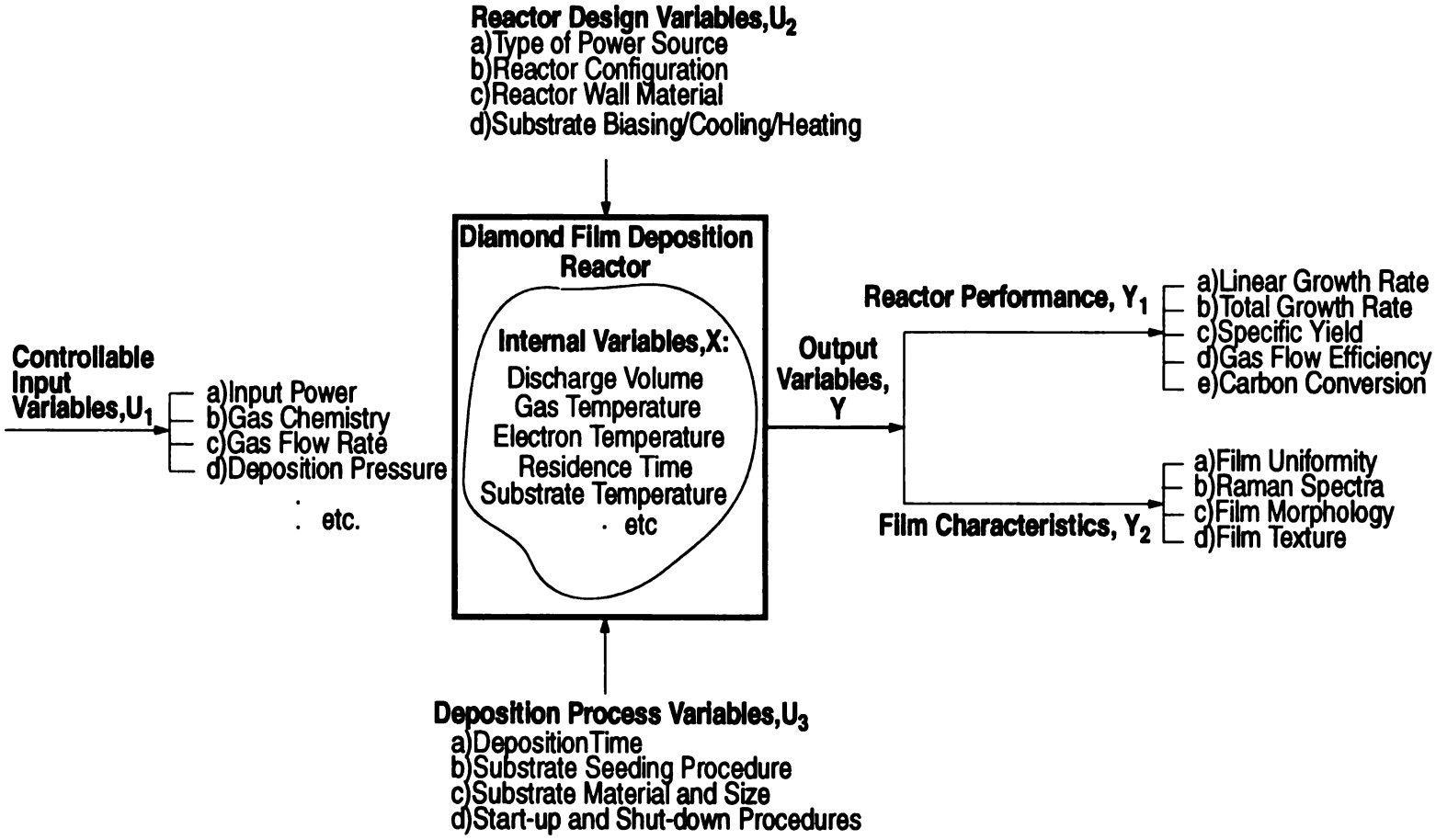

Figure 2.2 Multivariables of a diamond film deposition reactor.

2.3.2 "Figures of Merit" of Reactor Performance

In order to evaluate the performance of individual diamond film deposition reactors and compare the performance between different reactors, it is necessary to define the performance measures for a diamond film deposition reactor. These "figures of merit" may describe the efficiency of the deposition process or other important outputs of the deposition process such as film deposition rate. These figures of performance or merit can then be used to compare the performance of different deposition reactor concepts. The "figures of merit" that are employed in this dissertation are defined below:

(1) Linear Growth Rate (μm/h) is defined as the thickness increase of the diamond film (μm) divided by deposition time (h).

(2) Total Growth Rate (mg/h) is defined as the weight increase of the substrate (mg) divided by deposition time (h). Most papers in the open literature only report linear growth rate. Therefore if weight increase is not given in the reference then the total growth rate is calculated from the thickness increase by:
Weight Increase=(Thickness Increase)x(Deposition Area)x(Diamond Density of 3.51 g/cm^3).

(3) Specific Yield (kW-h/g) is defined as the power input (kW) per diamond film total growth rate (g/h)[9].

(4) Gas Efficiency (mg/liter) is defined as the total growth rate (mg/min) divided by total flow rate (liter/min). The total flow

rate is defined as the sum of all input gas flow rates[9].

(5) Carbon Conversion Efficiency is defined as the percentage of carbon atoms in the input gases which are converted into diamond[9],[16],[17].

2.4 Diamond Film CVD Reactor Technologies

Diamond film CVD reactors can be arranged into five major categories:

(1) Hot filament CVD (HFCVD) reactors;

(2) Direct current(DC) plasma-assisted CVD reactors;

(3) Combustion flame;

(4) RF plasma-assisted CVD reactors;

(5) Microwave plasma-assisted CVD reactors.

The state-of-art of (1)-(4) is briefly described in Section 2.4.1-2.4.5 below while in Section 2.5 microwave plasma assisted CVD reactors are reviewed in greater detail.

2.4.1 Notes on Literature Review

The review presented in the following sections is based on the experimental data that were published in the open literature. The input variables of a diamond film deposition reactor such as input power, gas chemistry, deposition pressure, reactor configuration, substrate material, etc., are directly cited from the references. However, except for the sub-

strate temperature, the internal variables of a diamond film deposition reactor are usually not described in the literature. The "figures of merit" of a diamond film deposition reactor examined in the following sections are estimated or calculated from the best data available in the references.

Some factors that can limit the accuracy of the "figures of merit" presented in this review are discussed below:

(1) In this review, deposition area is assumed to be the area of the entire substrate surface. It is assumed that the diamond film is deposited over uniformly the entire substrate surface. This assumption may result in overestimating some of the reactor "figures of merit".

(2) Linear growth rate may be measured differently by different research groups, resulting in the differences in the accuracy of "figures of merit" from on report to another. Some groups measure the film thickness from the SEM photos of the cross-sectional area of a diamond film while other groups use weight increase of the diamond film along with the deposition area and diamond density to calculate the film thickness. For both methods, the linear growth rate was obtained by dividing the thickness increase with the deposition time. If maximum linear growth rates are used, then the total growth rate expressed in mg/h is an overestimation of the growth rate unless the diamond film is uniformly coated over the entire deposition area.

(3) Since the method of determining film growth rate is different from one research group to another, the error bars for the "figures of

merit" may differ considerably from one reactor to another.

2.4.2 Hot Filament CVD (HFCVD) Reactors

2.4.2.1 Conventional HFCVD Reactor

Figure 2.3 schematically shows the conventional HFCVD reactor developed by Matsumoto *et al.*[18],[19] in 1982. After the reactor was evacuated to a low pressure by a vacuum pump, a gas mixture of methane and hydrogen was introduced from the top of the silica glass tube at a total flow rate of 4-200 sccm. A tungsten filament of 30 mm long, 0.15 mm in diameter[19] was placed several millimeters above the substrate. Once the reactor reached the operating pressure of 10-100 Torr, the filament was then heated by an electric current to a temperature of 2000°C. The gas mixture was thermally dissociated as it passed over the hot filament. A substrate (Si, Mo, natural diamond, etc.) was put on a silica holder and its temperature was monitored by a Pt-PtRh thermocouple set just below the silica holder.

Typical experimental variables that were reported or calculated in recently developed HFCVD reactors[20] are:

(A) Input Variables(U):

(1) Controllable input variables (U_1):

a) Input electrical power was not reported,

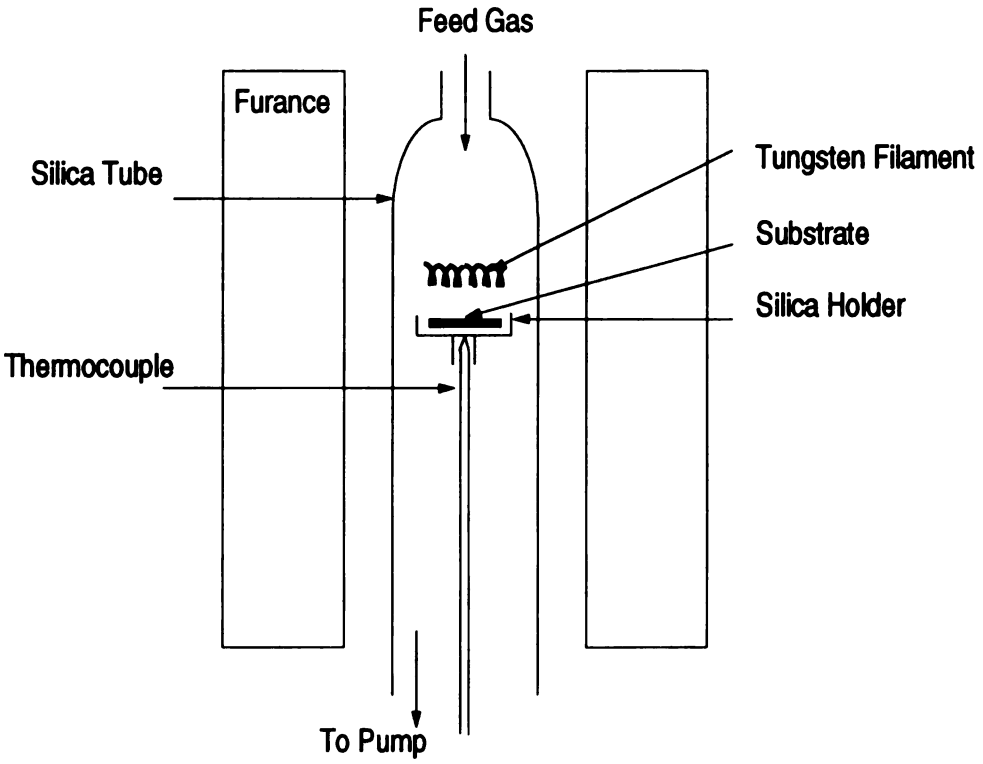

Figure 2.3 Schematic diagram of a conventional HFCVD reactor [18],[19].

b) Gas mixture: 0.067%-0.8%CH_4/H_2(CH_4 =0.1-1.2 sccm, H_2 =150 sccm),

c) Total flow rate~150 sccm.

d) Deposition pressure=25 Torr (3.33 kPa),

(2) Reactor design variables(U_2):

a) Type of Power source= DC power,

b) Reactor configuration is shown in Figure 2.3,

c) Reactor size: The filament was 10 mm long, 0.13 mm in diameter,

(3) Deposition process variables(U_2):

a) Deposition time=1 h,

b) Substrate seeding was not reported,

c) Substrate material and size= 1.5x1.5 mm^2 silicon,

d) Substrate was not biased, cooled or electrically heated,

(B) Internal variables(X):

(1) Substrate temperature=700-1060°C(973-1333°K),

(C) Figures of merit calculated for this review:

(1) Linear growth rate=1-4 μm/h,

(2) Deposition area=0.0225 cm^2,

(3) Total growth rate=0.008-0.03 mg/h,

(4) Specific yield is not available,

(5) Gas flow efficiency=0.0008-0.003 mg/liter,

(6) Carbon conversion efficiency~0.08%.

2.4.2.2 Electron-assisted HFCVD Reactor

An electron-assisted HFCVD reactor modified from the conventional HFCVD reactor has been used for diamond film growth. As an example, Figure 2.4 schematically displays the configuration of an electron-assisted HFCVD reactor[21],[22]. An AC current of 20A and 60V was applied and heated the filament to a temperature of 2000°C. In addition, a DC bias of approximately 90V was applied between the filament (negative) and the substrate (grounded, not shown in Figure 2.4). After the reactor was evacuated, a total flow rate of 50-100 sccm of a mixture of methane and hydrogen was supplied from the gas inlet and was forced to flow over the filament and substrate by the quartz tube shown in Figure 2.5. The reactor pressure was maintained at 30 Torr with a throttle valve. A tungsten filament of 20 mm long, 1.2 mm in diameter was supported approximately 1cm above the substrate. A substrate (Si, Mo, SiC, WC, etc.) was placed on a graphite holder, which in turn was placed on a water cooling stage. The substrate temperature was measured by a thermocouple attached to the back of the substrate.

Typical experimental variables that were reported or calculated from Ref.[22] are:

(A) Input Variables(U):

(1) Controllable input variables(U_1):

a) Input power level=1.2 kW,

b) Gas mixture= 1-8% CH_4/H_2 concentration,

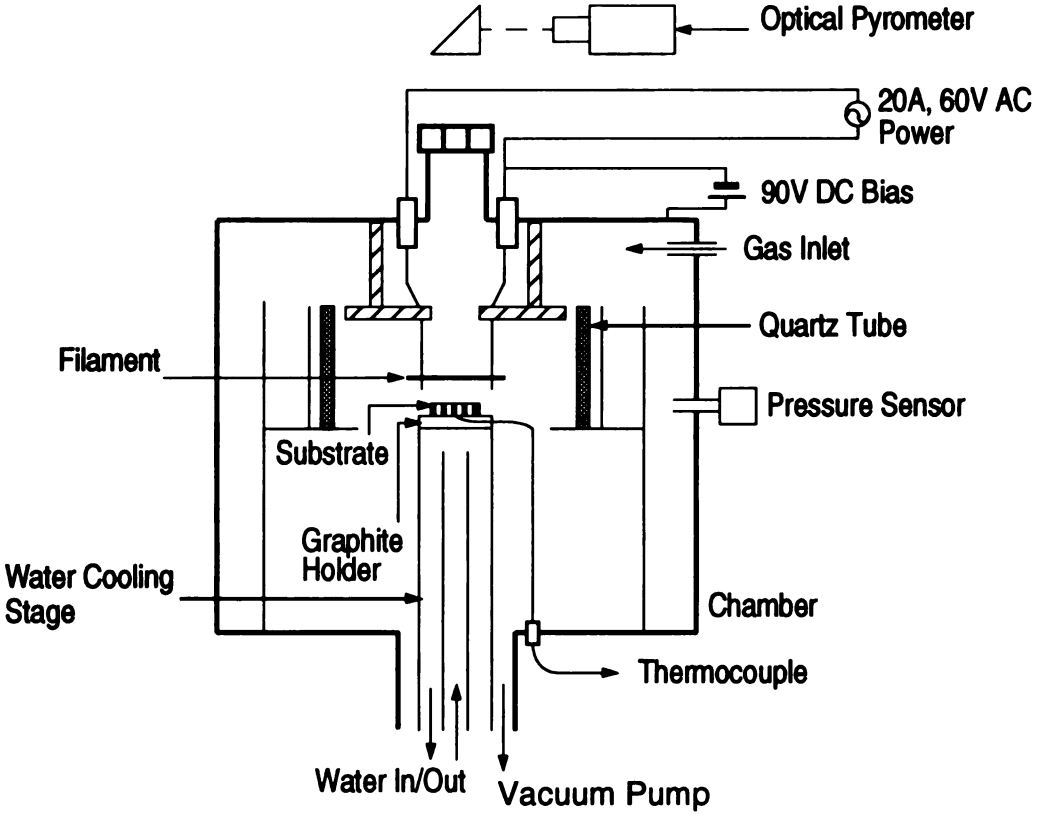

Figure 2.4 Schematic diagram of an Electron-assisted HFCVD reactor[22].

c) Total flow rate=100 sccm.

d) Deposition pressure=30 Torr (4 kPa),

(2) Reactor design variables(U_2):

a) Type of power source= AC power,

b) Reactor configuration is shown in Figure 2.4,

c) Reactor size: The filament was 20 mm long and 1.2 mm in diameter,

(3) Deposition process variables(U_2):

a) Deposition time=4-14 h,

b) Substrate seeding procedure was not reported,

c) Substrate material and size= 2x1cm^2 silicon,

d) Substrate was positively biased by 90V (with respect to filament) and was water cooled,

(B) Internal variables(X):

(1) Substrate temperature=750°C,

(C) Figures of merit calculated for this review:

(1) Linear growth rate=0.5-3 μm/h,

(2) Deposition area=2 cm^2,

(3) Total growth rate=0.35-2.1 mg/h,

(4) Specific yield=571-3428 kW-h/g,

(5) Gas flow efficiency=0.058-0.35 mg/liter,

(6) Carbon conversion efficiency=0.54-1.31%.

2.4.3 Direct Current (DC) Plasma CVD Reactors

2.4.3.1 Conventional DC Plasma CVD Reactor

Figure 2.5 schematically displays a conventional DC plasma CVD reactor[23],[24]. After the reactor was evacuated to 10^{-4} Pa(~7.5×10^{-4} mTorr), a gas mixture of CH_4 and H_2 was introduced at a total flow rate of 20-100 sccm. The input gas was distributed by a the water-cooled, grilled cathode. The reactor pressure was held at 200 Torr by a throttle valve. DC power was supplied to create a DC discharge between water-cooled anode and cathode when the chamber reached the operating pressure of 200 Torr. A substrate (Si, Mo, W, Al_2O_3, SiC, etc.) was mounted on the anode. This upward flow configuration allowed the impingement of dissociated species upon the substrate, resulting in the formation of diamond films. The temperature of the substrate during deposition was measured with an optical pyrometer[24].

Typical experimental variables that were obtained or calculated in this DC plasma CVD reactor are[24]:

(A) Input Variables(U):

(1) Controllable input variables(U_1):

a) Input power=3.14 kW,

b) Gas mixture= 2%CH_4/H_2,

c) Total flow rate=100 sccm.

d Deposition pressure=200 Torr (26.6 kPa),

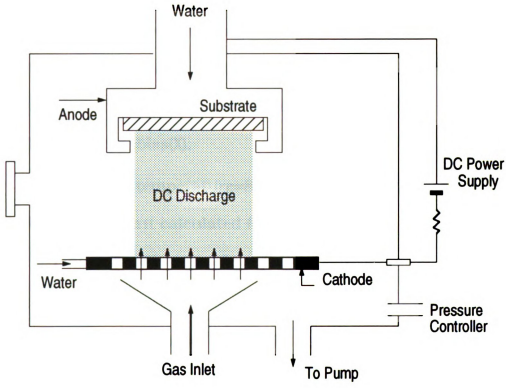

Figure 2.5 Schematic diagram of the DC plasma CVD reactor[23].

(2) Reactor design variables(U_2):

a) Type of power source= DC power,

b) Reactor configuration is shown in Figure 2.6,

c) Reactor size: Reactor consisted of a 1 cm diameter anode and a 2 cm diameter cathode,

(3) Deposition process variables(U_2):

a) Deposition time=30 min,

b) Substrate seeding procedure was not reported,

c) Substrate material and size= 5x5 mm^2 Si, Mo, W, etc.

d) Substrate was positively biased with 1kV (with cathode grounded) and was water cooled,

(B) Internal variables(X):

(1) Substrate temperature=850°C,

(C) Figures of merit calculated for this review:

(1) Linear growth rate=20 μm/h,

(2) Deposition area=0.25 cm^2,

(3) Total growth rate=1.76 mg/h,

(4) Specific yield=1784 kW-h/g,

(5) Gas flow efficiency=0.29 mg/liter,

(6) Carbon conversion efficiency=2.73%.

2.4.3.2 Enclosed DC Arc Jet CVD Reactor

A DC arc jet CVD reactor similar to the conventional DC plasma CVD reactors[24],[25] is illustrated in Figure 2.6[26]. During the diamond deposition, only Ar was passed through the plasma gun electrode gap, creating a high velocity plasma. The CH_4 and H_2 were introduced into the vacuum chamber through separate feed lines at a total flow rate of approximately 5.5 liter/min. The H_2 gas was injected 1 cm downstream of the electrode gap through opposing side ports integral to the plasma gun, while CH_4 gas injected 3.5 cm downstream from the H_2 ports through a stainless steel tube mounted onto the substrate holder. The reactor pressure was kept between 50-400 Torr by a throttle valve. The water-cooled molybdenum substrate with the size of 25mmx38mm was positioned 2.5 cm from the electrode gap. This downstream configuration allowed the impingement of dissociated species upon the substrate, resulting in the formation of diamond films.

Typical experimental variables that were reported or calculated in this DC plasma jet CVD reactor are[26]:

(A) Input Variables(U):

(1) Controllable input variables(U_1):

a) Input power=2.8-3.0 kW(20V, 140-150A DC Power),

b) Gas mixture: 2.7%-15%CH_4/H_2(Ar=13.7 liter/min, CH_4= 150-700 sccm, H_2=5.4 liter/min),

c) Total flow rate=20 liter/min,

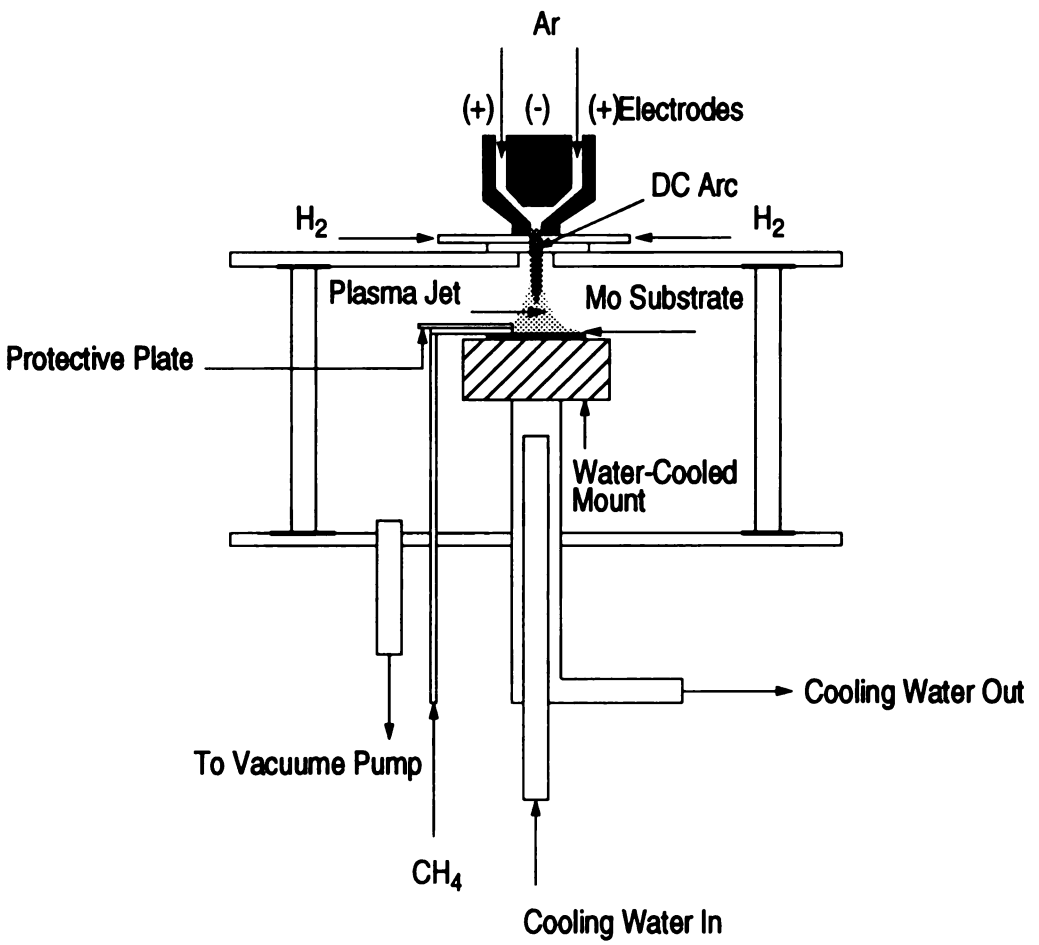

Figure 2.6 Schematic diagram of a DC plasma jet CVD reactor[26].

d) Deposition pressure=55-60 Torr (~18 kPa),

(2) Reactor design variables(U_2):

a) Type of power source= DC power,

b) Reactor configuration is shown in Figure 2.6,

c) Reactor size: The size of anode and cathode were not reported,

(3) Deposition process variables(U_2):

a) Deposition time was not reported,

b) Substrate seeding procedure was not reported,

c) Substrate material and size= 2.5x3.8 cm^2 silicon,

d) Substrate was electrically insulated and water cooled,

(B) Internal variables(X):

(1) Substrate temperature was not reported,

(C) Figures of merit calculated for this review:

(1) Linear growth rate=0.6-3.6 μm/h,

(2) Deposition area=9.5 cm^2,

(3) Total growth rate=2-12 mg/h,

(4) Specific yield=250-1500 kW-h/g,

(5) Gas flow efficiency=0.01-0.0017 mg/liter,

(6) Carbon conversion efficiency=0.06-0.12%.

Another DC plasma jet CVD reactor was operated at atmospheric pressure with two DC power supplies. The schematic of this reactor con-

figuration can be seen in Figure 2.7[27]. A secondary discharge was used to enhance the film growth rate using a DC substrate bias. As shown, a mixture of CH_4 and H_2 gases with flow rates of approximately 20 liter/min were fed from six injection ports located at the copper anode. In the meantime, Ar gas at a flow rate of 450 liter/min was fed into the anode-to-cathode spacing. The arcjet power supply provided the DC power to the tungsten cathode and copper anode, resulting in the formation of a DC arc around the converging nozzle. When input mixed gases passed downstream through the DC arc and the converging nozzle, the gas mixtures were dissociated and created a downstream plasma jet. These dissociated species impinged upon the substrate, resulting in the formation of diamond film on its surface. A substrate consisting of 1/2″ (1.27 cm) diameter molybdenum rod was threaded in a water-cooled copper holder as shown in Figure 2.7. This copper holder was DC biased by a biasing power supply and electrically insulated with a boron nitride (BN) insulator.

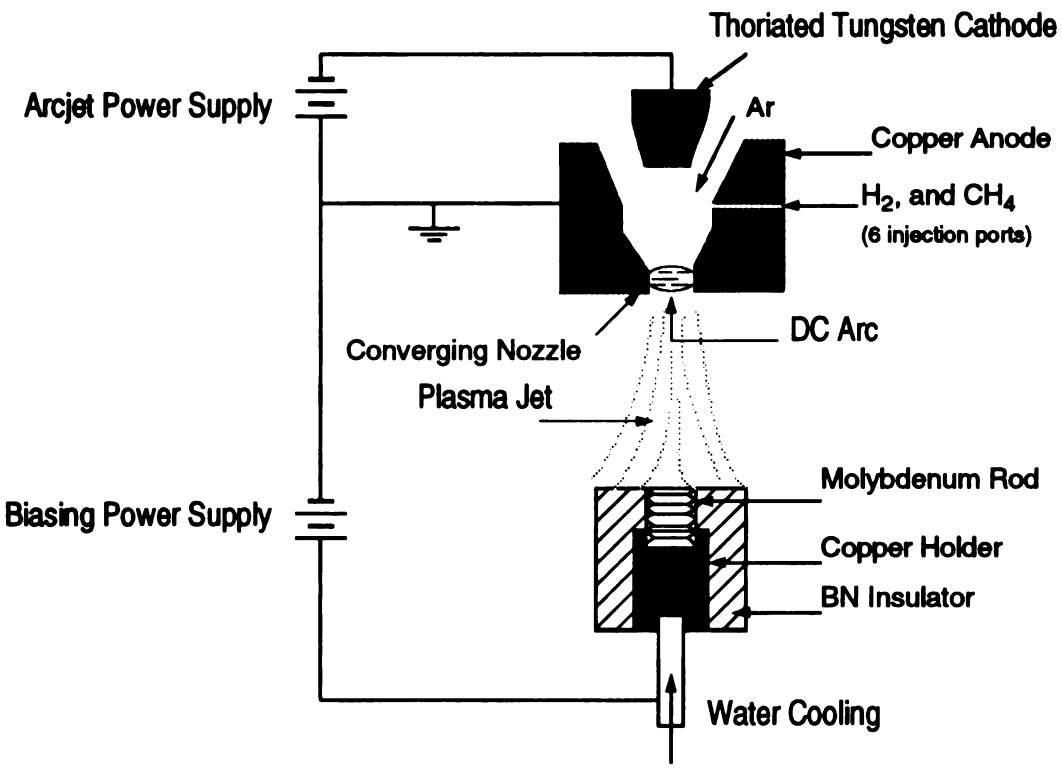

Figure 2.7 Schematic illustration of an atmospheric pressure DC arc jet CVD reactor and its substrate biasing system[27].

Typical experimental variables that were reported or calculated in this DC plasma jet CVD reactor are[27]:

(A) Input Variables(U):

(1) Controllable input variables(U_1):

a) Input power=100 kW,

b) Gas mixture=2.5%CH_4/H_2(CH_4=0.467 liter/min, H_2 = 19.125 liter/min, Ar=450 liter/min),

c) Total flow rate~470 liter/min,

d) Deposition pressure= atmospheric pressure,

(2) Reactor design variables(U_2):

a) Type of power source= Two DC power supplies

b) Reactor configuration is shown in Figure 2.7,

c) Reactor size: The size of anode and cathode were not reported,

(3) Deposition process variables(U_2):

a) Deposition time=1 h,

b) Substrate seeding procedure was not reported,

c) Substrate material and size=1/2″ diameter Mo rod,

d) Substrate was positively bias up to 200V and was also water cooled,

(B) Internal variables(X):

(1) Substrate temperature=1115^0C(1388^0K),

(C) Figures of merit calculated for this review:

(1) Linear growth rate=10-30 μm/h,

(2) Deposition area=1.27 cm^2,

(3) Weight gain=2.67-13.37 mg/h,

(4) Specific yield=7479 kW-h/g,

(5) Gas flow efficiency=$9.47x10^{-5}$-$4.74x10^{-4}$ mg/liter,

(6) Carbon conversion efficiency=0.018-0.089%.

2.4.4 Combustion Flames

2.4.4.1 Atmospheric Pressure Combustion Flame

The schematic drawing of a conventional combustion flame diamond film deposition reactor, which was operated at atmospheric pressure, is shown in Figure 2.8[28],[29],[30]. As shown, this combustion flame consists of torch, a torch nozzle, shroud, and the substrate assembly. A 0.95-1.27 cm diameter molybdenum rod was used as the substrate and was placed on a water-cooled block. A total flow rate of 2-6 liter/min of a mixture of C_2H_2 (acetylene) and O_2 was introduced from the top of the torch and flowed downstream to the torch nozzle and the shroud gas (N_2 or air) was fed downstream between torch and shroud. A flame of approximately 3000°C[27][29] was ignited by an electrical spark. The gas mixture of C_2H_2 and O_2 was dissociated by passing through the flame. Diamond films were then deposited on the substrate. The substrate temperature in this reactor was measured with an optical pyrometer.

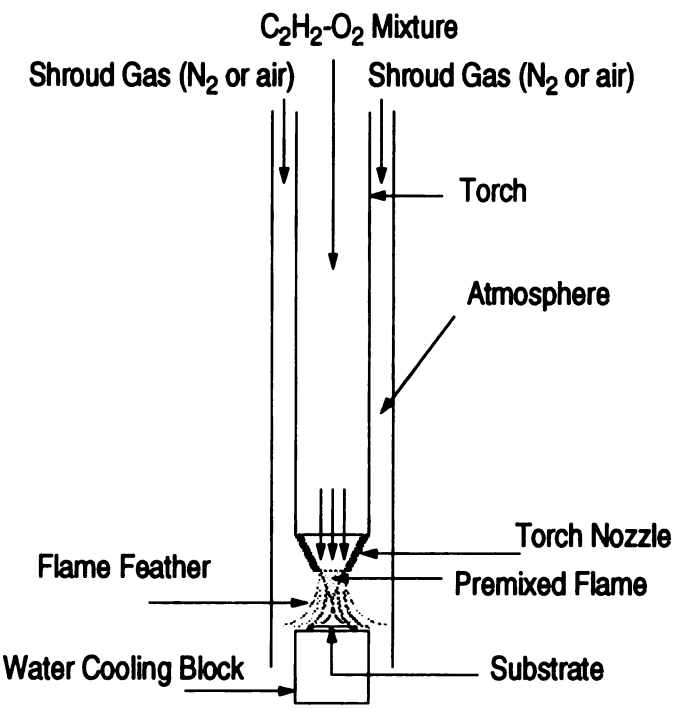

Figure 2.8 Schematic diagram of an atmospheric-pressure oxygen-acetylene combustion flame[29].

Typical experimental variables that were used in this combustion flame are[29]:

(A)Input Variables(U):

(1) Controllable input variables(U_1):

a) The flame power was not reported,

b)Gas mixture= C_2H_2 (0.643 liter/min), O_2 (0.607 liter/min) and N_2=1.5 liter/min,

c) Total flow rate=2.75 liter/min,

d) Deposition pressure= atmospheric pressure,

(2) Reactor design variables(U_2):

a) Type of power source= combustion flame,

b) Reactor configuration is shown in Figure 2.8,

c) Reactor size: the torch size was not reported

(3) Deposition process variables(U_2):

a) Deposition time=25 min,

b) Substrate was seeded by being polished with No.600 SiC sandpaper and 1 μm diamond paste,

c) Substrate material and size=3/8˝(0.95cm) diameter Mo,

d) Substrate was water cooled, no bias was applied.

(B) Internal variables(X):

(1) Substrate temperature=1050°C(1323°K),

(C) Figures of merit calculated for this review:

(1) Linear growth rate=10-15 μm/h,

(2) Deposition area=0.71 cm^2,

(3) Weight gain=2.49-3.74 mg/h,

(4) Specific yield was not available,

(5) Gas flow efficiency=0.033-0.050 mg/liter,

(6) Carbon conversion efficiency=0.006-0.009%.

2.4.4.2 Enclosed Flat Combustion Flame

A low-pressure flat flame was developed by Goodwin[31][32] and Cappelli[33][34] to deposit diamond film at the pressure ranging from 40 to 200 Torr. Figure 2.9 illustrates the reactor described in Ref.[33]. As shown, a multi-nozzle burner was supported by a T-stage. After the reactor was evacuated, a gas mixing chamber injected a mixture of O_2 and fuel (C_2H_2[19,20], CH_4[21], etc.) at flow rates between 9-21 liter/min through the multiple nozzles located on the top of burner and onto the substrate. The flame was ignited with an electric spark by an ignitor at proper pressure and the upward flow gas mixture then was dissociated in the flame. The dissociated species impinged on the substrate where the diamond films were deposited. The substrate used in this reactor was a threaded molybdenum rod of diameter ranging from 1.6 cm[33] to 5 cm[32], depending on the size of the burner. The substrate temperature was controlled by adjusting the amount of molybdenum that was threaded into the water-cooled block. The substrate temperature was measured by a two-color infrared pyrometer.

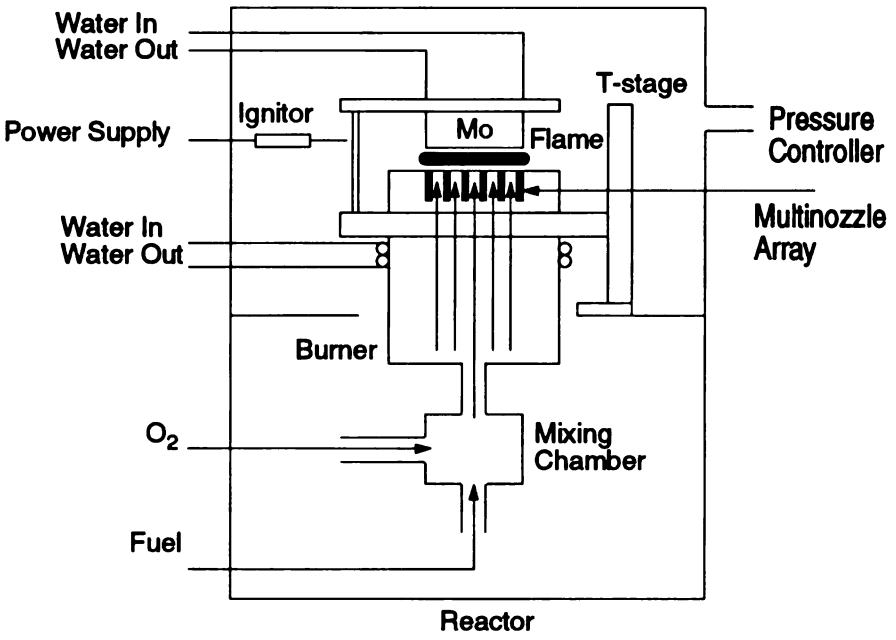

Figure 2.9 Schematic of an enclosed flat flame[32].

Typical experimental variables were given or calculated from the data supplied in Ref.[32] are:

(A)Input Variables(U):

(1) Controllable input variables(U_1):

a) Type of power source= combustion flame

b) Flame power was not reported,

c) Gas mixture:

- 0.6 liter/min-cm^2 of C_2H_2,i.e., 1.884 liter/min in a 2 cm diameter burner, and 7.536 liter/min in a 4 cm diameter burner,
- 1.3 liter/min-cm^2 of O_2,i.e., 4.082 liter/min in a 2 cm diameter burner, and 16.328 liter/min in a 4 cm diameter burner,

ii) Total flow rate=9.42-20.41 liter/min,

c) Deposition pressure=180 Torr (~24 kPa),

(2) Reactor design variables(U_2):

a) Reactor configuration is shown in Figure 2.9,

b) Reactor size: The diameter of the burner shown in Figure 2.10 was from 2 cm to 4 cm[31],[32],

(3) Deposition process variables(U_2):

a) Deposition time=2.5 h,

b) Substrate seeding information was not reported,

c) Substrate was a 5 cm diameter molybdenum rod,

d) Substrate was water cooled, no bias was applied.

(B) Internal variables(X):

(1) Substrate temperature=830°C(1103°K),

(C) Figures of merit calculated for this review:

(1) Linear growth rate=1 μm/h,

(2) Deposition area=19.6 cm^2,

(3) Weight gain=6.88 mg/h,

(4) Specific yield is not available,

(5) Gas flow efficiency=0.012-0.056 mg/liter,

(6) Carbon conversion efficiency=0.0014-0.0057%.

2.4.5 RF Plasma CVD Reactors

2.4.5.1 Conventional RF Plasma CVD Reactor

A schematic view of a conventional RF plasma CVD reactor operated at low pressure (3.75-22.5 Torr) is displayed in Figure 2.10[35]. As shown in Figure 2.10, the center section of quartz tube was coaxially surrounded by the working coil. The substrate was placed on a silica boat in the middle of quartz tube and experiments were performed without any external biasing or heating. After the reactor was evacuated, a mixture of CH_4/H_2 was fed into the quartz tube. One half to one kW of RF power was supplied by a 13.56 MHz generator. A RF plasma discharge was ignited at the center of quartz tube when the pressure was between 3.75 and 22.5

Torr. This plasma discharge dissociated the input gas mixtures and the radical species reacted on the substrate. Silicon, molybdenum, and silica glass plates were used as the substrate materials and the temperatures were monitored by an optical pyrometer during each experimental run.

Two example deposition results are[35]: (1) a 5 μm film was deposited under 7.5 Torr (1 kPa) with 700 W RF power at a substrate temperature of 800°C, and (2) a 20 μm film was deposited under 22.5 (3 kPa) with 1 kW RF power at substrate temperature of 940°C. Since the deposition time and the substrate size were not reported in Ref.[35], the "figures of merit" are not available.

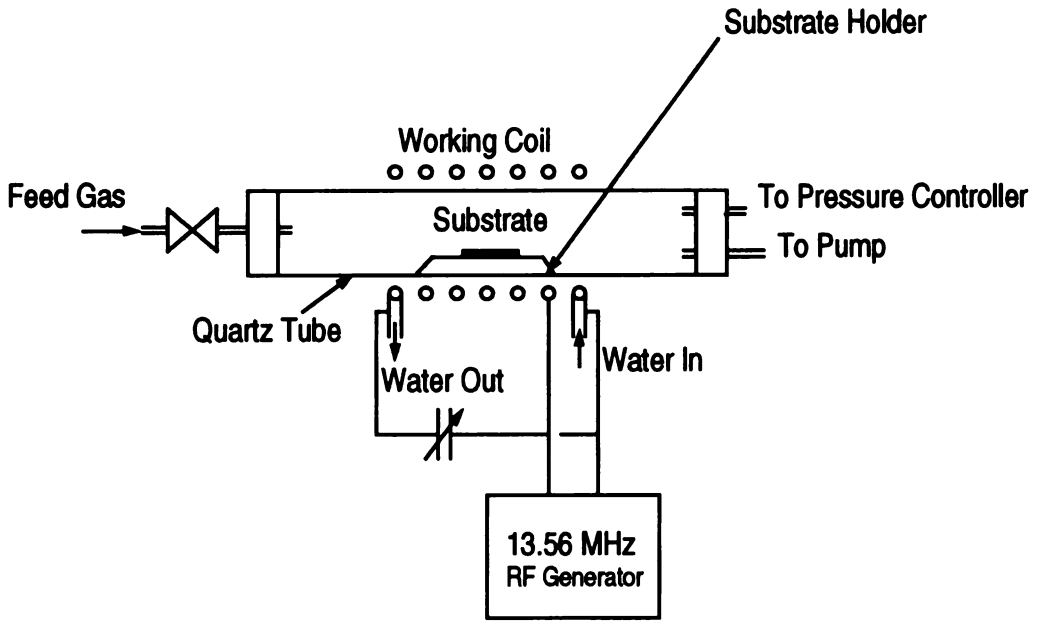

Figure 2.10 A schematic diagram of a conventional RF plasma CVD reactor[35].

2.4.5.2 RF Thermal Plasma CVD Torch

The schematic drawing of a RF thermal plasma diamond film deposition reactor is shown in Figure 2.11[36],[37]. As shown, the RF thermal plasma torch consists of a torch head, coaxial double quartz sleeves, and an RF working coil. The torch was mounted on the flange of a reactor chamber, where the water cooled substrate holder was positioned. After the chamber was evacuated, sheath gases (mixture of Ar, H_2 and CH_4) and plasma gas (Ar only) were introduced from the torch head. A 3.4-4 MHz RF power supply (not shown in Figure 2.11) was used to sustain the thermal plasma at deposition pressure of an atmosphere[36] or subatmosphere[37]. A molybdenum substrate of 10 cm diameter was placed within or at the end of the thermal plasma on a water-cooled substrate holder. Diamond film was deposited on the substrate as the dissociated gas species reacted on its surface.

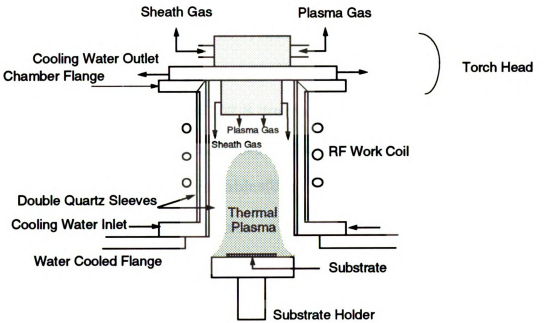

Figure 2.11 A schematic diagram of a RF thermal plasma torch[36][37].

The available experimental variables that can be obtained or calculated from Ref.[37] are summarized below:

(A)Input Variables(U):

(1) Controllable input variables(U_1):

a) Input power=60 kW,

b) Gas mixture:

-sheath gas: 4%CH_4/H_2(Ar=80 liter/min,H_2=20 liter/min,CH_4=0.8 liter/min),

- plasma gas: Ar=2 liter/min,

c) Total flow rate=102.8 liter/min,

d) Deposition pressure=150 Torr (20 kPa),

(2) Reactor design variables(U_2):

a) Type of power source= a 3.4 MHz RF power,

b) Reactor configuration is shown in Figure 2.11,

c) Reactor size: A 65 mm inner diameter quartz sleeve was used,

(3) Deposition process variables(U_2):

a) Deposition time was not reported,

b) Substrates were polished with 0.25 μm diamond paste,

c) Substrate was a 10 cm diameter molybdenum plate,

d) Substrate was water cooled, no bias was applied.

(B) Internal variables(X):

(1) Substrate temperature=800°C-950°C(1073°K-1223°K),

(C) Figures of merit calculated for this review:

(1) Linear growth rate=30 μm/h,

(2) Deposition area=78.5 cm^2,

(3) Weight gain=826.6 mg/h,

(4) Specific yield= 72.5 kW-h/g,

(5) Gas flow efficiency=0.134 mg/liter,

(6) Carbon conversion efficiency=3.21%.

2.5 Microwave Plasma assisted CVD Reactors

2.5.1 Magneto-microwave Plasma CVD Reactors

The schematic diagram of a magneto-microwave plasma CVD reactor is shown in Figure 2.12[38],[39]. This reactor was built to investigate the low temperature deposition of diamond films[40]. As shown, a magnetic field was established using a 15 cm diameter, 9 cm high Nd-Fe-B permanent magnet with a magnetic flux density of 0.42 T at the magnet pole face. Mantei *et al.*[39] indicated that the magnetic field was used to increase gas dissociation. A 2.45 GHz microwave power supply was pulse modulated at a repetition rate of 120 Hz with a fixed peak power level of 3 kW[38]. It is noted by the authors[39] that a high peak microwave power, i.e., 3 kW, was used to more completely dissociate the H_2 gas, while the average input microwave power is kept as low as 300 W for all deposition experiments.

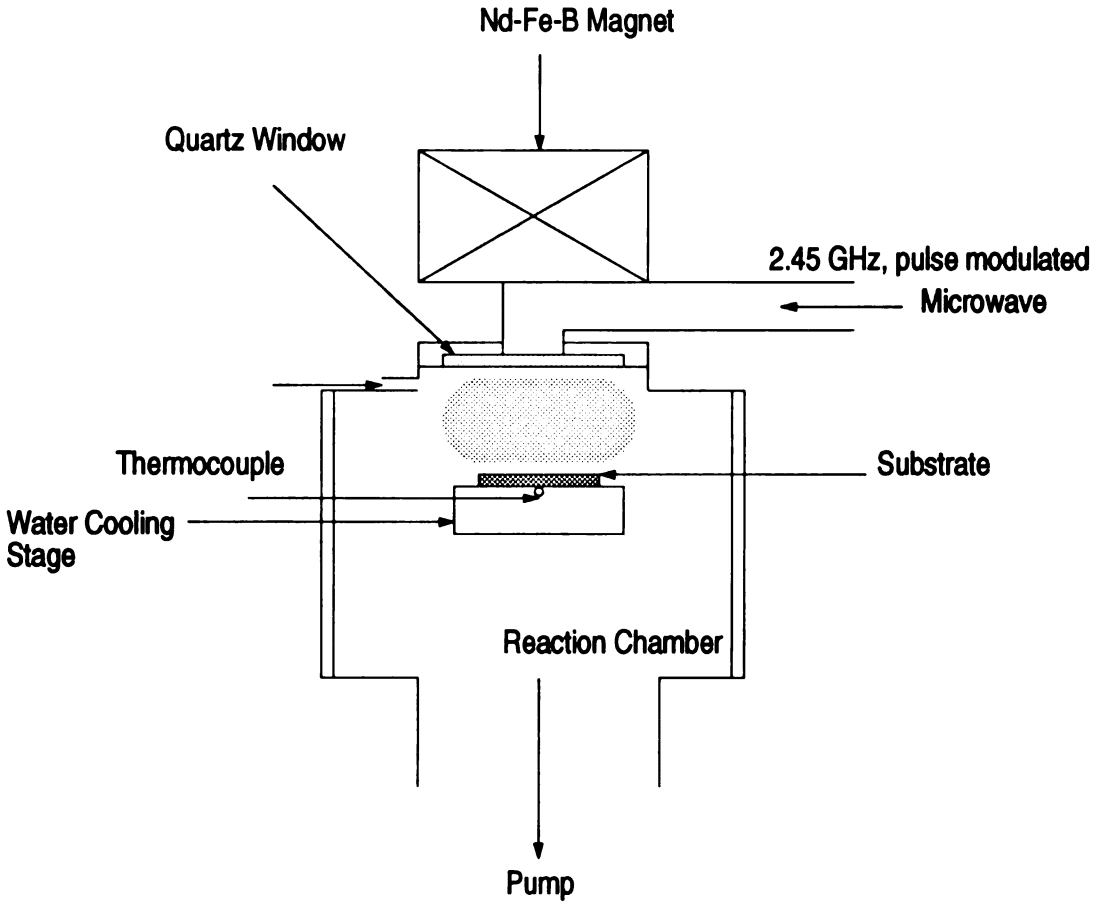

Figure 2.12 The schematic drawing of a magneto-microwave plasma CVD reactor[38],[39].

After the reaction chamber(15 cm in diameter) was evacuated to 15 mTorr, a mixture of CH_4-O_2-H_2 gases at flow rates between 100-400 sccm was introduced from the gas inlet located on the top of reaction chamber.

A plasma discharge was established by the 2.45 MHz, pulse modulated microwave power at pressure of 1-3 Torr. A 2.5 cm silicon wafer was placed on a water-cooled substrate holder, in which a thermocouple was inserted to the back side of the substrate to monitor the substrate temperature. A diamond film was formed on the substrate when the reactive gases were dissociated and reacted on its surface.

Detailed experimental variables that were obtained or calculated from Ref.[39] are:

(A)Input Variables(U):

(1) Controllable input variables(U_1):

a Input power: average microwave power is 300 W and peak microwave power is 3 kW,

b) Gas mixture: 10%CH_4/H_2, 9%O_2/H_2(H_2=100 sccm, CH_4= 10 sccm, O_2=9 sccm),

c) Total flow rate=119 sccm,

d) Deposition pressure=3 Torr (0.4 kPa),

(2) Reactor design variables(U_2):

a) Type of power source= a 2.45 GHz pulse modulated microwave generator,

b) Reactor configuration is shown in Figure 2.12,

c) Reactor size: A 15 cm diameter reaction chamber,

(3) Deposition process variables(U_2):

a) Deposition time=15 h

b) Substrates were polished with 5 μm diamond paste,

c) Substrate was a 2.5 cm diameter silicon wafer,

d) Substrate was water cooled. A permanent magnet was applied,

(B) Internal variables(X):

(1) Substrate temperature=300-600°C(573-873°K),

(C) Figures of merit calculated for this review:

(1) Linear growth rate=0.4-0.8 μm/h,

(2) Deposition area=4.91 cm^2,

(3) Weight gain=0.69-1.38 mg/h,

(4) Specific yield=217-434 kW-h/g,

(5) Gas flow efficiency=0.097-0.193 mg/liter,

(6) Carbon conversion efficiency=0.21-0.43%.

2.5.2 Tubular Microwave Plasma CVD Reactors

A schematic diagram of a typical tubular microwave reactor is shown in Figure 2.13[1]. The tubular microwave plasma reactor was developed in early 1980s by Kamo *et al.*[1] and became one of the most popular diamond film deposition reactor technologies. As shown, the input gas which is a mixture of hydrocarbon (CH_4[27-32,34],CO[33], etc.) and hydrogen with a flow rate less than 300 sccm was dissociated by the 2.45GHz microwave energy coupled into 40-44 mm diameter quartz tube[1]-[7] through a set of waveguides, power monitors, and three-stub tuner. A plunger was attached to the end of the waveguide to minimize the reflected power. A silicon substrate was placed in the middle of the quartz and its temperature was usually monitored with an optical pyrometer.

Typical experimental variables that were reported or calculated from the deposition experiments performed with a tubular microwave plasma-assisted CVD reactor are[8]:

(1) Controllable input variables(U_1):

a) Input power=600 W,

b) Gas mixture: 1%-2%CH_4/H_2(H_2=200-310 sccm, CH_4=2.8-3.6 sccm),

c) Total flow rate=202.8-313.6 sccm,

d) Deposition pressure=40 Torr (5.3 kPa),

(2) Reactor design variables(U_2):

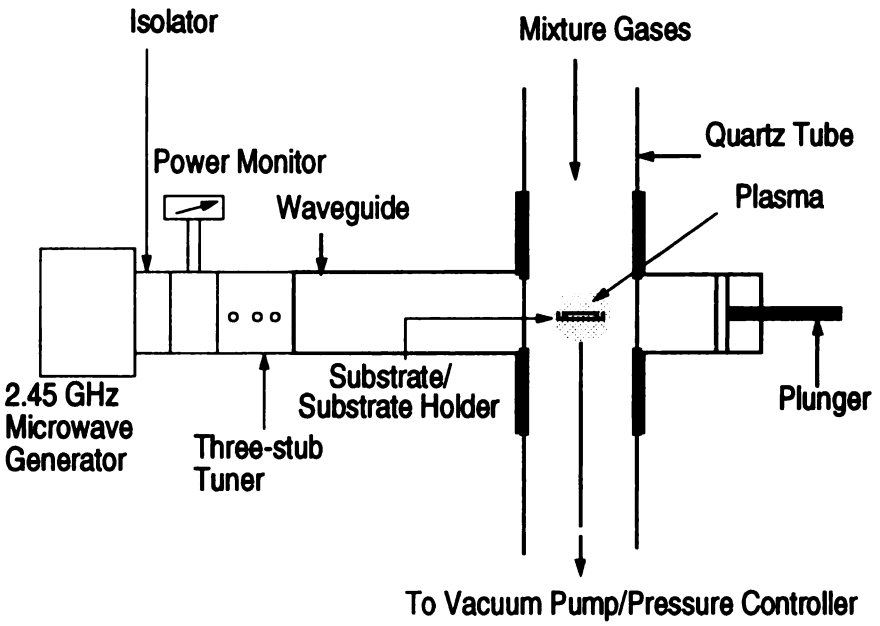

Figure 2.13 Schematic diagram of a tubular microwave plasma-assisted CVD reactor[1].

a) Type of power source: a 2.45 GHz microwave power,

b) Reactor configuration is shown in Figure 2.13,

c) Reactor size: Quartz tube size was approximately 40 mm in diameter,

(3) Deposition process variables(U_2):

a) Deposition time=6-7 h

b) Substrates were polished with 1-2 μm diamond paste for 30 min. The substrates were then agitated in an ultra-sonic bath containing propanol in which a small amount of diamond powder was suspended. The substrates were then degreased in 3 parts HCl and 1 parts HF solution, washed with distilled water, and dried.

c) Substrate size= 20x20 mm^2,

d) no substrate biasing, heating or cooling was applied,

(B) Internal variables(X):

(1) Substrate temperature=790-850°C(1063-1123°K),

(C) Figures of merit calculated for this review:

(1) Linear growth rate=0.8 μm/h,

(2) Deposition area=4 cm^2,

(3) Weight gain=1.12 mg/h,

(4) Specific yield=536 kW-h/g,

(5) Gas flow efficiency=0.059-0.092 mg/liter,

(6) Carbon conversion efficiency=0.97-1.24%.

2.5.3 Microwave Plasma Jet Reactors

Figure 2.14 schematically displays a microwave plasma jet torch system[41],[42]. The torch contained a rectangular waveguide, a microwave transition unit, and a coaxial waveguide. The coaxial waveguide consisted of a 57.2 mm diameter outer conductor and a 20 mm diameter center conductor. Microwave energy was excited in the TE_{01} mode in a rectangular waveguide by a 2.45 GHz microwave generator and then was transformed into the TEM mode by a rectangular to coaxial transition unit. Mixtures of hydrocarbon (CH_4,O_2), hydrogen, and argon were the feed gases which flowed radially into the coaxial waveguide and then passed through the nozzle (22 mm in diameter) and out of the reactor. A plasma jet was generated near the nozzle at atmospheric pressure and the dissociated species reacted on a silicon substrate, which was placed on a water cooled stage. The substrate temperature was monitored by an optical pyrometer during the experiment[41].

Detailed experimental variables that were reported or calculated from Ref.[42] are:

(1) Controllable input variables(U_1):

a) Input power=3.8-4.2 kW,

b) Gas mixture: 1.5%-4.5%CH_4/H_2(H_2= 20 liter/min, CH_4= 0.3-0.9 liter/min, O_2=0-0.525 liter/min, Ar=10 liter/min),

c) Total flow rate~ 40 liter/min,

d) Deposition pressure= atmospheric pressure,

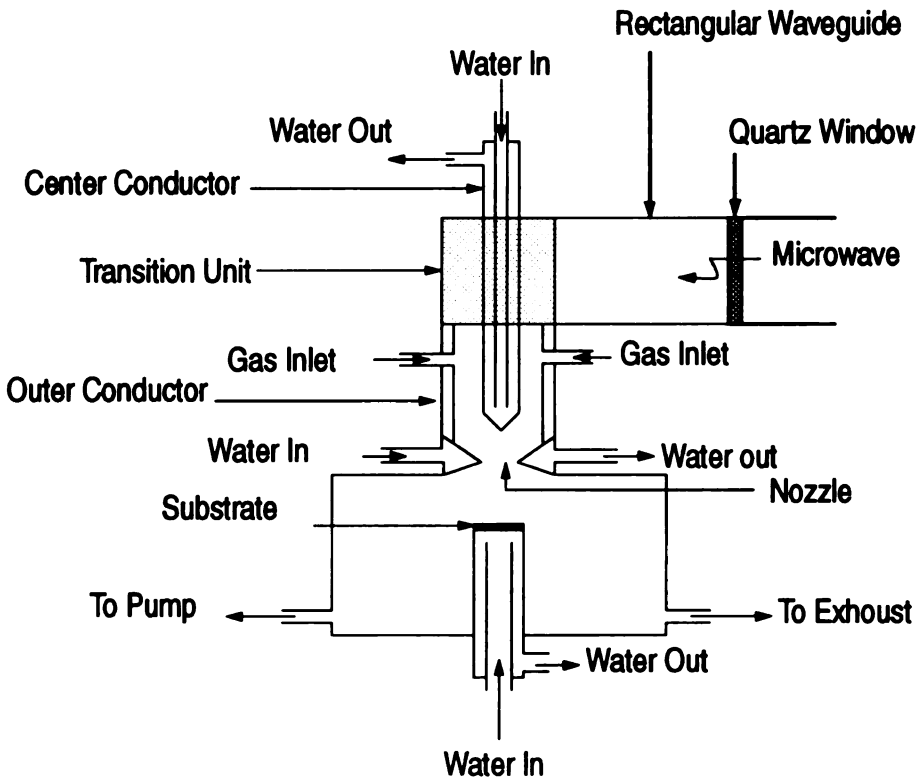

Figure 2.14 Schematic drawing of a microwave plasma jet torch[41].

(2) Reactor design variables(U_2):

a) Type of power source=a 2.45 GHz microwave power,

b) Reactor configuration is shown in Figure 2.14,

c) Reactor size: A 57.2 mm diameter outer conductor and a 20 mm diameter center conductor with a 22 mm jet nozzle

(3) Deposition process variables(U_2):

a) Deposition time=35 min,

b) Substrates were mechanical blasted for 2 h with SiC powder,

c) Substrate size=25x10 mm^2,

d) substrate was water cooled only,

(B) Internal variables(X):

(1) Substrate temperature=887-927°C(1160-1200°K),

(C) Figures of merit calculated for this review:

(1) Linear growth rate=6-12 μm/h,

(2) Deposition area=2.5 cm^2,

(3) Weight gain=5.27-10.53 mg/h,

(4) Specific yield=360-800 kW-h/g,

(5) Gas flow efficiency=0.002-0.004 mg/liter,

(6) Carbon conversion efficiency=0.018-0.109%.

2.5.4 Bell-jar Microwave Plasma-assisted CVD Reactors

2.5.4.1 Astex Bell-jar Microwave Plasma-assisted Reactor

The bell-jar microwave PACVD system, manufactured by Astex Inc., is schematically shown in Figure 2.15[43]-[46]. After the reactor was evacuated by the vacuum pump, a mixture of methane, hydrogen and oxygen was introduced from the gas inlet and guided into the bell jar by a cylindrical fused silica tube. The gas mixtures were dissociated by the microwave energy which was coupled into the cylindrical microwave cavity through the rectangular waveguide and coaxial antenna. The substrate, which can be silicon, fused silica, MgO, etc., was placed on a graphite holder and this holder was placed on the substrate cooling stage. A ball-shaped[44] plasma was created inside the quartz bell jar and the dissociated species reacted on the substrate surface, producing the diamond film over its surface.

Detailed experimental variables that were reported or calculated from Ref.[45] are:

(1) Controllable input variables(U_1):

a) Input power=1.5 kW,

b) Gas mixture: 0.5% CH_4/H_2,

c) Total flow rate=200-600 sccm,

d) Deposition pressure=40-70 Torr,

(2) Reactor design variables(U_2):

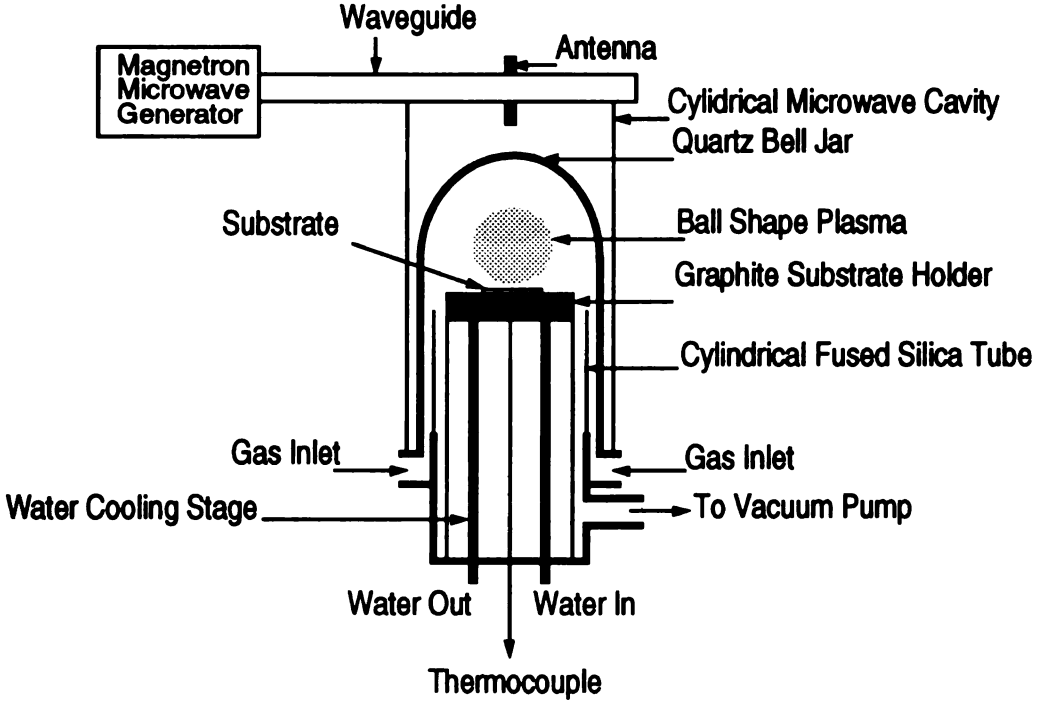

Figure 2.15 Schematic drawing of the Astex bell jar microwave PACVD reactor[43]-[46].

a) Type of power source: a 2.45 GHz microwave power,

b) Reactor configuration is shown in Figure 2.15,

c) Reactor size: A 4" diameter(10.16 cm) quartz bell jar,

(3) Deposition process variables(U_2):

a) Deposition time was not reported,

b) Substrates were polished by 0.5 μm diamond powder,

c) Substrate size=2 cm diameter,

d) substrate was water cooled only,

(B) Internal variables(X):

(1) Substrate temperature=850-1030°C(1123-1303°K),

(C) Figures of merit calculated for this review:

(1) Linear growth rate=3.5 μm/h,

(2) Deposition area=12.5 cm^2,

(3) Weight gain=15.4 mg/h,

(4) Specific yield=97 kW-h/g,

(5) Gas flow efficiency=0.42-1.28 mg/liter,

(6) Carbon conversion efficiency=16-48%.

2.5.4.2 UC-Berkeley Bell-jar Plasma-assisted CVD Reactor

A schematic diagram of a UC-Berkeley bell-jar MPACVD system is shown in Figure 2.16[47]-[50]. After the reactor chamber was evacuated to 30 mTorr[49], a mixture of CH_4 and H_2 gases with flow rates up to 100-300 sccm was fed into a 10.2 cm diameter quartz bell jar[48] via an annular gas feed system(not shown in Figure 2.16) in the circular metal baseplate. The mixture was then guided to the substrate by a short quartz tube, and was pumped out at the baseplate near the substrate holder. Microwave power entered the reaction chamber from the top and dissociated the gas mixtures. The substrate, which was a 25 mm diameter silicon wafer[49], was supported by a quartz sample holder at the position near the plasma ball. The dissociated species reacted on the substrate and formed the diamond film on its surface. The substrate temperature was measured from the back of the substrate by an infrared pyrometer.

Detailed experimental variables that were reported from Ref.[50] are:

(1) Controllable input variables(U_1):

a) Input power=560 W,

b) Gas mixture: 0.1% Vol. CH_4,

c) Total flow rate= approximately 300 sccm,

d) Deposition pressure=80 Torr,

(2) Reactor design variables(U_2):

a) Type of power source: a 2.45 GHz microwave power supply,

b) Reactor configuration is shown in Figure 2.16,

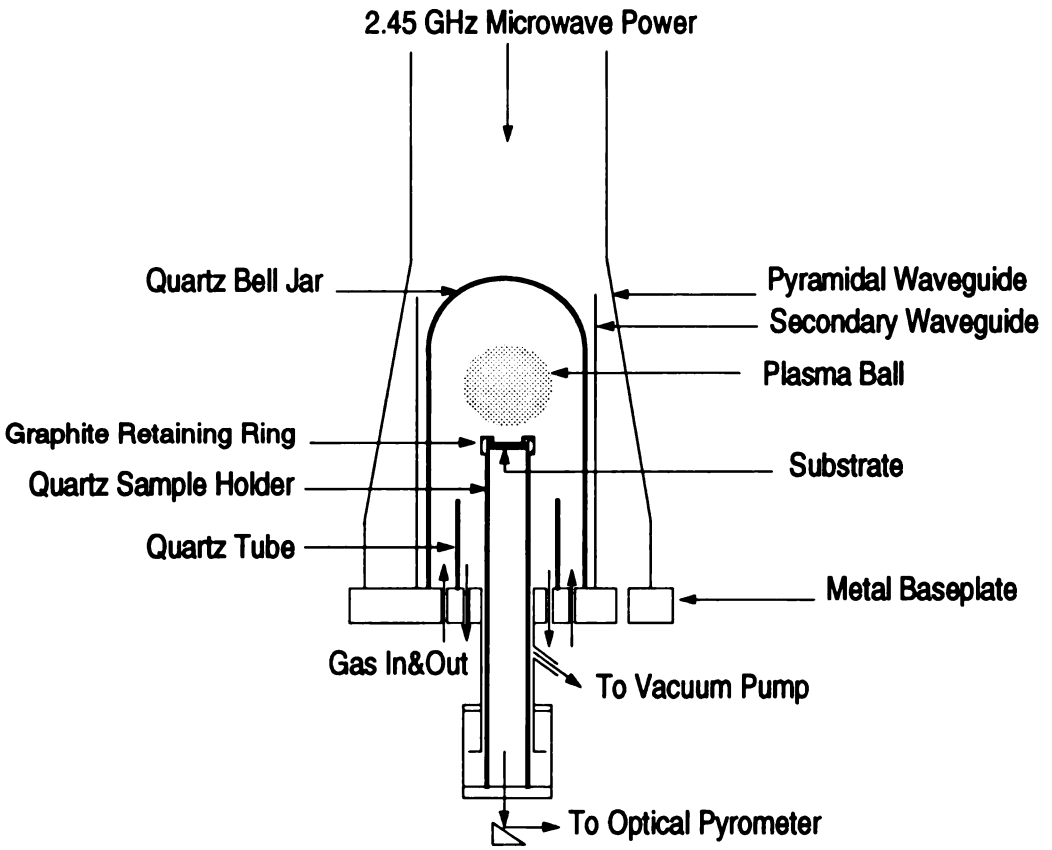

Figure 2.16 Schematic of the 4″ UC-Berkeley bell jar PACVD system[47]-[50].

c) Reactor size: A 10.2 cm diameter(4") quartz bell jar,

(3) Deposition process variables(U_2):

a) Deposition time =24 h,

b) Substrates were scratched with 1 μm diamond paste,

c) Substrate size=25 mm diameter,

(B) Internal variables(X):

(1) Substrate temperature=800-900°C(1073-1173°K),

(C) Figures of merit:

(1) Linear growth rate=0.02 μm/h,

(2) Deposition area=4.91 cm^2,

(3) Weight gain=0.034 mg/h,

(4) Specific yield=16470 kW-h/g,

(5) Gas flow efficiency=0.11 mg/liter,

(6) Carbon conversion efficiency=0.35%.

2.5.4.3 MSU Microwave Cavity Plasma Reactor (MCPR)

The schematic drawing of a microwave cavity plasma reactor (MCPR) developed at MSU in 1986-1991 is shown in Figure 2.17[9]. The microwave discharge was produced inside a quartz dome located at one end of a microwave cavity. After the chamber was evacuated to 1 mTorr, the reactive gases were introduced radially from the bottom of the cavity and flowed upward into and through the plasma. The gases then flowed out through a flow pattern regulator. The microwave energy was transmitted from a 2.45 GHz microwave generator through a rectangular waveguide into a 7″ cylindrical cavity via an end-feed probe. A 12 cm diameter hemisphere shaped plasma was created and stabilized by adjusting the length of the conduction probe and sliding short, i.e, L_p and L_s. A silicon substrate was placed on the flow pattern regulator. Thus the discharge was in direct contact with the substrate and also directly heated the substrate.

Detailed experimental variables that were reported or calculated from Ref.[51] are:

(1) Controllable input variables(U_1):

a) Input power=2.4 kW,

b) Gas mixture: 1.5%CH_4/H_2 (CH_4/H_2=6/400 sccm),

c) Total flow rate=406 sccm,

d) Deposition pressure=37 Torr (5 kPa),

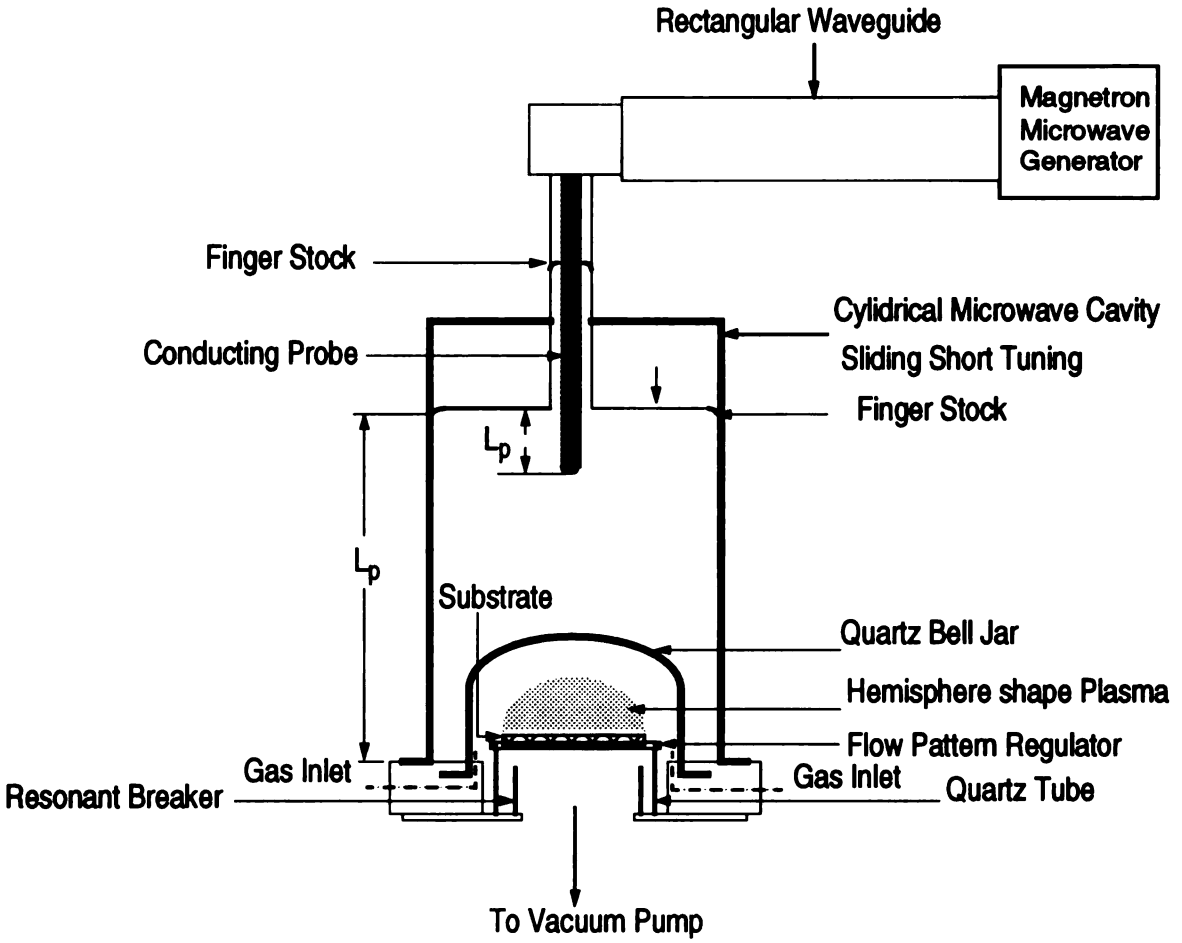

Figure 2.17 Schematic diagram of the moderate-pressure microwave cavity plasma reactor (MCPR)[9],[51].

(2) Reactor design variables(U_2):

a) Type of power source: a 2.45 GHz microwave power supply,

b) Reactor configuration is shown in Figure 2.17,

c) Reactor size: A 5″ diameter(12.7 cm) quartz bell jar,

(3) Deposition process variables(U_2):

a) Deposition time=8 h,

b) Substrates were seeded by 0.1 μm diamond powder/photoresist solution(detailed see Ref.[51])

c) Substrate size=3″ diameter (7.62 cm) diameter,

d) substrate was thermally isolated and no substrate bias was applied,

(B) Internal variables(X):

(1) Substrate temperature=1000°C(1273°K),

(C) Figures of merit calculated for this review:

(1) Linear growth rate=0.66 μm/h,

(2) Deposition area=45.60 cm^2,

(3) Weight gain= 10.56 mg/h,

(4) Specific yield=227 kW-h/g,

(5) Gas flow efficiency=0.43 mg/liter,

(6) Carbon conversion efficiency=2.19%.

2.5.5 Surface-wave Microwave PACVD reactor

A schematic diagram of a surface-wave microwave PACVD reactor is displayed in Figure 2.18[52]-[54]. After the chamber was evacuated to 10^{-6} Torr, mixtures of CH_4 and H_2 gases were fed into a fused silica vessel from the top of the reactor. The microwave energy was transmitted from a 2.45 GHz microwave generator through a waveguide surfatron into the fused silica vessel. A plasma was created and stabilized by adjusting the coaxial tuning stub and waveguide tuning stubs in the waveguide surfatron. A silicon substrate was placed on a molybdenum holder, which contained a tungsten filament heater.

Detailed experimental variables that were reported from Ref.[54] are:

(1) Controllable input variables(U_1):

a) Input power=1.15 kW,

b) Gas mixture:0.75%CH_4,

c) Total flow rate=100 sccm,

d) Deposition pressure=15 Torr (2 kPa),

(2) Reactor design variables(U_2):

a) Type of power source: a 2.45 GHz microwave power,

b) Reactor configuration is shown in Figure 2.18,

c) Reactor size=25 mm i.d quartz tube,

(3) Deposition process variables(U_2):

a) Deposition time=2h[53],

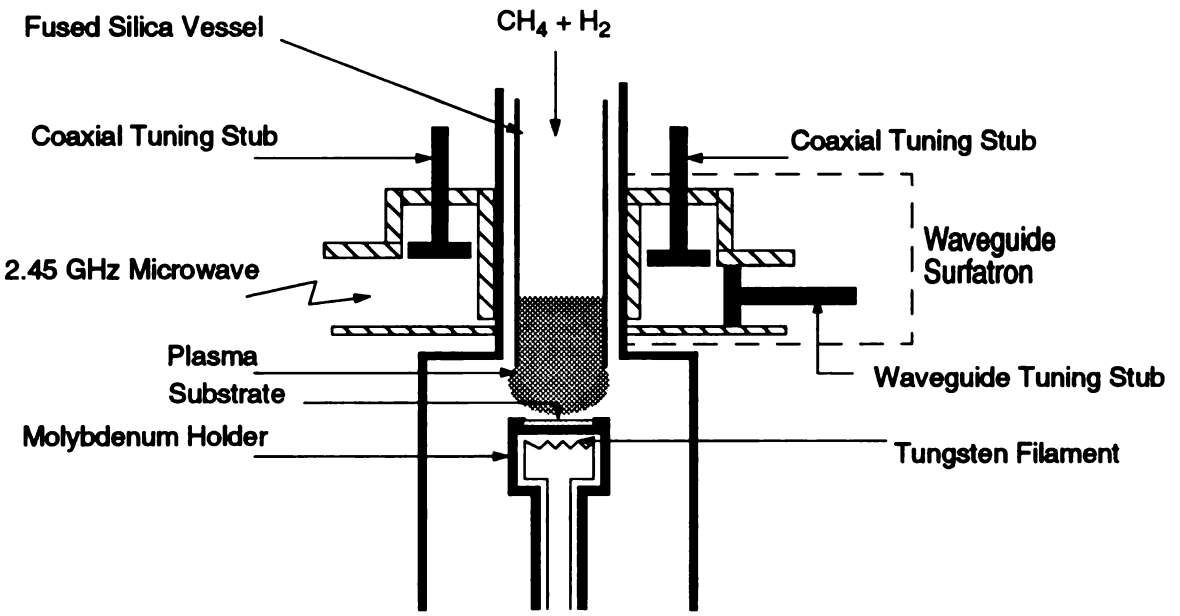

Figure 2.18 Schematic illustration of a surface-wave microwave PACVD apparatus[52]-[54].

b) Substrates were pretreated by 20-40 μm diamond powder in an ultrasonic methanol bath for 60 min, followed by cleaning with methanol,

c) Substrate size=2 cm in diameter,

d) substrate was heated by an external tungsten heater,

(B) Internal variables(X):

(1) Substrate temperature=950°C(1223°K),

(C) Figures of merit calculated for this review:

(1) Linear growth rate=0.4-0.6 μm/h,

(2) Deposition area= 3.14 cm^2,

(3) Weight gain=0.4-0.6 mg/h,

(4) Specific yield=2445 kW-h/g,

(5) Gas flow efficiency=0.08 mg/Liter,

(6) Carbon conversion efficiency=1.95.

2.6 Summary

The performance "figures of merit" of diamond film deposition reactors described in Section 2.4 and 2.5 are summarized in Table 2.1, Figure 2.19, and Figure 2.20. Table 2.1 lists the "figures of merit" of various diamond film deposition reactors. Figure 2.19 shows the relationships between linear growth rate (μm/h), area power density (defined as input power divided by deposition area, kW/cm^2), and specific yield (kW-h/Ct) of the diamond film deposition reactors. Note that performance data from all reactors except the microwave reactors are denoted by empty circles. Data from microwave diamond film deposition reactors are denoted by solid circles.

All of the diamond film synthesis techniques that have been reviewed in this chapter have the following aspects in common:

(1) Deposition rates increase as area power density increases. As shown in Figure 2.19, the conventional DC arcjet reactor(②), the atmosphere DC arcjet reactor(④), the RF thermal plasma torch(⑦), and the microwave plasma jet (⑩) employ high area power densities to produce high film growth rates.

(2) Figure 2.20 shows the relationship between the linear growth rate and deposition pressure. Deposition rates increase as deposition pressure increases. As shown, in the low-pressure nonequilibrium discharge regime (<80 Torr), linear growth rates are less than 3 μm/h. When the reactors operated in the high-pressure thermal discharge regime (>200 Torr) such as ⑦, ②, ④, ⑤, ⑩, growth rates are above 10 μm/h.

(3) Bell jar microwave plasma reactors described in Section 2.5.4

have better gas utilization efficiency of depositing diamond films than other plasma reactors.

(4) The carbon source in the reactive gases is less than 10% by the volume diluted in hydrogen,

(5) The substrate temperatures for synthesis of high quality diamond films are between 300-1100^{o}C.

(6) The best energy efficiency expressed in terms of energy/weight gain approaches 10 kW-h/Ct. Assuming an energy cost of ten cents per kW-h, the electrical energy costs approach one dollar/Ct. Using the data displayed in Figure 2.19 and Figure 2.20, this cost can be achieved by both low-pressure and high-pressure diamond film deposition reactors.

Table 2.1 Summary of "figures of merit"

Figures of Merits / Reactors	Linear Growth Rate (μm/h)	Total Growth Rate (mg/h)	Deposition Area (cm^2)	Specific Yield (kW-h/g)	Gas Flow Efficiency (mg/liter)	Carbon Conversion Efficinecy (%)
Conventional HFCVD[20]	1-4 μm/h	0.008-0.03 mg/h	0.0225 cm^2	N/A	$3x10^{-3}$ mg/liter	~0.08%
Electron-assisted HFCVD[22]	0.5-3.0 μm/h	0.35-2.1 mg/h	2 cm^2	571-3428	0.058-0.35 mg/liter	0.54-1.31%
Conventional DC Plasma[24]	20 μm/h	1.76 mg/h	0.25 cm^2	1784 kW-h/g	0.29 mg/liter	2.73%
Enclosed DC arc jet[26]	0.6-3.6 μm/h	2-12 mg/h	9.5 cm^2	250-1500	0.01-0.0017 mg/liter	0.06-0.12%
Atmospheric DC Arc jet[27]	10-30 μm/h	2.67-13.37 mg/h	1.27 cm^2	7479	$9.47x10^{-5}$ $4.74x10^{-4}$ mg/liter	0.018-0.089%
Atmospheric Combustion Flame[29]	10-15 μm/h	2.49-3.74 mg/h	0.71 cm^2	N/A	0.033-0.050 mg/liter	0.006-0.009%
Enclosed Flat Flame[32]	1 μm/h	6.88 mg/h	19.6 cm^2	N/A	0.012-0.056 mg/liter	0.0014-0.0057%
RF Thermal PACVD Torch[37]	30 μm/h	826.6 mg/h	78.5 cm^2	72.5 kW-h/g	0.134 mg/liter	3.21%
Magneto-microwave PACVD[39]	0.4-0.8 μm/h	0.69-1.38 mg/h	4.91 cm^2	217-434 kW-h/g	0.097-0.193 mg/liter	0.21-0.43%
Tubular Microwave PACVD[8]	0.8 μm/h	1.12 mg/h	4 cm^2	536 kW-h/g	0.059-0.092 mg/liter	0.97-1.24%
Microwave Plasma Jet[42]	6-12 μm/h	5.27-10.53 mg/h	2.5 cm^2	360-800 kW-h/g	0.002-0.004 mg/liter	0.018-0.109%
Astex Bell-Jar Micowave PACVD[45]	3.5 μm/h	15.4 mg/h	12.5 cm^2	97 kW-h/g	0.42-1.28 mg/liter	16-48%
UC-Berkery Microwave PACVD[50]	0.02 μm/h	0.034 mg/h	4.91 cm^2	16470 kW-h/g	0.11 mg/liter	0.35
MSU Moderate-Pressure MCPP[51]	0.55 μm/h	14.86 mg/h	81 cm^2	163 kW-h/g	0.61 mg/liter	2%-32%
MSU High-Pressure MCPR[11]	6.27 μm/h	44.68 mg/h	20.27 cm^2	69 kW-h/g	1.2 mg/liter	7.7%
Surface-wave PACVD[54]	0.4-0.6 μm/h	0.4-0.6 mg/h	3.14 cm^2	2445 kW-h/g	0.08 mg/liter	1.95

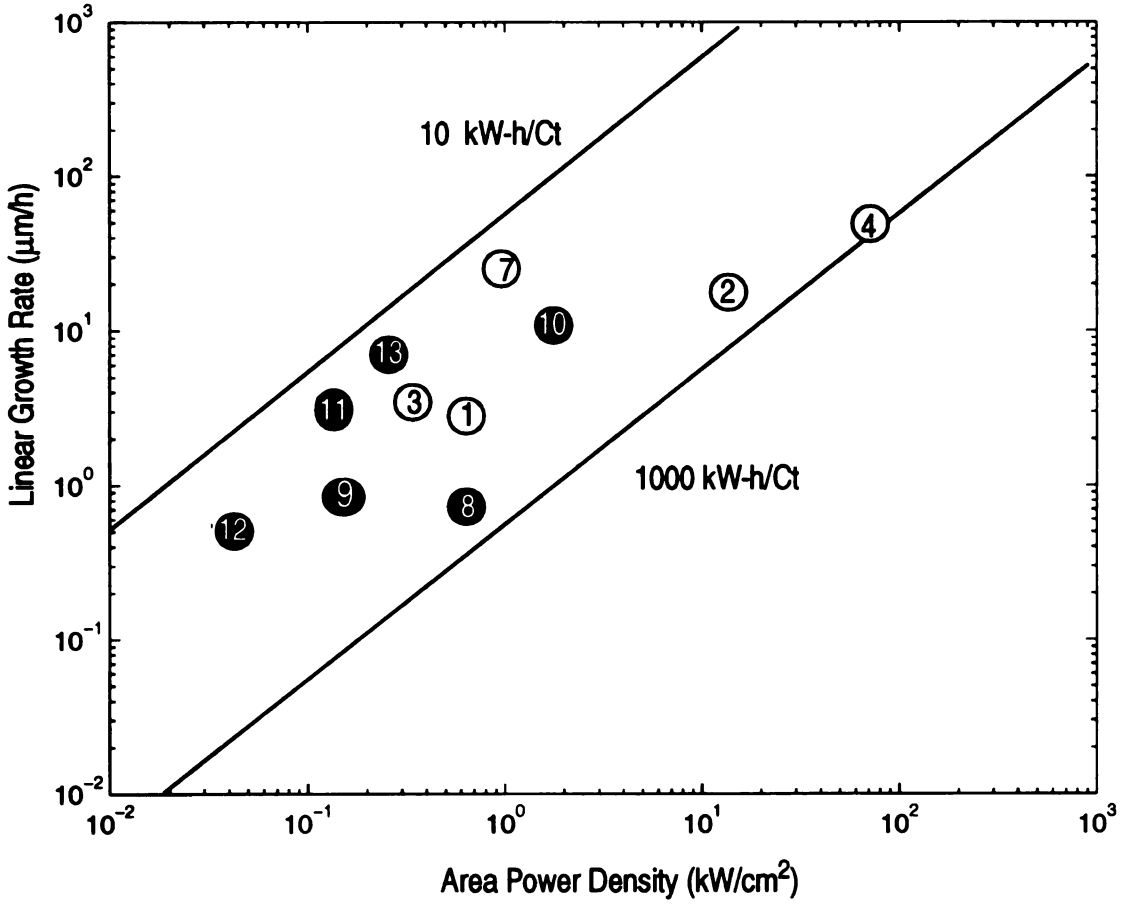

LEGEND

1.HFCVD[22]
2.Conventional DC CVD[24]
3.Enclosed DC Arcjet CVD[26]
4.Atmosphere DC Arcjet CVD[27]
7.RF Thermal Plasma Torch[37]
8.Magneto-microwave CVD[39]
9.Tubular Microwave CVD[8]
10.Microwave Plasma Jet CVD[42]
11.Astex Bell Jar Microwave CVD[45]
12.MSU Bell Jar Microwave CVD[51]
13.MSU Bell Jar Microwave CVD(High Pressure)[11]

Figure 2.19 Summary of linear growth rate vs. area power density for diamond film deposition reactors.

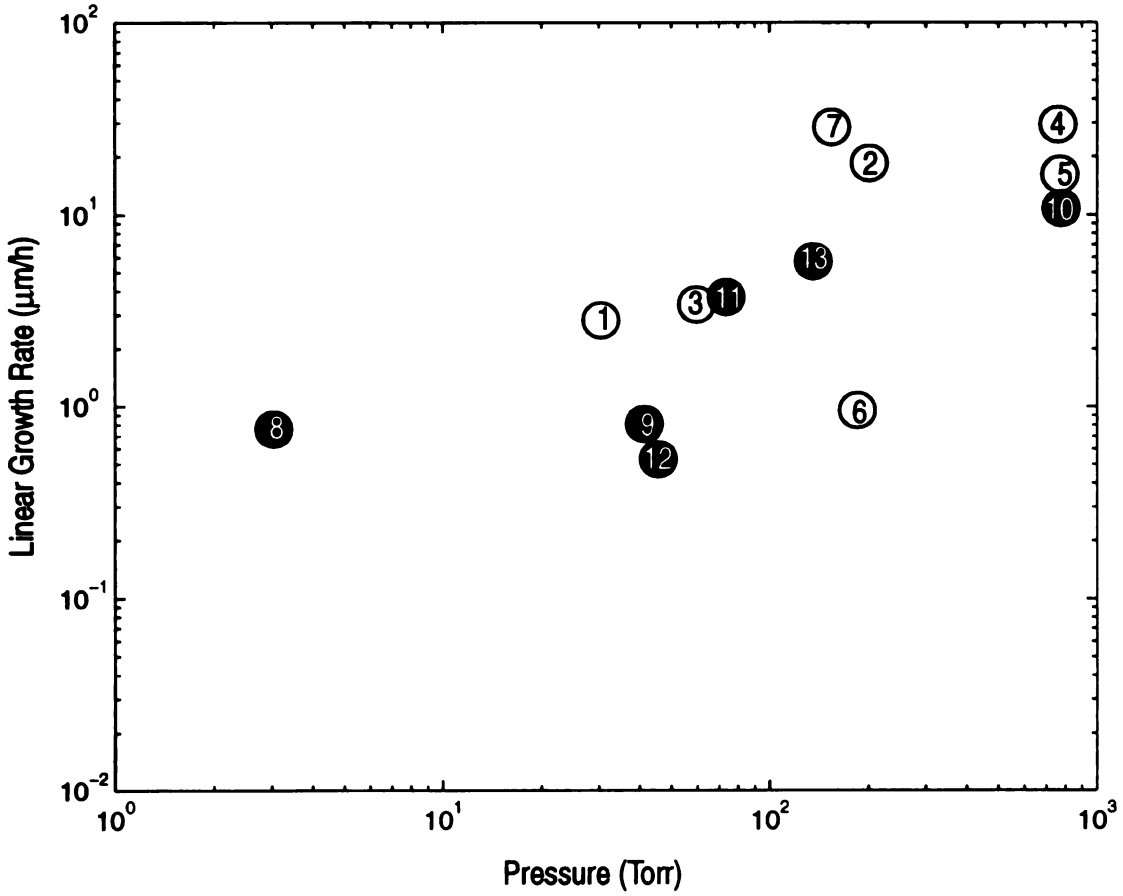

LEGEND

1.HFCVD[22]]
2.Conventional DC CVD[24]
3.Enclosed DC Arcjet CVD[26]
4.Atmosphere DC Arcjet CVD[27]
5.Atmosphere Combustion Flame[29]
6.Enclosed Combustion Flame[32]
7.RF Thermal Plasma Torch[37]
8.Magneto-microwave CVD[39]
9.Tubular Microwave CVD[8]
10.Microwave Plasma Jet CVD[42]
11.Astex Bell Jar Microwave CVD[45]
12.MSU Bell Jar Microwave CVD[51]
13.MSU Bell Jar Microwave CVD(High Pressure)[11

Figure 2.20 Summary of linear growth rate vs. pressure for diamond film deposition reactors.

CHAPTER 3

High-Pressure Microwave Cavity Plasma Reactor: Experimental Systems, Experimental Procedures, Experimental Parameter Space, Measurement Methodologies, and Reactor Configuration

3.1 Introduction

The objectives of this chapter were concerned with improving the moderate-pressure microwave cavity plasma reactor(MCPR) by extending its operation to higher pressures. Of particular importance was the objective of increasing the deposition rate and the energy efficiency of the microwave plasma reactors. In order to achieve these research objectives, the thermally floating MCPR reactor needed to be redesigned to operate at higher pressures (80-140 Torr) and higher input powers (2.5-4 kW). The redesigned reactor, identified here as high-pressure MCPR, includes a water-cooled substrate holder setup and a better air cooling system that is applied to cool the microwave cavity, bell jar, etc.

This chapter first presents the experimental systems that were employed in the experiments that are described in this chapter. The experimental systems consist of the microwave power supply and

waveguide/transmission systems, flow control and vacuum systems, and a computer monitor system. Then the common experimental procedures including the seeding procedure and start-up and shut-down procedures are described. The input and output parameter space that was used in the experiments presented in this thesis is also described. The design of water-cooled substrate holder setup which was needed in order to operate the reactor in high pressures is highlighted in the end of this chapter.

3.2 Experimental Systems

3.2.1 Introduction

The two microwave plasma diamond depositing reactors that are used in this thesis research, i.e., high-pressure MCPR (Chapter 3,4,5) and microwave plasma jet reactor (MPJR) (Chapter 6,7,8) use the same microwave power supply and waveguide/transmission system, vacuum pump and the gas flow control system, and computer monitor system. These systems are described below in Sections 3.2.2, 3.2.3, and 3.2.4.

3.2.2 Microwave power supply and waveguide/transmission system

Figure 3.1 schematically displays the microwave power supply and waveguide/transmission systems. The microwave power supply (1) consists of a magnetron (2), a circulator (3), and a dummy load (4). The waveguide/transmission systems consist of the rigid waveguides (5), a

dual-directional coupler (6), incident (7) and reflected (8) power meters, a flexible rectangular waveguide (9), and a rectangular waveguide to coaxial transition unit (10).

The microwave energy supplied by the magnetron (2), identified here as the incident power, P_{inc}, is propagated through a set of rectangular waveguides(5), (9), transmitted to a coaxial waveguide (11) by the transition unit (10), and coupled into the cavity applicator (12) through a mechanically tunable coaxial excitation probe (13). The excitation probe is located in the center of the sliding short (14) and the sliding short can be

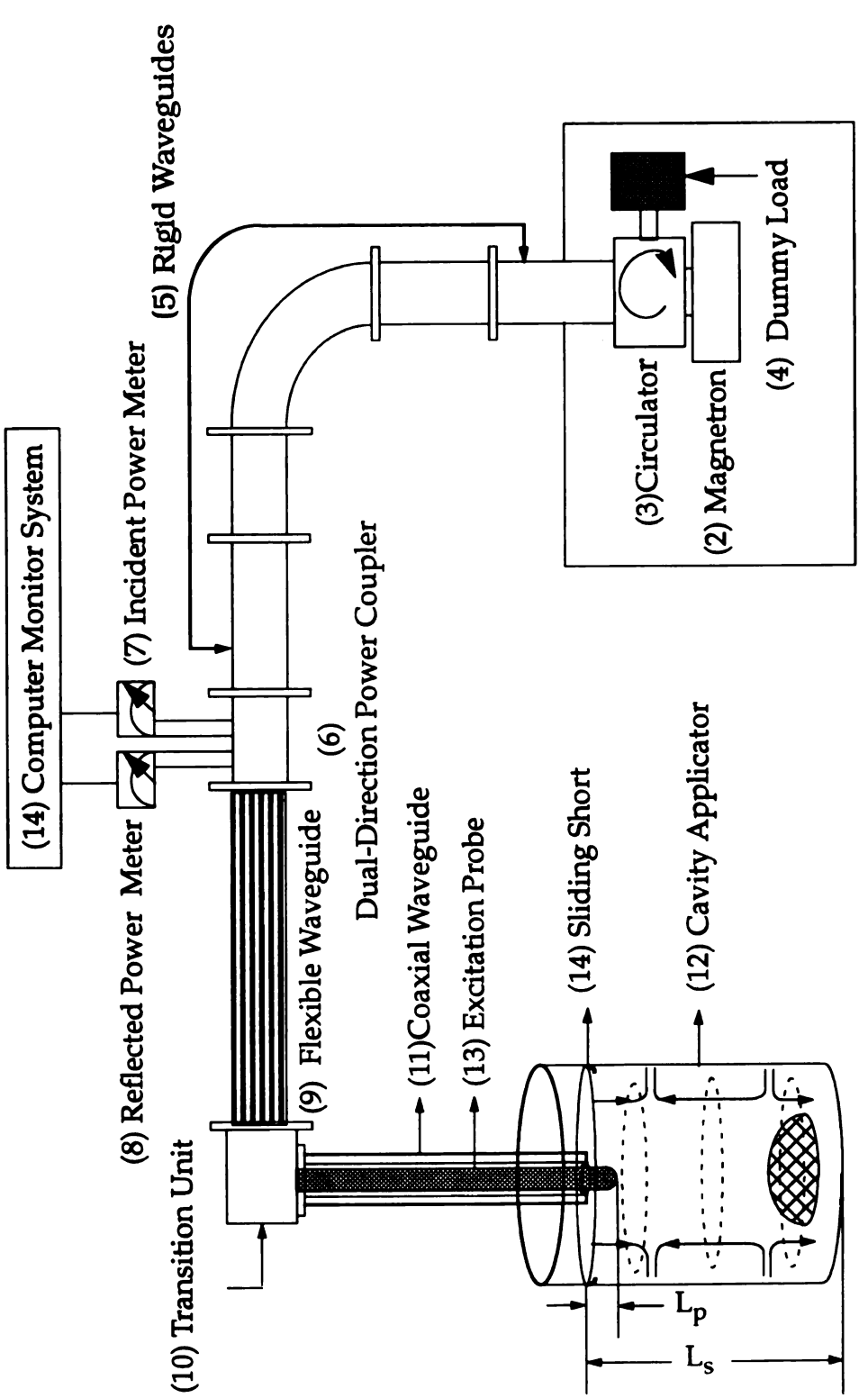

Figure 3.1 Microwave power supply and microwave waveguide/ transmission system for high-pressure MCPR and MJPR.

moved up and down along the reactor axis to control the applicator height, L_s. The depth of coaxial excitation probe, L_p, is also independently adjustable. In the case of any tuning mismatch, some of the incident power will be reflected back from the cavity applicator. This reflected power, P_{ref}, propagates through the dual-directional coupler (6) and is directed by the circulator (3) into the matched dummy load (4), where it is absorbed and dissipated as thermal energy. The power absorbed by discharge loaded applicator, P_t, is equal to the difference between the incident power and reflected power, i.e., $P_t = P_{inc} - P_{ref}$. The microwave power source is a Cober (Model No. S6F/4503), 2.45 GHz, 6 kW power source.

3.2.3 Flow Control and Vacuum Pump System

Figure 3.2 shows the schematic drawing of the flow control and vacuum systems. The source gases, which consist of CO_2 (1), H_2 (2), CO (3), and CH_4(4) of a respective purity of 99.9%, 99.999%, 99.9%, and 99.99%, are monitored by four MKS type 11159A mass flow controllers (5) along with a 4-channel MKS flow controller (6). The flow rates of source gases are set and displayed on this 4-channel MKS flow controller (6) by the system operator. The source gases with desired flow rates are mixed before they enter the baseplate (7). An ALCATEL 2033 type mechanical pump (12) is used to pump down the chamber pressure to ~5 mTorr, which is measured by a low pressure gauge (13). Operating pressure is set on the pressure controller (14) by the system operator and its value is

displayed on the high pressure gauge (10). A manual valve (11), which is normally open, is installed and can be used to manually control the

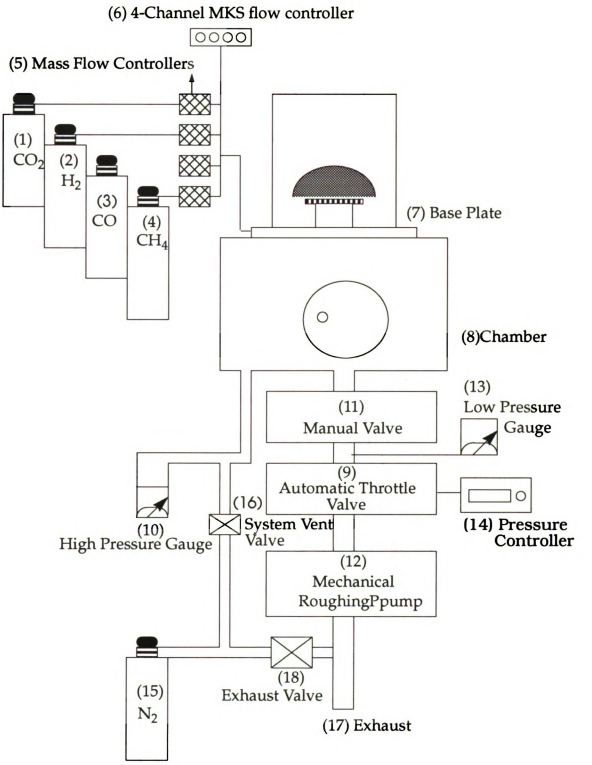

Figure 3.2 Flow control and vacuum system for high-pressure MCPR and MPJR.

pressure of the chamber if the automatic throttle valve fails. Nitrogen (15) is released at gas pressure of 10 psi through the system vent valve (16) to bring the chamber into the atmospheric pressure. It is also used to dilute the exhaust gases (17) through an exhaust valve (18). The mixing of nitrogen into the exhaust gas stream insures that the exhaust gases are below the flammable condition.

3.2.4 Computer Monitoring System

A computer monitoring system was used to observe and regulate the system operating conditions and control the shut down procedure in the experiments described in this thesis research. Figure 3.109 displays the flow chart of the computer monitoring program[9]. As shown, the experimental running time, reflected power upper limit, and the operating pressure threhold are first set in the computer. The experimental system is then enabled to allow the feed gases to flow and the microwave power to turn on. After the plasma is excited, a checking loop compares the pressure, reflected microwave power, and time with the preset values to determine the state of the experiment. An emergency shut down of the microwave power and feed gas is performed if the experimental running time, reflected power, and operating pressure are over the preset values at any time during the experiment. In the meantime, the automatic throttle valve is closed in order to isolate the vacuum pump from the process chamber. On the other hand, when the experiment is completed.

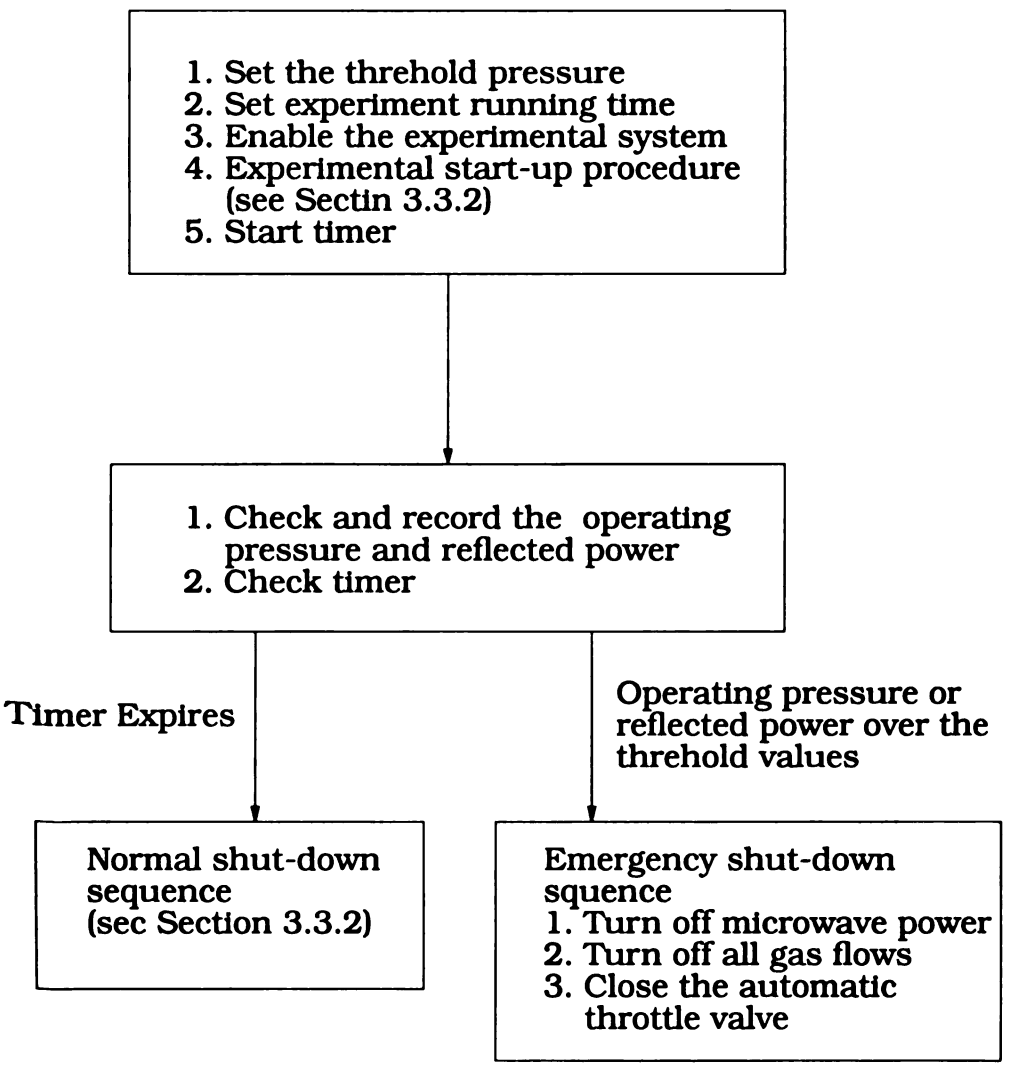

Figure 3.3 Flow chart of Computer monitor program[9].

the computer program directs the system into a normal shut-down sequence (see section 3.3.2).

3.3 Common Experimental Procedures

3.3.1 Seeding Procedure

A seeding procedure was performed on the substrate surface in preparation for the deposition experiments described in this dissertation. The diamond powder and photoresist were first mixed and then agitated in an ultrasonic bath. The resulting solution was then dropped over the entire substrate surface. The substrate was rapidly rotated in a spinner, resulting in the uniform seeding over the substrate surface. Using this photoresist seeding method, the diamond seeds were embedded more uniformly and the nucleation density was estimated to be $10^8 cm^{-2}$ [10],[51].

The recipe for the photoresist substrate seeding, which was routinely used in this research, is summarized as follows:

(1) bake 200 mg Amplex, 0.1μm diamond powder at 150°C for 30 minutes,

(2) pour 20 ml Shipley type A photo resist thinner into a 53 ml Shapely 1830 photo resist,

(3) mix 0.1 μm diamond powder in (1) with the solution in (2),

(4) ultrasonically agitate the mixture for 1 hour,

(5) drop the mixture onto the substrate surface with full coverage,

(6) spin the substrate at 4000 rpm for 40 seconds,

(7) bake the substrate at 150C for 15 minutes.

3.3.2 Start-up and Shut-down Procedures

After manually placing the substrate on the substrate holder and setting the cavity length (L_s~21 cm) and probe depth (L_p~3 cm), the reactor was pumped to 5 mTorr by a mechanical pump ((12) in Figure 3.2). Source gases with appropriate gas mixtures and flow rates were introduced into the reactor and then the chamber pressure was gradually increased. At chamber pressure of ~10 Torr, microwave power of 800 W was incident and ignited the discharge. The desired chamber pressures between 80-140 Torr were achieved in approximately five minutes by the value that was preset on the pressure controller ((14) in Figure 3.2.). Absorbed microwave power was adjusted between 3-4.5 kW so that the 2″ (5.08 cm) diameter substrate was covered with the discharge plasma. Substrate temperature was independently controlled between 700-1150^{o}C by varying the number of substrate discs (see Section 3.6.3.2 and 3.6.3.3). Methane and hydrogen were used as source gases and their flow rates were controlled by a 4-channel flow controller. During an actual deposition experiment, all the experimental input variables such as flow rate, deposition time, microwave power, etc. are monitored and recorded vs. running time by a computer (see Section 3.2.4). After the experiment

was completed, the experimental system was shut down with the procedures described below:

(1) automatically turn off CH_4, CO_2, and CO gas flow by shutting off the channels in gas flow controller,

(2) 3-minute self-cleaning process with H_2 plasma,

(3) automatically turn off microwave power,

(4) automatically turn off H_2 gas flow by shutting off the channel in gas flow controller,

(5) automatically evacuate the chamber by activating the throttle valve to the open position.

3.4 Experimental Parameter Space

3.4.1 Introduction

As mentioned in the literature review shown in Chapter 2, the output performance of a plasma diamond deposition reactor is a complex function of many experimental variables. Thus in a well understood and repeatable experimental system each of these experimental variables are identified and controlled. The reactor block diagram shown in Fig.2.2 arranges the reactor variables into three basic groups: (1) input variables, **U**, (2) the internal variables, **X**, and (3) the output variables, **Y**. Using the definitions of each variable group, as described in Chapter 2, a block diagram for the high-pressure MCPR diamond deposition reactor is dis-

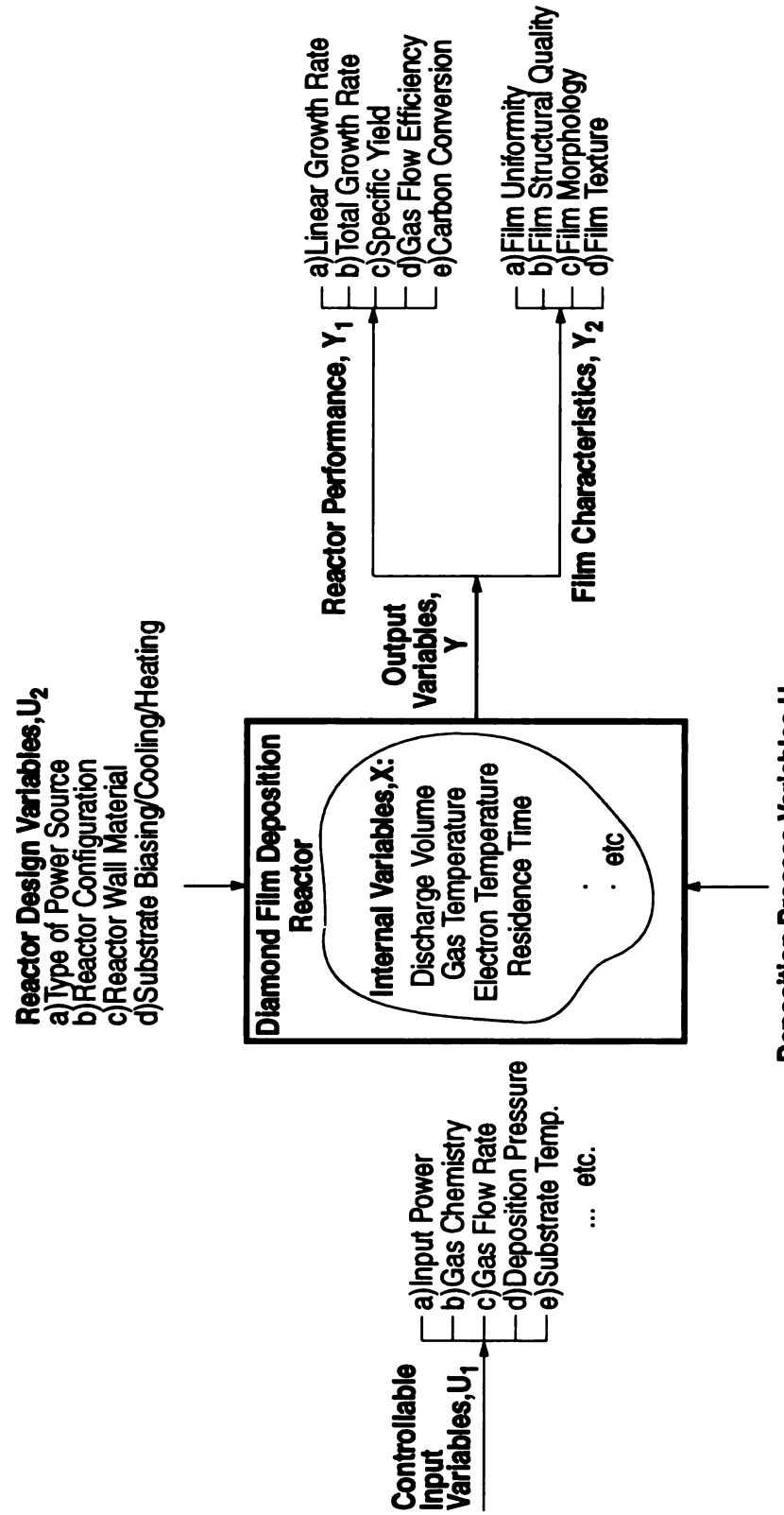

Figure 3.4 Multivariables for the high-presure MCPR a diamond film deposition reactor.

played in Figure 3.4. The detailed descriptions of each group are discussed in the sections below.

3.4.2 Independent Input Experimental Variables

Figure 3.4 shows a general block diagram of the experimental variables for a high-pressure MPCR CVD diamond deposition reactor. Table 3.1 identifies the range of experimental deposition variables chosen for this experimental investigation. The independent controllable input variables, $\mathbf{U_1}$, are substrate temperature T_s, pressure p, incident microwave power P_{inc}, gas chemistry c (expressed in $\%CH_4/H_2$)and total gas flow rate f_t. Their respective ranges varied from 700-1150C, 80-140 Torr, 3-5 kW, 1-8$\%CH_4/H_2$ and 100-1400 sccm. Reactor geometry variables, $\mathbf{U_2}$, were fixed except for the change in the substrate holders which allowed the substrate temperature to be independently varied. Deposition process variables, $\mathbf{U_3}$, include substrate size and material, seeding procedure and deposition time. Deposition time was varied from 4h to 100h. Undoped (100) 2″ diameter silicon wafers were used as substrates for all the experiments presented in this thesis. The substrates are seeded with a 0.1 μm diamond powder-photoresist solution as described in Section 3.3.1.

Table 3.1 Definition of the experimental variables for the high-pressure MCPR.

Input Variable, **U**	Controllable Input Variables, $\mathbf{U_1}$	a) Deposition Pressure, Variable: p=80-150Torr b) Absorbed Microwave Power, Variable: P_t=2.5-4.5kw c) Gas Chemistry, Variable: c=1-8% CH_4/H_2 d) Substrate Temperature, Variable: T_s=700-1150C e) Total Flow Rate, Variable: f_t=100-1400 sccm
	Reactor Geometry Variables, $\mathbf{U_2}$	a) Reactor Configuration, Variable: Substrate Holder Setups b) End-feed Excitation, Fixed c) Electromagnetic Mode and Cavity Tuning, Fixed at TM_{013} d) Quartz Dome Geometry, Fixed
	Deposition Process Variables, $\mathbf{U_3}$	a) Substrate Material and Size, Fixed: 2" dia. Silicon b) Substrate Seeding Procedure, Fixed: Seeded by a Spinner with 0.1μm Diamond Powder-Photoresist Solution c) Deposition Time, Variable: t=4-100 Hours
Internal Variable, **X**		a) Plasma Volume, V_d, Approximately Constant at $144cm^3$ b) Absorbed Power Density, Variable: $<P_V>=P_t/V_d$
Output Variable, **Y**	Reactor Performance, $\mathbf{Y_1}$:	a) Linear Growth Rate: 4-7 μm/h b) Total Growth Rate: 27-50 mg/h c) Specific Yield: 69-300 kw-h/g d) Gas Flow Efficiency: 0.6-1.2 mg/liter e) Carbon Conversion Efficiency: 1-12%
	Film Characteristics, $\mathbf{Y_2}$:	a) Film Uniformity: 10% or better over 2" dia. area b) Film Structural Quality: FWHM=3-8 cm^{-1} c) Film Morphology: mostly (111) morphology d) Film Texture: mostly <110> texture

3.4.3 Dependent Internal Experimental Variables

The experimentally measured internal variables, **X**, in the high-pressure MCPR were (1) the power absorbed by the reactor, P_t, (2) the plasma volume, V_d, and (3) the absorbed power density, $\langle P \rangle = P_t/V_d$. The power absorbed by the reactor P_t, is defined as the difference between the incident microwave power P_{inc} and the reflected power P_{ref}, i.e. $P_t = P_{inc} - P_{ref}$. The plasma volume V_d was always adjusted so that the hemispherical discharge covered the substrate and produced good deposition uniformity. As the pressure varied from run to run the absorbed power was adjusted to produce a discharge that covered the substrate. Thus the discharge volume was approximately constant at 144 cm^3 for all experiments and P_t and $\langle P \rangle$ increased with pressure.

3.4.4 External Output Experimental Variables

As shown in Figure 3.4, the reactor output variables (**Y**) in the high-pressure MCPR are defined as reactor performance variables ($\mathbf{Y_1}$) and film characteristic variables ($\mathbf{Y_2}$). The reactor performance variables contain film linear growth rate, film total growth rate, specific yield, gas flow efficiency, carbon conversion efficiency. The film characteristic variables include film uniformity, film structural quality, film morphology, and film texture. Each of the reactor performance variables has been defined in Chapter 2 (see page 16-18). The techniques of measuring the film

characteristic variables are described in the next section.

3.5 Measurement of Experimental Output Variables

3.5.1 Measurement of Film Characteristics

3.5.1.1 Measurement of Film Uniformity

Film uniformity was determined by (1) breaking the wafer and measuring the thickness vs. position by a SEM, or (2) for thick films by directly measuring the thickness of free standing films with micrometer. Percent uniformity is defined by the difference between the maximum and minimum thickness measurements divided by the average thickness measurement over the 5 cm diameter substrate.

3.5.1.2 Measurement of Film Structural Quality

The Raman Spectroscopy equipment was developed by Mossbrucker *et.al.*[67] at MSU. In the system, the Raman spectra were excited with the 514 nm line of a green Ar^+ laser with an output power of 600 mWatt. A 60X optical objective lens that illuminated a spot with a diameter of 30 μm was used for all the Raman spectra reported here.

In the later chapters, the full width at half of its height maximum (FWHM) of Raman spectra for the diamond peak at 1332 cm^{-1} will be used as an indication of the structural quality of diamond films. Since the laser

has a non-zero, small but finite band width, the corrected FWHM will be broadened by the following equation[67],[68]:

$$M = \sqrt{F_{Sample}^{2} + F_{Mono}^{2} + F_{Laser}^{2}},$$

where M = Corrected FWHM measurement,

F_{Sample} = Measured FWHM of the sample,

F_{Mono} = FWHM of the monochromator,

F_{Laser} = FWHM of the laser.

3.5.1.3 Measurement of Film Texture

X-ray diffraction (XRD) measurement of films with film thickness greater than 5 μm[69] provide an indication of growth orientation in the crystalline films[70]. The location of XRD peaks and their relative intensities in a powder pattern is shown in Table 3.2. Generally, the diffractometer for XRD spectra reported in this dissertation use a stop size of 0.1^{o} and a 3 second integration. The growth orientation ratio utilized in the later chapters is defined by the ratio of [220] peak height to [111] peak height, i.e., I[220]/I[111]. Since the powder pattern intensity of [111] peak is dominant over other XRD peaks (note that the powder is spread randomly on the detecting stage), a growth orientation ratio << 1 indicates little orientation in that crystallographic direction while a ratio >> 1 shows significant orientation of these crystal grains in the film[22].

Table 3.2 Location of XRD peaks and their relative intensity in a powder pattern.

XRD peak	2θ Position	Powder Pattern Intensity
[111]	43.9°	100%
[220]	75.3°	25%
[311]	91.5°	16%
[400]	119.5°	8%
[331]	140.6°	16%

3.5.1.4 Measurement of Film Morphology

Since Scanning Electron Microscopy (SEM) is a well known technique that has higher resolution, as well as a wider and higher magnification range than light microscopy[71], it has been utilized for identifying the surface morphology and thickness of the diamond films reported in this dissertation.

In order to get a good SEM photo, the diamond film sample was required to be (1) devoid of solvents, water, or grease that may vaporize in the vacuum, (2) firmly mounted on the specimen stage, and (3) electrically conductive. Using these techniques, a typical SEM image that resulted from the JEOL 6400 SEM at MSU is shown in Figure 3.5. The terminology of surface morphologies used in this dissertation is also defined in Figure 3.5[72],[73].

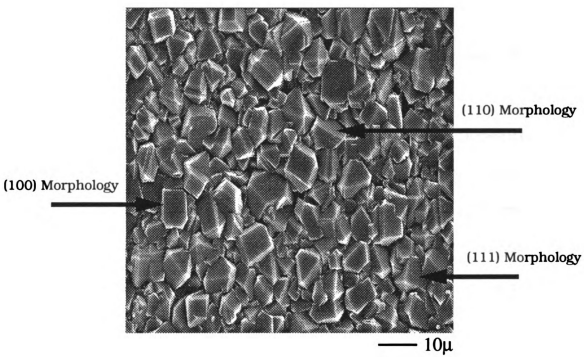

Figure 3.5 A typical SEM photo from JEOL 6400 at MSU.

3.5.2 Calculation of Reactor Performance

3.5.2.1 Measurement of Film Growth Rate

Film total growth rate, W in mg/h was determined by measuring the total weight gain of the substrate, W_t, during an experimental run and dividing this gain by the deposition time t. The average linear growth rate(μm/h), d, was determined from $d = \frac{W}{A \cdot D}$, where W is the weight gain per hour, A is the deposition area, D is the diamond density of 3.51 g/ cm^3[14].

As an example, the linear growth rate for the high-pressure MCPR is calculated here. As shown in Table 2.1, the total growth rate for the high-pressure MCPR is measured to be 44.86 mg/h over 2" diameter silicon substrate (with experimental conditions of CH_4/H_2=18/600 sccm and absorbed microwave power of 3.1 kW). Then the linear growth rate is:

$$\text{linear growth rate } (\mu m/h) = \frac{44.68 \ \frac{mg}{h} \times \frac{10^4 \mu m}{cm}}{20.27 cm^2 \times 3.51 \frac{g}{cm^3} \times \frac{10^3 mg}{g}}$$

$$= 6.27 \ \mu m/h.$$

3.5.2.2 Measurement of Specific Yield

Specific Yield (kW-h/g) is defined as the power input (kW) per diamond film total growth rate in the units of g/h[9]. Using the same exam-

ple that is described in the section above, the total growth rate in the high-pressure MCPR is 44.86 mg/h over 2″ diameter silicon substrate, then the specific yield is:

$$\text{specific yield (kW-h/g)} = \frac{3.1\text{kW}}{44.68\ \frac{\text{mg}}{\text{h}} \times \frac{\text{g}}{10^3\text{mg}}}$$

$$=69\ \text{kW-h/g.}$$

3.5.2.3 Measurement of Gas Efficiency

Gas Efficiency (mg/liter) is defined as the total growth rate (mg/min) divided by total flow rate (liter/min). The total flow rate is defined as the sum of all input gas flow rates[9]. Using the same example that is described in the section above, i.e. the total growth rate in the high-pressure MCPR is 44.86 mg/h over 2″ diameter silicon substrate, then the gas efficiency is:

$$\text{gas efficiency (mg/liter)} = \frac{44.68\ \frac{\text{mg}}{\text{h}}}{618\frac{\text{cc}}{\text{min}} \times \frac{1}{10^{-3}\text{liter}} \times \frac{60\text{min}}{\text{h}}}$$

$$=1.2\ \text{mg/liter.}$$

3.5.2.4 Measurement of Carbon Conversion Efficiency

Carbon Conversion Efficiency is defined as the percentage of carbon atoms in the input gases which are converted into dia-

mond[9],[16],[17]. If the total growth rate in the high-pressure MCPR is 44.86 mg/h over 2″ diameter silicon substrate, then the carbon conversion efficiency is:

carbon conversion efficiency (%)

$$= \frac{44.68\ \frac{mg}{h} \times \frac{g}{10^3 mg} \times \frac{1h}{60min} \times \frac{mole}{12g} \times \frac{6.02 \times 10^{23} atom}{mole}}{18\frac{cc}{min} \times \frac{liter}{10^3 cc} \times \frac{mole}{22.4liter} \times \frac{6.02 \times 10^{23} atom}{mole}} \times 100\%$$

=7.7%.

3.6 Design of High-Pressure MCPR

3.6.1 Introduction

As mentioned in Section 3.1, the objectives of this chapter research were to increase the deposition rate and energy efficiency of the thermally floating MCPR that was developed by Zhang[9]. In order to achieve these objectives, the reactor has to be operated in a higher pressure, higher power density regime (see Figure 2.19 and Figure 2.20). However, when the reactor was operated in this regime, the temperature of the substrate increases above 1150°C where diamond deposition does not take place and the reactor components such as quartz bell jar, microwave cavity, etc., became overheated. A reactor operating field map for the thermally floating reactor, which was developed by Zhang[9] and Khatami [51],

shows that as the operating pressure and absorbed microwave power increase, the substrate temperature also increases.

As shown in Figure 3.6, the substrate temperature reaches 1000°C at pressure of 56 Torr. Thus the addition of a water cooling stage and a better air cooling system became necessary when the operation of thermally floating MCPR is extended to higher pressures. This section begins with the description of the original MCPR that was developed by J. Zhang[9]. Then the design of the water cooling stage setups and the air cooling system that were developed and employed during the course of this thesis research is described.

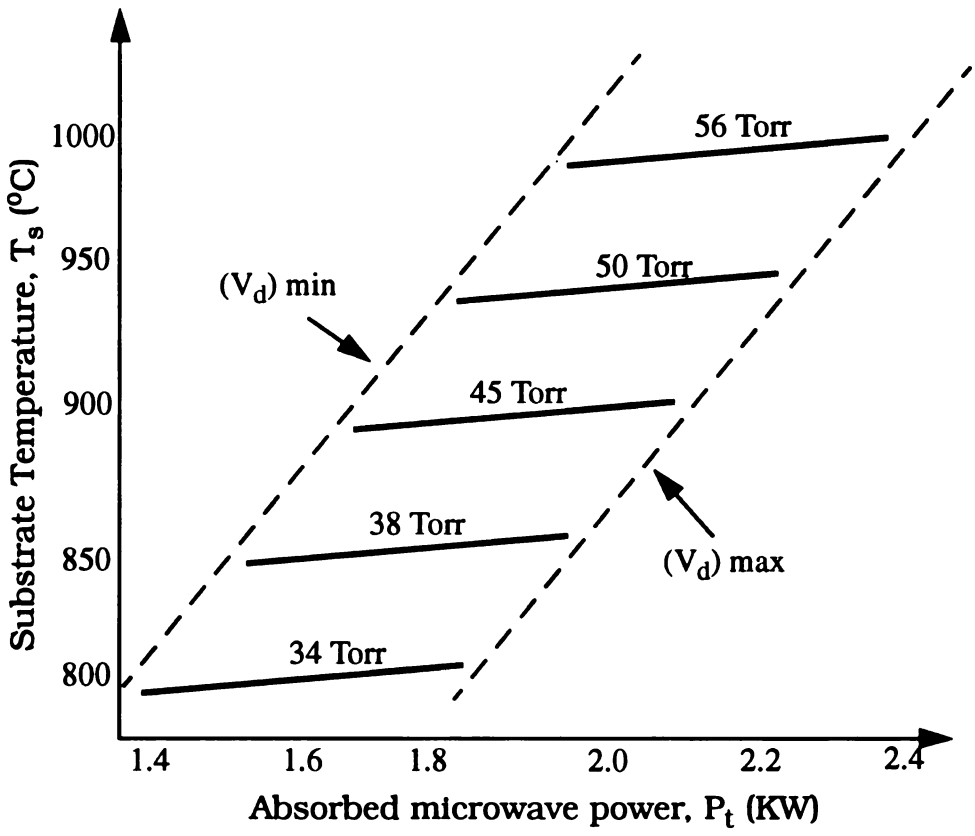

Figure 3.6 Reactor operating field map under thermally floating configuration For 5" quartz dome/3" substrate reactor configuration[51].

3.6.2 Operation of The Thermally Floating MCPR

3.6.2.1 Operation of Microwave Cavity Excitation and Tuning

A cross sectional view of the thermally floating MCPR is shown in Figure 3.7. As shown, the applicator side wall(1) consists of a 17.8 cm inside diameter cylindrical brass tube. This brass tube is electrically connected to a water-cooled baseplate assembly(2-4) and a water cooled sliding short(11) via finger stock(12). Thus the cylindrical volume bounded by the sliding short, the side walls and the baseplate forms the cylindrical cavity applicator electromagnetic excitation region. As shown, 2.45 GHz (CW) microwave power is coupled into the cylindrical cavity applicator through a mechanically tunable coaxial excitation probe(13) located in the center of the sliding short. The sliding short can be moved up and down along the reactor axis to control the applicator height, L_s, and the depth of coaxial excitation probe, L_p, is also independently adjustable. Thus by changing the probe depth and the cavity height, the applicator can be excited and matched to the desirable electromagnetic resonance.

3.6.2.2 Operation of Air Cooling System

The only air cooling system that was used in the thermal floating MCPR consists of a air blower with 60 CFM (cubic foot per minute). As

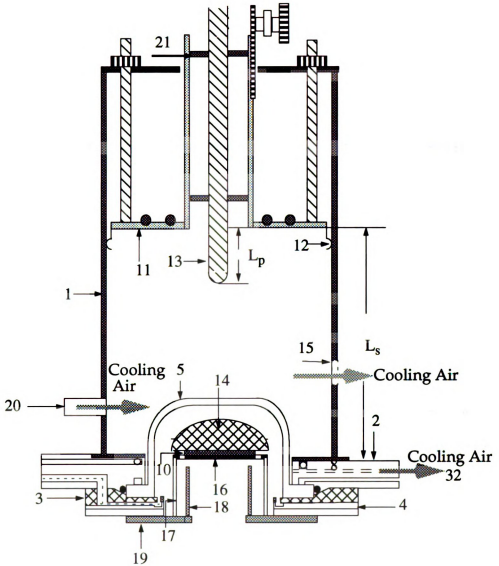

Legend

(1)	Cavity Side Wall	(2)	Baseplate	(3)	Annular Plate
(4)	Distribution Plate	(5)	Quartz Dome	(10)	Substrate
(11)	Sliding Short	(12)	Finger Stock	(13)	Excitation Probe
(14)	Plasma Discharge	(15)	View Window	(16)	Flow Pattern
(17)	Quartz Tube	(18)	Metal Tube	(19)	Metal Plate
(20)	Air Blower Inlet	(21)	Teflon Pieces	(32)	Laser Ports

Figure 3.7 The cross sectional view of the thermally floating MCPR system.

shown in Figure 3.7, this air blower forms an air cooling stream by blowing the cooling air from the air blower inlet (20), onto the bell jar (5) and cavity side walls (1), and finally flows out of the cavity through the view window (15) and two pairs of laser diagnostic ports (32).

3.6.2.3 Operation of Thermally Floating Substrate Holder Setup

The baseplate assembly consists of a water-cooled and air-cooled baseplate(2), an annular input gas feed plate(3), a gas distribution plate(4), a 12.5cm i.d. quartz dome(5), the thermally floating substrate holder setup assembly (16-19), and the substrate itself (10). The baseplate, the annular gas plate, and the gas distribution plate introduce an uniform ring of input gas into the quartz dome volume. A hemisphere shaped discharge(14) is positioned over and is adjusted to be in direct contact with the top of the substrate surface by varying L_p and L_s to excite and match the TM_{013} plasma-loaded resonant mode. The discharge can be viewed through the screened side window(15) and the substrate temperature is measured by focusing an optical pyrometer through the screened side window(15). The substrate (10) is placed on top of a flow pattern regulator (16) which is supported by a quartz tube (17). Quartz tubes of different heights may be used to change the position of the substrate with respect to the plasma. A metal tube (18) which serves as a conductive tube is placed inside the quartz tube (17) and prevents the plasma discharge from forming underneath the substrate by reducing the

the substrate by reducing the electric field underneath the substrate. The metal tube (18) and quartz tube (17) are placed on a metal plate (19) which has 30 mm diameter hole in its center to pass the hot gases from with the quartz dome (5) to the pump.

3.6.3 Operation of The High-Pressure MCPR

3.6.3.1 Introduction

This section first presents the change in the air cooling system that was used to cool the microwave cavity and bell jar. Then the design of the water-cooled substrate holder setup that replaced the thermally floating substrate holder setup in the MCPR (described in section above) is described. Since the high-pressure MCPR, which is shown in Figure 3.8, used the same microwave cavity and microwave power deliver systems, the operation of microwave cavity excitation and tuning is referred to Section 3.6.2.1.

3.6.3.2 The Change In The Air Cooling System

In order to utilize the air blower existing inside the Cober microwave power supply and add another air cooling stream into the high-pressure MCPR, two Teflon pieces (as shown in (21) Figure 3.8) were drilled four of 1/8" diameter through holes. This change allows the cooling air (from the air blower in the microwave power supply, not shown in

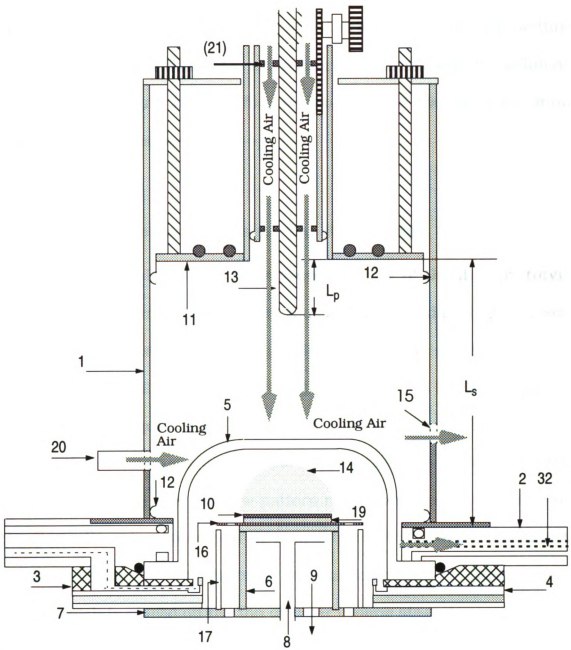

Legend

(1)	Cavity Side Wall	(2)	Baseplate	(3)	Annular Plate
(4)	Distribution Plate	(5)	Quartz Dome	(6)	Cooling Stage Wall
(10)	Substrate	(11)	Sliding Short	(12)	Finger Stock
(13)	Excitation Probe	(14)	Plasma Discharge	(15)	View Window
(16)	Flow Pattern Regulator	(17)	Quartz Tube	(19)	Insulation Disc Set
(20)	Air Blower Inlet	(21)	Teflon Pieces	(32)	Laser Ports

Figure 3.8 The cross sectional view of the high-pressure MCPR system.

Figure 3.8) to flow through the coaxial waveguide, onto the bell jar (5) and cavity side walls (1), and to flow out of the view window(15) and the three laser ports (32). This additional air cooling not only allowed the additional cooling of the quartz bell jar (5) but also provided cooling of the input coaxial waveguide system.

3.6.3.3 Substrate Cooling Stage - The First Design

Figure 3.9 shows the cross sectional view of the first prototype water-cooled substrate holder setup that was developed for high-pressure diamond film deposition in Michigan State University. As shown, a 2″ in diameter silicon substrate(Figure 3.9(a)) was placed on the 2″ in diameter graphite holder(Figure 3.9(b)). A boron nitride ring(Figure 3.9(c)) was used to keep the substrate at the center of the reactor. A set of insulating discs(Figure 3.9(d)), the gas flow pattern regulator(Figure 3.9(e)), and the 2″ tall, 3″ diameter water cooling stage(Figure 3.9(f)) were employed to control the substrate temperature. The gas flow pattern regulator(Figure 3.9(e)), which is placed on the top of water cooling stage, is an electrically conducting disc (made from either graphite or molybdenum) with a ring of holes circumferentially surrounding the substrate holding recess. Substrate temperature could be independently controlled by placing different layers of either graphite or boron nitride insulation disks(Figure 3.9(d) between the gas flow pattern regulator(Figure 3.9(e)) and the 2″ diameter graphite holder(Figure 3.9(b)).

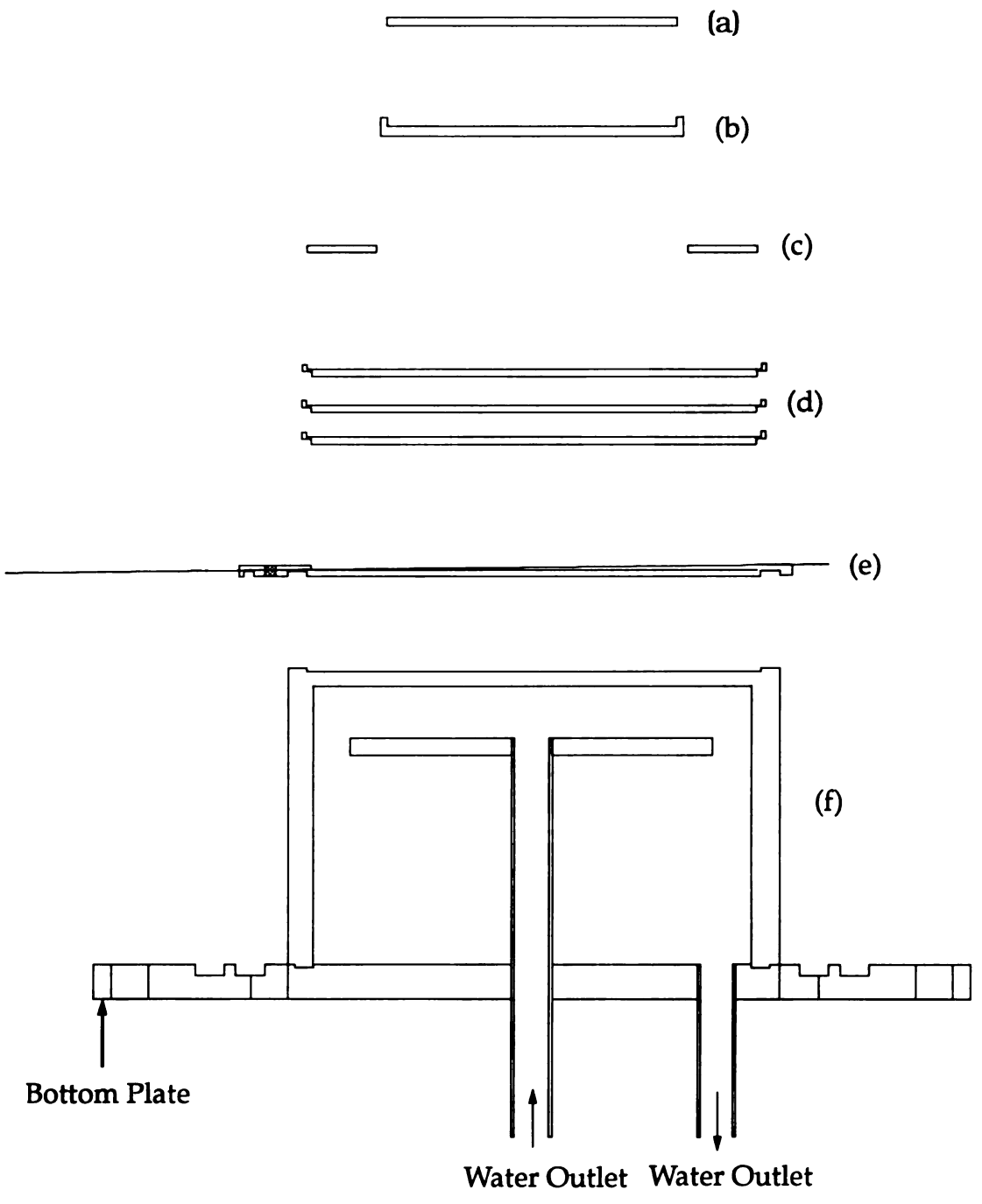

Figure 3.9 Typical substrate holder setup used in high-pressure MCPR for diamond film deposition: (a) 2″ silicon wafer, (b) 2″ graphite substrate holder, (c) boron nitride ring, (d) insulation discs, (e) graphite flow regulator, (f) water coolling stage.

Figure 3.10 and Figure 3.11 schematically illuminate the construction of the prototype water cooling stage. The can body, which is shown in Figure 3.10, consists of a 3.125″ inside diameter stainless plate and a 2″ tall stainless steel tube. These two parts were jointed by a vacuum weld. The bottom body, which is shown in Figure 3.11, contains the water inlet tube, the water outlet tube, and bottom plate. The cooling water was guided to the center of the body can by the 0.25″ in diameter inlet tube and then released through the 0.25″ in diameter outlet tube.

3.6.3.4 Drawbacks of The First Design

The first substrate holder setup design and water cooling stage had the following drawbacks:

Substrate holder setup:

(1) The edge of 2″ graphite holder was etched by the plasma after each run. This resulted in an unknown and an additional amount of carbon contribution to the diamond film deposition process. The maintenance of the reactor was also increased by the need to replace the 2″ graphite holder.

(2) The resulting temperature at the center of the substrate was higher than the temperature at the edge of the substrate area. This is due to the observation that the plasma shape becomes more arc-like than hemisphere-like at high pressure regime.

Water cooling stage:

(1) The 0.25″ in diameter water inlet and outlet were easily plugged

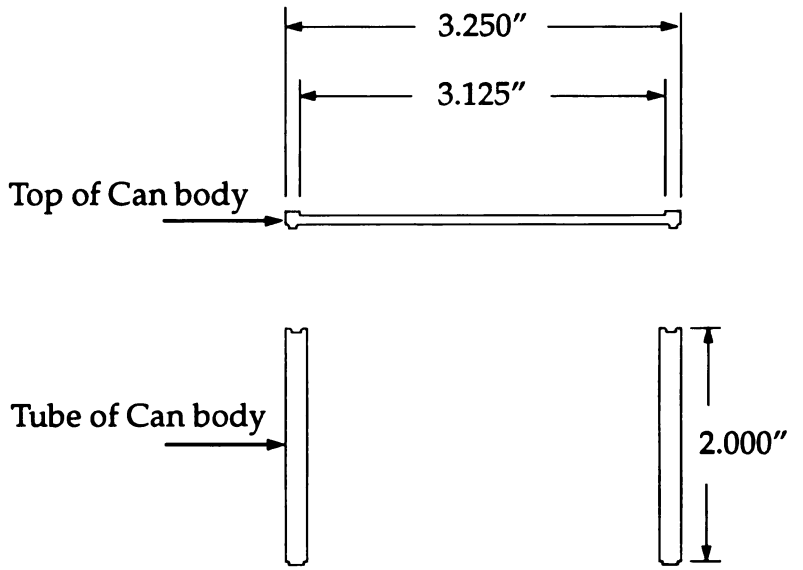

Figure 3.10 Can Body of the 3" Water Cooling Stage[107]

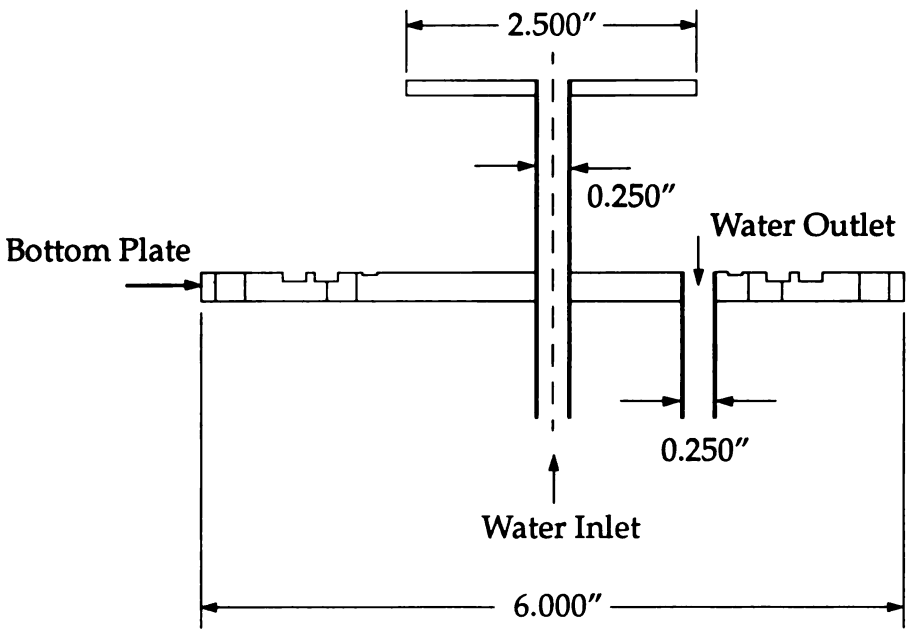

Figure 3.11 Bottom Body of the 3" Water Cooling Stage[107].

by the debris from the university water. The installation of water filters became necessary.

(2) A water leak from the welding section between the top of can body top and the tube of can body (shown in Figure 3.10) was observed.

A redesigned substrate holder setup and water cooling stage eliminated these drawbacks. This redesigned system is described in the sections below.

3.6.3.5 Final Substrate Cooling Stage Design

Figure 3.12 schematically shows the redesigned high-pressure MCPR configuration for diamond film deposition. The major differences between the revised configuration and prototype version are:

For substrate holder setup:

(1) 2″ graphite holder was replaced by 2″ conductive plate. This replacement can prevent the substrate holder from being etched by the plasma discharge.

(2) The 2″ conductive plate, as shown in Figure 3.12, was curved. This configuration solved the problem of temperature nonuniformity over the substrate that was described in Section 3.2.3.

For water cooling stage:

(1) As shown in Figure 3.13, the can body was machined from one solid piece of stainless steel. This prevented the problem of water leakage.

(2) As shown in Figure 3.13, the inside surface of top body can was

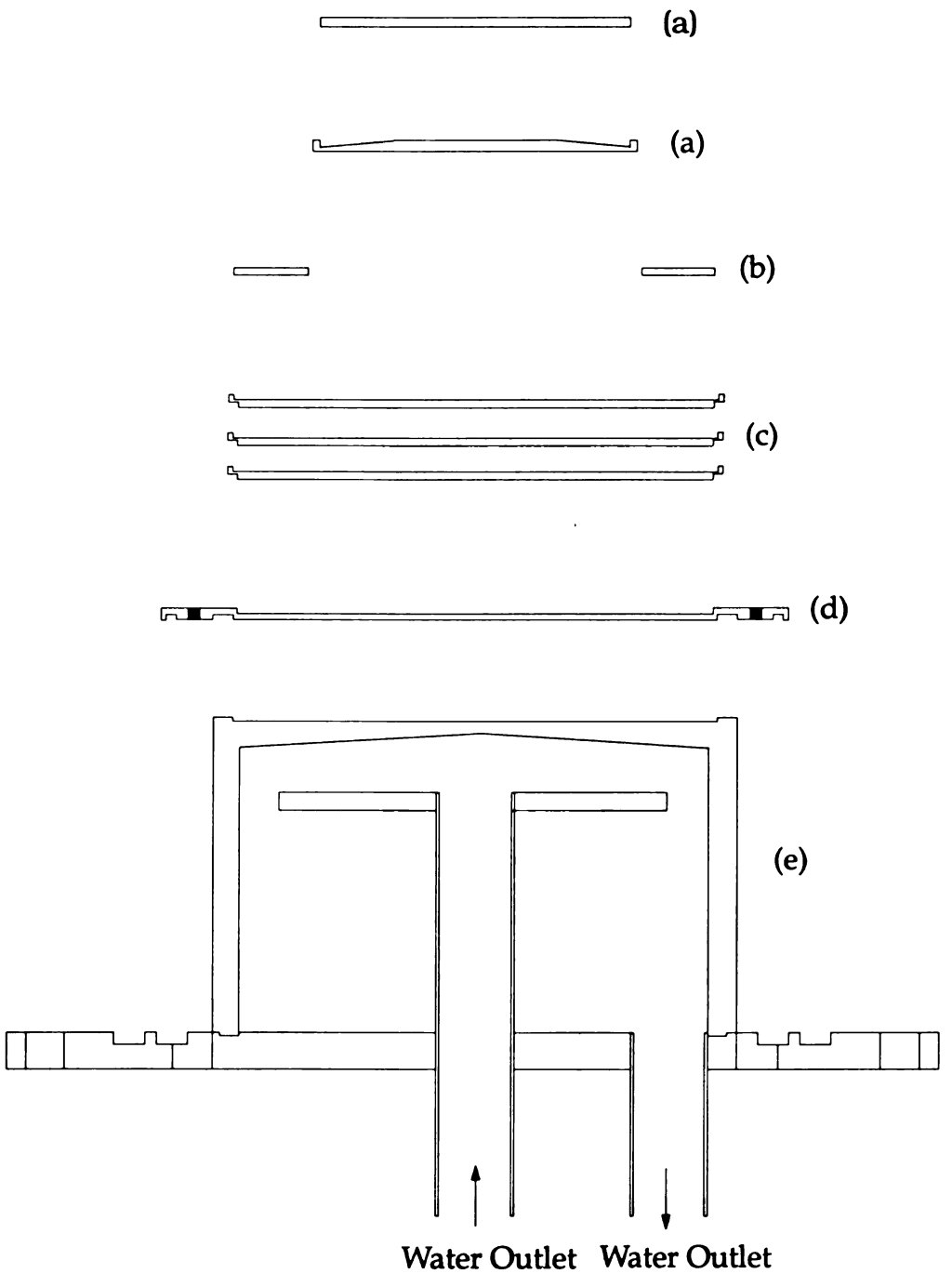

Figure 3.12 Typical substrate holder setup used in high-pressure MCPR for diamond film deposition: (a) 2˝ silicon wafer, (b) 2˝ conductive plate, (c) boron nitride ring, (d) insulation discs, (e) graphite flow regulator, (f) water coolling stage.

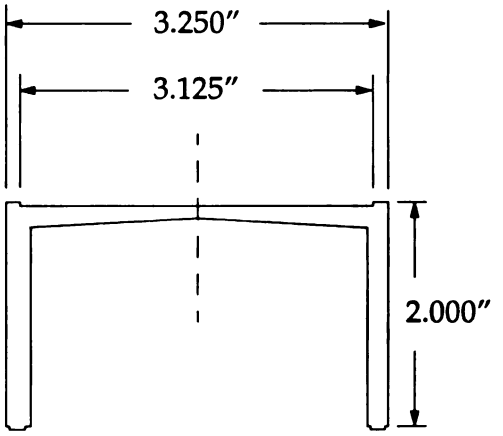

Figure 3.13 Can Body of the 3″ Water Cooling Stage[107].

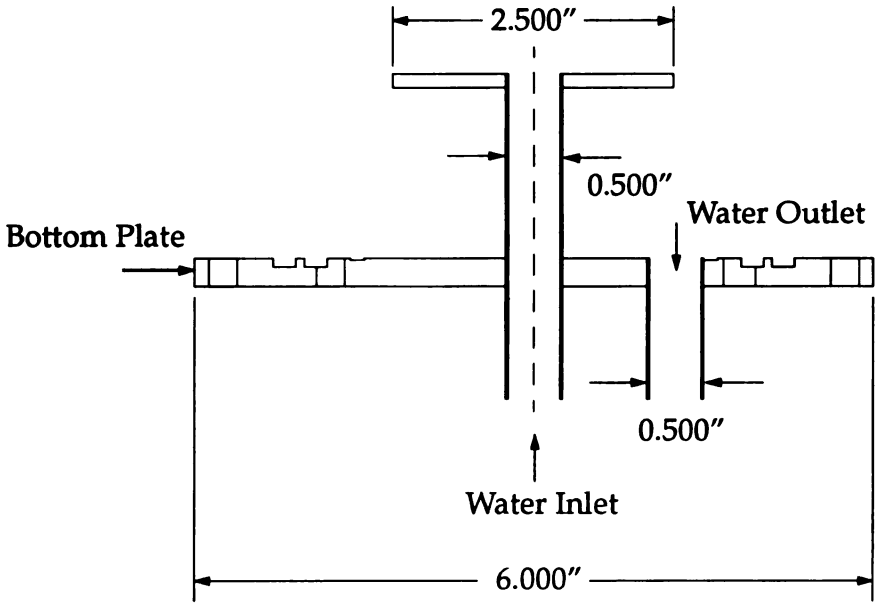

Figure 3.14 Bottom Body of the 3″ Water Cooling Stage[107].

machined from a flat surface to a curved surface. This revision enhanced the cooling at the center of body can, where higher temperature takes place under thermal plasma discharge condition.

(3) As shown in Figure 3.14, stainless steel tubes for water inlet and outlet were extended from 0.25″ to 0.5″ in diameter. This revision allowed more cooling water to flow inside the can body and prevented the input and output cooing tubes from being plugged by debris from university cooling water.

3.7 Summary

As described earlier in this chapter, a 12.5 cm diameter plasma reactor, identified as thermally floating MCPR, was developed by Zhang[9] and Khatami[51] and applied to diamond thin film deposition over 3″ or 4″ in diameter substrates in the 20-70 Torr pressure regime[9],[51]. As shown in Table 2.1, the total growth rate and specific yield over 3″ silicon substrates for this reactor are 14.86 mg/h(0.55 μm/h) and 163 kW-h/g, respectively. This chapter has described a redesigned thermally floating MCPR reactor which includes a water-cooled substrate holder setup and a better air cooling system. With these additions, the reactor, identified here as high-pressure MCPR, can be operated under the higher pressure (80-150 Torr) and higher power (2-4.5 kW) regime. When operating under these higher pressure higher power conditions the plasma changes from a non-equilibrium discharge to a more thermal-like discharge. The next two chapters describe the operational performance and the characteristics of

the diamond films synthesized by this new reactor configuration.

CHAPTER FOUR

Reactor Experimental Output Performance -

Reactor Performance ($\mathbf{Y_1}$)

4.1 Introduction

In general, the output performance of the reactor ($\mathbf{Y}$) is a function of many input variables, i.e., $\mathbf{Y}=f(\mathbf{U_1}, \mathbf{U_2}, \mathbf{U_3})$. As shown in Figure 4.1, the input variables are divided into three groups, (1) independent input variables $\mathbf{U_1}$ which include (a) methane concentration, (b) total flow rate, (c) substrate temperature, (d) absorbed microwave power, (e) deposition pressure; (2) reactor geometry variables $\mathbf{U_2}$ which include (a) quartz dome size, (b) water cooling stage geometry, (c) substrate type and size, (d) reactor size, L_s, (e) coupling probe position, L_p; (3) process variables, $\mathbf{U_3}$, which include (a) seeding procedure, (b) start-up and shut-down procedures, and (c) deposition time (t). Important internal variables $\mathbf{X}$ are the discharge plasma volume V_d and the absorbed microwave power density $\langle P_V \rangle$. The plasma volume V_d is held constant at ~144 cm^3 for all the experimental runs in this chapter and chapter 5. As shown in Figure 4.1,

absorbed microwave power (P_t), deposition pressure (p), and microwave power volume density ($<P_V>$) are not independent of each other, i.e.,,$<P_V>=P_t/V_d$. Thus the absorbed power and the pressure are directly related in all the experiments and thus these variables are referred to as a doublet input variable, i.e., as the absorbed microwave power- deposition pressure (P_t-p) variable.

As also shown in Figure 4.1, the outputs of the reactor (**Y**) can be divided into two groups. Outputs $\mathbf{Y_1}$ are concerned with the reactor performance such as growth rate, specific yield, and carbon conversion efficiency. A second group of outputs $\mathbf{Y_2}$ are concerned with the film properties such as morphology, structural quality, and texture. The understanding of the reactor behavior is very difficult not only because of the numerous variables but also because the input vs. output behavior of each variable is nonlinear and complex. Theories that describe and predict reactor behavior do not exist.

Therefore it is necessary to experimentally explore the operational behavior of the redesigned high pressure MCPR. The experimental data presented in this chapter are the result of over 100 separate experiments representing over 1,000 hours of experimental operation. The resulting multiple dimensional input/output experimental variable space is difficult to visualize and plot. Thus this chapter presents an overview of the high pressure MCPR reactor performance $\mathbf{Y_1}$ versus a selected number of input variables. Each experimental run represents a data point in the

multic

ments

tor in

experi

and T

concer

ture,

p. As

fixed,

electr

man

T_s, t

film

exp

effi

Exp

forr

plot

able

gle i

each

multidimensional input/output variable space. In each of these experiments the output reactor performance $\mathbf{Y_1}$ was measured for specific reactor inputs. The reactor input and output variables and their associated experimental ranges explored in this chapter are displayed in Figure 4.1 and Table 4.1. The independent input variables chosen were (a) methane concentration, c=%CH_4/H_2, (b) total flow rate, f_t, (c) substrate temperature, T_s, (d) absorbed microwave power (P_t), and (e) deposition pressure, p. As indicated in Figure 4.1 and Table 4.1, all other input variables were fixed, i.e., the substrates were limited to two inch (100) silicon wafers, the electromagnetic excitation was fixed at TM_{013} mode, etc.

This chapter presents an overview of the output reactor performance $\mathbf{Y_1}$ versus the five dimensional input variable space, i.e., $\mathbf{Y_1}$=f(c, f_t, T_s, t, P_t-p). The output performance variable $\mathbf{Y_1}$ that are of interest are (a) film linear growth rate, expressed in μm/h, (b) total growth rate, expressed as mg/h, (c) specific yield, expressed as kW-h/g, (d) gas flow efficiency, expressed in mg/liter, and (e) carbon conversion efficiency. Experimental data in this chapter is only presented for films with an uniformity of 15% or better.

The multiple dimensional experimental variable space is difficult to plot on a single graph. Therefore the various reactor performance variables $\mathbf{Y_1}$ are plotted as a group of experimental data points versus a single input variable, i.e., $\mathbf{Y_1}$=f (c), $\mathbf{Y_1}$=f(f_t), $\mathbf{Y_1}$=f(T_s), $\mathbf{Y_1}$=(t), and $\mathbf{Y_1}$=f(P_t-p). In each of these plots the other input variables are varied over their respec-

tive ranges described in Figure 4.1 and Table 4.1. Thus for each performance curve there is considerable scatter of the experimental data as the other four input variables are changed. However, a shaded curve is included in each plot to represent the performance boundary of the reactor. It is this performance boundary (or surface in the multidimensional input/output variable space) that describes the experimental performance of the MCPR reactor.

The high pressure MCPR output performance, i.e., growth rate, specific yield, and carbon conversion efficiency are summarized in the sections below. These reactor outputs are then compared with the performance of other reactors that were described in Chapter 2.

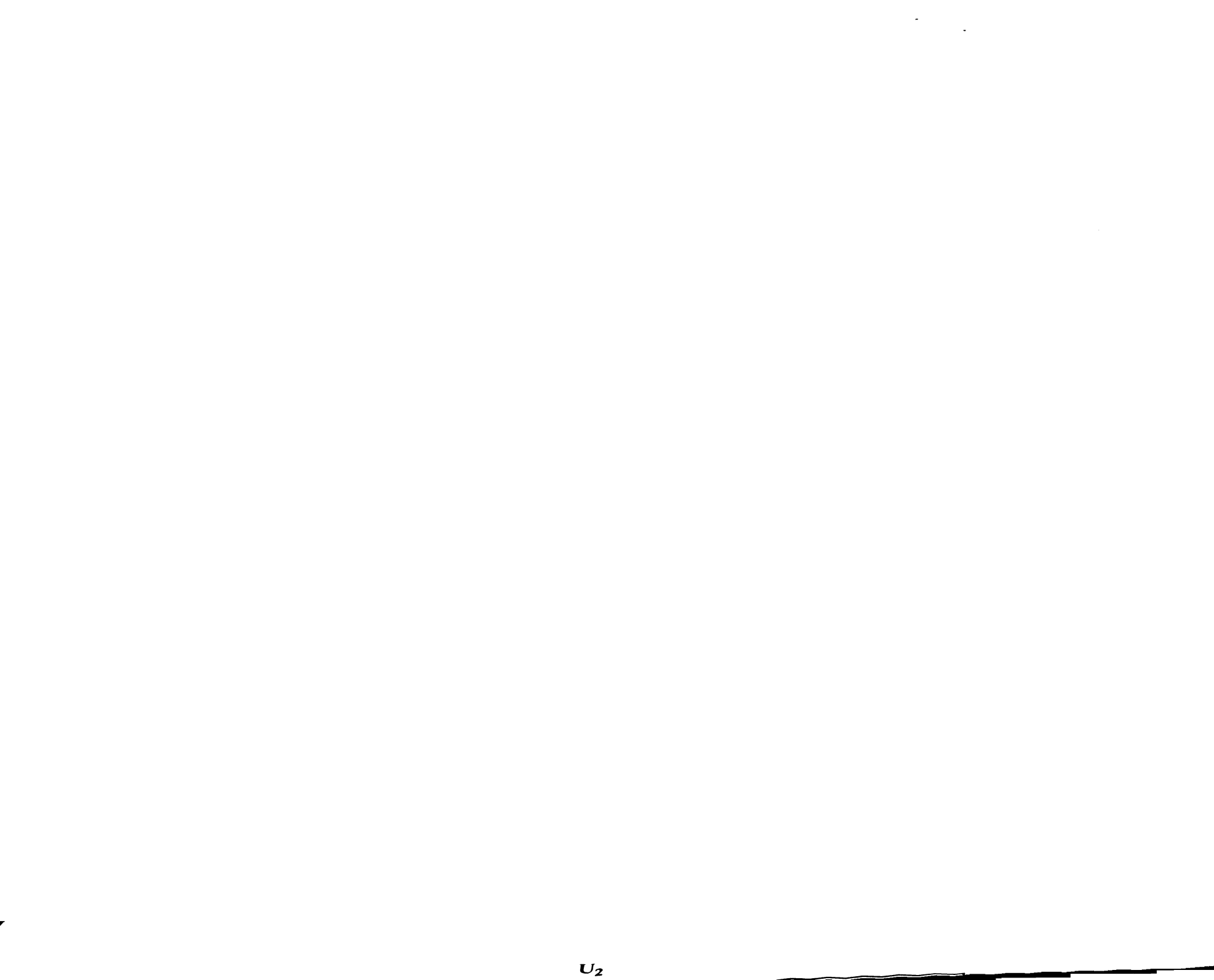
U_2

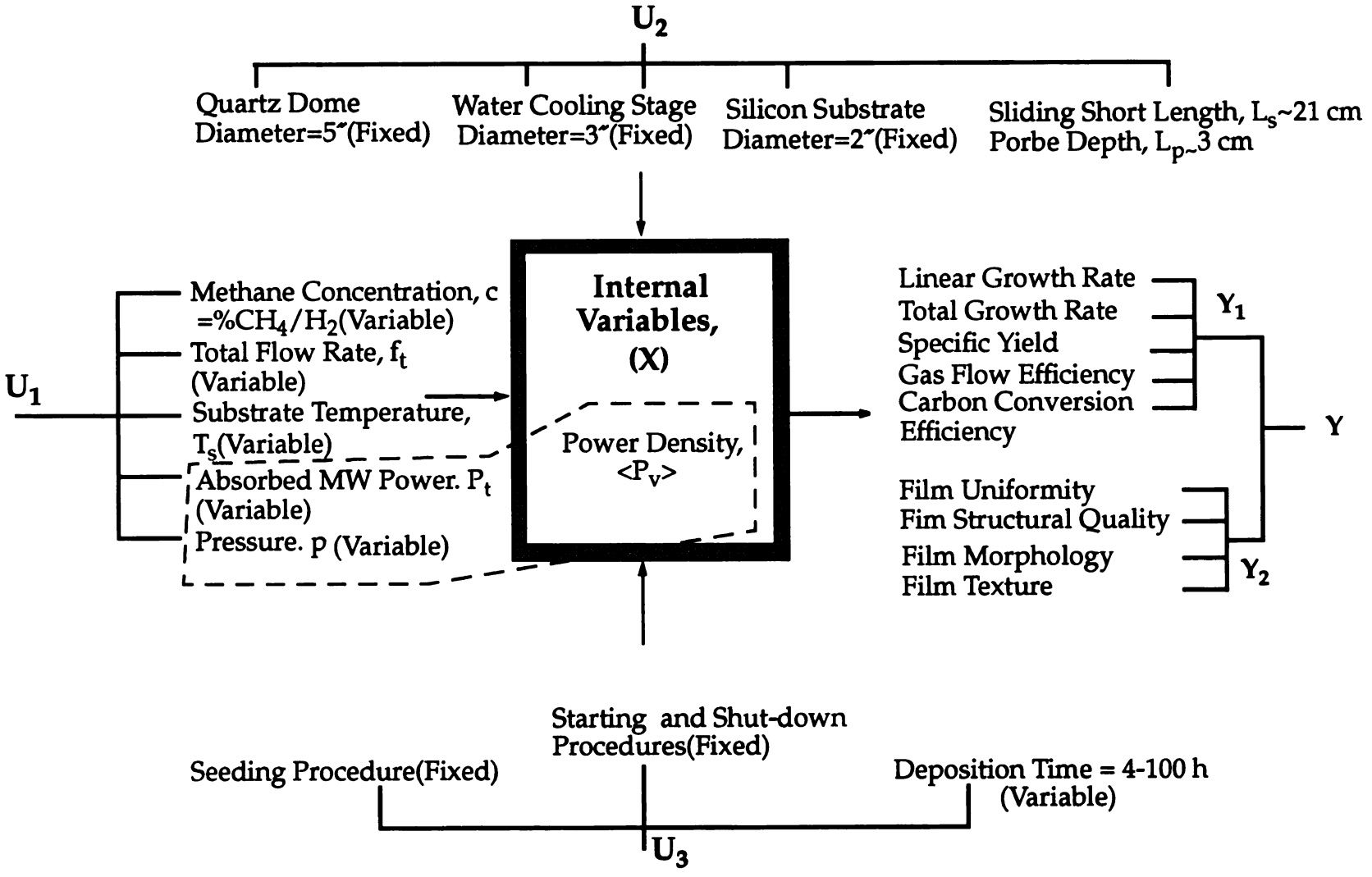

Figure 4.1 High-pressure MCPR block diagram for the experiments described in this chapter.

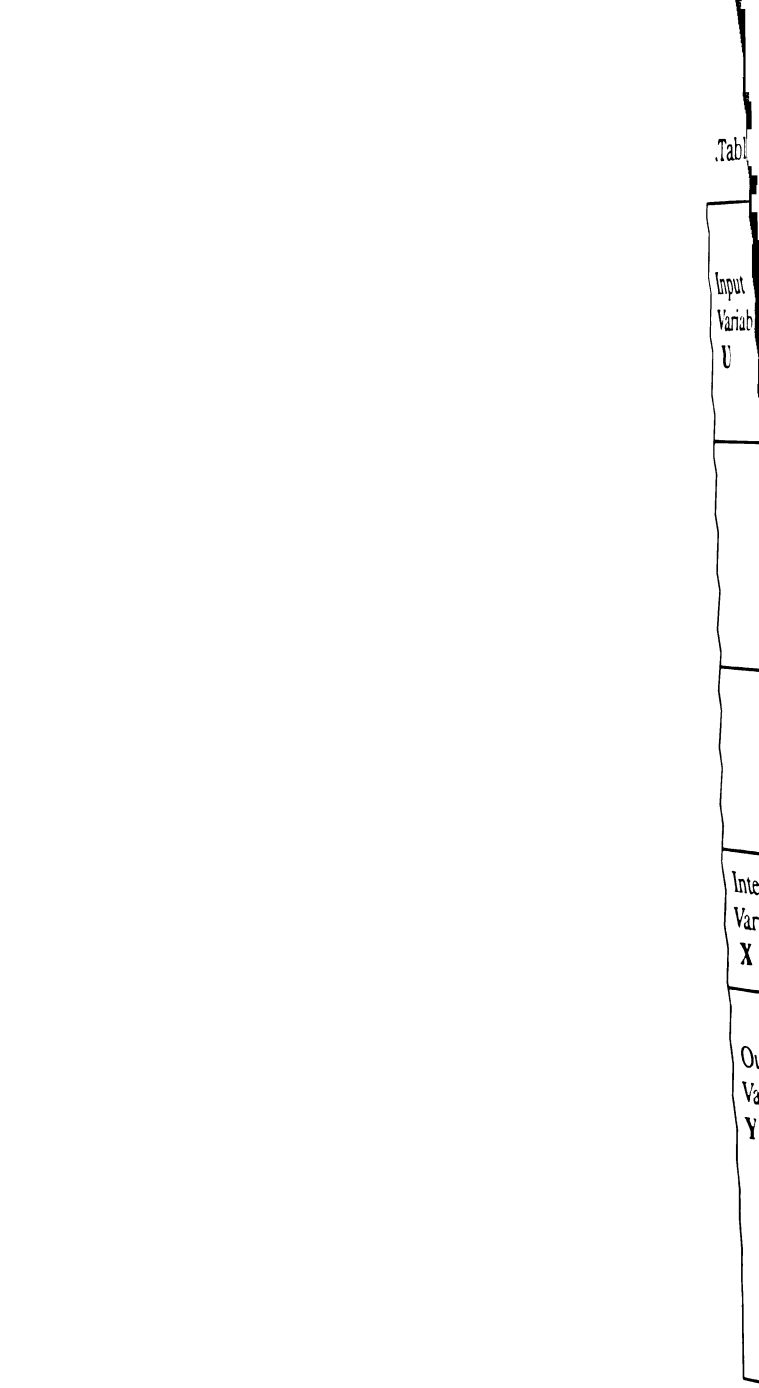
Input
Variab
U
Inte
Var
X
Ou
Va
Y

.Table 4.1 The Ranges of reactor variables investigated in this chapter

Input Variable **U**	Controllable Input Variables, U_1	a) Deposition Pressure, Variable: p=80-140Torr b) Absorbed Microwave Power, Variable: P_t=3-5kw c) Methane Concentration, Variable: c=1-8% CH_4/H_2 d) Substrate Temperature, Variable: T_s=800-1130C e) Total Flow Rate, Variable: f_t=100-1400 sccm
	Reactor Geometry Variables, U_2	a) Quartz Dome, Fixed b) Water Cooling Stage Configuration, Fixed c) Sliding Short Length L_s~21cm and Probe Depth L_p ~3cm Approximately Fixed(at TM_{013} Excitation Mode) d) Substrate Material and Size, Fixed: 2" dia. (100) Si
	Deposition Process Variables, U_3	a) Starting and Shut-down Procedure, Fixed b) Substrate Seeding Procedure, Fixed c) Deposition Time, Variable: t=4-100 Hours
Internal Variable **X**		a) Plasma Volume, V_d, Approximately Constant at 144cm^3 b) Absorbed Power Density, Variable: $<P_v>=P_t/V_d$
Output Variable **Y**	Reactor Performance, Y_1:	a) Linear Growth Rate: 4-7 μm/h b) Total Growth Rate: 27-50 mg/h c) Specific Yield: 69-300 kw-h/g d) Gas Flow Efficiency: 0.6-1.2 mg/liter e) Carbon Conversion Efficiency: 1-12%
	Film Characteristics Y_2:	a) Film Uniformity: 10% or better over 2" dia. area b) Film Structural Quality: FWHM=3-8 cm^{-1} c) Film Morphology: mostly (111) morphology d) Film Texture: mostly <110> texture

4.2 Reactor Performance (Y_1)- Linear Growth Rate

4.2.1 Linear Growth Rate=f(c,f_t,T_s,t)

Figure 4.2 to Figure 4.5 display the linear growth rate as a function

of a single input variable, i.e., the growth rate is plotted as a function of the CH_4/H_2 concentration, c, (Figure 4.2), of total flow rate, f_t , (Figure 4.3), of substrate temperature, T_s, (Figure 4.4), and of deposition time, t, (Figure 4.5). The right hand vertical axis in Figure 4.2 displays the total growth rate in mg/h. Since all the films were reasonably uniform over the two inch diameter, the relationship between the total growth rate, W, and the linear growth rate, d, is a constant determined from d~ W/(AD)~W/ 7.1, where A is the deposition area(~20.27 cm^2) and D is the diamond density (3.51 g/cm^3). The relationship between these two growth rates is the same for all figures in this chapter.

As shown, the shaded curves in each performance map represent the performance boundary of the reactor's growth rate versus the specific input variables and thus defines the experimental performance of the high pressure MCPR. Instead of plotting these curves versus a single variable the same data points can be displayed vs. two variables. For example in Figure 4.6 the same experimental growth rate data is displayed vs. substrate temperature and methane concentration. The shaded colored curves in this figure represent an upper boundary for the maximum growth rate at either a constant T_s (red curve T_s=1080°C) or a constant c (green curve c=3%). Indeed in Figure 4.6 there exists a three dimensional surface (not shown) that represents the upper boundary of the growth rate vs. T_s or c.

It is interesting to compare the CH_4/H_2 deposition regions for the moderate pressure MCPR[9],[51] and for the high pressure MCPR. Figure 4.7 displays a corner of the "well known" Bachmann Phase Diagram for CVD diamond deposition[45]. When both reactors use only CH_4/H_2 chemistry the "zone" of diamond deposition occurs along the H/H+C line. In the moderate pressure MCPR, good diamond films were grown between methane concentrations of 0.6-4.75% corresponding to the H/H+C values of 0.997-0.979[9],[51]. In high pressure MCPR, diamond films were grown between methane concentrations of 1-8% corresponding to the H/H+C values of 0.995-0.967.

Figure 4.8 shows the locations of diamond deposition zones vs. three independent input variables c, f_t, and T_s for both high pressure and moderate pressure MCPRs. As shown, the three dimensional zone where diamond deposition occurs was increased in the high pressure MCPR. This deposition zone was increased by extending c from 0.6-5% to 1-8%, f_t from 60-200 sccm to 400-1400 sccm, and T_s from 700-1000C to 600 to 1130C. This significant increase in the volume of diamond deposition zone is believed to be due to the shift of the discharge plasma chemistry from a non-equilibrium cold plasma regime to a thermal-like plasma discharge regime.

The experimental data displayed in Figure 4.2 to Figure 4.6 also indicates that the maximum uniform film growth rate using high pressure MCPR is 6.27 μm/h(or~45 mg/h) and it is achieved at c=3%, f_t=618 sccm,

T_S~1C

funct

pholo

space

prese

descr

allow

carb

sent

T_s~1060°C, t=100h, and p=135 Torr. Clearly film growth rate is a strong function of c, f_t, T_s, t, and p. The details of how the growth rate, film morphology, film texture, etc. change vs. the multiple dimensional variable space can be investigated by taking cross sectional slices of the data set presented here. This output performance vs. single input variables will be described in the next chapter. The experimental data set presented here allow the calculation of reactor performance such as specific yield and carbon conversion efficiency. The results of these calculations are presented in Section 4.3.

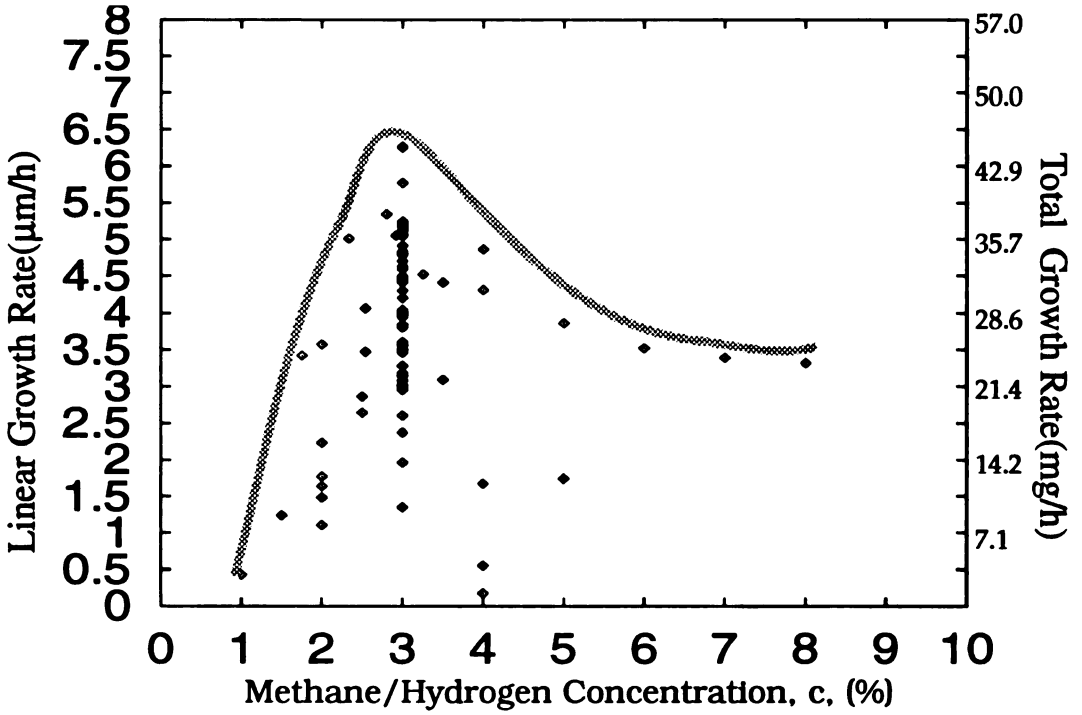

Figure 4.2 Summary of growth rate vs. methane/hydrogen concentration in high-pressure MCPR.

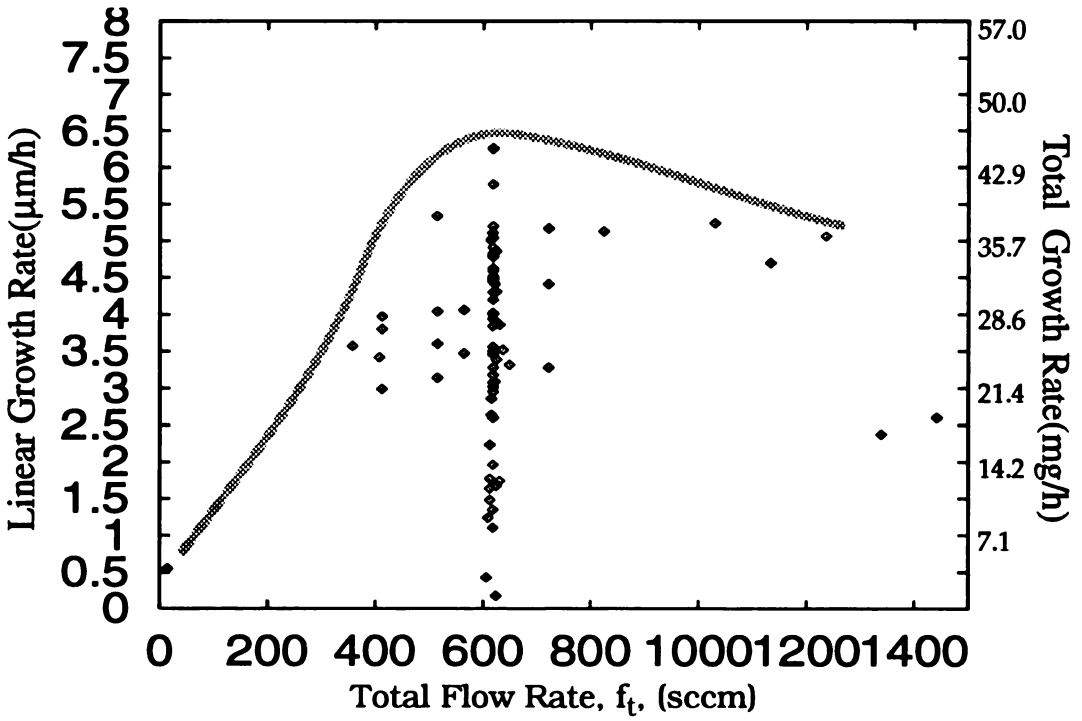

Figure 4.3 Summary of growth rate vs. total flow rate in HPMCPR.

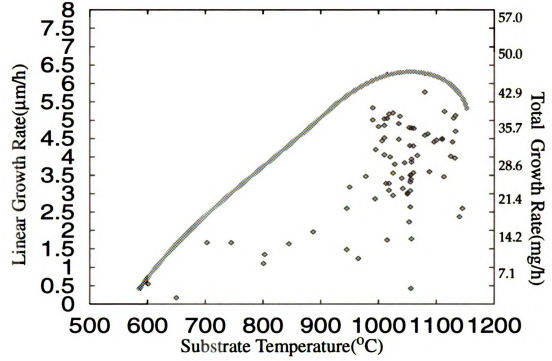

Figure 4.4 Summary of linear growth rate vs. substrate temperature.

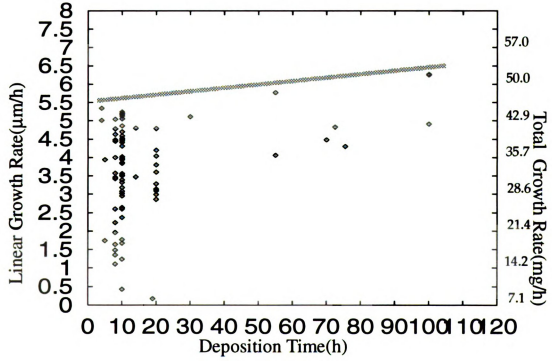

Figure 4.5 Summary of linear growth rate vs. deposition time.

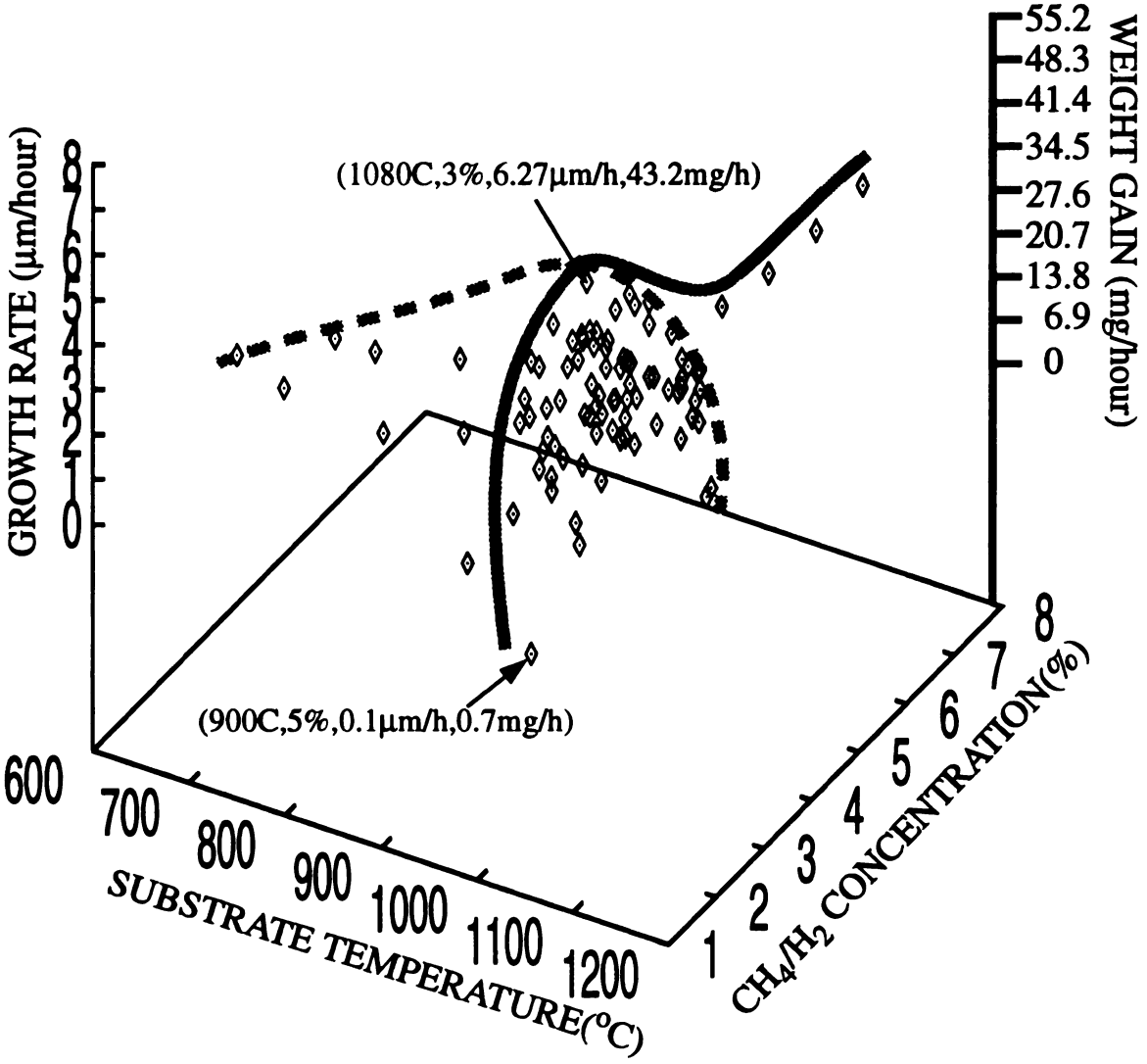

Figure 4.6 Summary of growth rate vs. methane/hydrogen concentration and substrate temperature in the high-pressure MCPR. Solid curve represents an upper boundary for the maximum growth rate at constant c=3% and dash curve presents an upper bounday for the maximum growth rate at constant T_s=1080°C.

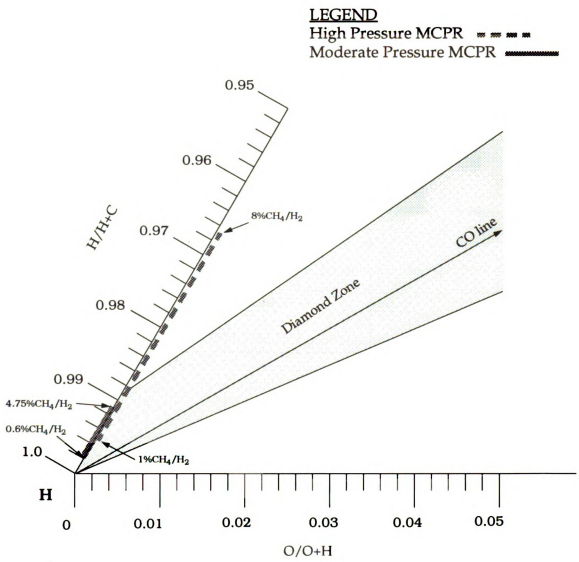

Figure 4.7 Locations of different methane concentrations for the experiments that were investigated in this thesis. The solid curve represents the diamond growth region for the moderate pressure MCPR[9],[51] and the dash curve represents the growth region for the high pressure MCPR discribed in this thesis.

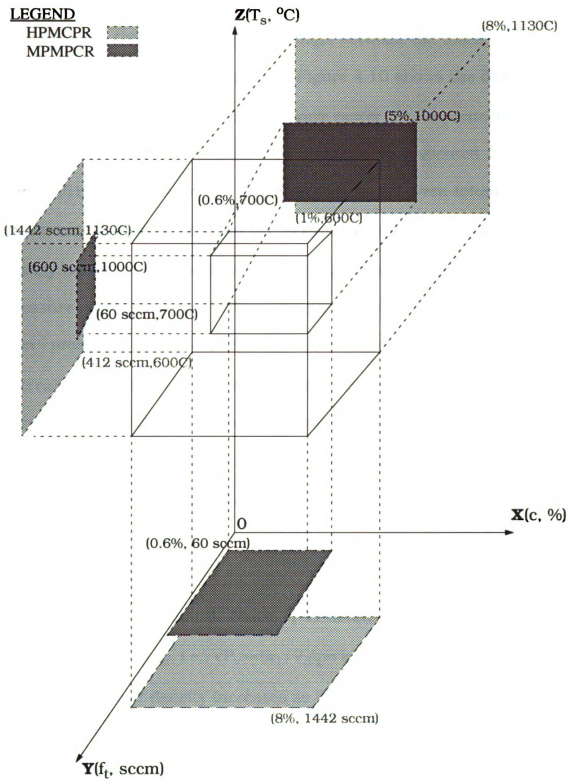

Figure 4.8 Location of diamond zones vs. c, f_t, and T_s for high pressure and moderate pressure[51] MCPRs.

4.2.2 Linear Growth Rate=f(P_t-p)

Figure 4.9 shows the relationships between the linear growth rate and doublet input variable P_t-p and Figure 4.10 shows the linear growth rate as a function of absorbed microwave power. The experimental growth rates for the moderate pressure MCPR are also presented for comparison[9],[51]. The data points shown in Figure 4.9 were taken under the experimental conditions when the plasma volume (V_d) was held approximately constant as deposition pressure (p) was increased in 70-140 Torr pressure regime. In order to keep the plasma volume constant as deposition pressure increased, the absorbed microwave power (P_t) was increased. The dashed curve in Figure 4.9 presents the experimentally measured increase in the power density ($<P_v>=P_t/V_d$) as the pressure increased. The solid curve is again an upper boundary for the growth rate versus deposition pressure for the high pressure MCPR.

The dashed curve presents the experimentally measured power density as a fuction of the pressure, i.e., $P_t=k_1p$ (k_1 was approximately measured to be constant). Since P_t is defined as $<P_v>V_d$, then $P_t=k_1p$ becomes $<P_v>V_d=k_1p$, i.e., $<P_v>=(k_1/V_d)p= k_2p$ ($k_2=k_1/V_d$~constant). Thus the volume power density increases as the deposition pressure increases. The other important experimental power density, area power density $<P_A>$, which is also shown on the left hand axis in Figure 4.9. This power density is defined as $<P_A>=P_t/A$ where A is the deposition area. The rela-

tionship between the $<P_V>$ and $<P_A>$ is a constant determined from $<P_A>= (V_d/A)<P_V>\sim 7.1<P_V>$, where A is the deposition area(~20.27 cm^2) and V_d is the plasma volume (~144 cm^3).

As the pressure increases from 30 Torr to 80 Torr to over 100 Torr, the discharge plasma changes from a non-equilibrium discharge to a more thermal like discharge. When the reactor is operated in the thermal plasma regime, the film growth rate increases. Figure 4.9 shows that increasing the operating pressure from the 20-80 Torr pressure regime to the 80-140 Torr regime increases the maximum deposition rate by a factor of five.

Also as shown in Figure 4.9 for a constant pressure the growth rate data displays a considerable variation. For example at the thermal-like plasma regime (p=80-140 Torr), the growth rate varies between a maxima of 6.5 μm/h(~43 mg/h) to a minima of 0.5 μm/h(~3 mg/h). This variation indicates that at a constant pressure the growth rate is strong function of many input variables such as methane concentration (c), substrate temperature (T_s), total flow rate (f_t), etc., and varies considerably as these input variables are changed.

It is interesting to compare the growth rates and the associated area power densities of the low pressure and the high pressure MCPRs in this section. The low pressure MCPR operated with an area power density of 0.03- 0.04 kW/cm^2 [51] which resulted in the maximum growth rate of ~0.55 μm/h. The area power densities for the high pressure MCPR, as

shown in Figure 4.9, are mostly in the range of 0.15 and 0.25 kW/cm^2. The area power density of high pressure MCPR is almost 10 times that of the low pressure MCPR. Interestingly, the linear growth rates of the high pressure MCPR are also approximately ten times the linear growth rates of the low pressure MCPR. Thus the linear growth rate, i.e., the deposition per substrate area, increases directly as the discharge area power density increases.

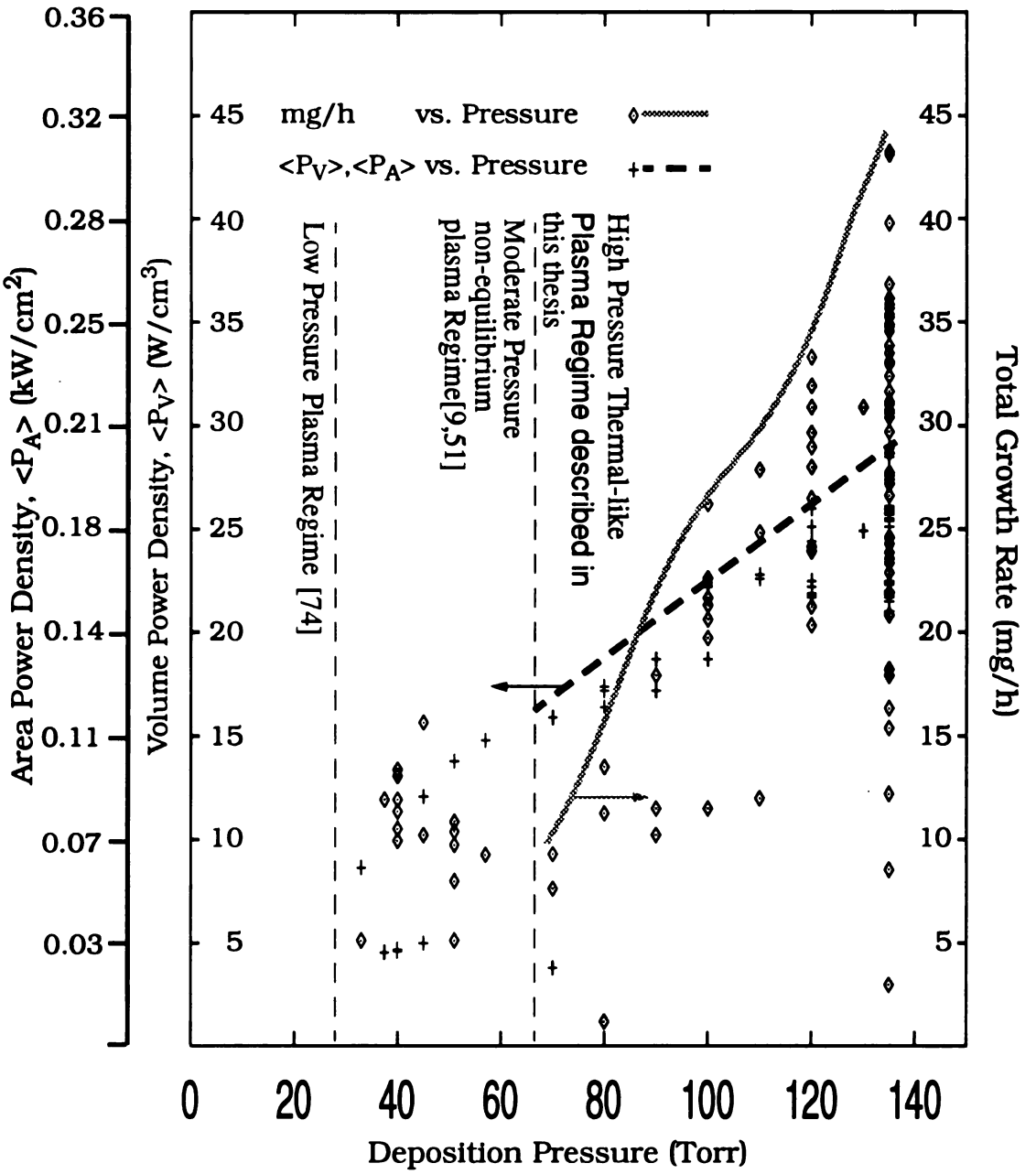

Figure 4.9 Summary of growth rate vs. pressure for the high pressure MCPR.

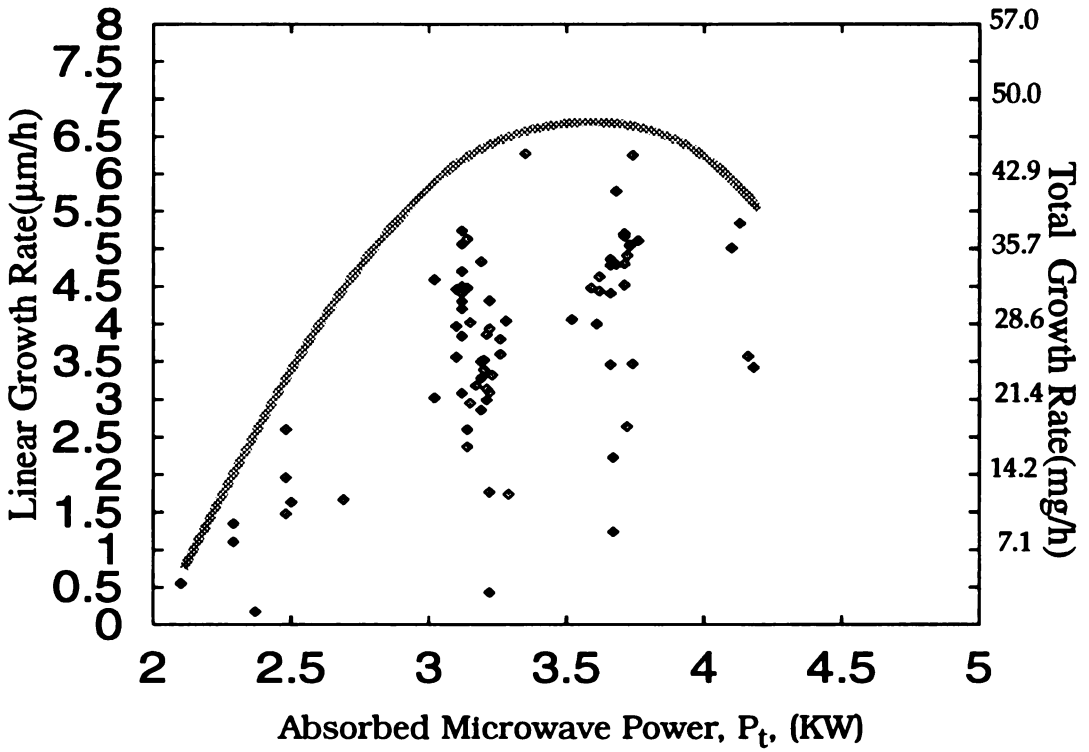

Figure 4.10 Summary of film growth rate vs. absorbed power.

4.3 Reactor Performance (Y_1)- Specific Yield

4.3.1 Specific Yield=f(c, f_t, T_s, t)

Specific yield is a measure of the electrical efficiency of the deposition process. That is, the lower the specific yield the fewer electrical energy kW-h required to deposit a given weight of diamond. As shown in Figure 4.11, the specific yield first decreased with increasing c and then reached a minimum around c=3%, and then slightly increased with continued increasing c. From Figure 4.11 the specific yield was found to be bounded at 220 kW-h/g, 100 kW-h/g, 70 kW-h/g, and 150 kW-h/g at c=1%, 2%, 3%, and 4-8%, respectively.

Figure 4.12 displays the variation of the lower bound of specific yield as flow rates were varied from 50 sccm to 1400 sccm. The best specific yield was achieved by using the total flow rate at around 600 sccm. Figure 4.13 displays the variation of specific yield versus the substrate temperature, T_s. Low specific yield occurred in the high substrate temperature range when the deposition rate is the highest. Conversely, poor specific yield was produced in the low substrate temperature region. It is also observed from Figure 4.13 that the specific yield decreased to a minimum and increased with increasing substrate temperature. As shown in Figure 4.14, the specific yield slightly decreases as the deposition time increases. This is no doubt caused by the fact shown in Figure 4.5 that the deposition rate increases as the film thickness and crystal size increase.

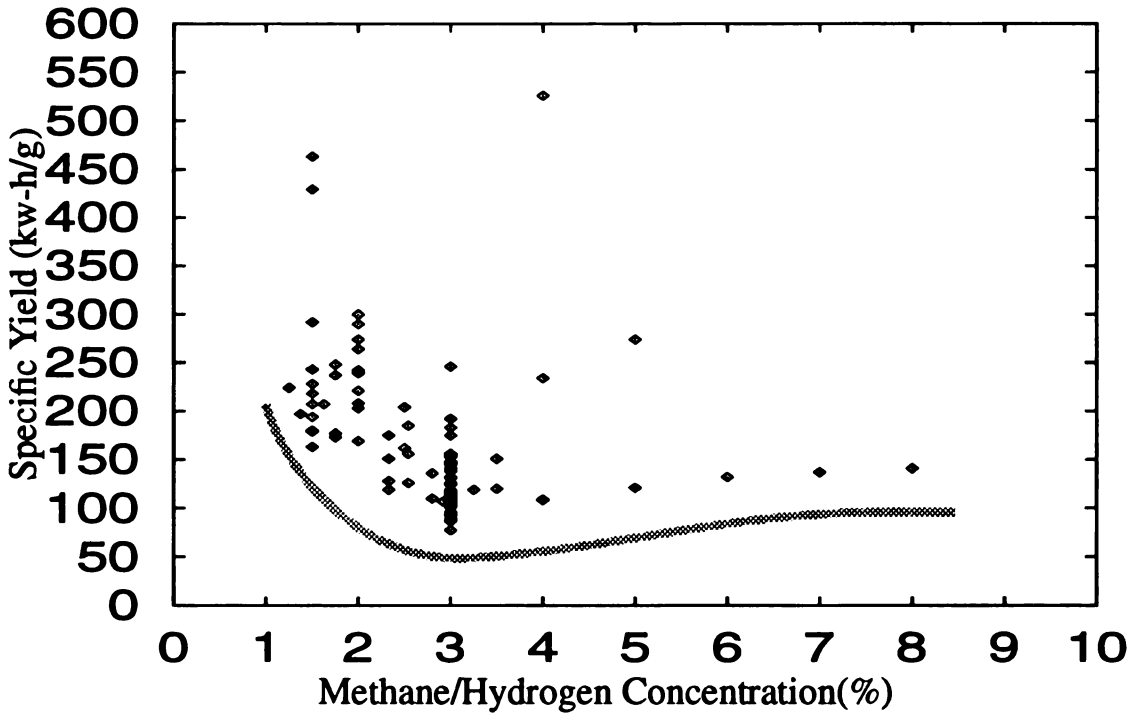

Figure 4.11 The effect of $\%CH_4/H_2$ on the specific yield in high-pressure MCPR.

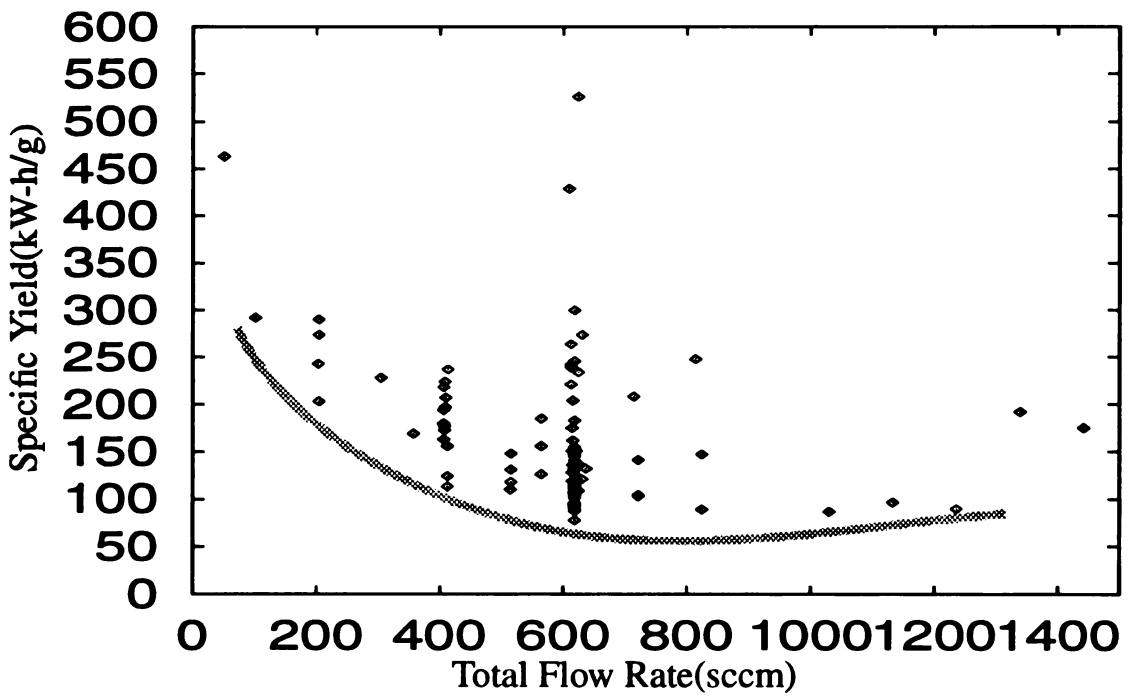

Figure 4.12 Summary of specific yield vs. total flow rate in the high-pressure MCPR.

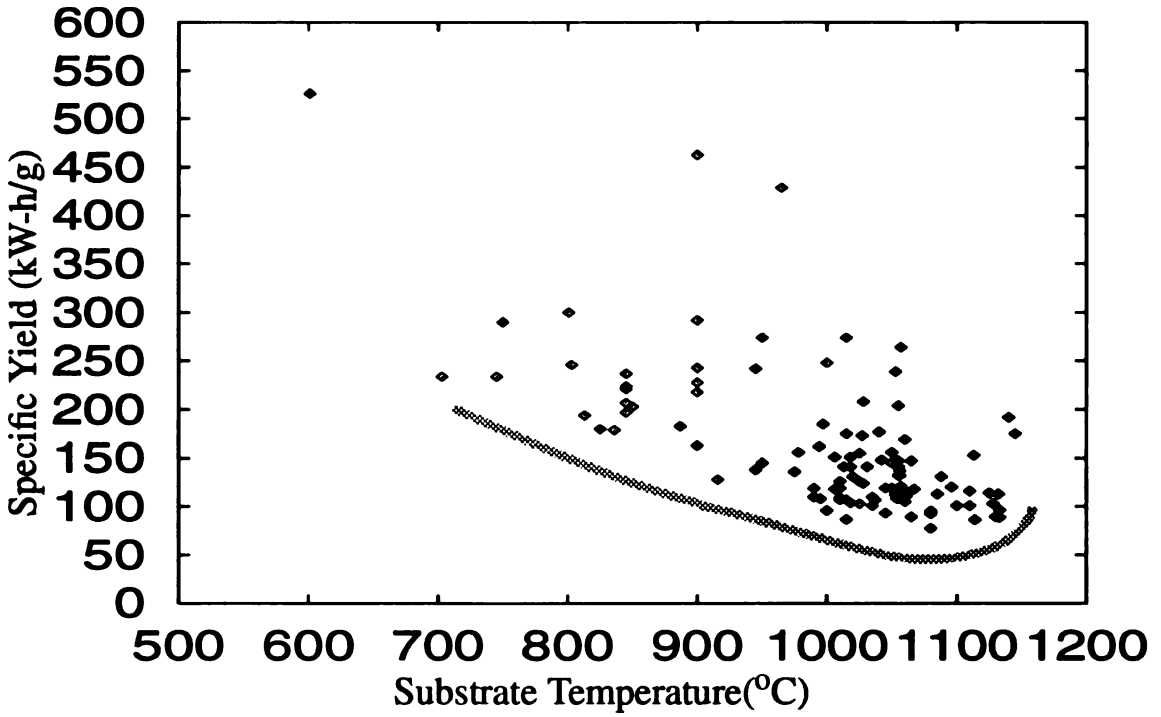

Figure 4.13 Summary of specific yield vs. T_s in high pressure MCPR.

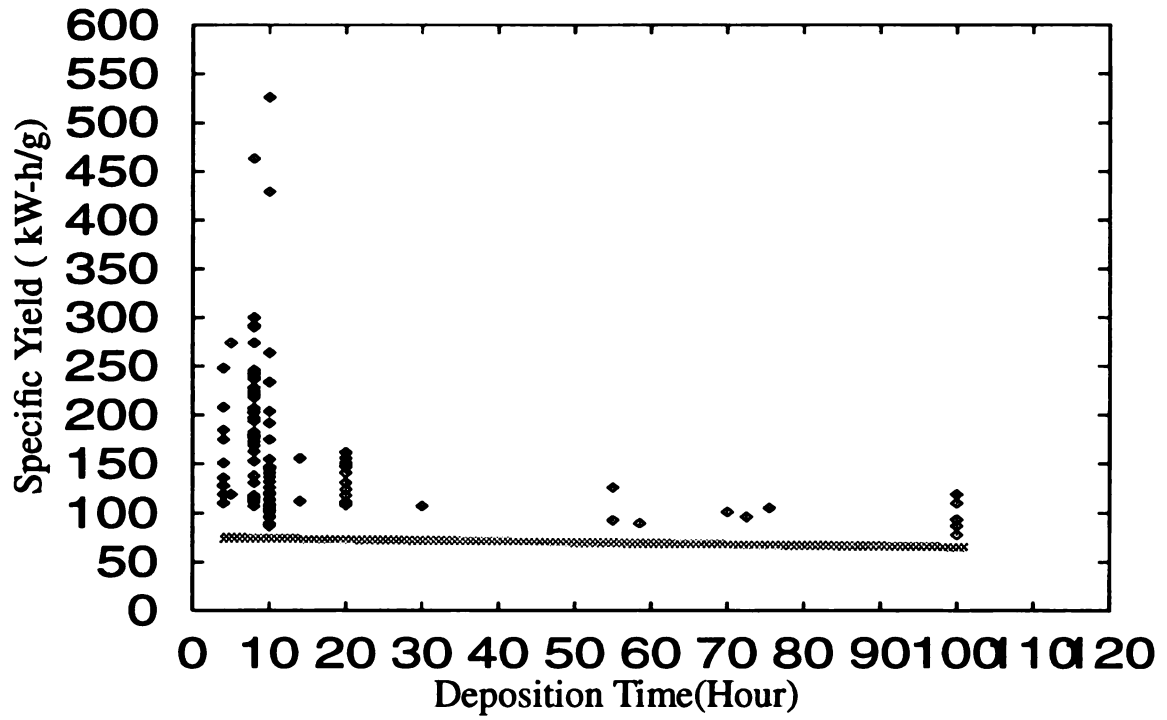

Figure 4.14 Summary of specific yield vs. deposition time in high-pressure MCPR.

4.3.2 Specific Yield=f(P_t-p)

Figure 4.15 shows the effect of absorbed microwave power on specific yield. As shown, the specific yield decreased to a minimum of 70kW-h/g around 3-4 kW.

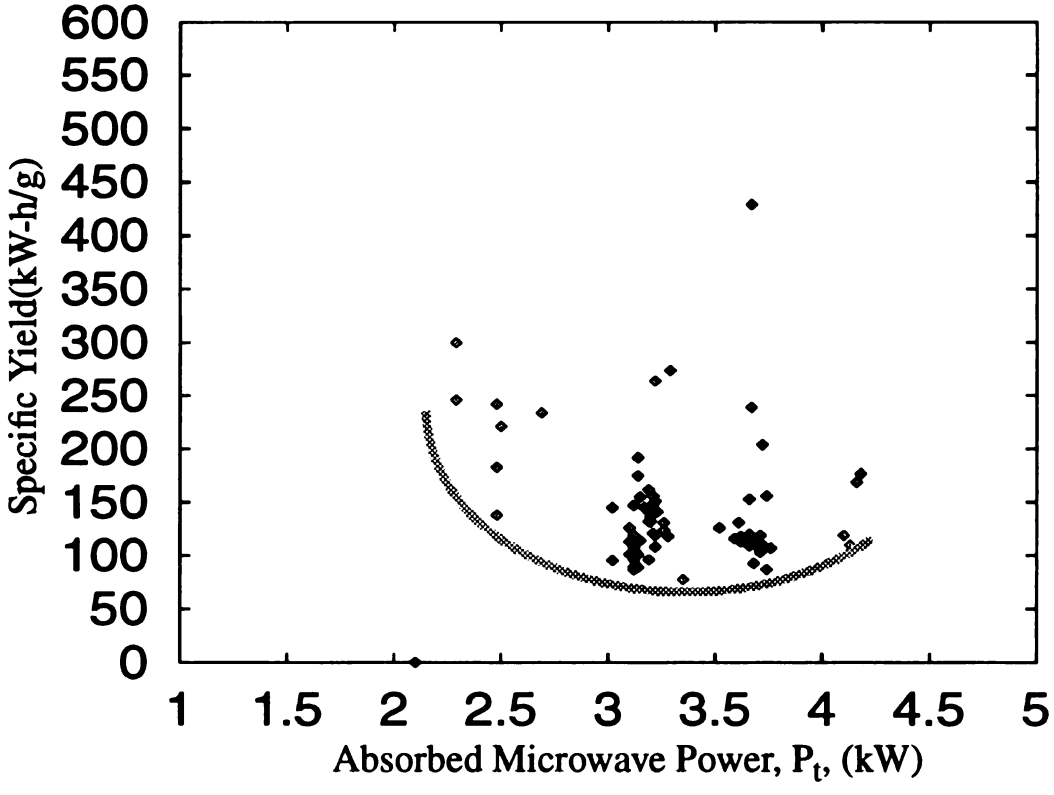

Figure 4.15 Summary of specific yield vs. absorbed micorwave power in HPMCPR.

4.4 Reactor Performance (Y_1)- Carbon Conversion Efficiency

4.4.1 Carbon Conversion Efficiency=f(c,f_t,T_s,t)

Carbon conversion efficiency is a measure of the amount of input carbon that is deposited in the diamond film. Figure 4.16-Figure 4.19 display the variation of carbon conversion efficiency versus c, f_t, T_s, t, and P_t-p. Clearly carbon conversion efficiency is high under low total flow rates, low methane concentrations, and at high temperature conditions. Carbon conversion efficiency as high as 12% can be achieved and take place under relatively high film growth conditions.

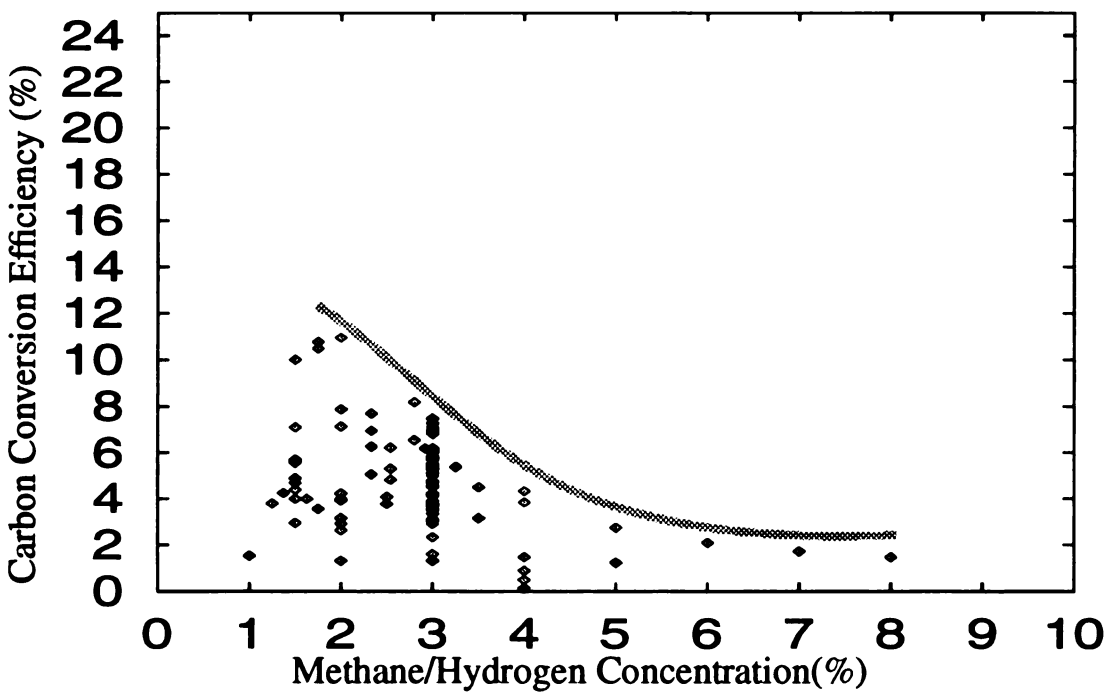

Figure 4.16 Summary of carbon conversion efficiency vs. %CH_4/H_2.

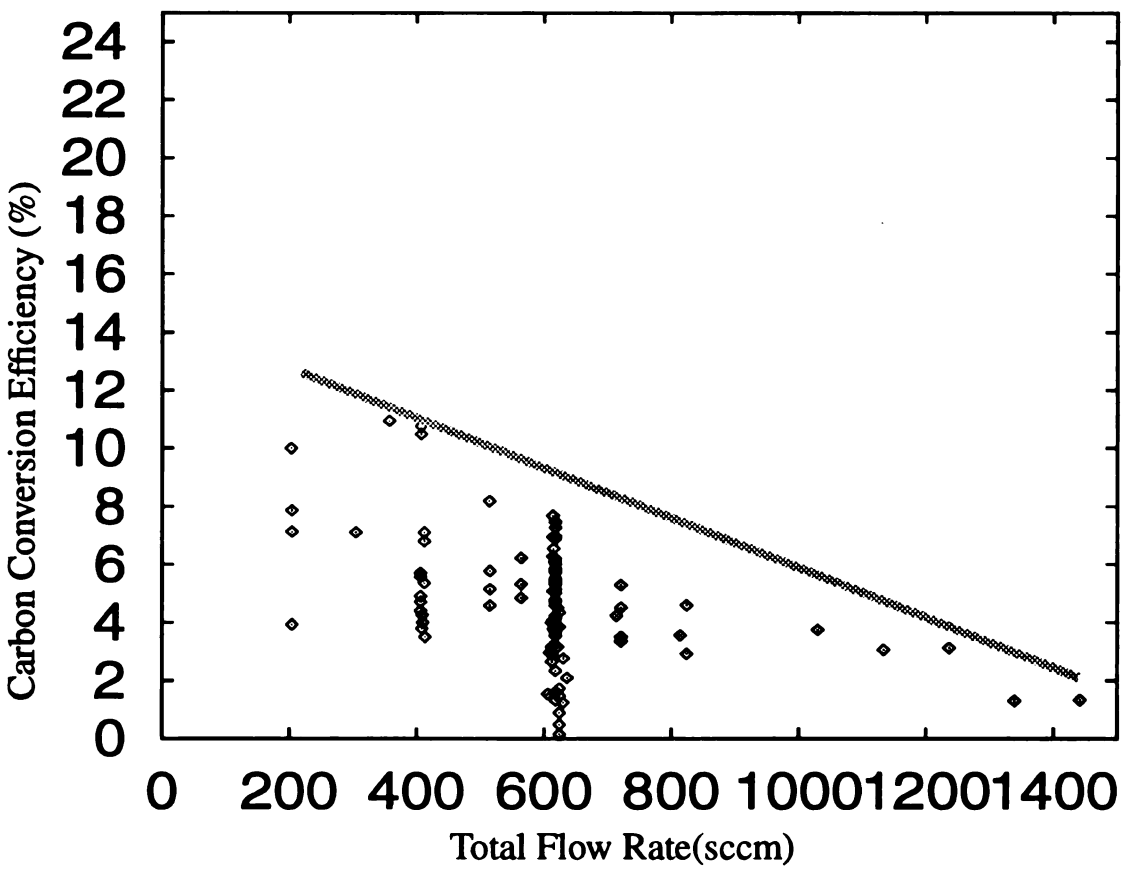

Figure 4.17 Summary of carbon conversion efficiency vs. total flow rate.

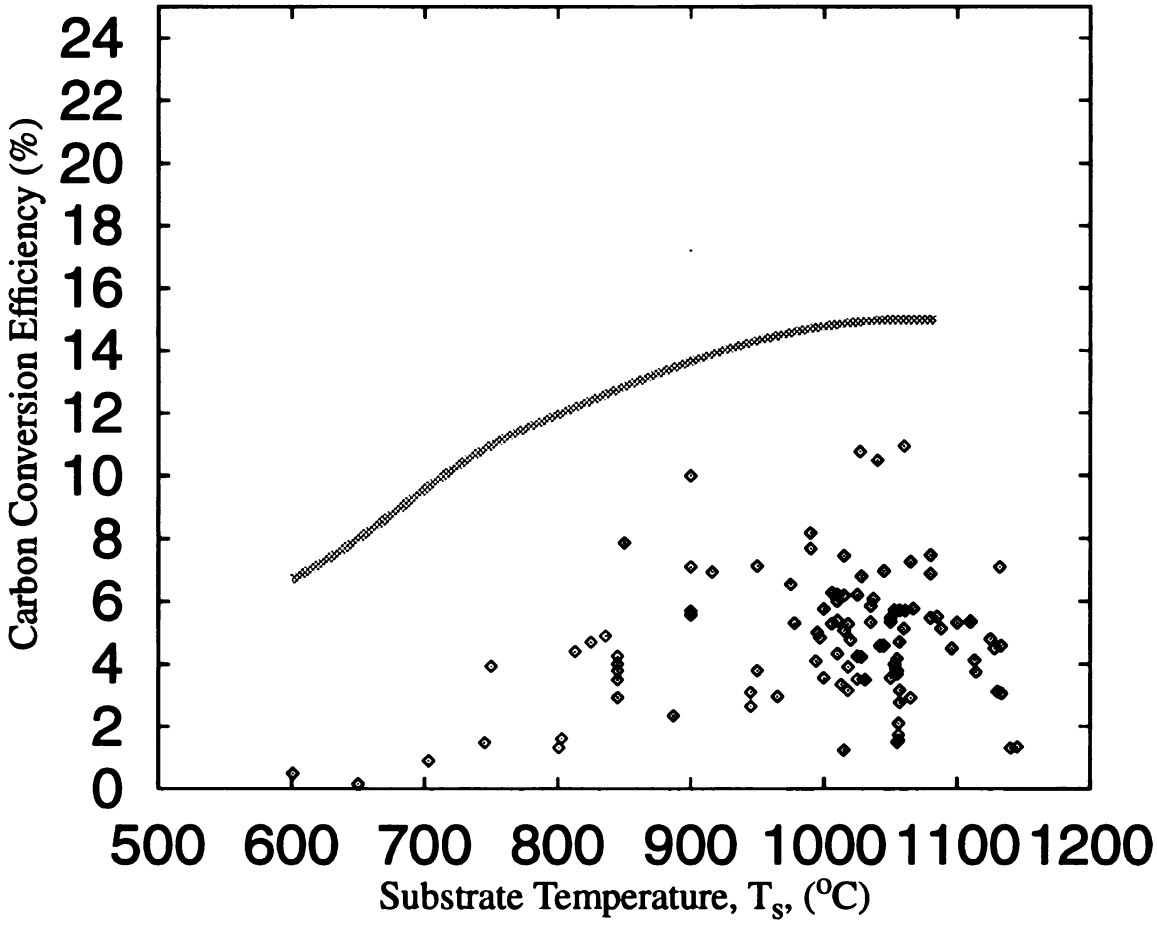

Figure 4.18 Summary of carbon conversion efficiency vs. T_S.

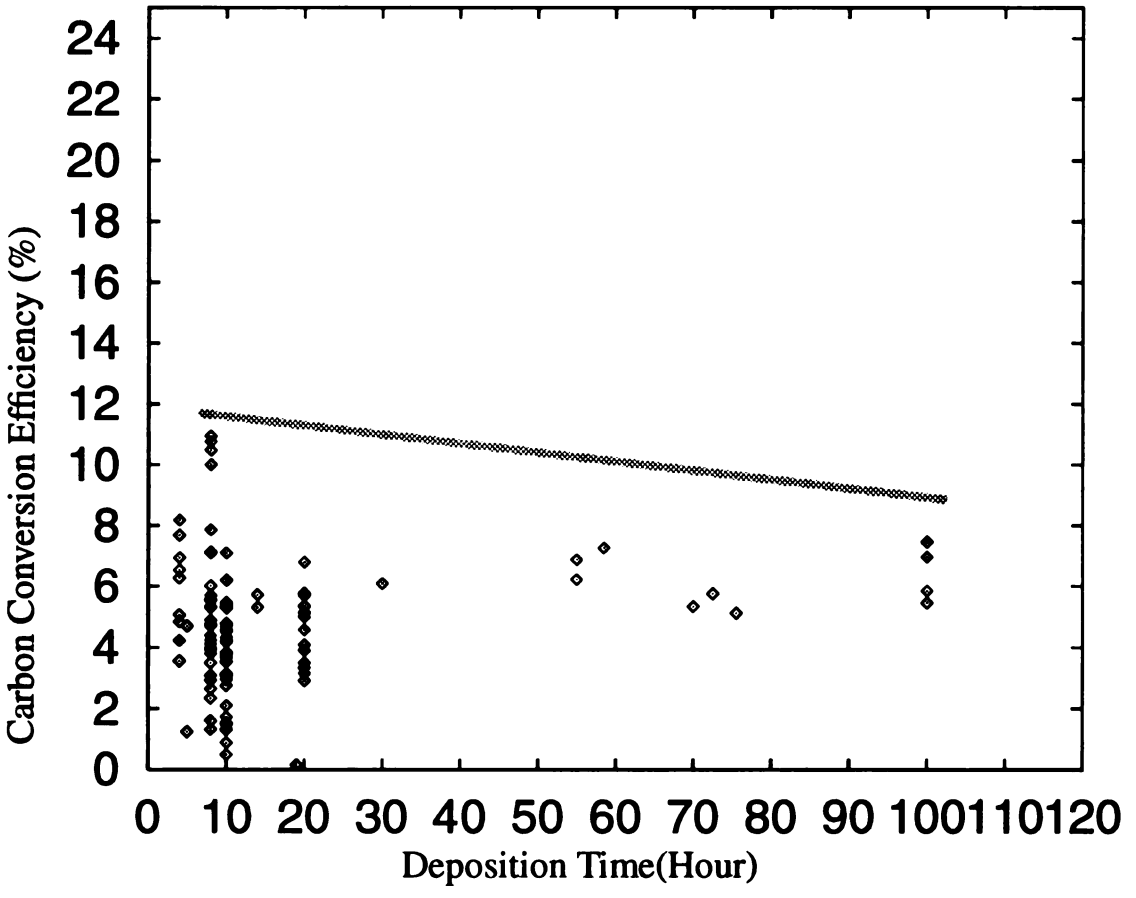

Figure 4.19 Summary of carbon conversion efficiency vs. deposition time.

4.4.2 Carbon Conversion Efficiency=f(P_t-p)

Figure 4.20 shows the effect of absorbed microwave power on carbon conversion efficiency. From Figure 4.20, the carbon conversion efficiency did not vary significantly with respect to the absorbed microwave power. Thus carbon conversion efficiency is not a strong function of the input variable of P_t-p.

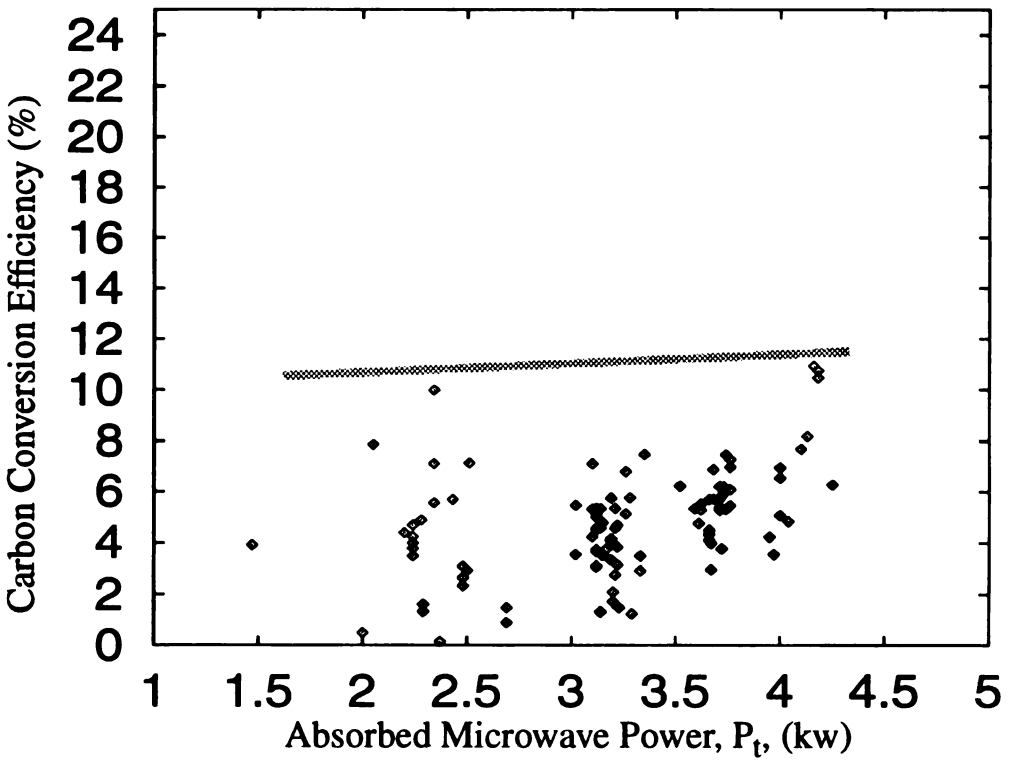

Figure 4.20 Summary of carbon conversion efficiency vs. absorbed microwave power in the high pressure MCPR.

4.5 The Growth of Thick Free Standing Diamond Films

Section 4.2 -4.4 presented the reactor performance of a high pressure MCPR diamond deposition reactor versus experimental controllable input variables. These experimental investigations yielded a " high growth recipe". Using the high growth rate input variable conditions thick diamond films were synthesized on two inch substrate. In particular, two inch diameter free-standing CVD diamond films of <110> orientation and (111) morphology with approximate thickness of 7 mm were routinely produced using high-pressure MCPR system. This recipe was derived from the experimental input parameters that produced the best growth rate, i.e., the experimental input variables were pressure=135 Torr(Figure 4.9), CH_4/H_2=3%(18/600 sccm) from Figure 4.2, total flow rate~600 sccm(Figure 4.3), substrate temperature = 1060C (Figure 4.4), deposition time = 100h (Figure 4.5), absorbed microwave power~3.5 kW(Figure 4.9). After synthesis, a free standing diamond film was produced by back etching the silicon using 50%HNO_3-25%HF-25%CH_3COOH solution. An example of the surface morphology of these films is displayed in Figure 5.21(f).

4.6 Summary

Using high pressure MCPR microwave plasma assisted diamond thin film synthesis was experimentally investigated with CH_4/H_2 gas

mixtures at 80-140Torr. Some of the important performance data is plotted in Figure 2.19, and Figure 2.20 and in Table 2.1 where it can be directly compared with the published performance of other reactors.

The performance of the high pressure MCPR can be summarized as follows:

(1) Optimum diamond film growth conditions of the high-pressure MCPR are CH_4/H_2=3-4%, f_t=600-700sccm, T_s=1060-1100C, p=120-135Torr, and $<P_V>$=30W/cm^3. The reactor performance (Υ_1) under these conditions are:

(a) linear growth rate= 6.27 m/h,

(b) total growth rate=44.68 mg/h,

(c) specific yield= 69 kW-h/g

(d) Gas flow efficiency= 0.08 mg/liter

(e) Carbon conversion efficiency=7.7%.

(2) The low pressure MCPR reactor[9],[51] operates with an area power density of 0.03-0.04 kW/cm^2, resulting in maximum linear deposition rates of approximately 0.55 μm/h. The area power densities for the high pressure MCPR is 0.15- 0.25 kW/cm^2, i.e., almost ten times the area power density of the low pressure MCPR. Interestingly, the maximum linear growth rates of the high pressure MCPR are also approximately ten times the linear growth rates of the low pressure MCPR. Thus the linear growth rate, i.e., the deposition per substrate area, increases directly as the area power density increases.

(3) A comparison of the specific yield of the moderate pressure MCPR and high pressure MCPR indicates that the energy efficiency improves considerably from 163 kW-h/g to 69 kW-h/g as the operating pressure increases, i.e., a thermal like high pressure microwave discharge improves the specific yield by a factor of two and one half.

(4) The volume in the input variable space when the diamond deposition occurs was increased considerably by changing the operating pressure of the MCPRs from a 20-80 Torr non-equilibrium plasma regime, to a 80-140 Torr thermal-like plasma regime.

(5) Carbon conversion efficiency was not significantly affected by the shift of operating the MCPRs from a non-equilibrium plasma regime to a thermal-like plasma regime.

CHAPTER FIVE

Reactor Experimental Output Performance-

Film Characteristics ($\mathbf{Y_2}$)

5.1 Introduction

Chapter 4 presented an overview of the high pressure MCPR's output reactor performance $\mathbf{Y_1}$ versus five dimensional input variable space, i.e., $\mathbf{Y_1}$= f (c, f_t, T_s, t, P_t-p). As pointed out in the summary of Chapter 4, there exists an optimum diamond growth zone in this five dimensional input variable space, i.e., the maximum diamond deposition rate takes place under the experimental input conditions of c~3%, f_t~600 sccm, T_s~1080°C, P_t~3.3 kW, and p~135 Torr. This optimum diamond growth zone can be visualized versus the two dimensional input variable space shown in Figure 4.6. In this chapter the reactor output performance $\mathbf{Y_2}$ (referred as the diamond film property) is evaluated by taking cross sectional experimental data slices from these multidimensional plots. In particular, a series of experiments were performed by observing the change in output film properties $\mathbf{Y_2}$ versus changes in one independent input variable. Experiments are varied around the maximum deposition conditions shown in Figure 4.6.

Independent experimental variables $\mathbf{U_1}$ such as methane concentration, total flow rate, and substrate temperature are the selected experimental input variables. The absorbed microwave power and pressure were fixed at the optimized conditions of 3.3 kW and 135 Torr, respectively. Reactor geometry variables $\mathbf{U_2}$ were held constant and deposition process variables $\mathbf{U_3}$ were also held constant except the deposition time, which is considered as the fourth input variable in this chapter. The plasma volume, V_d, was held approximately constant at 144 cm^3, while the volume power density as described earlier in Figure 4.9, also remains constant, i.e., $\langle P_V \rangle = P_t/V_d \sim 23$ W/cm^3. Film output properties $\mathbf{Y_2}$ that were investigated include film morphology, film texture, and film structural quality. Thus output film properties $\mathbf{Y_2}$ were investigated as a function of methane concentration, total flow rate, substrate temperature, and deposition time, i.e., $\mathbf{Y_2} = f(c, f_t, T_s, t)$.

The first set of experiments, described in Section 5.2, contain eight separate experimental runs using different methane concentrations (c=1-8%) while holding other independent experimental variables $\mathbf{U_1}$ constant such as $f_t \sim 600$ sccm, $T_s \sim 1060^oC$, $P_t = 3.22$ kW, and p=135 Torr. Reactor geometry variables $\mathbf{U_2}$ and deposition process variables $\mathbf{U_3}$ are held constant (deposition time =5h) for these eight experimental runs. Thus $\mathbf{Y_2}$ is investigated as a function of methane concentration, i.e., $\mathbf{Y_2} = f(c)$. The second set of experiments, described in Section 5.3, contain six separate

experimental runs using different total flow rates (f_t= 400, 600, 800, 1000, 1200, 1400 sccm) while holding other independent experimental variables $\mathbf{U_1}$ constant such as c=3%, T_s~1080°C, P_t= 3.22 kW, and p=135 Torr. Reactor geometry variables $\mathbf{U_2}$ and deposition process variables $\mathbf{U_3}$ (deposition time=10h) are held constant for these six experimental runs. Thus $\mathbf{Y_2}$ is investigated as a function of total flow rates, i.e., $\mathbf{Y_2}$=f(f_t). The third set of experiments, described in Section 5.4, contain six separate experimental runs using different substrate temperatures (T_s=950, 1025, 1050, 1075, 1100, 1125 °C) by varying the number of insulation discs in water-cooled substrate holder setup (see Section 3. 6) while holding other reactor geometry variables $\mathbf{U_2}$ such as the quartz dome size and the substrate material constant. Independent experimental variables $\mathbf{U_1}$ such as c, f_t, P_t, and p are held constant at 3%, 618 sccm, 3.22kW, and 135 Torr, respectively. Deposition process variables $\mathbf{U_3}$ were also held constant (deposition time=10h) for these six experiments. Thus $\mathbf{Y_2}$ is investigated as function of substrate temperature, i.e., $\mathbf{Y_2}$=f(T_s). The fourth set of experiments, described in Section 5.5, contain six separate experimental runs using different deposition time (t= 5, 10, 20, 30, 55, 100 h) while holding other deposition process variables $\mathbf{U_3}$ such as starting and shut-down procedures and seeding procedures constant. Independent experimental variables $\mathbf{U_1}$ such as c, f_t, T_s, P_t, and p are held constant at 3%, 618 sccm, 3.22kW,1080°C, and 135 Torr, respectively. Reactor geometry

variables $\mathbf{U_2}$ were held constant. Thus $\mathbf{Y_2}$ is investigated as function of deposition times, i.e., $\mathbf{Y_2}$=f(t).

5.2 Effect of Methane Concentration (c)

5.2.1 Introduction

This section presents an experimental investigation of the film output properties $\mathbf{Y_2}$ as a function of methane concentration. Eight experiments were performed by starting at optimized film growth conditions and then carefully varying methane concentrations from 1% to 8%. This section first presents the experimental conditions for the eight experiments that were investigated and then the influence of methane concentration on film growth rate, film morphology, film texture, and film structural quality is described.

5.2.2 Experimental Variables

(A) Input variables(U):

(1) Controllable input variables (U_1):

a) Gas mixture: **Variable, c=1% to 8%,**

b) Total flow rate~600 sccm,

c) Substrate temperature=1058^{0}C,

d) Absorbed microwave power=3.22 kW,

e) Deposition pressure=135 Torr (18 KPa),

(2) Reactor geometry variable(U_2):

a) Quartz dome size: 5˝ in diameter,

b Water cooling state configuration: fixed (see Section 3.6.3.5)

c) Substrate: 2˝ (100) silicon substrate

(3) Deposition process variables(U_3):

a) Deposition time=5 h,

b) Substrate seeding procedure: fixed(see Section 3.3.1)

c) Start-up and shut-down procedures: fixed (see Section 3.3.2),

(B) Internal variables(**X**):

(1) Power Density= 23 W/cm^3,

(2) Area Power Density= 0.16 kW/cm^2,

(3) Plasma volume~144 cm^3.

5.2.3 Growth Rate=f(c)

The dependence of diamond film weight gain and growth rate on methane concentration is shown in Figure 5.1. As might be expected, the growth rate increases with increasing methane flow rate and drops at high methane concentrations (>3.5%). The possible explanation is that as CH_4 concentration is increased for a constant hydrogen flow rate, the number of atomic hydrogen is no longer sufficient to etch sp^2 graphite.

Thus the high-order growth of diamond can not be continued on the layer of graphite, resulting in a lower growth rate and the formation the black cauliflower-like microcrystalline gains.

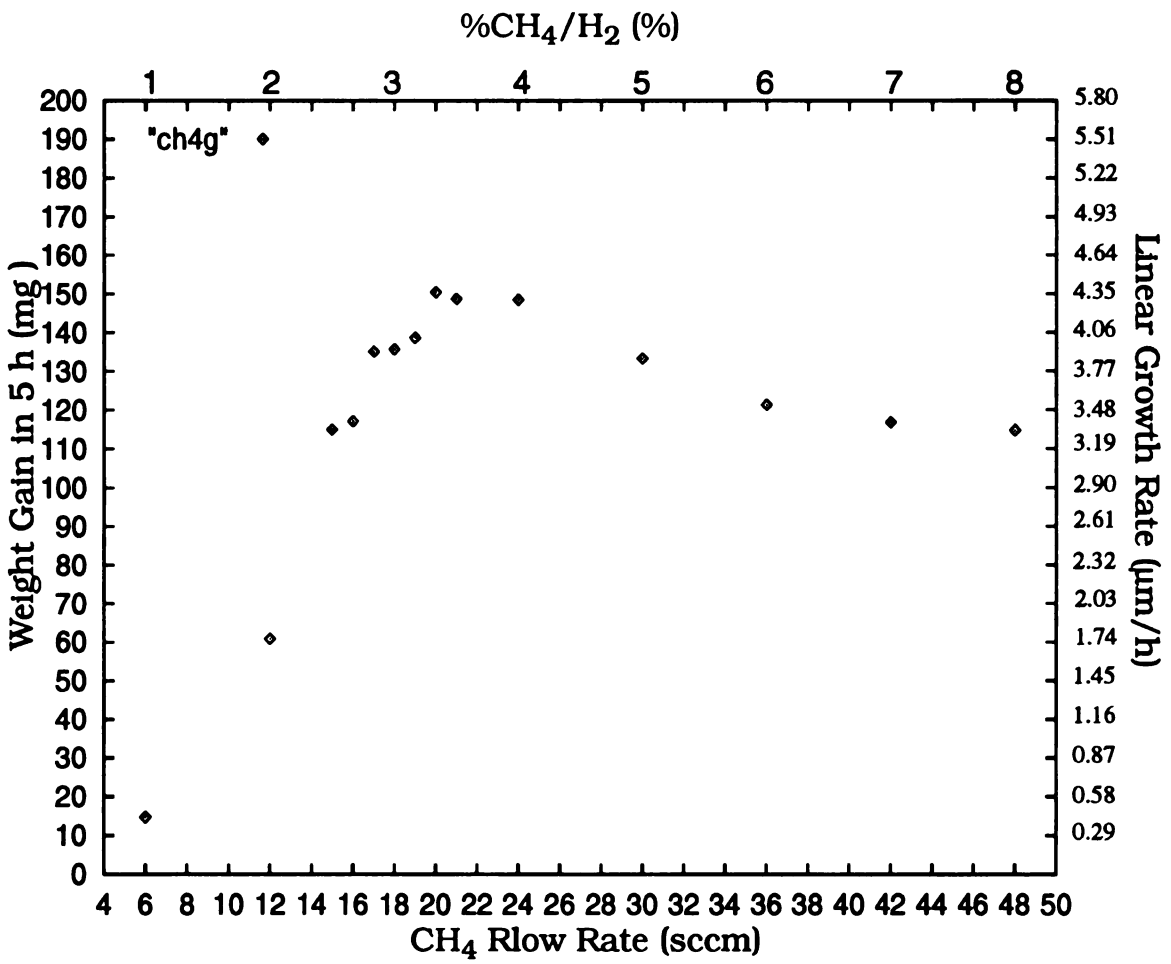

Figure 5.1 Linear growth rates (weight gain) versus methane concentrations. The experimental conditions are shown in Section 5.2.2

5.2.4 Film Morphologye=f(c)

The Scanning Electron Microscopy photographs of the films deposited for 5 hours using different methane concentrations, c, in hydrogen are shown in Figure 5.2(a) - 4(h). At c=1% [see Fig.5.2(a)], only small diamond crystals were formed. These crystals have (100) and (110) cubo-octahedron morphologies. The discontinuous diamond films that were obtained at c=1% deposition condition, indicate the characteristic source gas boundary (lowest methane concentration) for the high pressure MCPR. When c=2% [see Fig.5.2(b)], the film surfaces consist of densely populated diamond grains. As shown in Fig.5.2(b), the diamond films consist of well-faceted grains having square (100) faces and some (110) roof-like facets. When c=3%[see Fig.5.2(c)], the film surfaces show both (110) roof-like and (111) triangular morphologies. At c=4%[see Fig.5.2(d)] (110) roof-like facets become less and (111) triangular facets dominate. When c=5%, the films completely exhibit (111) triangular morphologies. For 6% < c <8%, the film became microcrystalline and there is no crystallographic planes of diamond observed. The surface of Fig.5.2(f) to (h) has the so-called "cauliflower" structure.

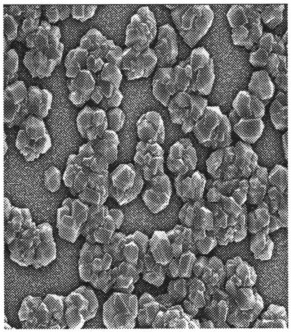

Figure 5.2(a) c=1%

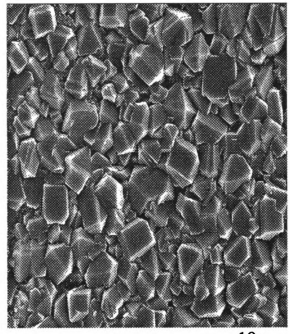

Figure 5.2(b) c=2%

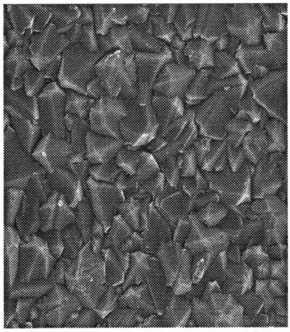

Figure 5.2(c) c=3%

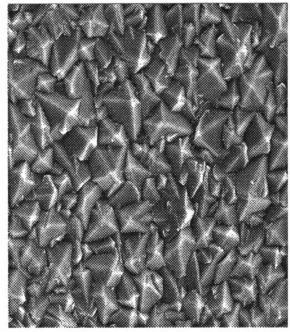

Figure 5.2(d) c=4%

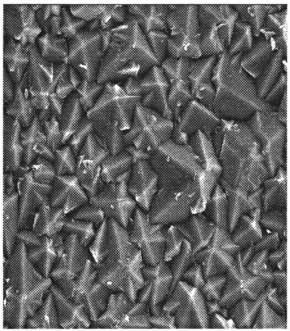

Figure 5.2(e) c=5%

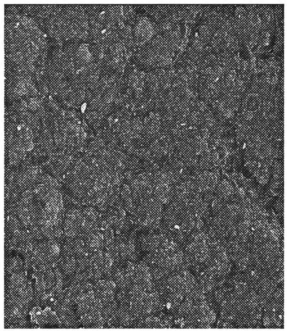

Figure 5.2(f) c=6%

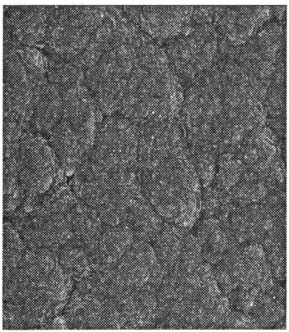

Figure 5.2(g) c=7%

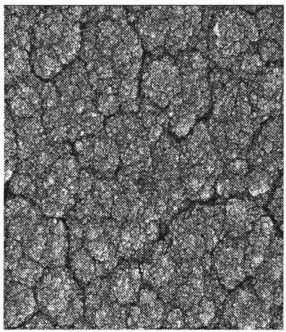

Figure 5.2(h) c=8%

Figure 5.2(a)-(h) Surface morphology vs. $\%CH_4/H_2$ varied from 1% to 8%.

5.2.5 Film Texture=f(c)

The resulting XRD spectra of different methane concentrations are shown in Figure 5.3(a) to (g). Figure 5.4 shows the ratio of intensities of <220> and <111> peaks from XRD. The positions of the lines at $2\theta \sim 43.9^{o}$ and $2\theta \sim 75.3^{o}$ are the indication of the <111> film texture and <220> film texture. In order to analyze the degree of diamond grain orientation, the intensity of each line was recorded from the original computer control system with the same sensitivity of x-ray detection for all spectra. At low methane concentrations of c=1% and 2%, the I(220) / I(111) ratio is less than one, indicating that the films have no preferred film texture. As methane concentration increased to c=4% and 5%, the I(220) / I(111) ratio becomes larger than one, indicating that the degree of <110> orientation was further enhanced and the films were textured in the <110> direction. When 6% < c < 8%, the I(220) / I(111) ratio decreases to the value of 0.4, indicating the presence of the cauliflower films showing no preferred film texture.

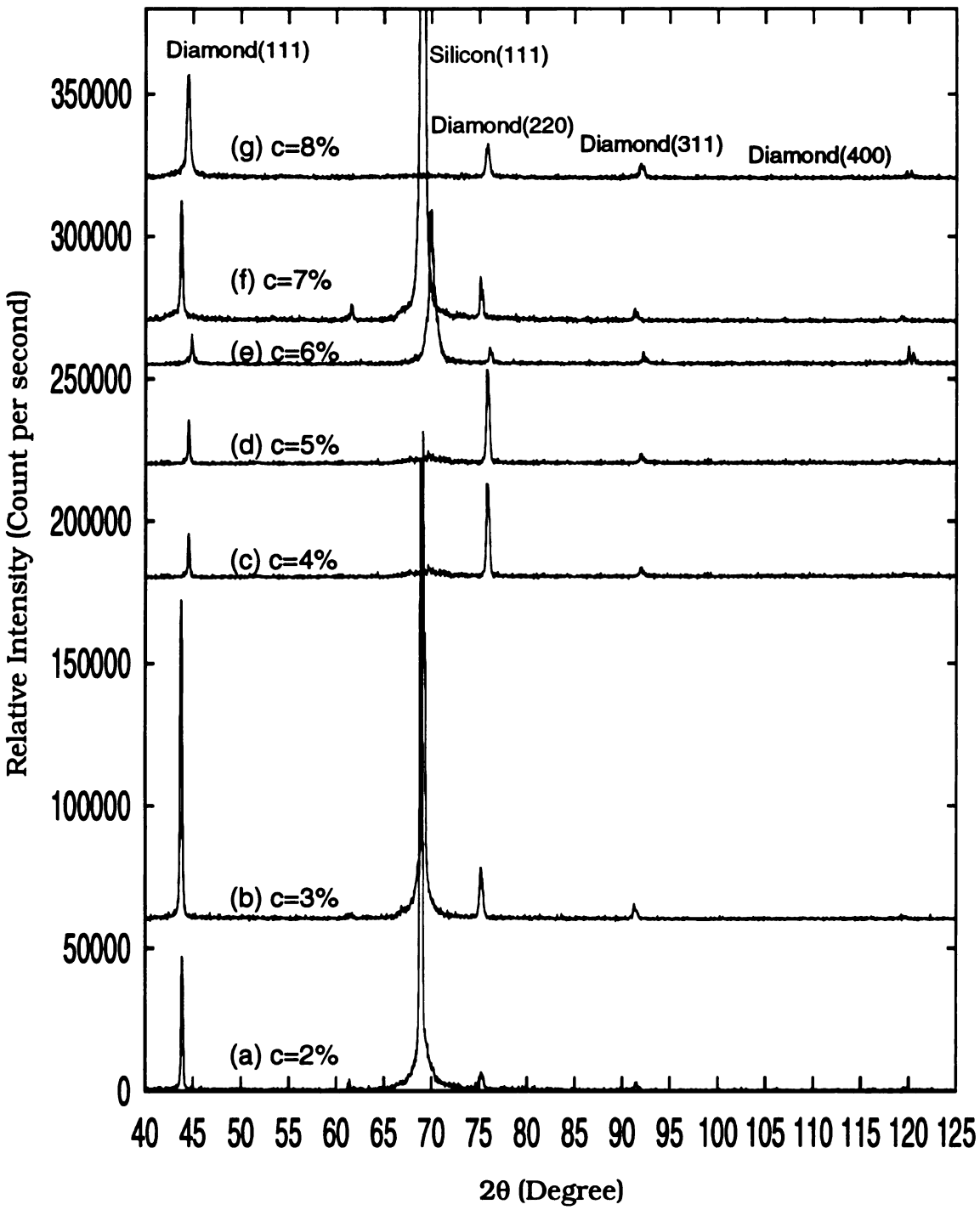

Figure 5.3 The X-ray diffraction spectra as a function of methane concentrations of (a) 2%, (b) 3%, (c) 4%, (d) 5%, (e) 6%, (f) 7% and (g) 8%. Maximum ratio of I(220)/I(111) was observed at c=4% and 5%. They are summarized in Figure 5.4.

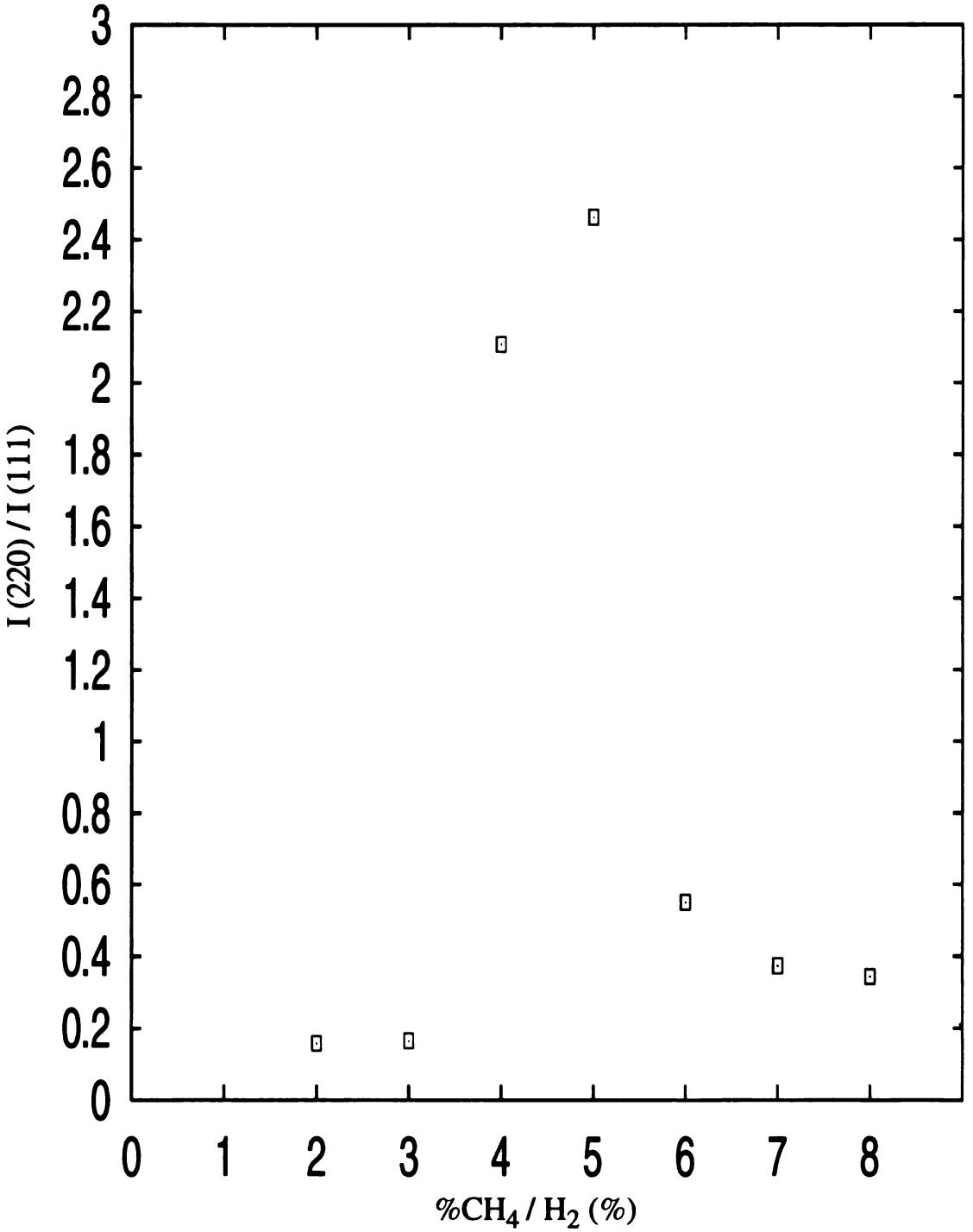

Figure 5.4 The ratio of the XRD peak height of (220) to (111) versus the methane concentration. The experimental conditions are shown in Section 5.2.2.

5.2.6 Film Structural Quality=f(c)

Typical Raman spectra of the diamond films deposited on Si(100) at eight different concentrations of methane, ranging from 1% to 8%, are shown in Figure 5.5. The Raman spectra shown in Figure 5.5 exhibit three main features: (1) the appearance of the peak at 1332 cm^{-1} from 1% to 8%, which is the characteristic line of crystalline diamond, (2) the appearance of a broad peak centered at about 1580 cm^{-1} for the methane concentration above 6%, which is characteristic of polycrystalline graphite or amorphous carbon with graphite bonding, (3) the 6% and 8% films show a broad peak at about 1280 cm^{-1} whose origin is not yet fully understood. For 6% < c <8%, the films exhibit a relatively low diamond peak at 1332 cm^{-1} and relatively strong contribution from nondiamond carbon. The films that contain certain amount of nondiamond carbon exhibit the cauliflower morphology(shown in Figure 5.2(f)-(h)). Compared to 6% < c <8%, the Raman spectra of the 1% < c< 5% films display a sharp diamond peak at 1332 cm^{-1} and no contribution from nondiamond carbon. The films show well-faceted crystalline diamond morphologies as shown in Figure 5.2(a)-(e).

Figure 5.6 displays the full width at half maximum (FWHM) of the 1332 cm^{-1} peak as a function of methane concentration. A FWHM of 2.0 cm^{-1} is plotted as a reference for natural diamond. As seen in Figure 5.6, the FWHM decreases from 17.43 cm^{-1} for the c=1% to 8.77 cm^{-1} for c=2%

and remains approximately constant up to 5% methane concentration.

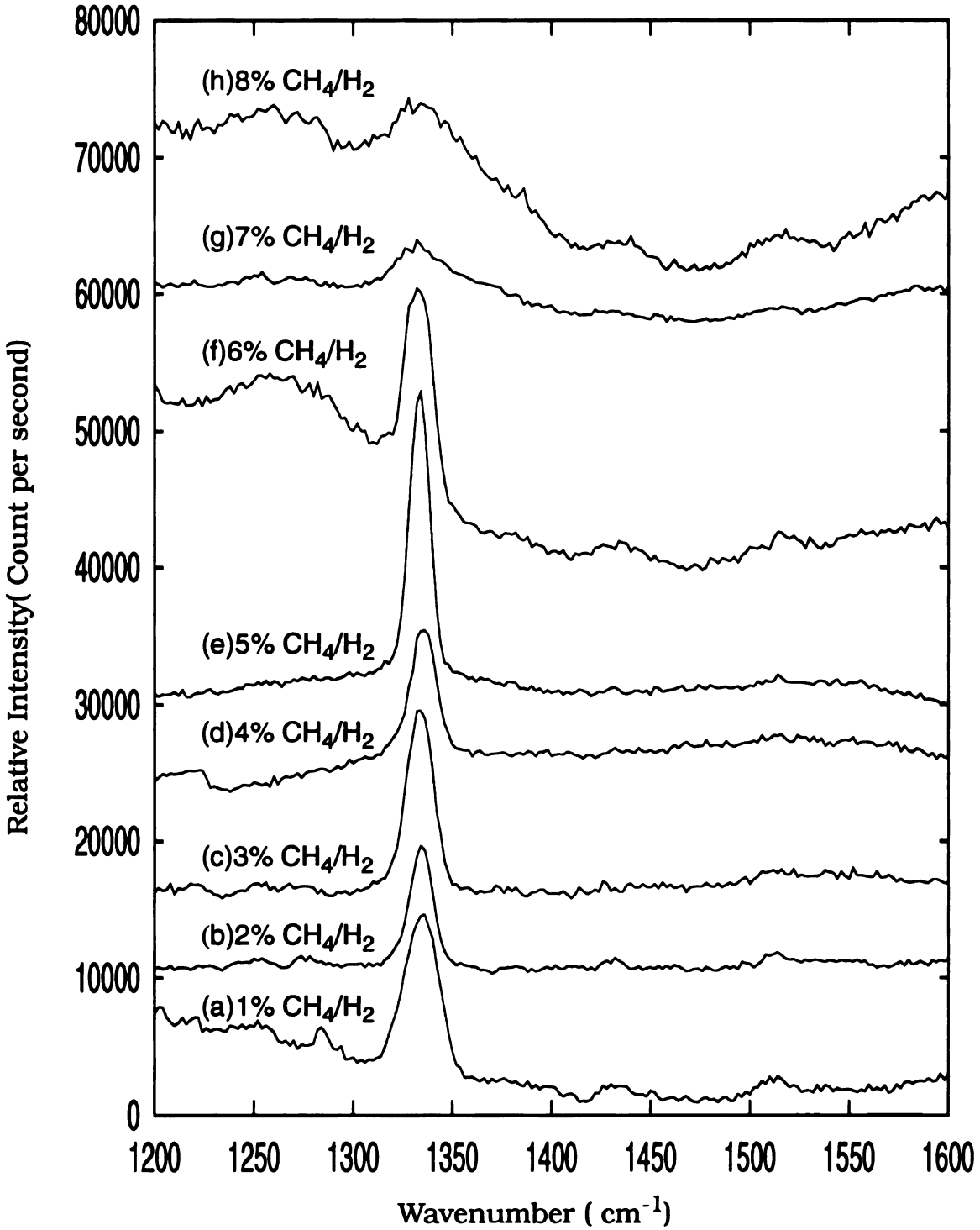

Figure 5.5 Raman spectra of various methane concentrations.The Experimental conditions are shown in Section 5.2.2.

The FWHM then increased abruptly from 8.42 cm^{-1} for c=5% to 72.14 cm^{-1} for c=8%.

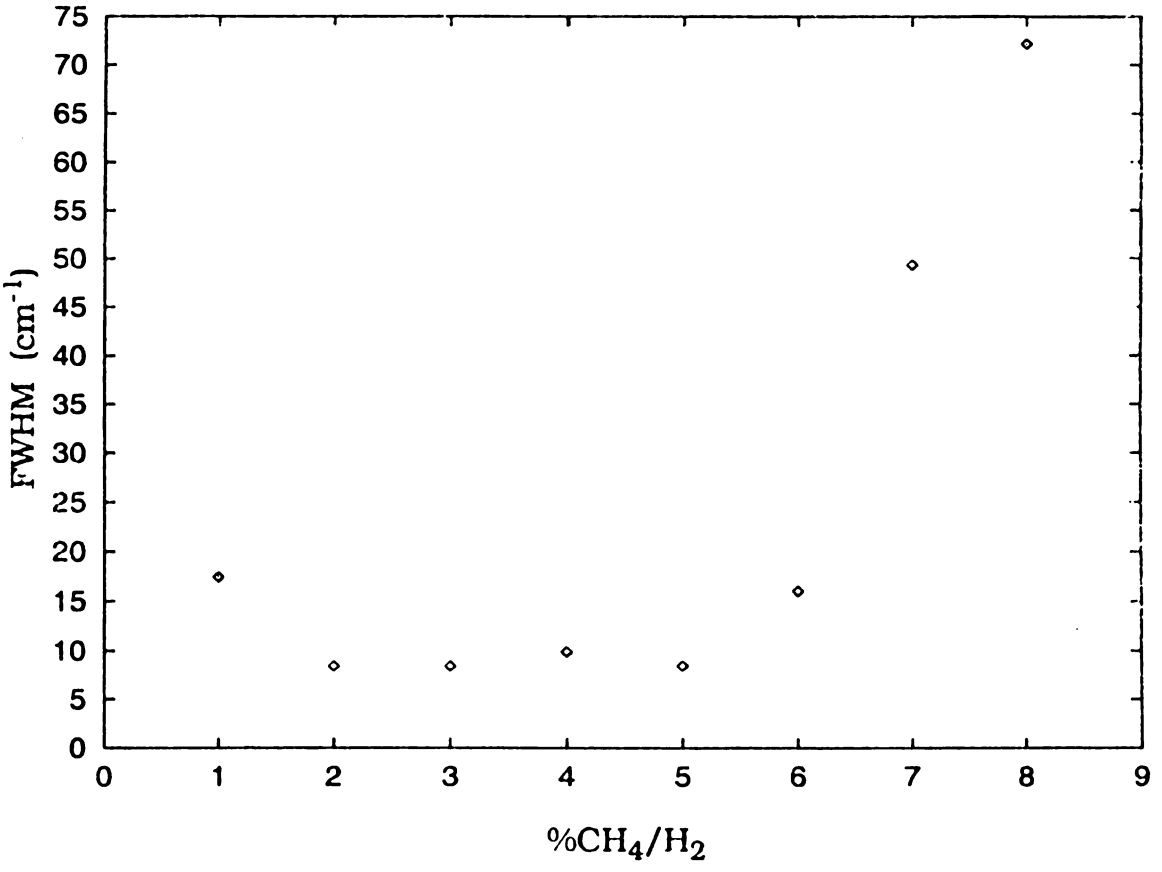

Figure 5.6 FWHM of Raman spectra as a function of CH_4/H_2 concentration. The experimental conditions are shown in Section 5.2.2.

5.3 Effect of Total Flow Rate (f_t)

5.3.1 Introduction

This section presents an experimental investigation of the film output properties $\mathbf{Y_2}$ as a function of total flow rate. Six experiments were performed by varying the flow rate from 412 sccm to 1442 sccm around optimized deposition conditions. The section first describes the experimental conditions for these six experiments and then the variation of film growth rate, film morphology, film texture, and film structural quality versus total flow rates are described in the later section.

5.3.2 Experimental Variables

(A) Input variables(U):

(1) Controllable input variables (U_1):

a) Gas mixture: 3%CH_4/H_2,

b) Total flow rate= **Variable from 412-1442 sccm**,

c) Substrate temperature=1080°C,

d) Absorbed microwave power=3.22 kW,

e) Deposition pressure=135 Torr (18 KPa),

(2) Reactor geometry variable(U_2):

a) Quartz dome size: 5" in diameter,

b Water cooling state configuration: fixed (see Section 3.6.3.5

c) Substrate: 2″ (100) silicon substrate

(3) Deposition process variables(U_3):

a) Deposition time=10 h,

b) Substrate seeding procedure: fixed(see Section 3.3.1),

c) Start-up and shut-down procedures: fixed (see Section 3.3.2),

(B) Internal variables(X):

(1) Power Density= 23 W/cm^3,

(2) Area Power Density= 0.16 kW/cm^2,

(3) Plasma volume~144 cm^3.

5.3.3 Growth Rate=f(f_t)

The effect of the total flow rate (denoted as f_t) on film growth rate is shown in Figure 5.7. The experimental conditions for different flow rate (CH_4/H_2=12/400, 18/600, 24/800, 30/1000,36/1200 and 42/1400 sccm) are shown in Section 5.4.2. It is noted that CH_4/H_2 concentration is kept at 3% for different flow rates. As shown in Figure 5.7, the growth rate increased from 3.92 μm/h at CH_4/H_2=12/400 sccm and increases to a maximum of 5 μm/h at CH_4/H_2=30/1000 sccm and then decreases to a relatively low growth rate of 2.61 μm/h at CH_4/H_2=42/1400 sccm. Therefore growth rate of the diamond film is affected by flow rate while CH_4/H_2 concentration, pressure, substrate temperature, microwave

input power and deposition time remain unchanged.

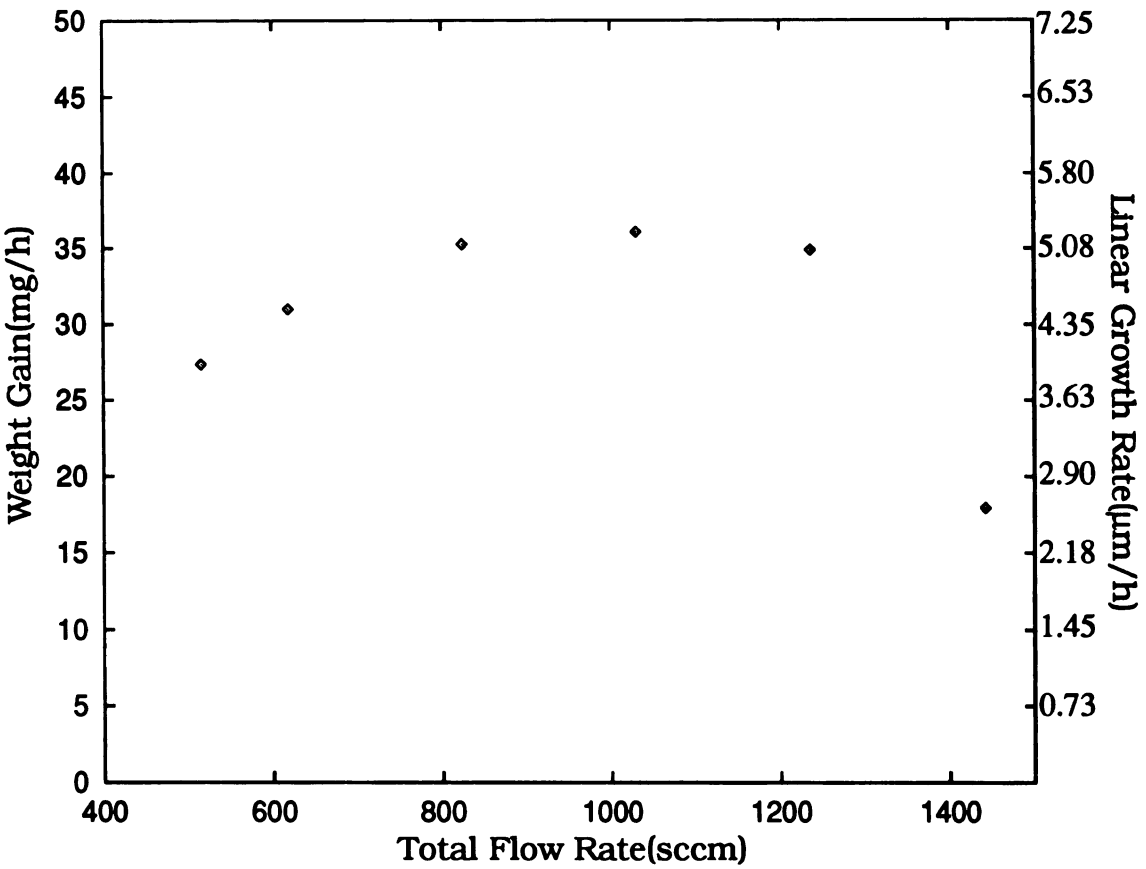

Figure 5.7 Linear growth rate as a function of total flow rate at fixed methane/hydrogen concenctration(3%).

5.3.4 Film Morphology=f(f_t)

The film morphologies that resulted as the total flow rate was varied are shown in Figure 5.8(a)-(f). As shown diamond films exhibit mixed (110) roof-like and (111) triangular morphologies when f_t=412 sccm(CH_4/

H_2= 12/400), 618 sccm(CH_4/H_2=18/600 sccm), and 824 sccm (CH_4/ H_2=24/800 sccm) are used. As f_t increases to 1030 sccm (CH_4/H_2 =30/ 1000 sccm) the film exhibits completely (111) triangular morphology. When flow rate further increases to 1236 sccm(CH_4/H_2 =36/1200 sccm), (110) roof-like facets are again observed in the film. As flow rate increases to 1442 sccm(CH_4/H_2=42/1400 sccm), the film shows (100), (110) and (111) morphologies. It is noted that the maximum growth rate again occurs when the film completely exhibits (111) triangular morphology at flow rate of CH_4/H_2 =30/1000 sccm. Also (100) facets are observed in the film that produced at CH_4/H_2 =42/1400 sccm, which has the minimum film growth rate.

Figure 5.8(a) f_t=412 sccm

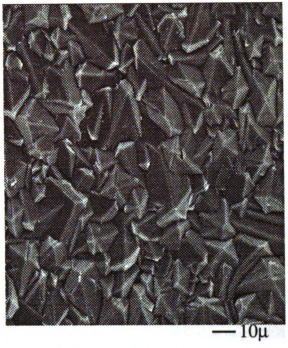

Figure 5.8(b) f_t=618 sccm

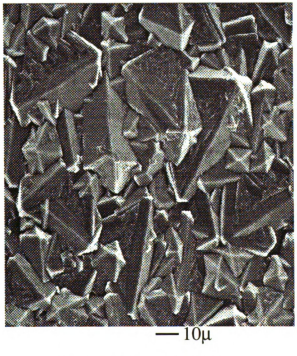

Figure 5.8(c) f_t=824 sccm

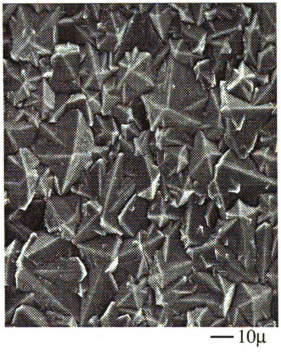

Figure 5.8(d) f_t=1030sccm

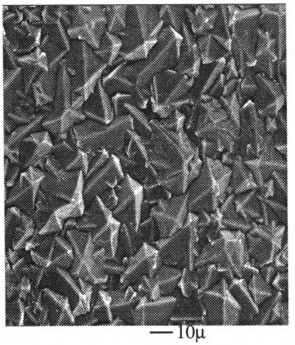

Figure 5.8(e)f_t=1236 sccm

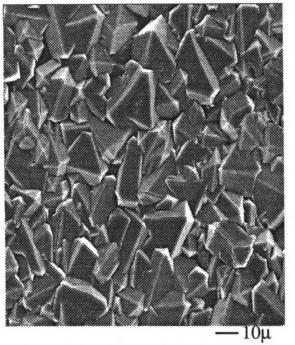

Figure 5.8(f) f_t=412 sccm

Figure 5.8(a)-(f) Film morphologies vs. total flow rates. The experimental conditions are shown in Section 5.3.2.

5.3.5 Film Texture=f(f_t)

The XRD spectra of diamond films synthesized by different total flow rates are shown in Figure 5.9. Ratios of I(220) to I(111) for different f_t are shown in Figure 5.10. As shown in Figure 5.10 the relative height of I(220) with respect to I(111) reaches its maximum at f_t=618 sccm (CH_4/H_2 =18/600).The films synthesized for 10 h under the conditions shown in Section 5.4.2 show no preferred textures at f_t=412 sccm (CH_4/H_2 =12/400) and f_t=1442 sccm(CH_4/H_2 =42/1400 sccm) and exhibit <110> texture at f_t=618 sccm (CH_4/H_2=18/600), 824 sccm (CH_4/H_2 =24/800), 1236 sccm (CH_4/H_2 =36/1200 sccm).

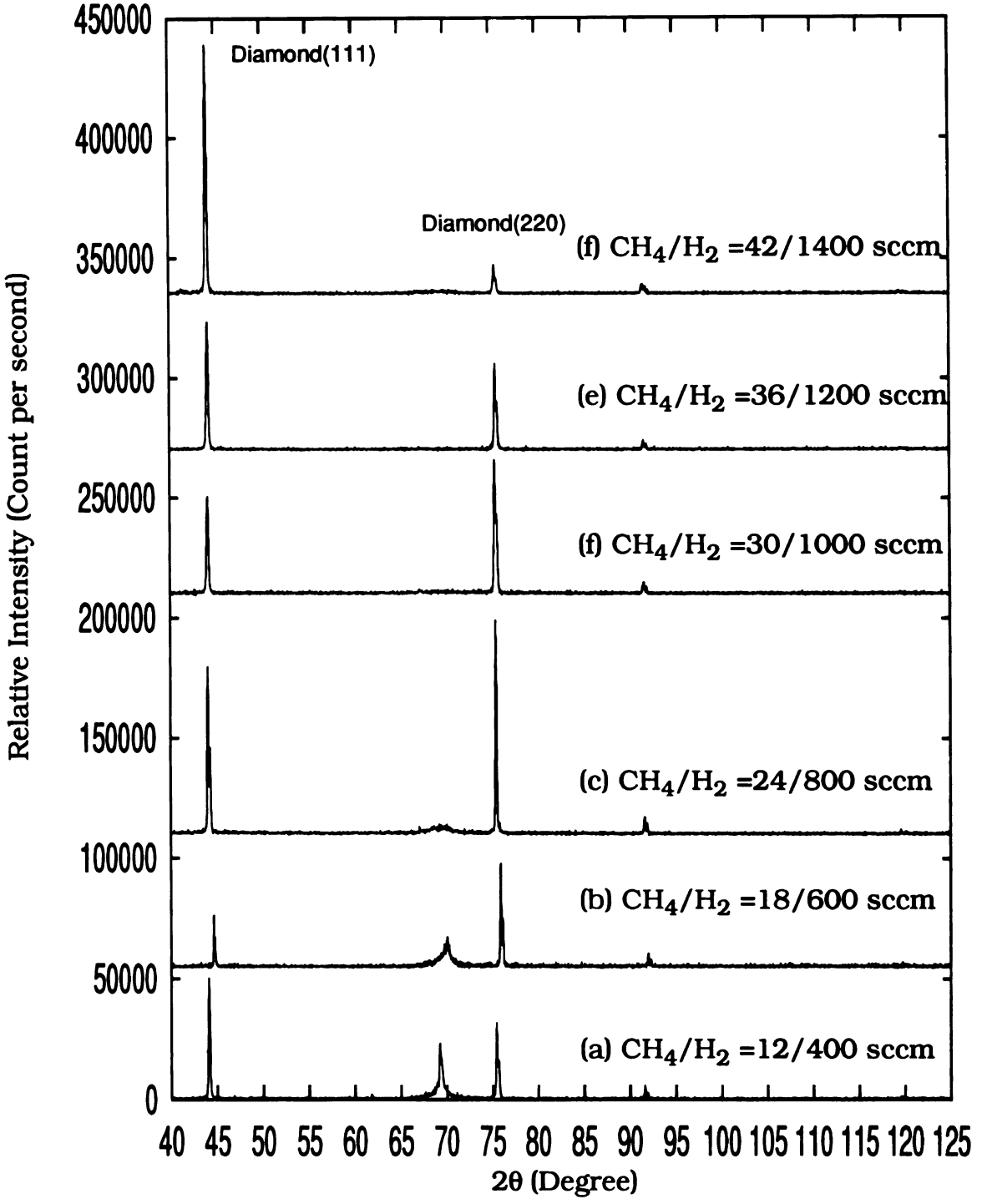

Figure 5.9 XRD spectra of diamond films synthesized by CH_4/H_2 flow rates of (a)12/400 sccm, (b)18/600 sccm, (c) 24/800 sccm, (d) 30/1000 sccm, (e) 36/1200 sccm and (f) 42/1400 sccm, using the experimental conditions described in Section 5.3.2.

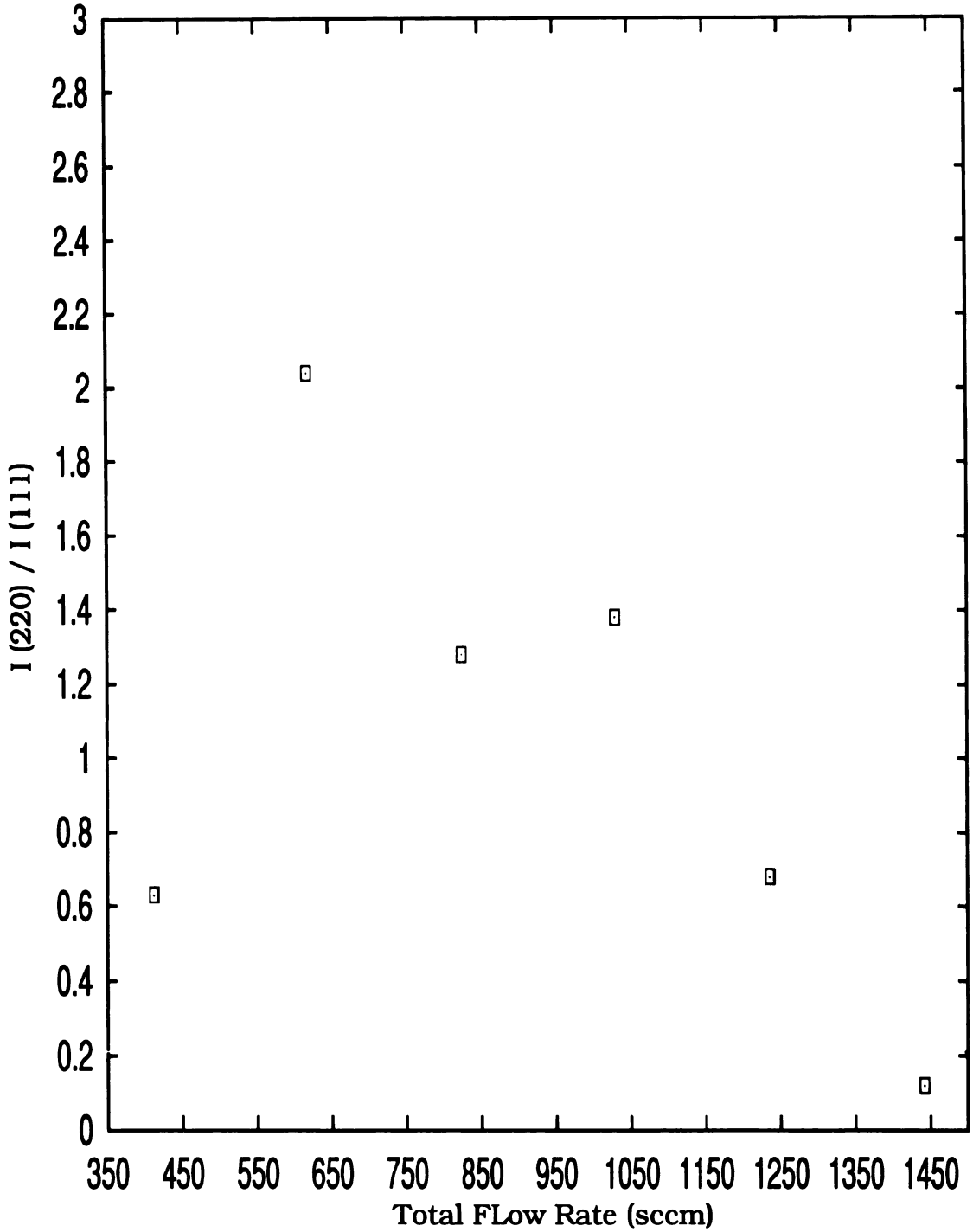

Figure 5.10 The XRD height of (220) relative to that of (111) as function of total flow rate in microwave plasma cavity system. The experimental conditions for these experiments are described in Section 5.3.2.

5.3.6 Film Structural Quality=f(f_t)

Raman spectra of diamond film produced by different flow rates are displayed in Figure 5.11. The FWHM of these Raman spectra are in Figure 5.12. As shown in Figure 5.12, FWHM remains approximately constant at 5.85 cm^{-1} for flow rates of f_t=412, 618, 824 sccm and decreases to 4.79 cm^{-1} at f_t=1236 sccm and further decreases to 3.50 cm^{-1} at f_t=1442 sccm, which has the FWHM that is very close to that of nature diamond, i.e., 2.3 cm^{-1}.

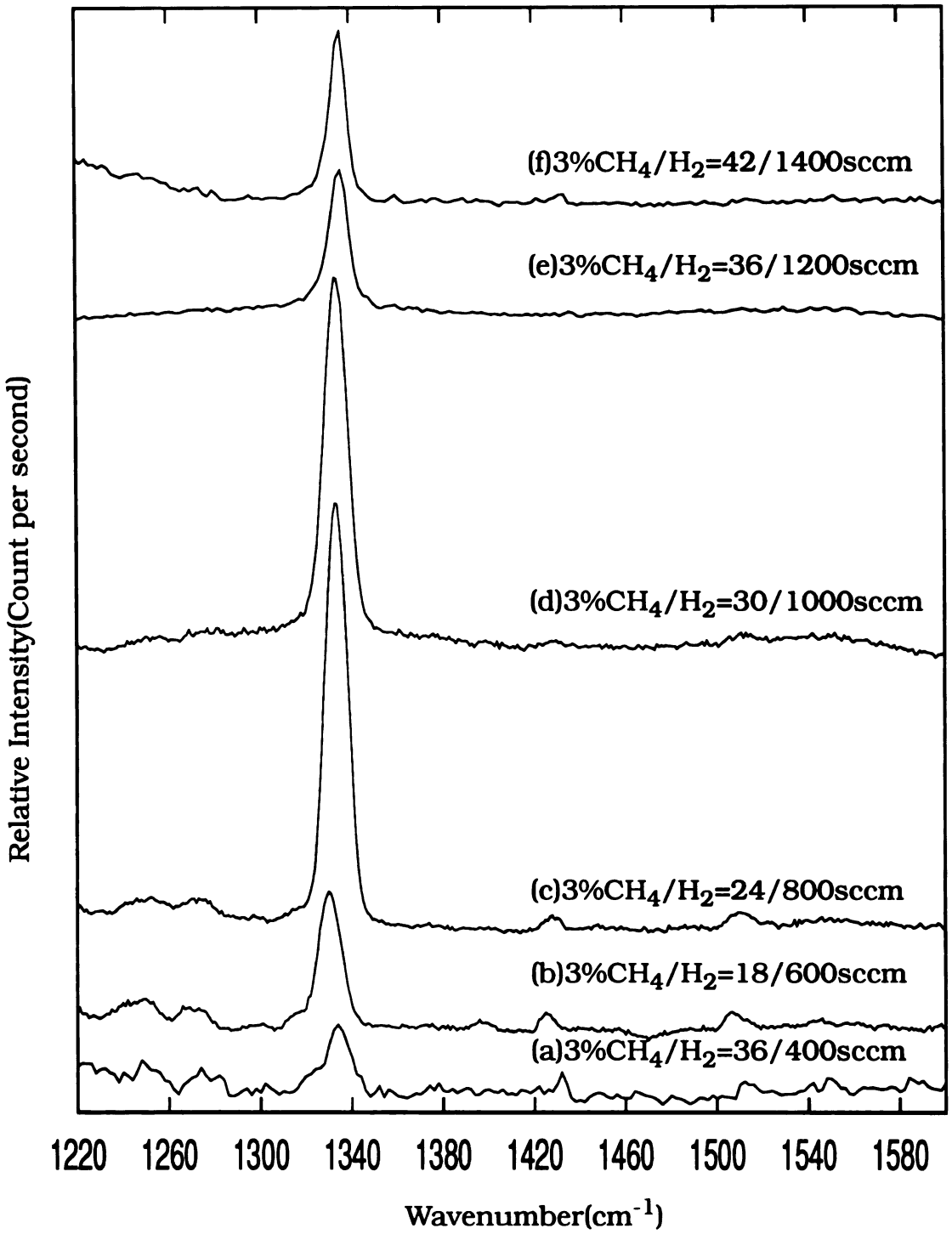

Figure 5.11 The effect of total flow rate on Raman spectrum. The experimental conditions are listed in Section 5.3.2.

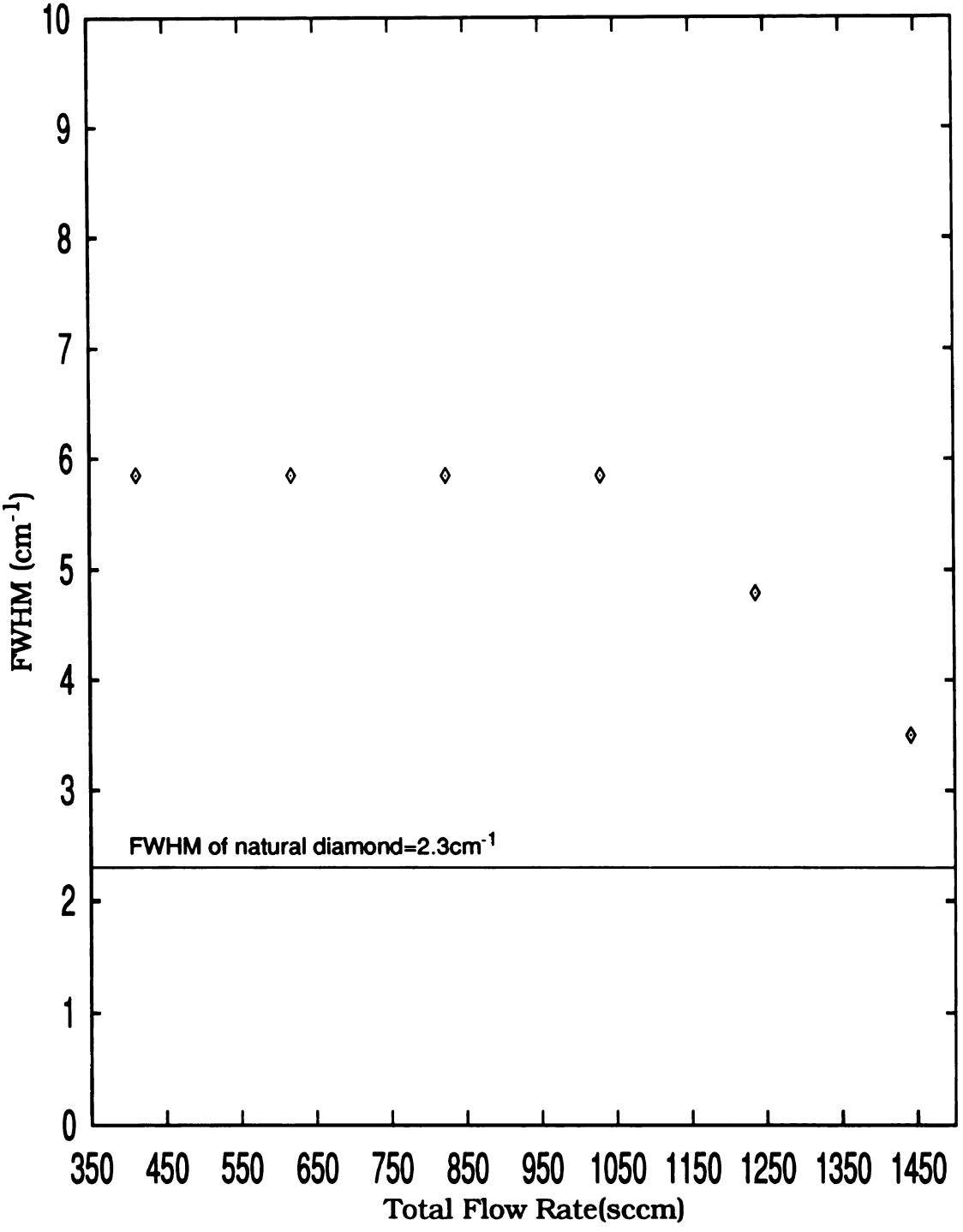

Figure 5.12 The effect of total flow rate on FWHM of Raman spectrum. The experimental conditions are shown in Section 5.3.2.

5.4 Effect of Substrate Temperature (T_s)

5.4.1 Introduction

The six experiments presented in this section were performed by varying T_s from 950 to 1125°C while holding the other experimental variables constant.This section first describes the experimental conditions for the six experiments that were investigated and then the influence of substrate temperatures on film growth rate, film morphology, film texture, and film structural quality are presented in the following section.

5.4.2 Experimental Variables

(A) Input variables(U):

(1) Controllable input variables (U_1):

a) Gas mixture: 3%CH_4/H_2(18/600 sccm),

b) Total flow rate= 618 sccm,

c) Substrate temperature: **Variable from 950-1125°C**,

d) Absorbed microwave power=3.22 kW,

e) Deposition pressure=135 Torr (18 KPa),

(2) Reactor geometry variable(U_2):

a) Quartz dome size: 5″ in diameter,

b Water cooling state configuration: fixed (see Section 3.6.3.5

c) Substrate: 2˝ (100) silicon substrate

(3) Deposition process variables(U_3):

a) Deposition time=10 h,

b) Substrate seeding procedure: fixed(see Section 3.3.1)

c) Start-up and shut-down procedures: fixed (see Section 3.3.2),

(B) Internal variables(**X**):

(1) Power Density= 23 W/cm^3,

(2) Area Power Density= 0.16 kW/cm^2,

(3) Plasma volume~144 cm^3,

5.4.3 Growth Rate=f(T_s)

The growth rate as a function of substrate temperatures is shown in Figure 5.13. The rest of experimental conditions are shown in Section 5.4.2. A water cooling stage, as shown in Figure 3.12, is utilized to control the substrate temperature by adding or removing the graphite holder layers. Therefore the substrate temperature can be independently studied without changing the experimental input variables such as deposition pressure, MW input power, substrate position which could also influence the substrate temperature. Experiments with substrate temperatures of 950C, 1025C, 1050C, 1075C, 1100C and 1125C were performed at c=3% while holding the other experimental variable approximately constant. As shown, growth rate increases from T_s=950C and reaches a maximum at

T_s=1100C and then decreases with increasing T_s.

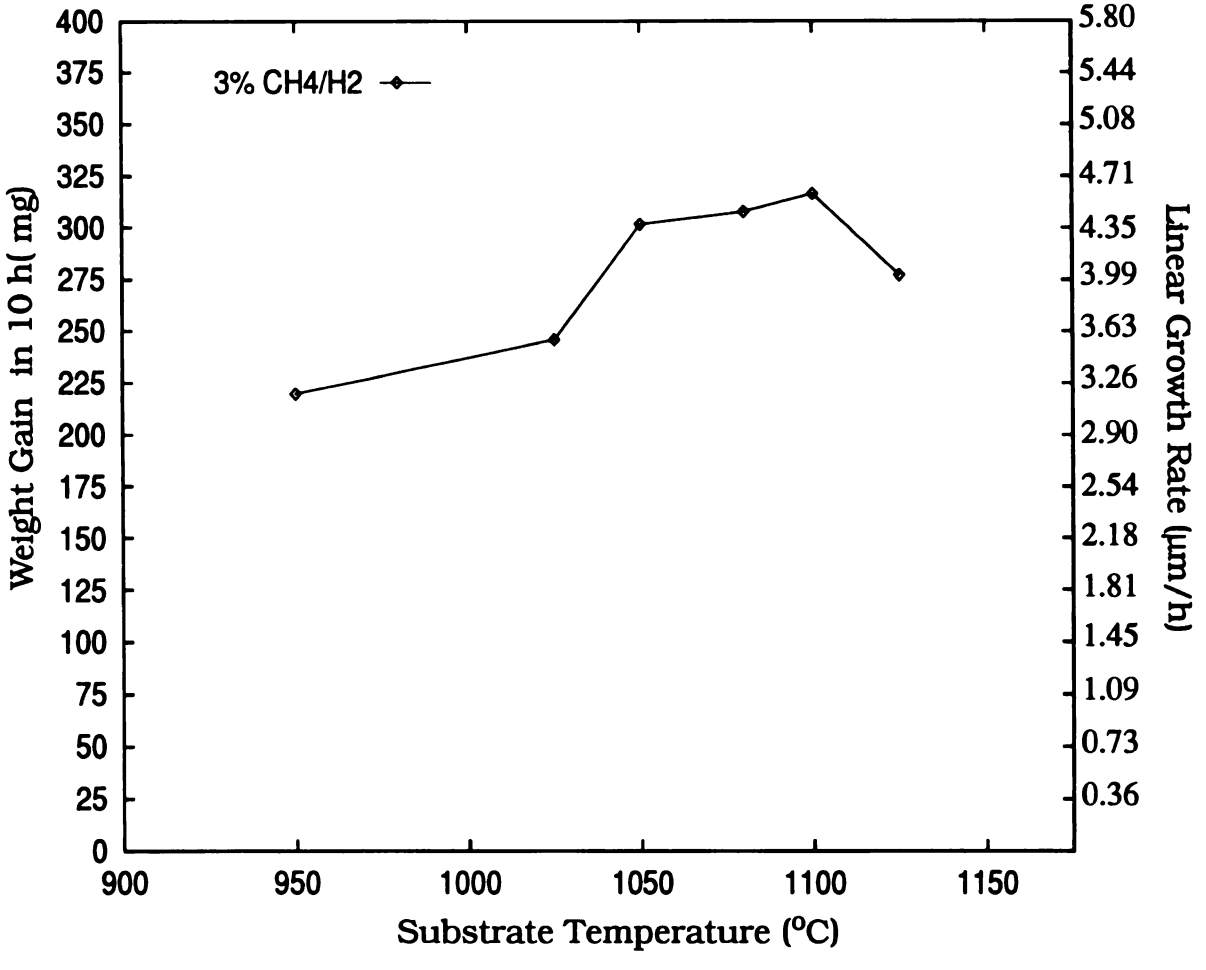

Figure 5.13 The effect of T_s on the film growth rate.

5.4.4 Film Morphology=f(T_s)

The film morphologies inspected by the SEM were shown in Figure 5.14(a) -(f). The experimental conditions are shown in Section 5.4.2. As shown, the film exhibits both (100)square and (110) roof-like morphologies at T_s=950C and then shows mostly (111) triangular and some (110) roof-like facets at T_s=1025, 1050C and 1075C. When T_s increases to 1100C the film exhibits only (111) triangular facets. Then when T_s increases to 1125C, the film mostly exhibits (111) triangular facets and begins to shown the (110) roof-like morphology. Since (111) triangular faces are highly defective, the structural defects of (111) triangular faces will promote nucleation and growth of diamond[56],[65]. It is believed that (111) triangular facets are more favored under high growth rate conditions than (110) roof-like or (100) square facets. It is noted that crystal size also increases as substrate temperature increases.

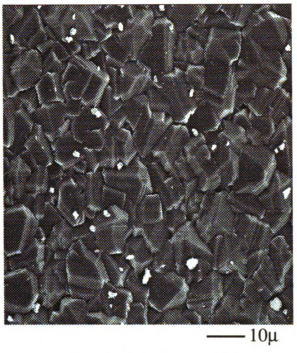

Figure 5.14(a) T_s=950C

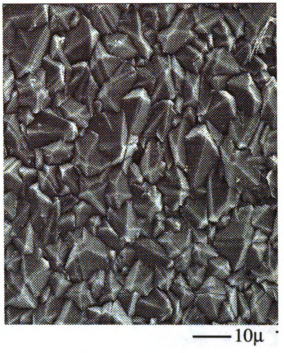

Figure 5.14(b) T_s=1025C

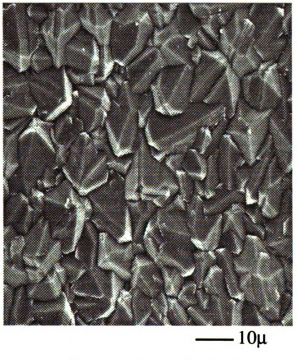

Figure 5.14(c) T_s=1050C

Figure 5.14(d) T_s=1075C

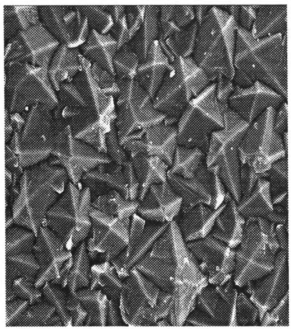

—— 10μ

Figure 5.14(e) T_s=1110C

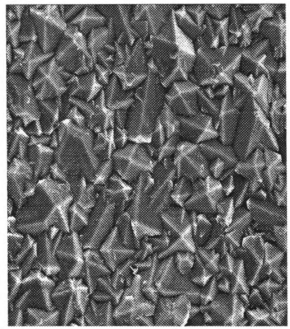

—— 10μ

Figure 5.14(f) T_s=1125C

Figure 5.14(a)-(f) Film morphologies vs. substrate temperatures. The experimental conditions are described in Section 5.4.2.

5.4.5 Film Texture=f(T_s)

The X-ray diffraction spectra for different substrate temperatures are shown in Figure 5.15(a)-(f). The comparison of the intensity ratio of <220> to <111> for the diamond films deposited at different substrate temperate is shown in Figure 5.16. As seen in Figure 5.16, the I(220)/ I(110) ratio increased from 0.3 (at T_s=1025C) to 0.78 (at T_s=1050C) and 0.8 for T_s= 1075C. The I(220)/I(110) ratio shows a maximum value of 1.6 at T_s=1100C. This indicates that the film texture in the direction of <110> was enhanced as substrate temperature increased to 1100C and then suppressed with further increase in the substrate temperature.

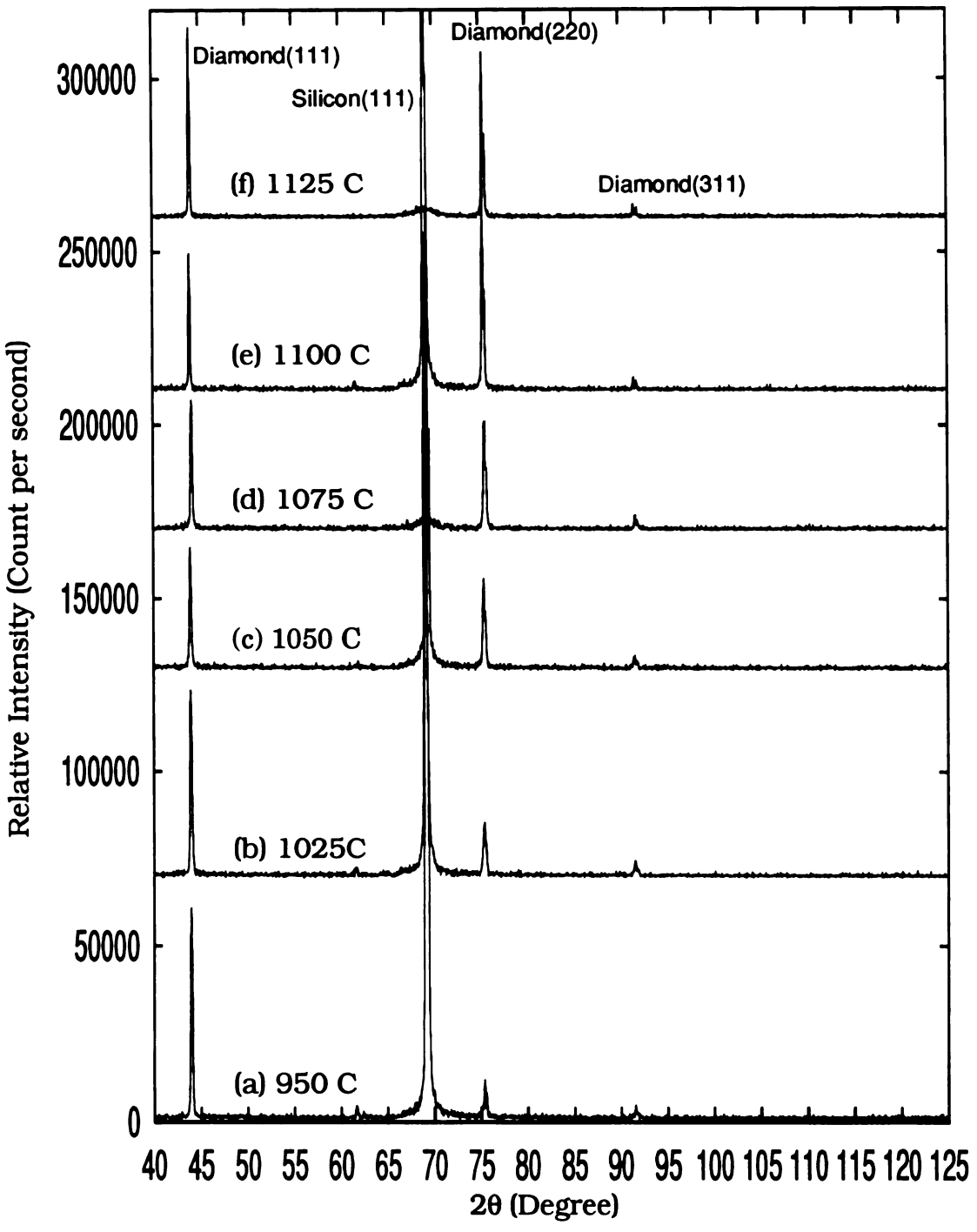

Figure 5.15 X-ray diffraction spectra of diamond films synthesized for (a) 950C, (b) 1025C, (c) 1050C, (d) 1075C, (e) 1100C and (f) 1125C. Maximum ratio of I(220)/I(111) was observed at (e) 1100C. They are summarized in Figure 5.16.

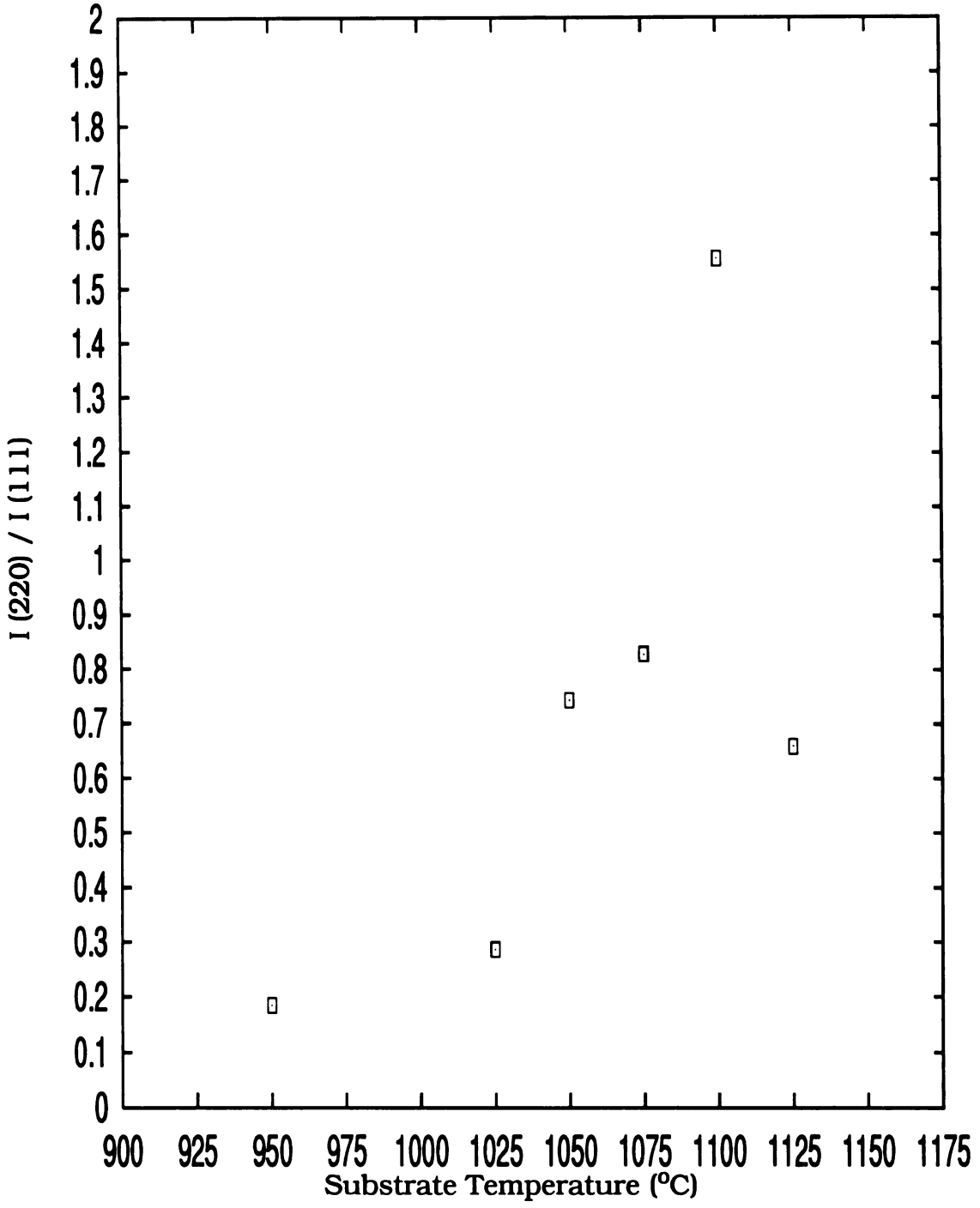

Figure 5.16 The XRD peak height of (220) relative to that of (111) as a function of substrate temperature. The experimental conditions for these experiments are shown in Section 5.4.2.

5.4.6 Film Structural Quality=f(T_s)

The FWHM of diamond peak lines from Raman spectra using different substrate temperatures are displayed in Figure 5.17. The Raman spectra are shown in Figure 5.18. As shown in Figure 5.17, the FWHM is not affected significantly by the substrate temperature. As seen in Figure 5.18, the strong diamond peak at 1332 cm^{-1} is observed and the sp^2 graphite at 1580 cm^{-1} and nondiamond carbon background are not observed from these Raman spectra.

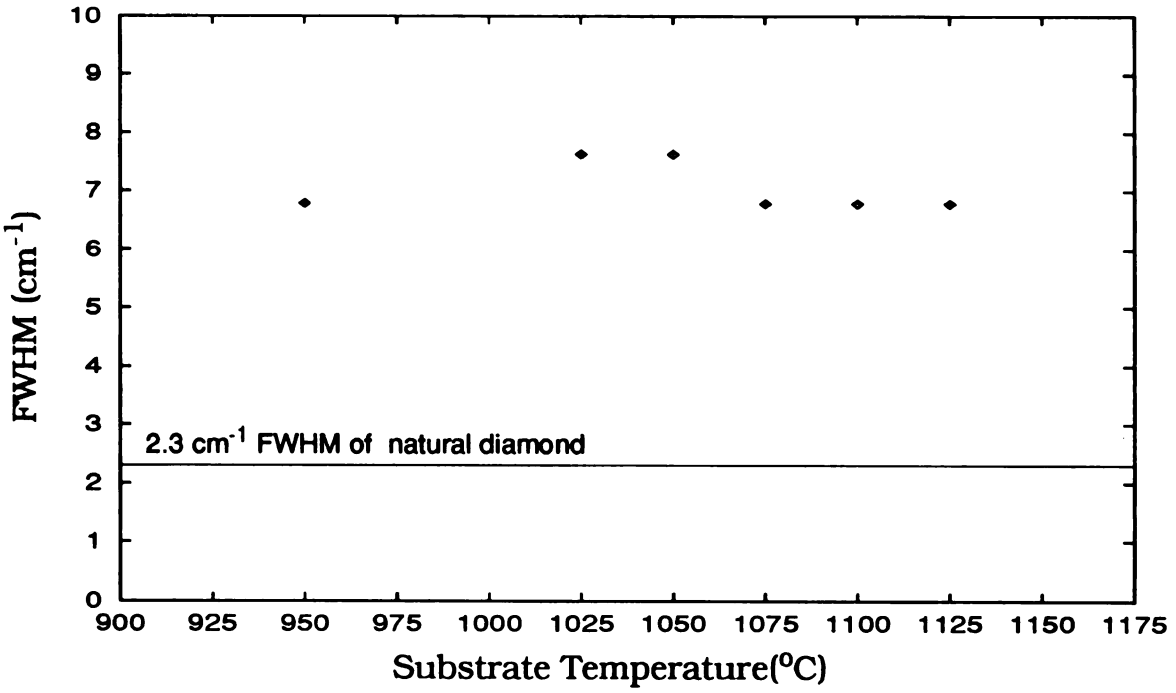

Figure 5.17 The effect of substrate temperatures on FWHM of diamond peak lines from Raman spectra. Their Raman spectra are shown in Figure 5.18.

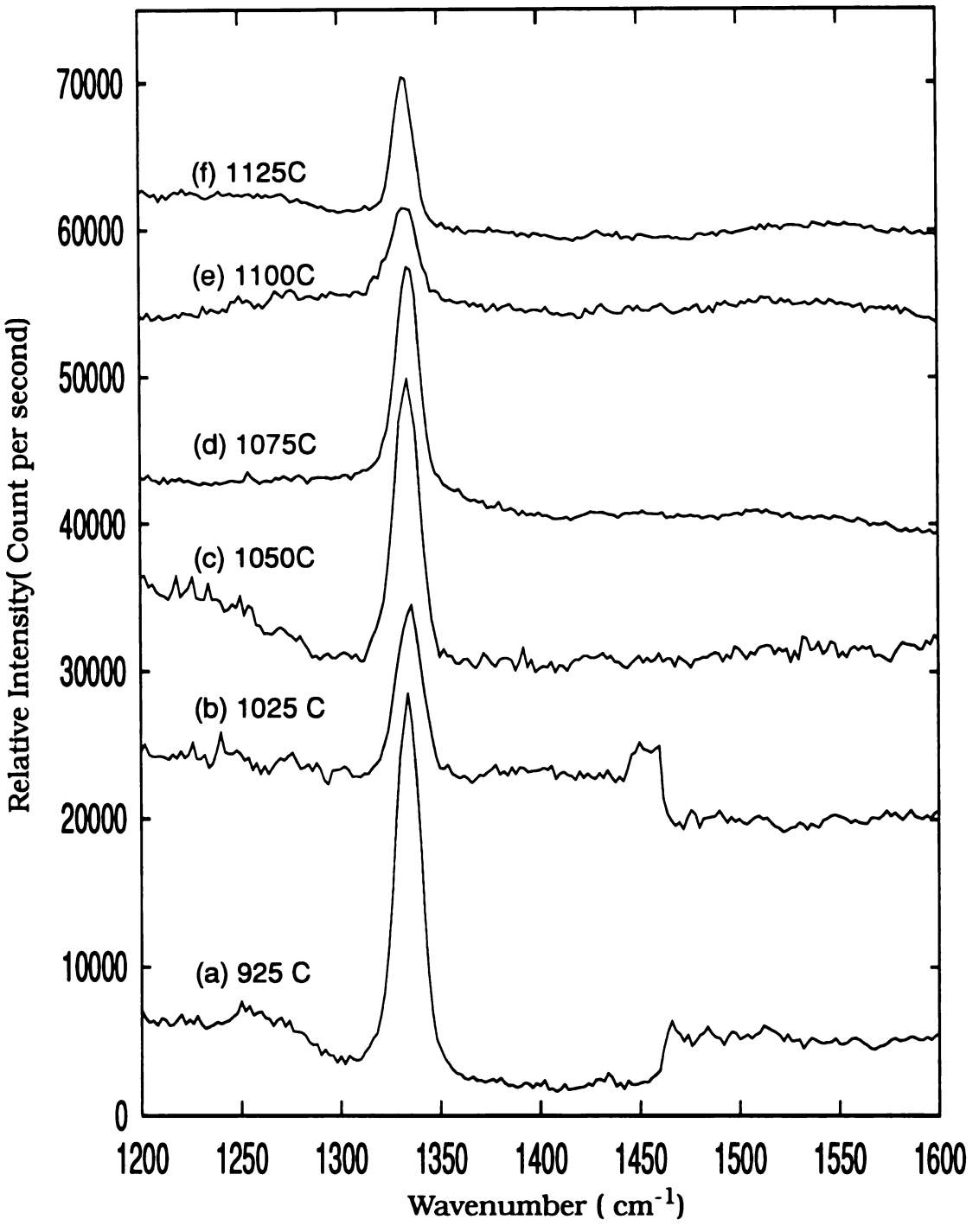

Figure 5.18 The effect of substrate temperature on Raman spectra. The experimental conditions are listed in Section 5.4.2.

5.5 Effect of Deposition Time (t)

5.5.1 Introduction

The six experiments presented in this section were performed by varying the deposition time, t, from 5 to 100 hours while holding the other experimental variables constant.This section first presents the experimental conditions for six experiments and then influence of the deposition time on film growth rate, film morphology, film texture, and film structural quality are presented.

5.5.2 Experimental Variables

(A) Input variables(U):

(1) Controllable input variables (U_1):

a) Gas mixture: 3%CH_4/H_2(18/600 sccm)

b) Total flow rate= 618 sccm.

c) Substrate temperature= 1080°C

d) Absorbed microwave power=3.22 kW,

e) Deposition pressure=135 Torr (18 KPa),

(2) Reactor geometry variable(U_2):

a) Quartz dome size: 5″ in diameter,

b Water cooling state configuration: fixed (see Section 3.6.3.5

c) Substrate: 2″ (100) silicon substrate

(3) Deposition process variables(U_3):

a) Deposition time: **Variable from 5-100 h**,

b) Substrate seeding procedure: fixed(see Section 3.3.1)

c) Start-up and shut-down procedures: fixed (see Section 3.3.2),

(B) Internal variables(**X**):

(1) Power Density= 23 W/cm^3,

(2) Area Power Density= 0.16 kW/cm^2,

(3) Plasma volume~144 cm^3,

5.5.3 Growth Rate=f(t)

The experiments performed in this section have identical experimental input variables except that different deposition times (denoted as t) were used. The experimental conditions and the effect of deposition time on film growth rate are shown in Section 5.5.2 and Figure 5.19, respectively. As shown in Figure 5.19, the film growth rate slightly increases as deposition time increases. It is believed that the slowly increasing growth rate with the increasing deposition time is attributed to the success of cyclically higher-order diamond growth[3].

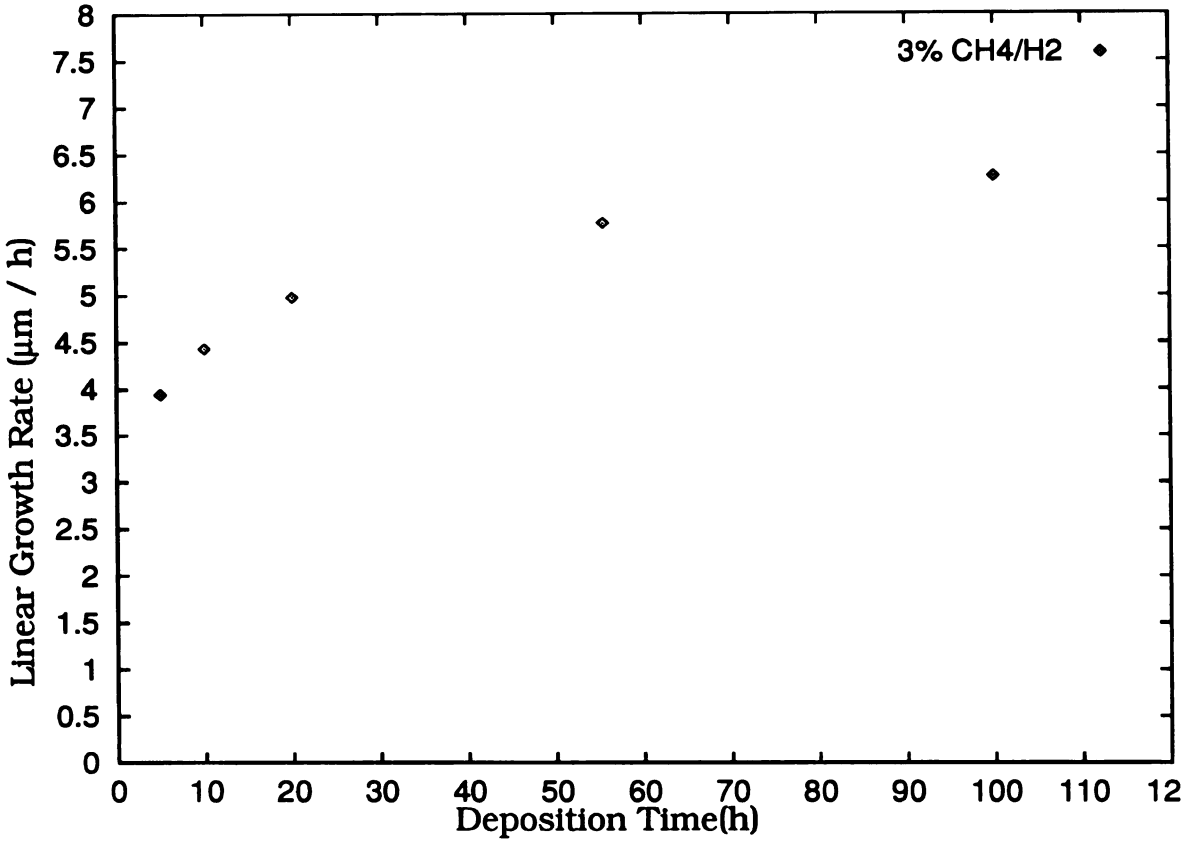

Figure 5.19 Linear growth rate as a function of deposition time. The experimental conditions are described in Section 5.5.2.

5.5.4 Film Morphology=f(t)

The film morphologies produced from different deposition times are shown in Figure 5.20(a)-(f). At t=5h, the film exhibits (110) roof-like and some (111) triangular morphologies. These morphologies are also shown at t=10h. At t=20h the film mostly develops the (111) triangular facets and the number of (110) roof-like facets has decreased. At t 30h, the films completely exhibit (111) triangular morphologies. On the other hand, no (110) roof-like facet is observed when t=30h. The average of dia-

mond grain size increases from 8mm at t=5h to 30mm at t=30h and then reaches its maximum of more than 250 μm at t=100h. It is noted that 630 μm film thickness with 250 μm crystal sizes are synthesized in the MCPR operating at the pressure of 135 Torr.

Figure 5.20(a) t=5h

Figure 5.20(b) t=10h

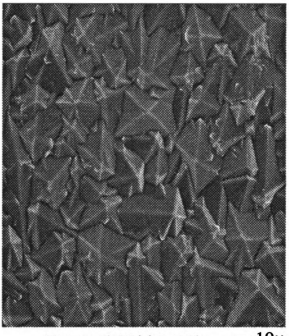

Figure 5.20(c) t=20h — 10μ

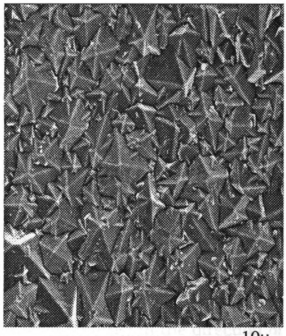

Figure 5.20(d) t=30h — 10μ

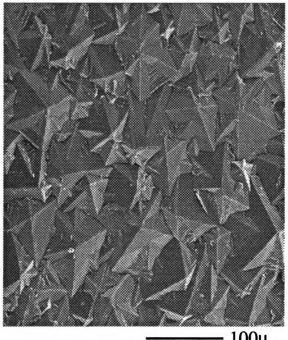

Figure 5.20e) t=55h ——— 100μ

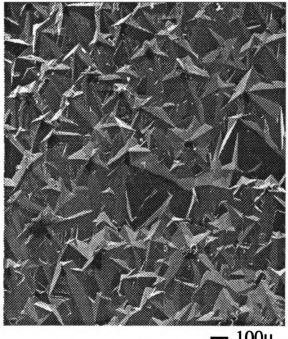

Figure 5.20(f) t=100h — 100μ

Figure 5.20 (a)-(f) Film morphology vs. deposition time. The experimental conditions are shown in Section 5.5.2.

5.5.5 Film Texture=f(t)

X-ray diffraction spectra of diamond film synthesized for 5h to 100h are shown in Figure 5.21. As shown the peak height in the <111> direction, which has $2\theta=43.9^{o}$, and in the <110> direction, which has $2\theta=75.3^{o}$, vary with the deposition time. At t=5h and 10h ratio of I(220) to I(111) is less than 1, indicating that the films do not have preferred orientation. As film is synthesized longer the ratio of I(220) to I(111) increases. At t 30h the peak height of <111> direction becomes very small while that of <110> becomes larger. This indicates that the films which were synthesized longer than 30h are highly textured in the direction of <110>. The XRD height of (220) relative to that of (111) as function of deposition time is shown in Figure 5.22.

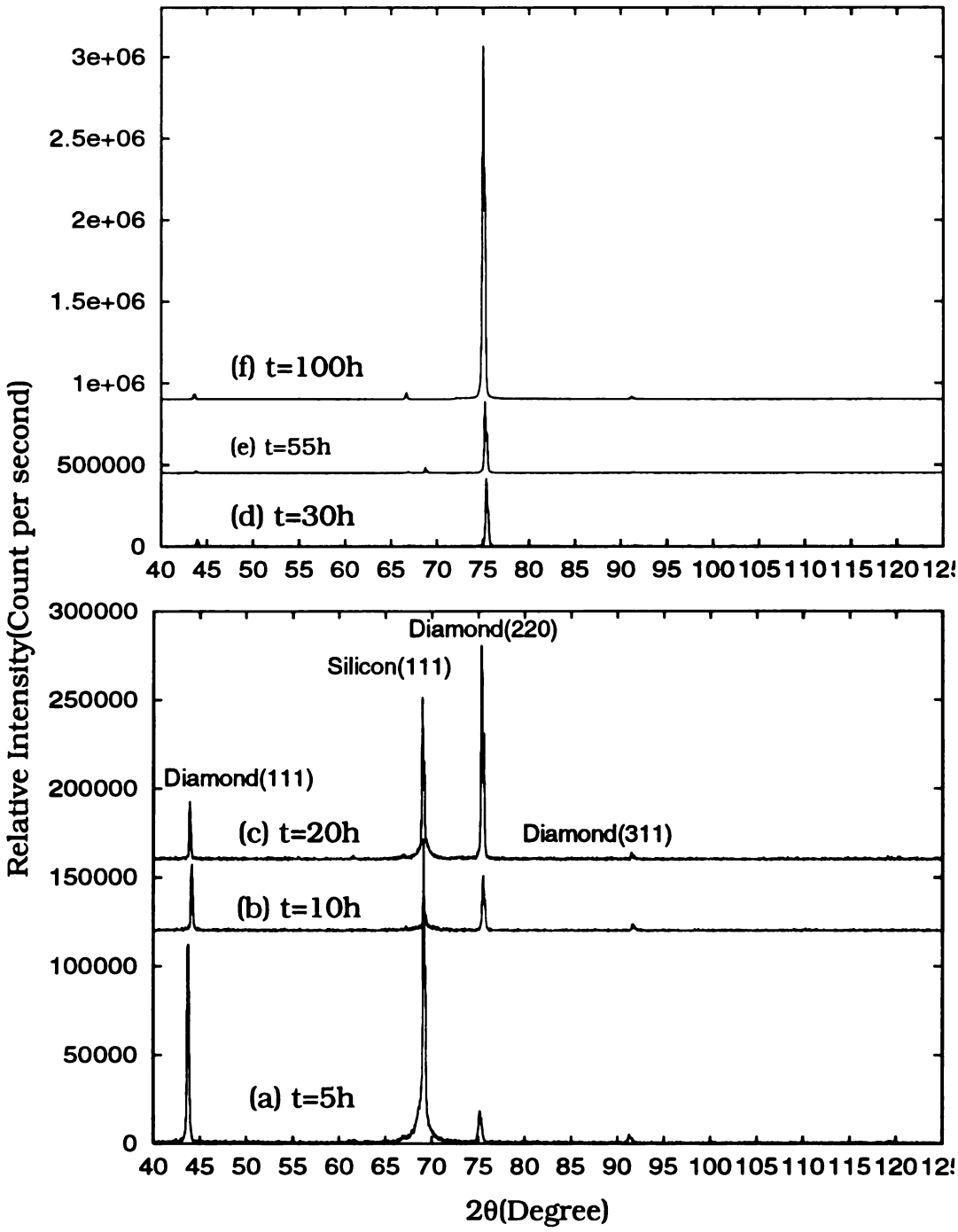

Figure 5.21 X-ray diffraction spectra of diamond films synthesized for (a) 5 h, (b) 10 h, (c) 20 h, (d) 30 h, (e) 55 h and (f) 100 h, using the experimental conditions described in Section 5.5.2.

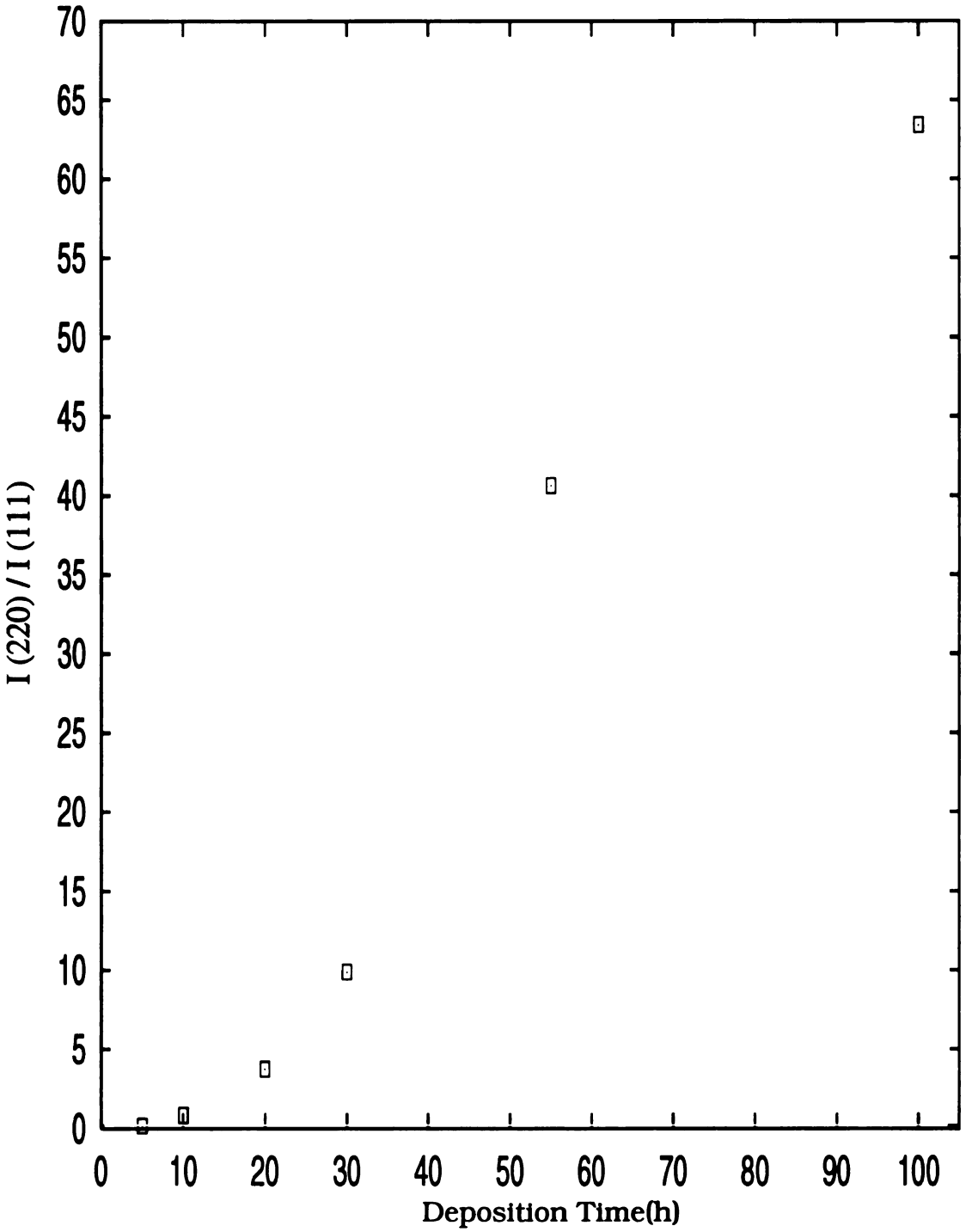

Figure 5.22 The XRD height of (220) relative to that of (111) as a function of deposition time in high pressure MCPR.

5.5.6 Film Structural Quality=f(t)

The influence of deposition times on FWHM is shown in Figure 5.23. Raman spectra of the diamond films produced by different deposition time is displayed in Figure 5.24. As shown in Figure 5.23, FWHM is reduced as the deposition time is increased. The narrowest FWHM of 2.84 cm^{-1} is measured from a diamond film synthesized for 100h. This value is very close to the value of natural diamond(2.3 cm^{-1}). As shown in Figure 5.24, a sharp peak of 1332 cm^{-1} is observed and no graphite or nondiamond carbon background is observed in these Raman spectra.

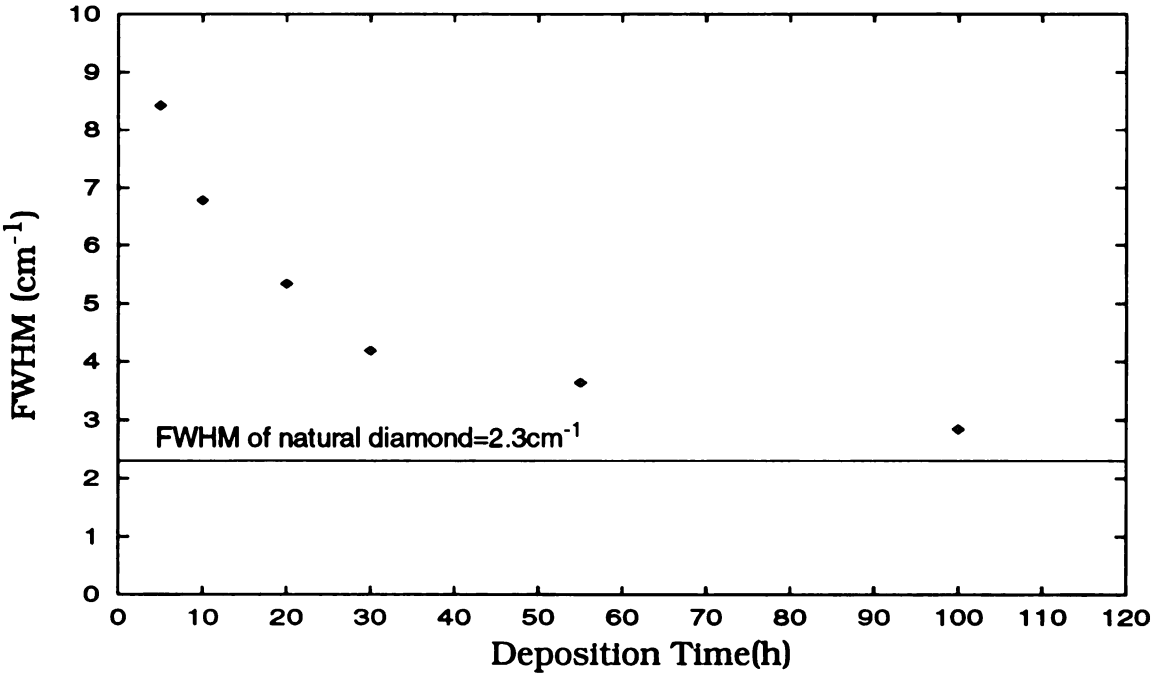

Figure 5.23 FWHM of the diamond peak lines vs. deposition times. Their Raman spectra are shown in Figure 5.24.

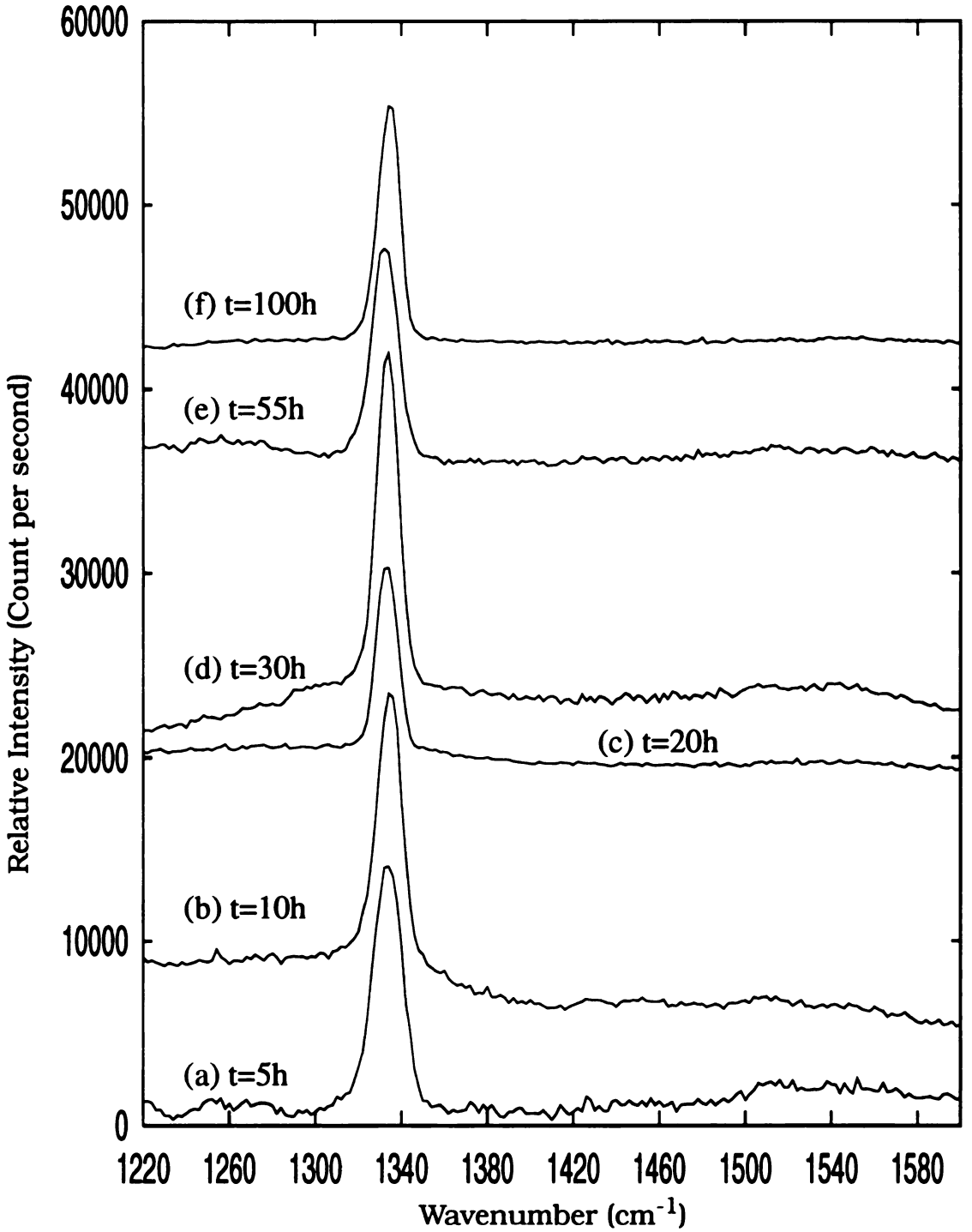

Figure 5.24 The effect of deposition time on Raman spectrum. The experimental conditions are listed in Section 5.5.2.

5.6 Summary

Diamond films that were deposited within the optimized diamond growth zone (centralized at c~3%, f_t~600 sccm, T_s~1080°C, P_t~3.3 kW, p~135 Torr, t= 100 h) showed various film morphologies, film textures, and film structural qualities as one of these independent experimental input variables was varied around the optimized deposition conditions. When c was varied between 1% and 8% while holding f_t~ 600 sccm, T_s~1080°C, P_t~3.3 kW, p~135 Torr, t=5 h), diamond films partially exhibited (100) square morphology at c=2%, (110) roof-like and (111) triangular morphologies at c=3%~5%, and showed cauliflower morphology at c 6%. Raman spectra showed the strong diamond peaks at 1332 cm^{-1} when c was between 2% and 5%. These methane concentrations produced the diamond films with crystalline diamond morphologies. However, Raman spectra showed a large graphite peak at c=6-8%. These methane concentrations produced the diamond films with microcrystalline morphologies. When f_t was varied between 412 sccm and 1442 sccm, the resulting films mostly exhibited (110) roof-like and (111) triangular morphologies and strong Raman diamond peaks. When T_s was varied from 950 to 1125°C, diamond films showed partially (100) square morphology at T_s=950°C and films exhibited (110) roof-like and (111) triangular morphologies when T_s 950°C. The films showed strong Raman

diamond peaks in this temperature region. As deposition times were varied from 5 to 100 hours, the resulting films displayed both (110) roof-like and (111) triangular morphologies at t<30h. When films synthesized with deposition times longer than 30 h, the films completely exhibited (111) triangular morphology. Films that exhibited both (111) triangular morphology and <110> film texture were synthesized under conditions of maximum growth rate.

CHAPTER SIX

Development and Optimization of the Microwave Plasma Jet Reactor

6.1 Introduction

This chapter presents the development and optimization of the microwave plasma jet reactor (MPJR) for the deposition of diamond films on irregular and conducting substrate materials. The MPCR apparatus described in Chapter 3-5 was used to create a uniform coating on flat substrate surfaces. This apparatus was difficult to be reproducibly used when coating surfaces with complex geometries such as ring seals and drills. The problem of uncontrollable and nonuniform deposition was especially evident if the surface to be coated was electrically conductive. The conductive surface interfered the electromagnetic fields within the cavity and made it very difficult to form a uniform and controllable plasma around the substrate surface. Often intense, nonuniform discharges were formed on the edges of the substrate. It was therefore an objective of the present research to design an apparatus and develop processes for the treatment of a surface with a complex geometry such as drill bits and or even substrates with very small and fragile structure

such as carbon fibers.

The experimental work in this chapter carries on from the earlier research by J. Zhang[9],[110]. The early and basic versions of the MPJR, where originated from the work of Zhang and Asmussen [9],[110], are described and the historical development of this reactor concept is presented. Then the optimization of these MPJRs for diamond deposition on round tools and carbon fibers and its final version are described. The experimental work described in Chapter 6 and 7 involved over 100 experiments and over 1,000 hours of reactor operation. The experimental work involved the process of the reactor design, experimental evaluation and test.

6.2 Development of the MPJR

6.2.1 Experimental Systems

The MPJR described in this chapter utilizes the same experimental systems as those of the high pressure MCPR. These common experimental systems include microwave power supply/waveguide transmission systems, flow control/vacuum pump systems, computer monitoring system, microwave tuning assembly, microwave cavity, and gas baseplate assemblies. They have been described in chapter 3. Indeed the major difference between high pressure MPCR (described in Chapter 3-5) and MPJR (described in Chapter 6-7) systems is the reactor configuration

inside the bell jar (i.e., substrate holder setup). These different reactor configurations can be loaded and unloaded from the systems manually by the system operator. Thus the operation procedures such as starting and shut down procedures are very similar for all of the configurations described in this thesis except that the cavity length (L_s) is approximately 20 cm for the high pressure MCPR and is approximately 19 cm for the MPJR.

6.2.2 Early Version of MPJR

The MPJR rector concept originated from the earlier work of Zhang and Asmussen[110]. The early version of MPJR is shown in Figure 6.1[9]. As shown, the substrate (10) and substrate holder (16) are located in a region separated from the plasma discharge (14). The metal stage (7) and quartz tube (17b) are connected together with a tight fit in order to force the input gas to flow through the jet grid (23). This jet grid is an electrically conducting plate (22) in which one or more holes are present to allow the input gas to flow from above the plate, onto the deposition region below the plate. A plasma discharge is created above the conducting plate and the input gases are then forced through the plasma, through the grid plate (22), and onto a substrate located below the grid plate (22). This design reduces the input gas by passing of the discharge, i.e., all the input gas must flow through the discharge and thus improves the gas utilization efficiency. Since the input gases are flowed through the discharge

and through one or more small orifices, this configuration is called a plasma jet. It was expected that the jet-like design would result in a high deposition rates similar to other jet reactors[41]-[42],[93]-[96]. The design also has the advantage of having very low microwave fields in the substrate deposition region. Ionization takes place above the grid plate or in the grid hoes. The deposition volume is essentially microwave field free where the excited species and radicals were created above the grid, flowed/diffused onto and around the substrate. Therefore this configuration also allows the diamond deposition on irregular and conducting substrate materials.

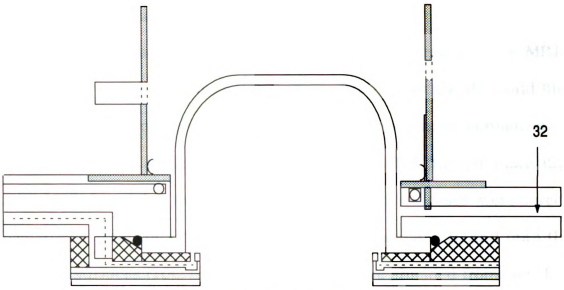

(A) Microwave Cavity, Bell Jar, and Gas Plate Assemblies

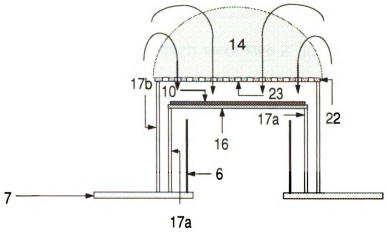

(B) Substrate Holder Setup

Legend of (B)

(6)	Resonant Breaker	(7)	Metal Stage	(10)	Substrate
(14)	Plasma Discharge	(16)	Substrate Holder	(17a)	Quartz Tube
(17b)	Quartz Tube	(22)	Grid Plate	(23)	Jet Grid
(320	Laser Port				

Figure 6.1 Cross sectional view of the early version of MPJR for high rate diamond film deposition on flat substrates[9].

6.2.3 Basic Configuration of the MPJR for Diamond Film Deposition on Round Tools

Figure 6.2 schematically displays the basic version of the MPJR developed by Zhang[110] that was first used to deposit the diamond film on irregular shaped objects such as drill bits. This reactor configuration utilized a plasma discharge that was created below the jet plate (22) instead of above the jet plate. As shown the input gases were forced downstream from the nozzle (23), through the plasma (14), and onto the substrate surfaces (10). The deposition area were shielded from the electromagnetic fields by the jet plate and thus the downstream discharge can cover many irregular shaped substrates.

The substrates(10), which were **two** 2″ long, $\frac{3}{8}$″ diameter WC-6%Co round tools, were placed on the metal stage (7) and supported by a graphite holder (16). This graphite holder was mounted on a 10 mm long, 4″ diameter quartz tube (17a). A jet nozzle plate (22) with one $\frac{1}{2}$″ diameter nozzle(23) at its center was placed on a 77 mm long, 4″ diameter quartz tube (17b). This jet plate was used to force the source gas mixtures of CH_4 and H_2 to flow through the nozzle and onto the substrates. A plasma discharge (14) was created in the substrate region where the electromagnetic field strength is low. With this substrate holder configuration, uniform but weakly adhering diamond films were deposited on the surfaces of the two round tools. However when the number of the tools was increased to

six, nonuniform diamond film deposition on the tool surface was observed for all of the six tools.

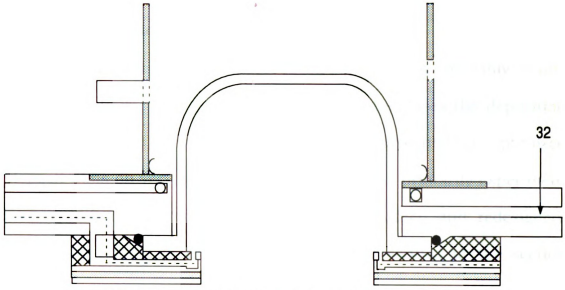

(A) Microwave Cavity, Bell Jar, and Gas Plate Assemblies

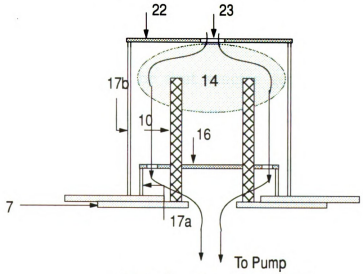

(B) Substrate Holder Setup

Legend of (B)

(7)	Metal Stage	(10)	Substrate	(14)	Plasma Discharge
(16)	Substrate Holder	(17a)	10mm Quartz Tube	(17b)	77mm Quartz Tube
(22)	Jet Nozzle Plate	(23)	Jet Nozzle	(32)	Laser Ports

Figure 6.2 The cross sectional view of the basic version of MPJR for diamond film coating on two WC-6%Co round tools[110].

6.3 Optimization of the MPJR for Diamond Film Deposition on Round Tools

6.3.1 Introduction

While the first prototype MPJR could deposit films uniformly on one or two round tools, as the number of the tools increases the deposition became nonuniform. Thus reactor concept was redesigned and optimized to deposit films on very many tools. This study was primarily experimental where different geometries were tested, evaluated and redesigned. Some of the results of this investigation are described in the section below.

6.3.2 Optimization

Figure 6.3 displays the first reactor geometry that was modified from the basic configuration of MPJR. This first variation was used to deposit diamond films on **six** $1\frac{1}{2}$" long, $\frac{1}{8}$" diameter WC-6%Co round tools. It is noted that this reactor variation used the different size of round tools from previous deposition experiments. These $1\frac{1}{2}$" long, $\frac{1}{8}$" diameter WC-6%Co round tools were used as the benchmark substrate in these optimization. As shown, substrates(10), which were six $1\frac{1}{2}$" long, $\frac{1}{8}$" diameter WC-6%Co round tools, were placed on a graphite holder (16).

This graphite holder was mounted on a 17 mm long, 4" diameter quartz tube (17a). A jet nozzle plate (22) with one $\frac{1}{4}$" diameter nozzle(23) at its center was placed on a 77 mm long, 4" diameter quartz tube (17b). This jet plate was used to force the source gas mixtures of CO and H_2 to flow through the nozzle and onto the substrates. A plasma discharge (14) was created in the substrate region. With this substrate holder configuration, uniform and adherent diamond films were deposited on the surfaces of the six round tools. However nonuniform films were deposited on the tool surfaces when the number of the tools was increased to eighteen.

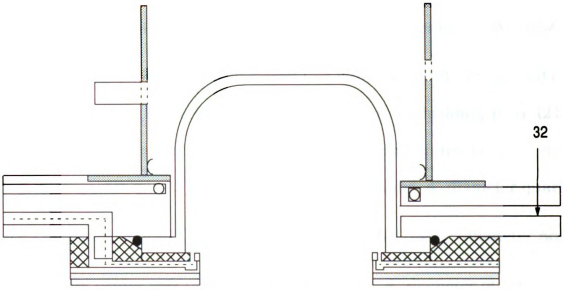

(A) Microwave Cavity, Bell Jar, and Gas Plate Assemblies

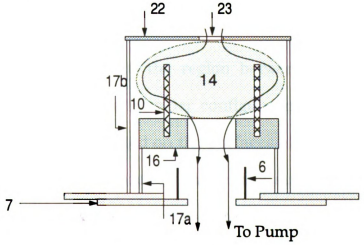

(B) Substrate Holder Setup

Legend of (B)

(6)	Resonant Breaker	(7)	Metal Stage	(10)	Substrate
(14)	Plasma Discharge	(16)	Substrate Holder	(17a)	17mm Quartz Tube
(17b)	77mm Quartz Tube	(22)	Jet Nozzle Plate	(23)	Jet Nozzle
(32)	Laser Ports				

Figure 6.3 The cross sectional view of the first variation of MPJR for diamond film coating on six WC-6%Co round tools.

Figure 6.4 shows the second variation of MPJR that was used to deposit diamond films on **eighteen** $1\frac{1}{2}$" long, $\frac{1}{8}$" diameter WC-6%Co round tools. As shown, eighteen round tool substrates(10) were placed on a graphite holder (16) and supported by a graphite shielding plate (21). The graphite holder and the shielding plate were mounted on a 17 mm long, 4" diameter quartz tube (17a) and a 10 mm long, 4" diameter quartz tube (17b), respectively. A jet nozzle plate (22) with one $\frac{1}{4}$" diameter nozzle(23) at its center was placed on a 77 mm long, 4" diameter quartz tube (17c). This jet plate was used to force the source gas mixtures of CO and H_2 to flow through the nozzle and onto the substrates. A plasma discharge (14) was created in the region between two conducting plates (21,22). With this substrate holder configuration, uniform and adherent diamond films were deposited on the surfaces of the eighteen round tools. Uniform diamond film deposited on the tool surface was observed when the number of the tools was increased to thirty six. This substrate holder setup demonstrated the repeatability and resulted in uniform diamond film deposition over the thirty six round tool substrates.

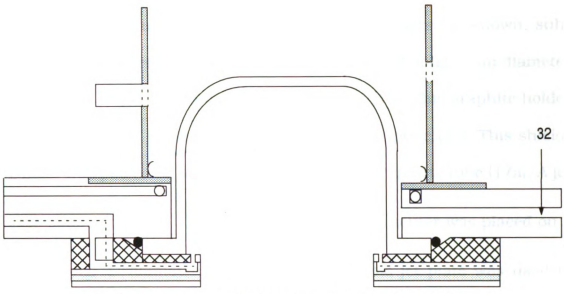

(A) Microwave Cavity, Bell Jar, and Gas Plate Assemblies

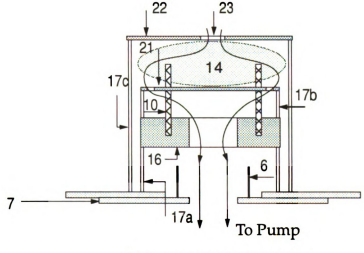

(B) Substrate Holder Setup

Legend of (B)

(6)	Resonant Breaker	(7)	Metal Stage	(10)	Substrate
(14)	Plasma Discharge	(16)	Substrate Holder	(17a)	17mm Quartz Tube
(17b)	10 mm Quartz Tube	(17c)	77mm Quartz Tube	(22)	Jet Nozzle Plate
(23)	Jet Nozzle	(32)	Laser Ports		

Figure 6.4 The cross sectional view of the first variation of MPJR for diamond film coating on eighteen and thirty six WC-6%Co round tools.

Figure 6.5 displays another design of MPJR that was used to deposit diamond films on 7 μm diameter carbon fibers. As shown, substrates(10), which consisted of two thousand 4.5 inch long, 7 μm diameter carbon fibers, were placed on a graphite holder (16). This graphite holder was mounted on a 4" diameter graphite shielding plate (21). This shielding plate was placed on a 40 mm long, 4" diameter quartz tube (17a). A jet nozzle plate with one $\frac{1}{4}$" diameter nozzle(23) at its center was placed on a 20 mm long, 4" diameter quartz tube (17b). This jet plate was used to force the source gas mixtures of $CO/CH_4/ H_2$ to flow through the nozzle and onto the substrates. A plasma discharge (14) was created in the region between these two conducting plates (21,22). With this substrate holder configuration, uniform and adherent diamond films were deposited on the surfaces of carbon fibers. This substrate holder setup demonstrated repeatable experiments and resulted in uniform diamond film deposition on thousands of carbon fibers.

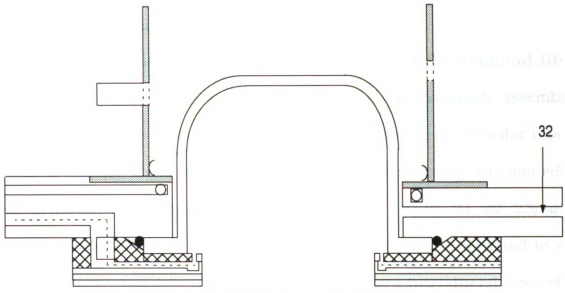

(A) Microwave Cavity, Bell Jar, and Gas Plate Assemblies

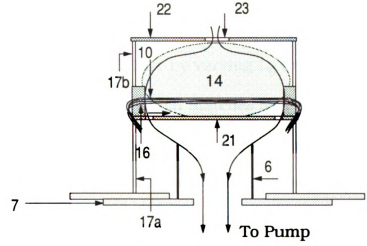

(B) Substrate Holder Setup

Legend

(6)	Resonant Breaker	(7)	Metal Stage	(10)	Substrate
(14)	Plasma Discharge	(16)	Substrate Holder	(17a)	40mm Quartz Tube
(17b)	20mm Quartz Tube	(22)	Jet Nozzle Plate	(23)	Jet Nozzle
(32)	Laser Ports				

Figure 6.5 The cross sectional view of the thirdth variation of MPJR for diamond film coating on many carbon fibers.

6.3.3 Operation of the Optimized MPJR for Diamond Film Deposition on Round Tools

The final configuration of MPJR optimized for diamond film deposition on round tools is shown in Figure 6.6. The baseplate assembly consists of a water-cooled and air-cooled baseplate(2), an annular input gas feed plate(3), a gas distribution plate(4), a 12.5cm i.d. quartz dome(5), the MPJR substrate holder setup assembly (6, 7, 16, 17, 21, 22, 23) and the substrate itself (10). After the reactor chamber was evacuated to ~5 mTorr, source gas mixtures of $CH_4/CO/H_2$ were introduced from the baseplate (2), the annular gas plate (3), and the gas distribution plate (4) into the quartz dome (5) volume. A plasma discharge(14) is created at pressures between 25-50 Torr by varying L_p and L_s to the position of ~3 and ~ 19 cm, respectively, which matches and excites the TM_{013} plasma-loaded resonant mode. By adjusting the cavity length to ~19 cm, the plasma discharge was positioned in the substrate region below the jet plate (22) and can be viewed through the laser diagnostic ports (32). The substrate temperature was measured by focusing an optical pyrometer through these ports. A metal tube (6) which served as an electromagnetic field resonance breaker was placed inside the quartz tube (17a) and prevents the plasma discharge from forming underneath the substrate by reducing the electric field underneath the substrate. The metal tube (6) and quartz tube (17a) are placed on a metal stage (7) which has 30 mm diameter hole in its center to pass the hot gases to the pump.

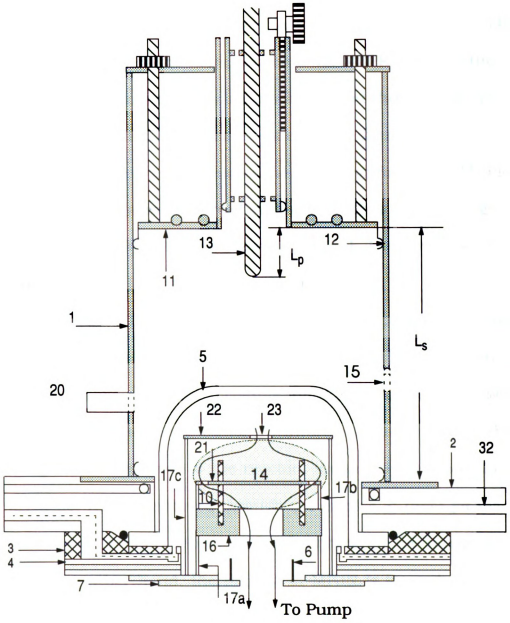

Legend

(1)	Cavity Walls	(2)	Baseplate	(3)	Gas Annular Plate
(4)	Gas Distribution Plate	(5)	Quartz Bell Jar	(6)	Resonant Breaker
(7)	Metal Stage	(10)	Substrate	(14)	Plasma Discharge
(16)	Substrate Holder	(17a)	10mm Quartz Tube	(17b)	77mm Quartz Tube
(22)	Jet Nozzle Plate	(23)	Jet Nozzle	(32)	Laser Ports

Figure 6.6 The cross sectional view of the final optimized configuration of MPJR which was used for diamond film coating on eighteen and thirty six WC-6%Co round tools.

6.4 Summary

The MPJR is a new microwave plasma reactor concept, which has several advantages over the more conventional MCPR. First all the input gases are forced to flow through the discharge and thus gas bypassing is eliminated. The MPJR also utilizes a different configuration of creating a plasma jet discharge from the microwave discharge formed in MCPRs. In MPJR, the reactive gases are forced to flow through a nozzle or a group of nozzle-like holes ((23) in Figure 6.2 - Figure 6.4). Then they are dissociated in the plasma (14) which is located in the holes and in between two conducting plates (21,22). The dissociated reactive species then flow/diffuse onto the substrate (10). In other CVD jet reactors[89]-[97], significant amount of volume and surface recombinations of dissociated reactive species are observed when they are forced through a nozzle. Hence, the gas flow and power efficiencies of the reactors are greatly reduced. In addition, when hot gases are forced through the nozzles in these jet reactors, the problems of erosion, deposition, and melting on the nozzle are also found. On the other hand, the plasma in MPJR is located downstream from the nozzle (23). Thus the problem of recombination in the nozzle is significantly reduced. The input gas flow serves as a natural cooling agent to the nozzle (23) and thus also drastically reduces the nozzle erosion and hence film contamination. The excited radical species are located in a microwave field free region and thus allows deposition on irregular shaped and conducting substrates. This new reactor configuration pro-

duces the discharge adjacent to the substrate, thus the discharge is not any larger than necessary, resulting in efficient use of microwave energy.

The plasma created in the MPJR and CVD process are relatively independent of the geometry and material of the substrates. Therefore it becomes possible to use this apparatus to coat the substrates with complex geometries and different materials, such as cylindrical cemented carbide inserts (1/8″ in diameter) and fine carbon fibers (7 μm in diameter). The experimental parameter space and experimental results for diamond film deposition using MPJR are presented in the next chapter.

CHAPTER SEVEN

The Experimental Performance of the Microwave Plasma Jet Reactor

7.1 Introduction

This chapter presents the experimental performance of the optimized MPJR. The experimental input/output variable space and experimental procedures are first described. Then the optimized experiments that produced uniform and adherent, approximately 1-5 μm diamond films on round tools and carbon fibers are presented. It is expected that the optimum deposition conditions presented in this chapter will be useful when evaluating process scale up for round tools and carbon fibers deposition.

7.2 Experimental Input/Output Variable Space

During this thesis research over 100 experimental runs representing over 1000 hours of reactor operation were performed. The resulting experimental parameter space that was used to deposit uniform and adherent diamond films on the benchmark substrates is displayed in Figure 7.1. Table 7.1 summarizes the ranges of the experimental variables

that have achieved excellent diamond film deposition on the benchmark substrates. In Section 3.4 it was pointed out that the microwave plasma deposition process is very complex. It consists of a large number of input ($\mathbf{U}=[\mathbf{U_1},\mathbf{U_2},\mathbf{U_3}]$), internal ($\mathbf{X}$), and output variables ($\mathbf{Y}$). The output variables ($\mathbf{Y}$) are dependent upon the input and internal variables, i.e., $\mathbf{Y}=g(\mathbf{U},\mathbf{X})$ and the internal variables are dependent upon the input variables ($\mathbf{X}=f(\mathbf{U})$).

As shown in Figure 7.1 and Table 7.1, the controllable input variables ($\mathbf{U_1}$) include the gas mixture, total flow rate, deposition pressure, and absorbed microwave power. Two gas concentrations, i.e., the methane concentration ($c_1=\%CH_4/H_2$) between 0.5% and 2% and the carbon monoxide concentration ($c_2=\%CO/H_2$) between 2.5% and 10% were used to achieve useful diamond film deposition. Total flow rates, denoted as f_t, were varied between 100 and 600 sccm. As indicated by the dashed curve in Figure 7.1, deposition pressure (p=13-50 Torr), absorbed microwave power (P_t=0.8-1.5 kW), and substrate temperature (T_s=600-1050°C) are directly related since the MPJR is operated in a thermally floating configuration[51]. Thus these three input variables are not independent of each other and for the experiments presented in this chapter are referred to as a triad input variable, namely, $p\text{-}P_{inc}\text{-}T_s$. Using the ranges of these experimental controllable input variables, good to excellent diamond films were deposited on the surface of benchmark substrates.

The reactor geometry variables (U_2) were (1) a quartz dome with inner base diameter of 5" (12.7 cm), (2) the MPJR substrate holder setup,(3) the substrate. The quartz dome size is fixed for the experiments presented in this chapter. Two optimized MPJR substrate holder setups (Figure 6.6 and Figure 7.14) were used to investigate diamond film deposition on the irregular shaped substrates. Note also that the substrates themselves were variables, i.e., the number and placement of the round tools and carbon fibers could be changed from run to run.

The deposition process variables (U_3) such as start-up/shut-down procedure and substrate seeding procedure were held constant except the deposition time, which was varied from 4h to 30h. The experiments that were investigated in this chapter did not utilize any substrate pretreatment procedure (including substrate cleaning, etching and seeding). The output performance variables that were of interest were film growth rate, film uniformity, film structural quality, and film morphology. Note that only experimental runs where the films were observed to stick to the substrates after the experimental run was completed were included as useful experimental data.

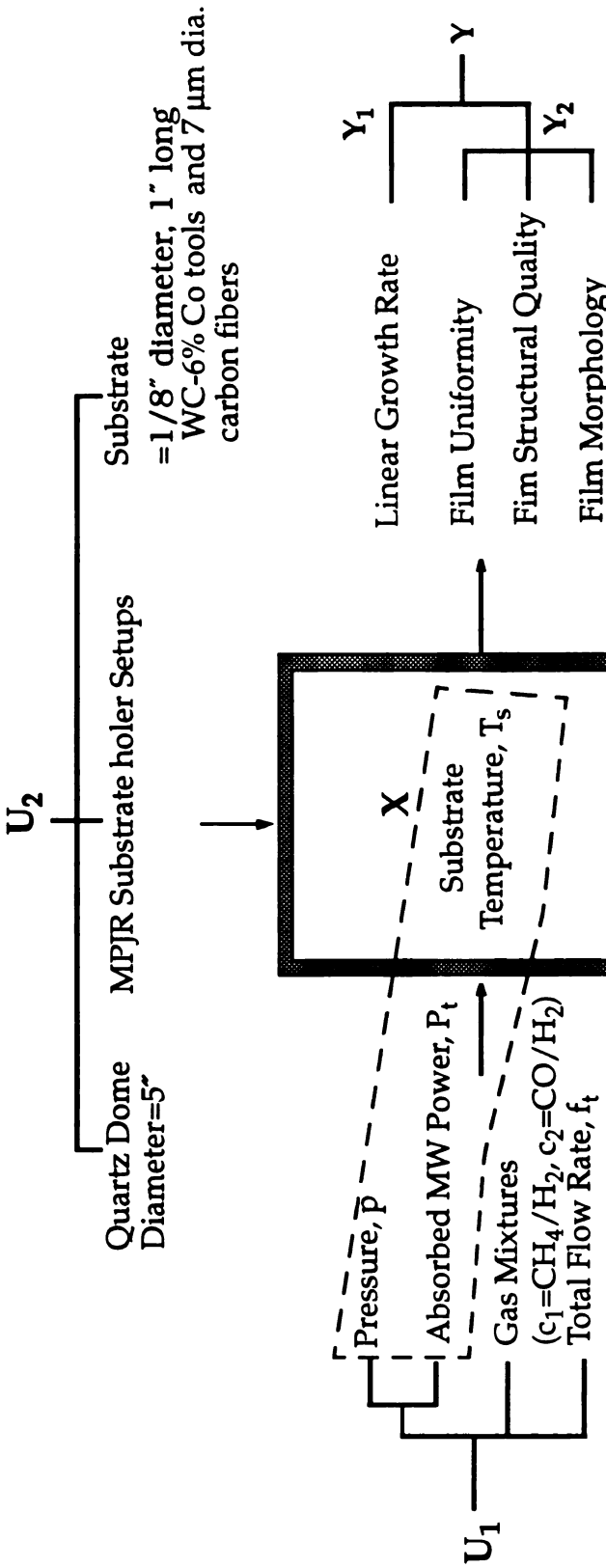

Figure 7.1 MPJR block diagram for diamond thin film deposition on the benchmark substrates. The dashed curve encircles the p, P_t, and T_s variables indicating that this triad of variables can be considered as a single variable for this investigation.

Table 7.1 Reactor input/internal/output variables investigated in this and next chapters.

Input Variable, **U**	Controllable Input Variables, $\mathbf{U_1}$	a) Deposition Pressure, Variable: p=13-50Torr b) Absorbed Microwave Power, Variable: P_t=0.8-1.5 kW c) Gas Chemistry, Variable: c_1=0.5-2% CH_4/H_2,c_2=2.5-10% CO/H_2 e) Total Flow Rate, Variable: f_t=100-600 sccm
	Reactor Geometry Variables, $\mathbf{U_2}$	a)Quartz Dome Size, fixed at 5" diameter b) Reactor Configuration, Variable: Substrate Holder Setups c) Substrate Material and Size, variable: WC-6% Round Tools and Carbon Fibers d) End-feed Excitation, Fixed e) Electromagnetic Mode and Cavity Tuning, Fixed at TM_{013}
	Deposition Process Variables, $\mathbf{U_3}$	a) Starting and Shut-down Procedures, fixed b) No Substrate Seeding Procedure c) Deposition Time, Variable: t=4-30 Hours
Internal Variable, **X**		a) Substrate Temperature, Variable: T_s=600-1050C
Output Variable, **Y**	Reactor Performance, $\mathbf{Y_1}$:	a) Linear Growth Rate
	Film Characteristics, $\mathbf{Y_2}$:	a) Film Uniformity b) Film Structural Quality c) Film Morphology

7.3 Experimental Procedures

7.3.1 Substrate Pretreatment Procedure

The experiments presented in this chapter used gas chemistries that were different from the CH_4/H_2 experiments presented in Chapter 3-

5. As shown in Figure 7.1 and Table 7.1, two different carbon containing gases, CO and CH_4, were mixed with the hydrogen gas. The mixtures of these two gases are denoted as c_1=CH_4/H_2 and c_2= CO/H_2. The addition of CO/H_2 was found to increase the deposition rate three to five times over the deposition rate achieved by using CH_4/H_2. The CO/H_2 gas mixtures also were able to produce films without any special substrate seeding. Thus no substrate seeding procedure was necessary for the experiments presented in this chapter.

7.3.2 Start-up and Shut-down Procedures

Since MPJR used the same experimental systems that were used in high pressure MCPR, the start-up and shut-down procedures are referred to Section 3.6.2. The reactor operation is referred to Section 6.3.3.

7.3.3 Measurement of Substrate Temperature

The substrate temperature was measured by an optical pyrometer. Optical pyrometer temperature measurements are performed through the side laser ports ((32) in Figure 6.1 - Figure 7.2) focusing directly upon the rod tools or the carbon fibers.

7.3.4 Measurement of Reactor Output Variables Y

7.3.4.1 Measurement of Reactor Performance Variable (Y_1)

The linear growth rate is the only reactor performance variable that was investigated for MPJRs. The thickness of the resulting film was measured from the cross sectional view of the SEM photo. The linear growth rate is defined as the thickness divided by the deposition time.

7.3.4.2 Measurement of Film Characteristic Variables (Y_2)

The film uniformity over the substrate was determined by two thickness measurements from SEM cross sectional photos over the broken tools or fibers. The two measured spots were located in the opposite position on the broken surface. One thickness measurement, referred as the minimum thickness measurement, and the other thickness measurement, referred as the maximum film thickness measurements, were recorded for each tool cross section. Film uniformity was calculated as:

Film Uniformity= (Maximum Thickness Measurement-Minimum Thickness Measurement/Maximum Thickness X 100%.

Raman Spectroscopy was performed on the deposited diamond to assess the diamond structural quality. Film morphology was identified by SEM.

7.4 Diamond Film Deposition on WC-6%Co Round Tools

7.4.1 Reactor Configuration

Figure 6.6 displays a cross-sectional view of the MPJR that was used to deposit uniform diamond films on round tools (10). As shown thirty six 1/8" diameter, $1\frac{1}{2}$" long, WC-6% wt Co round tools were used as the substrates (10). These tools were held in a vertical position by a graphite holder (16) and supported by a shield plate (21). This substrate holder (16) and shielding plate (21) were mounted on the quartz tubes (17a) and (17b), respectively. A plasma (14) is created in the region between the jet pattern plate (22) and the shielding plate (21) below a nozzle (23) by tuning cavity length and probe length at 19 cm and 3 cm, respectively. The metal stage plate (7) and quartz tube (17c) are placed together so that the source gas is forced to flow through the nozzle (23) of the jet pattern plate (22), through the plasma (14), and flows out through a ring of holes in the shielding plate (21) and finally through the center hole of the substrate holder (16). The plasma discharge (14) was confined between two conductive parallel plates (21),(22). The one inch top surfaces of the round tools were placed between (21) and (22) so that the discharge and the free radicals could freely diffuse over these irregular surfaces. The following sections present the optimized experimental input variables and the reactor output performance.

7.4.2 Experimental Controllable Input Variables (U) and Internal Input Variables (X)

The optimized independent experimental input variables (**U**) and internal input variables (**X**) that were used to produce the uniform (4% or better), thin (~3 μm) diamond films over 36 round tools per run were:

(1) Controllable input variables (U_1):

a) Power input:

i) Power source: a 2.45 GHz microwave generator,

ii) P_{abs}= 1.35 KW,

b) Gas input:

i) Gas mixture: CO/H_2 =10/400 sccm, CH_4/H_2=0,

ii) Total flow rate=410 sccm,

c) Deposition pressure=30 Torr (4 kPa),

(2) Reactor geometry variables(U_2):

a) Reactor Configuration:

- A 5″ diameter(12.7 cm) quartz bell jar,

- Substrate holder setup for tool coating (Figure 7.1) was applied,

b) No external substrate heating, cooling or biasing,

(3) Deposition process variables (U_2):

a) Deposition time= 8 h,

b) No Substrate pretreatment procedures such as cleaning, seeding, etc. were applied,

c) Substrate size and material=1/8″ diameter, $1\frac{1}{2}$″ WC-6%Co

round tools,

(B) Internal variables(X):

(1) Substrate temperature=754-800°C(1027-1073°K).

Using these experimental input conditions, the reactor performance (Y_1) and film characteristics (Y_1) are presented in the sections below.

7.4.3 Reactor Performance (Y_1) - Linear Growth Rate

Figure 7.2 shows two thickness measurements for each round tools (totally 36 round tools) that were produced from a single run using the experimental conditions described in Section 7.4.2. Two measured spots were chosen as the thickness measurement for each tool using the SEM. The first spot was picked on one edge of the breaking tool surface and the second spot was on the other side. Film thickness of 2.0 μm-3.6 μm were deposited on these 36 tools after a 8 hour experimental run. The average linear growth rate is 0.25-0.45 μm/h.

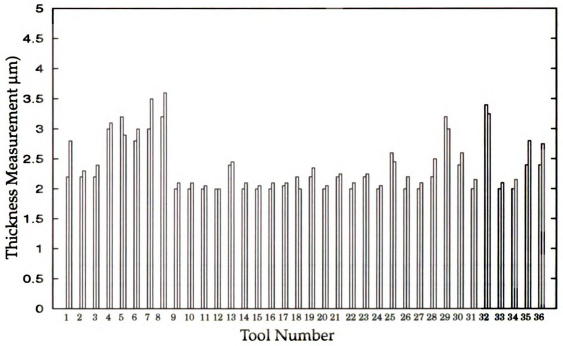

Figure 7.2 Thickness measurements of 36 WC-6%Co round tools.

7.4.4 Film Characteristic (Y_2)

7.4.4.1 Film Uniformity

Figure 7.3 shows the film uniformity of thirty six round tools that were diamond coated in a single experimental run. Film uniformity is calculated from the thickness data shown in Figure 7.2 according to the formula described in Section 7.3.4.2. One representative cross sectional

SEM photo of the diamond film deposited on the round tools is shown in Figure 7.4.

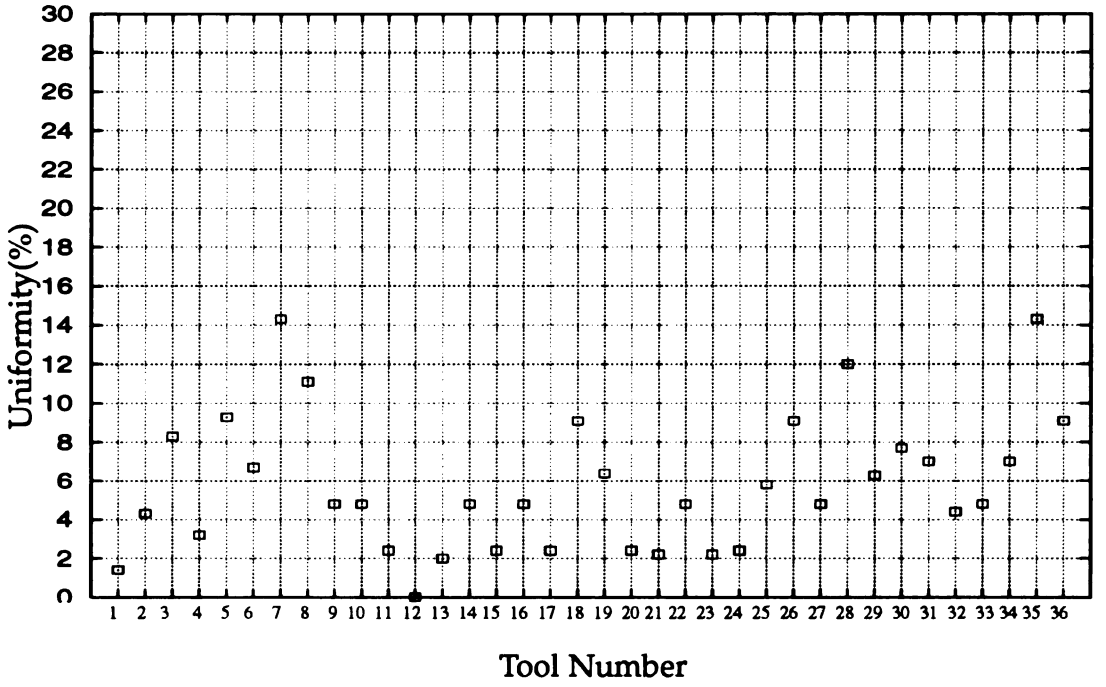

Figure 7.3 Film Uniformity of diamond films for thirty six WC-6%CO round tools.

7.4.4.2 Film Morphology

Film morphologies of the WC-6%Co surface that were deposited with diamond films at different times were shown in Figure 7.4-Figure 7.12. The experimental input variables shown in Section 7.2 were held constant except that the deposition time was varied from 0.5 h(Figure 7.5), 1 h(Figure 7.6), 2 h(Figure 7.7), 3 h(Figure 7.8), 4 h(Figure 7.9), 5 h(Figure 7.10), 6 h(Figure 7.11), and 8 h(Figure 7.12). Figure 7.4 shows the surface morphology of a WC-6%Co before deposition.

As shown in Figure 7.5, the WC surface was nucleated by the CO/ H_2 plasma in the first 0.5 hour. At t=1h(Figure 7.6), some octahedron diamond crystals were deposited on the etched surfaces. At t=2h(Figure 7.7), more octahedron diamond crystals covered the surfaces. However the round tool surface was not fully covered by the diamond film at this moment. It was observed that these 1 μm big octahedron diamond crystals were believed to be the first layer of the diamond film growth on the WC tools. They offered the nuclearation of high-order growth. At t=3h(Figure 7.8), the WC round tool surfaces were fully covered by cauliflower diamond films with some square diamond films. At t=4h(Figure 7.9), the situation described in t=3h became more obvious that more square diamond films were observed. At t=5h(Figure 7.10), square and triangular facets were both observed. At t=6h(Figure 7.11), the grain size increased with the same morphologies described at t=4h. At t=8h(Figure 7.12), same morphologies were observed with increasing grain sizes.

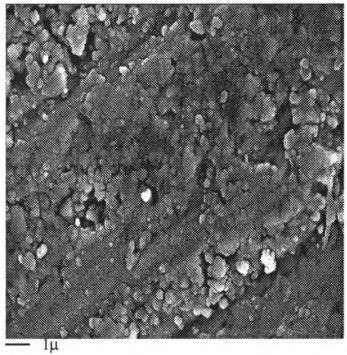

Figure 7.4 SEM photo of the pre-deposited WC-6%Co round tool surface.

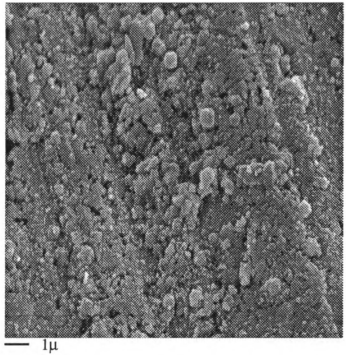

Figure 7.5 SEM photo of a diamond film deposited WC-6%Co surface. The deposition time is 0.5 h.

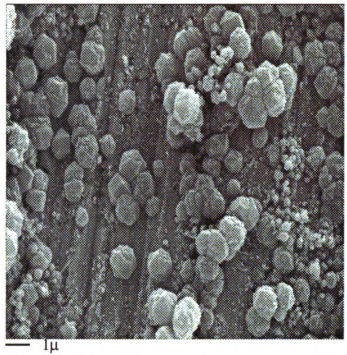

Figure 7.6 SEM photo of a diamond film deposited WC-6%Co surface. The deposition time is 1 h.

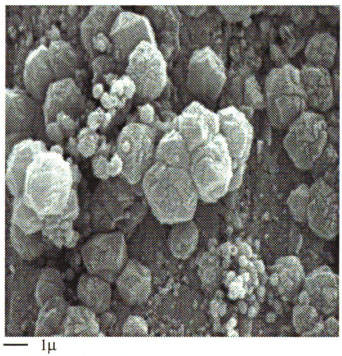

Figure 7.7 SEM photo of a diamond film deposited WC-6%Co surface. The deposition time is 2 h.

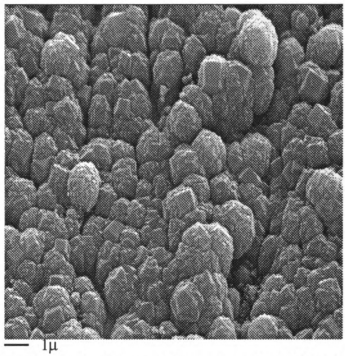

Figure 7.8 SEM photo of a diamond film deposited WC-6%Co surface. The deposition time is 3 h.

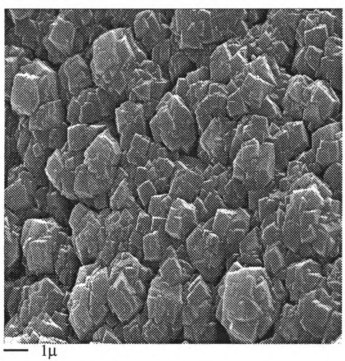

Figure 7.9 SEM photo of a diamond film deposited WC-6%Co surface. The deposition time is 4 h.

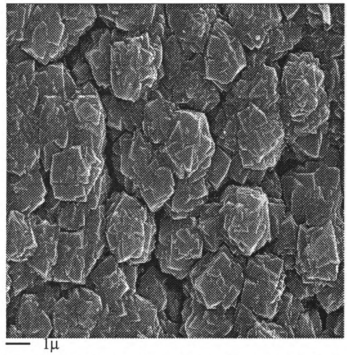

Figure 7.10 SEM photo of a diamond film deposited WC-6%Co surface. The deposition time is 5 h.

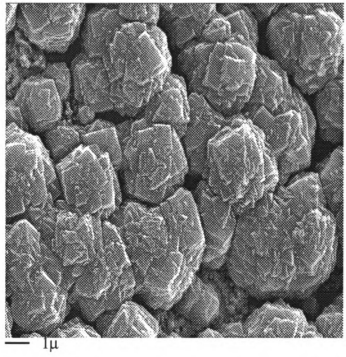

Figure 7.11 SEM photo of a diamond film deposited WC-6%Co surface. The deposition time is 6 h.

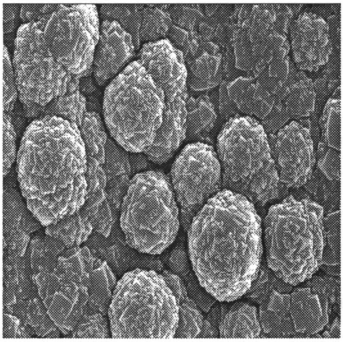

— 1μ

Figure 7.12 SEM photo of a diamond film deposited WC-6%Co surface. The deposition time is 8 h.

7.4.4.3 Film Structural Quality

Figure 7.13 shows the Raman spectrum of the diamond film deposition experiment that was described in Section 7.2. Raman Spectroscopy, which has approximately 30 μm spot size, shows the diamond peak at 1332 cm^{-1}.

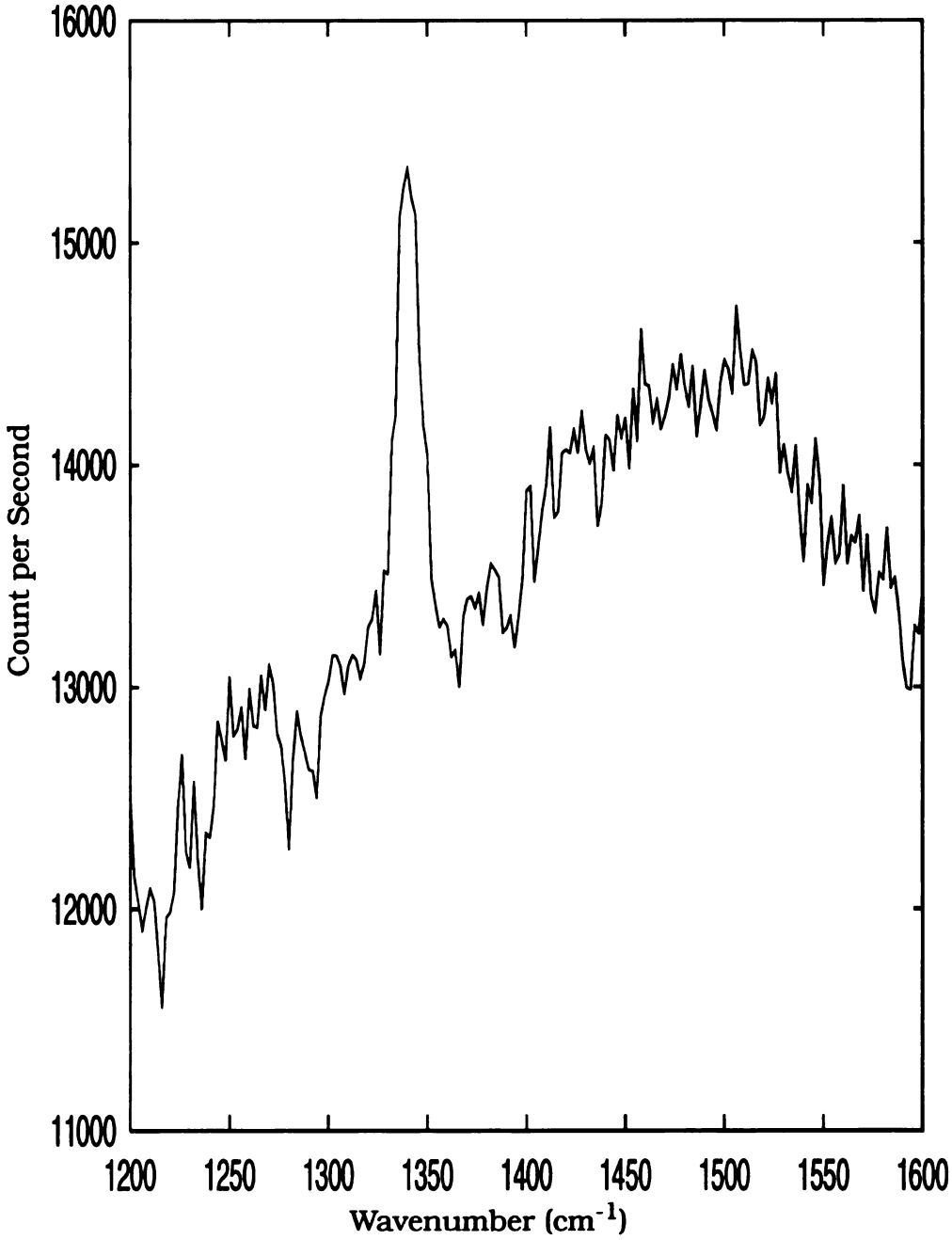

Figure 7.13 Raman spectrum of the diamond film that was deposited on a WC-6%Co round tool surface.

7.5 Diamond Film Deposition on Carbon Fibers

7.5.1 Reactor Configuration

Figure 7.14 shows schematic cross-sectional view of an apparatus for diamond thin coating of the carbon fiber substrate (10), wherein the substrate (10) being coated is supported by a graphite holder (16). This substrate holder (16) is mounted on a graphite shielding plate (21) which stands on a quartz tube (17) used to change the position of the substrate (10). A plasma (14) is created in the region between the jet pattern (22) and the graphite shielding plate by coupling microwave power into the plasma (14). The metal stage (7) and quartz tube (17) are sealed together to force the source gas to flow through the orifice (23) of jet pattern plate. The rest of the components of this apparatus are identical to those of the MCPR for diamond film synthesis on silicons and the MPJR for diamond film coating on cemented carbide round tools, which were described in Section 3.5 and Section 7.4.1, respectively.

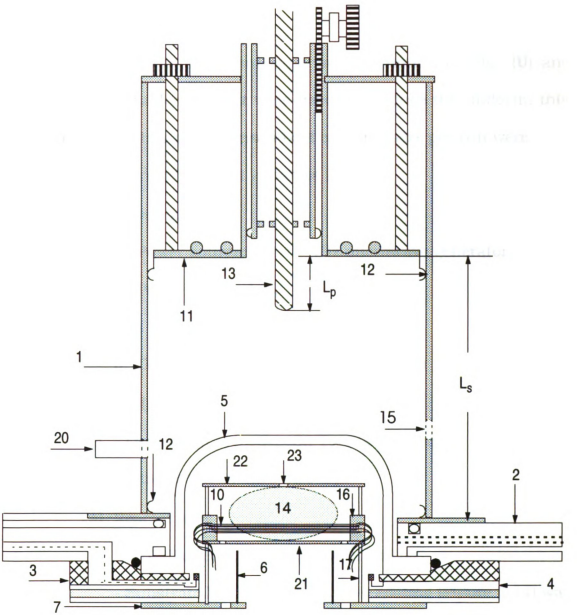

Legend

(1)	Cavity Side Wall	(2)	Baseplate	(3)	Annular Gas Plate
(4)	Gas Distribution Plate	(5)	Quartz Dome	(6)	Resonant Breaker
(7)	Metal Stage	(10)	Carbon Fiber Substrate	(11)	Sliding Short
(12)	Finger Stock	(13)	Excitation Probe	(14)	Plasma Discharge
(15)	Screen Side View	(16)	Substrate Holder	(17)	Quartz Tube
(21)	Shielding Plate	(22)	Jet Nozzle Plate	(23)	Jet Nozzle
(32)	Laser Ports				

Figure 7.14 The cross sectional view of the microwave plasma jet reactor for diamond thin film coating on carbon fibers[14].

7.5.2 Experimental Controllable Input Variables (U) and Internal Input Variables (X)

The optimized independent experimental input variables (**U**) and internal input variables (**X**) that were used to produce the uniform, thin (~1 μm) diamond films over thousands of carbon fibers per run were:

(1) Controllable input variables (U_1):

a) Power input:

i) Power source: a 2.45 GHz microwave generator,

ii) Power level=1 kW,

b) Gas input:

i) Gas mixture: $CH_4/H/_2$ =4/400 sccm

ii) Total flow rate=404 sccm,

c) Deposition pressure=35 Torr (4.66 kPa),

(2) Reactor geometry variables (U_2):

a) Reactor size:

- A 5" diameter(12.7 cm) quartz bell jar,

- Substrate holder setup for fiber coating (Figure 7.14) was used,

b) No external substrate heating, cooling or biasing,

(3) Deposition process variables (U_2):

a) Deposition time=28 h,

b) Substrates were pretreated in a CO/H_2(10/400 sccm) plasma for 20 minutes,

c) Substrate size and material=7 μm diameter carbon fibers

(B) Internal variables(X):

(1) Substrate temperature=1000°C(1273°K).

7.5.3 Film Characteristic (Y_2)

Figure 7.15 and Figure 7.16 show the SEM photos of diamond thin film deposition on carbon fibers. Since the film thickness is approximately 1.5 μm after a 28 hour run, the average linear growth rate is approximately 0.05 μm/h. From both figures, the diamond films were uniformly deposited on the carbon fiber surface.

Figure 7.17 shows the Raman spectrum of the diamond film that was deposited on the surface of carbon fiber. It is noted that the spot size of this Raman measurement is approximately 5 μm in diameter, which is referred as micro-Raman measurement.

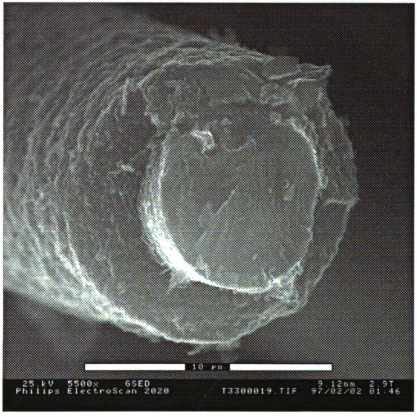

Figure 7.15 The SEM picture of a diamond film coated carbon fiber. The experimental conditions are shown in Section 7.3.2.

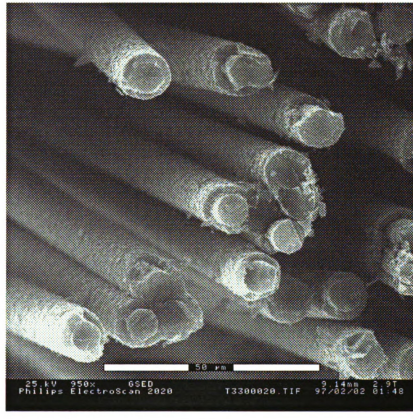

Figure 7.16 The SEM picture of the diamond film on carbon fibers. This figure is an enlarge of Figure 7.15 that contains more carbon fibers.

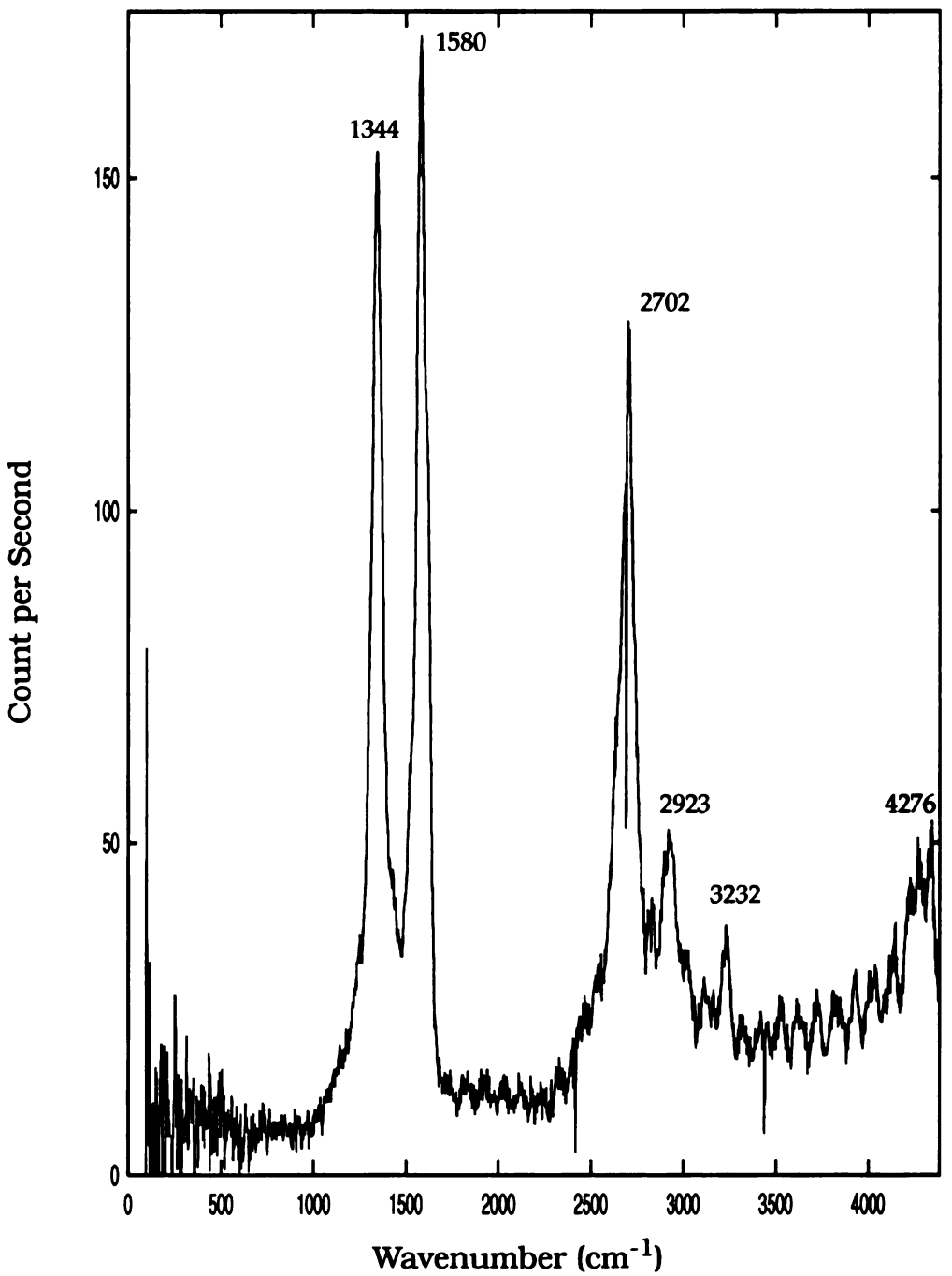

Figure 7.17 Raman spectrum of the diamond film on the carbon fibers.

7.6 Summary

The configuration of the microwave plasma jet reactor and its optimized experimental input conditions that were used for the uniform diamond film coating on irregular shaped objectives are presented in this chapter. Rather, the original experiments intelligently chose several starting points, i.e., the substrate setups, $CO/CH_4/H_2$ chemistries, jet pattern plates, and then varied the experimental input variables in promising directions to achieve deposition uniformly over the irregular objects with reasonable adhesion and deposition rates.

Achieving excellent adhesion was not an objective of this study. However, experimental exploration of the original experimental variable space was achieved with the exception of following variables:

(1) experiments were limited to less than 1,500Watt input power,

(2) total gas flow rates were held under 600 sccm,

(3) no experiments were performed with CO_2 input gas,

(4) high packing capacity was achieved,

(5) no substrate pretreatment was included,

(6) uniform, well-adhered diamond thin films(0.5~5 μm) were coated irregular objects such as WC-6%Co round tools and carbon fibers,

(7) diamond quality was identified(by Raman Spectroscopy),

(8) smooth diamond thin films were observed(by SEM).

CHAPTER EIGHT

Conclusions

8.1 Introduction

The experiments described in this dissertation have demonstrated the successful operation of two new prototype reactor configurations. The first, identified as an improved microwave cavity plasma reactor (MCPR) concept has demonstrated considerable improvement of performance when compared with other lower pressure microwave plasma thin film deposition reactors. This reactor operates at pressures between 80 to 150 Torr and produces a thermal-like plasma which is able to deposit uniform films over two to three inch substrates. This new reactor modified an existing low pressure microwave plasma reactor by incorporating a water cooled substrate holder and increasing the gas air cooling of the reactor. These design improvements allowed operation at higher pressures, higher input power levels and also achieved independent control over substrate temperatures.

The output performance of the redesign, as measured by film growth rate, deposition efficiency (specific yield, carbon conversion efficiency, etc.), demonstrated considerable improvement over the published

performance of other microwave reactors. Deposition rates are of the order 50 mg/h with energy efficiencies of 70 kW-h/g (or 14 kW-h/ct) while still achieving carbon conversion efficiencies of 5-10%. These performance measures compare well with the best overall performance of any CVD diamond deposition reactor. Clearly, an original objective of this thesis research which was to increase the deposition rate has been achieved. A scaled up version of the MPCR, i.e., a thirteen inch diameter discharge reactor, excited at 915 MHz has been constructed and is in operation at Norton Diamond Film Corporation. While the performance measures of this larger reactor remain unpublished, if these performance measures are similar to those presented in this thesis then the larger scale up reactor is capable of high deposition rates, expressed in weight gain per hour, over large areas. This thesis research has demonstrated the ability to improve the deposition performance (deposition rate and deposition area) of microwave reactors. Thus this reactor concept itself opens up the possibility of applying microwave plasma reactors to both thin film and thick film deposition applications.

The second prototype reactor, i.e., microwave plasma jet reactor (MPJR), is operated at pressures between 10 to 45 Torr. This reactor concept has the specific design advantages of (1) preventing gas bypassing, (2) providing a forced flow of input gases into the deposition region and even sometimes onto the deposition surfaces, and (3) reducing the electromagnetic field in the deposition volume. The MPJR utilizes a new pat-

tromagnetic field in the deposition volume. The MPJR utilizes a new patented force-flow concept to create a microwave plasma discharge in a region where the electromagnetic field strength is low. This ensures that only the plasma is produced adjacent to the substrate which can be conductive and can have a complex geometry. $CO/CH_4/H_2$ source gases together with this force-flow concept are utilized to enhance the diamond film growth on irregular shaped, conducting materials with sharp edges, and on fragile materials. In the experiments presented in chapter six and seven demonstrate that the MPJR is able to deposit uniform diamond films on many of 1/8" diameter tungsten carbide round tools and thin films on 5-7 μm diameter carbon fibers.

8.2 Operational Characteristics of a High-Pressure MPCR

8.2.1 Introduction

Using CH_4/H_2 chemistries the MPCR was experimentally characterized in the high-pressure 80-150 Torr regime. In this pressure regime the microwave absorbed power density increases to 20-30W/cm^3 and the discharge produces a thermal-like plasma where the translational temperatures and hydrogen electronic temperature are both within the 2000-2200k ranges. Under these conditions the maximum uniform film deposition rates increase to 4.6-7μm/h(45mg/h on 5.08 cm diameter substrate). Thus the deposition rate have increased by a factor

of five over the deposition rates of low pressure nonequilibrium microwave discharge reactors. Using the approach of J. Angus [15], where the performance of different reactors are compared by relating growth rate vs. reactor area power density (i.e. P_{abs} divided by deposition area), the specific energy of this reactor can be calculated. The reactor performance is displayed as point ● in Figures 2.19 and 2.20. The area power density is 0.15-0.25 kW/cm^2 yielding a specific deposition energy of 14-20 kW-h/ct or specific yield of 70-100 kW-h/g. Optimum growth conditions are CH_4/H_2=3-4%, f_t=600-700sccm, T_s=1060-1100C, p=120-135Torr, and $<P_V>$=30 W/cm^3. Deposited films exhibit (111) morphology and <110> film texture under high growth rate conditions. The reactor performance is very repeatable and controllable with respect of the growth rate, morphology, etc. Both thick films and thin films can be deposited using many substrate materials. Using reactor scaling laws described earlier [112-115], this reactor concept with 915MHz excitation can create much larger thermal microwave discharges and thus has the ability to deposit films uniformly at high growth rates over much larger areas.

8.2.2 Diamond Film Deposition on 2″ Silicon Wafers

An experimental study of diamond film deposition on 2″ silicon wafers was investigated by performing a series of experiments where different CH_4/H_2 concentrations, substrate temperatures, deposition times

and total flow rates were important variables and measured various film growth rate, film uniformity, film Raman Spectrum, film morphologies, and film textures were measured as the output variables. The volume in input variable space, i.e., a volume in CH_4/H_2, T_s, and f_t space, where diamond films with excellent quality were synthesized was identified and compared to analogous volume for lower pressure microwave reactors. This three dimensional diamond deposition volume is much larger for the MCPR than the associated volume for the lower pressure, nonequilibrium microwave plasma reactors. This significant increase in the input variable space for good diamond deposition is believed to be caused by the shift of the discharge chemistry from a nonequilibrium cold plasma regime to a thermal-like plasma discharge. Films with excellent, well-defined crystal facets could be synthesized at high growth rate under much higher temperature (>1000C) and higher CH_4/H_2 concentrations (>3%).

Other results of this study are briefly summarized as below:

(1) The optimum growth conditions in the high-pressure MPCR system are 3%~4% CH_4/H_2 concentrations with total flow rate between 600 sccm and 800 sccm, substrate temperature of ~1050C, deposition pressure of 120-135 Torr, and absorbed MW power ~3.4 kW. The resulting growth rate is approximately 5.5 μm/h (or 46 mg/h).

(2) High quality diamond films of thickness between 10 to 100 μm with uniformity better than 10% have been routinely deposited on 2" diameter silicon substrates. The high quality of the diamond film has

been demonstrated by its linewidth of Raman Spectra (3-8 cm^{-1}).

(3) 2" thick (>100 μm) free-standing diamond films with uniformity better than 15% have been routinely produced. High quality of the free-standing diamond film has been demonstrated by its linewidth of Raman Spectra (~3 cm^{-1}) and thermal conductivity (10-15 W/cm-K)[116].

(4) Diamond films show different morphologies as CH_4/H_2 concentration varies while other experimental conditions are kept constants. These constant experimental controllable input variables include the substrate temperate (1060C), deposition pressure (135 Torr), total flow rate (600 sccm), substrate temperate (5 h), and absorbed microwave power (3.4 kW).

(i) diamond films exhibit mixed (100) square, (110) roof-like, and (111) morphologies at CH_4/H_2=2%.

(ii) Diamond films mostly exhibit (111) triangular morphology at CH_4/H_2=3%~5%.

(iii) Diamond films show cauliflower morphology at CH_4/H_2 6%.

(4) Diamond films show different morphologies versus variations in substrate temperature while other experimental controllable input variables are kept constant. These variables include CH_4/H_2 (3%), deposition pressure (135 Torr), total flow rate (600 sccm), deposition time (10h), absorbed microwave power (3.4 kW).

(i) At substrate temperatures between 800C and 950C

diamond films show mixed (100) square, (110) roof-like and (111) triangular morphologies.

(ii) At substrate temperatures between 950C and 1125C diamond films mostly exhibit (111) triangular morphology.

(5) Diamond films display different morphologies vs. the deposition time. These constant input variables include CH_4/H_2 (3%), substrate temperature (1060C), deposition pressure (135 Torr), total flow rate (600 sccm), absorbed microwave power (3.4 kW).

(i) At deposition times between 4h and 30h the resulting films show both (110) roof-like and (111) triangular morphologies.

(ii) When films are synthesized longer than 30h, the films completely exhibit (111) triangular morphology.

(6) Diamond films display different morphologies vs. the total flow rates. These constant input variables include CH_4/H_2 (3%), substrate temperature (1060C), deposition pressure (135 Torr), deposition time (10 h), absorbed microwave power (3.4 kW).

(i) At total flow rates between 600 and 800 sccm, the resulting films show (111) triangular morphology.

(ii) When films synthesized with $200<f_t<600$ and 800 sccm$<f_t<$1400 sccm, the films exhibit mixed (110) and (111) morphologies.

8.3 Operational Characteristics of the MPJR

8.3.1 Diamond Film Deposition on 1/8" diameter WC-Co Round tools

The experimental investigation of diamond film coating on WC-6%Co round tools using the microwave plasma jet reactor was conducted. The results of this investigation can be summarized as follows:

(1) An optimized substrate tool holder setup demonstrated uniform and adherent diamond film deposition on 36 WC-6%Co round tools.

(2) A gas mixture of 2.5%-10% CO/H_2 was utilized to pretreat the round tool surfaces and deposit adhering diamond films. This method simplifies the substrate pretreatment procedure such as cleaning, etching, and seeding.

(3) Deposition of uniform diamond thin films on the thirty six cutting tool inserts is experimentally repeatable. This result is unique in that it is the only report in the open literature that was using a microwave discharge to deposit diamond films on batches of many round tools.

(4) The utilization of force-flow concept of the MPJR together with the substrate holder setups and CO/H_2 gas mixtures provide the possibility of commercializing the synthesis of diamond films on the cutting tools if the MPJR is scaled up from 2.45 GHz to 915 MHz.

8.3.2 Diamond Film Deposition on 5-7 μm diameter Carbon Fibers

The experimental investigation of diamond film coating on carbon fibers using the microwave plasma jet reactor was conducted. The results of this investigation can be summarized as follows:

(1) An improved substrate holder setup was proved to be capable of depositing diamond films on many carbon fibers.

(2) A gas mixture of $CO/CH_4/H_2$ was utilized to pretreat the carbon fibers and deposit well-adhered diamond films. This recipe simplifies the substrate pretreatment procedures such as cleaning, etching, and seeding, which is the first time reported in the open literature.

(3) Deposition of uniform diamond thin films on numbers of carbon fibers is experimentally repeatable.

(4) The utilization of force-flow concept of the MPJR together with the substrate holder setups and $CO/CH_4/H_2$ gas mixtures provide the possibility of commercializing the synthesis of diamond films on large diameter carbon fibers when the MPJR is scaled up from 2.45 Gaze to 915 MHz.

8.4 Recommendations for Future Research

8.4.1 High-Pressure MPCR

(1) In order to obtain a better understanding of the interaction between electromagnetic field and plasma discharge, electric field mea-

surements in high-pressure MPCR should be conducted. A new cavity with electric field measurement probe holes has been built.

(2) For diamond film applications such as lithography, heat sink, hard coating, etc., it is necessary to deposit different morphologies of diamond films at higher growth rates. Since only a preliminary investigation of diamond film morphologies versus experimental conditions was performed, more detailed investigation of diamond film morphologies versus multiple experimental inputs in high-pressure MPCR should be conducted.

(3) In order to be able to better control the diamond film deposition process in the high-pressure MPCR, not only must the relationship between output and input variables be investigated, but also the relationship between internal variables and the input and output variables must be studied. Deposition experiments where the internal variables are carefully measured must be carried out. Some of these internal variables are plasma species concentrations, gas temperatures, in-situ film growth measurements.

(4) Investigation of the use of $CO/CH_4/H_2$ gas mixtures to improve the diamond film growth rates and gas flow efficiencies using the high-pressure MPCR.

8.4.2 MPJRs

(1) In order to have a better understanding of the plasma dis-

charge in MPJRs, the electromagnetic field patterns and electric field strengths both above and below the jet pattern plate should be investigated.

(2) The adhesion of the diamond thin films on cutting tools using CO/H_2 chemistries should be continued to be investigated. This investigation should include varying the experimental inputs such as substrate temperature and concentration CO/H_2, etc., and evaluating the corresponding film adhesion by indentation tests.

APPENDICES

APPENDIX A

A.1 Experimental Conditions of the Diamond Films Presented in Chapter 3 and Chapter 4

Table A.1 shows the experimental conditions of the diamond films presented described in Chapter 3 and 4.

Table A.1 Experimental conditions of the diamond films presented in Chapter 3 and 4.

Sample	p (Torr)	T_s (°C)	P_t (kW)	c (%)	f_t (sccm)	t (h)	μm/h	Specific Yield (kW-h/g)	$\langle P_v \rangle$ (W/cm^3)	$\langle P_A \rangle$ (W/cm^2)
TK35	135	1113	3.66	3	618	8	3.46	153	25.4	180
ST235	135	1057	3.68	3	618	20	4.79	111	25.5	181
ST248	135	1037	3.76	3	618	30	5.11	107	26.1	185
TK3	135	1080	3.68	3	618	55	5.77	92.5	25.5	181
ST233	135	1015	3.74	3	618	100	6.25	86.8	26.0	185
ST188	120	1055	3.12	3	618	10	3.08	147	21.7	154
ST185	120	995	3.12	3	618	20	4.20	108	21.7	154
ST179	120	1035	3.14	3	618	70	4.48	101	21.8	155
ST81	120	978	3.74	2.54	564	14	3.47	156	26.0	185

Table A.1 (cont'd)

Sample	p (Torr)	T_s (^oC)	P_t (kW)	c (%)	f_t (sccm)	t (h)	μm/h	Specific Yield (kW-h/g)	$\langle P_v \rangle$ (W/cm^3)	$\langle P_A \rangle$ (W/cm^2)
ST79	120	1010	3.52	2.54	564	55	4.06	126	24.4	173
ST231	135	1015	3.73	2.92	617.5	10	5.05	107	25.9	185
ST225	135	1025	3.71	3	618	10	5.20	103	25.8	184
ST230	135	1010	3.71	3	618	10	4.52	119	25.8	184
ST249	135	965	3.67	1.5	609	10	1.24	429	25.5	181
ST247	135	1053	3.67	2	612	8	2.23	239	25.5	181
TK38	135	1055	3.72	2.5	615	10	2.64	204	25.8	184
TK37	135	1053	3.71	3	618	14	4.80	112	25.8	184
TK33	135	1096	3.66	3.5	621	10	4.41	120	25.4	181
TK40	135	1010	3.66	4	624	10	4.86	109	25.4	181
ST63	135	990	4.13	2.8	514	4	5.34	110	28.7	203
ST64	135	990	4.10	2.33	614	4	5.01	119	28.5	202
ST48	135	1060	4.16	2	357	8	3.57	169	28.9	205
ST44	135	1040	4.18	1.75	407	8	3.42	177	29.0	206
ST227	135	1018	3.71	3	721	10	5.17	104	25.8	184
ST65	120	916	4.00	2.33	614	4	4.53	128	27.8	197
TK9	120	1085	3.62	3	618	8	4.63	113	25.1	178
ST199	120	1045	3.12	3	618	10	3.84	119	21.7	154
ST200	120	1055	3.19	3	618	10	3.50	132	22.2	157
ST188	120	1055	3.12	3	618	10	3.08	147	21.7	154
ST198	120	1025	3.15	3	618	10	2.95	155	21.9	155
TK7	130	1110	3.59	3	618	8	4.48	116	24.9	172
TK31	135	1010	3.73	3	618	8	5.04	107	25.9	184
TK32	135	1061	3.66	3	618	8	4.78	111	25.4	181
TK14	135	1006	3.62	3	618	8	4.44	118	25.1	179
TK34	135	1020	3.61	3	618	8	4.00	131	25.1	178
TK35	135	1113	3.66	3	618	8	3.46	153	25.4	181
ST221	120	1050	3.76	3	618	100	4.58	119	26.1	185
ST220	120	1045	3.76	3	618	100	5.85	93.2	26.1	185
ST215	135	1035	3.72	3	618	100	4.91	110	25.9	183

Table A.1 (cont'd)

Sample	p (Torr)	T_s (°C)	P_t (kW)	c (%)	f_t (sccm)	t (h)	μm/h	Specific Yield (kW-h/g)	$\langle P_V \rangle$ (W/cm^3)	$\langle P_A \rangle$ (W/cm^2)
ST233	135	1015	3.74	3	618	100	6.25	86.8	26.0	184
MO5	135	1080	3.35	3	618	100	6.27	77.5	23.3	165
ST190	135	1065	3.76	3	618	58	6.10	89.4	26.1	185
ST192	120	1000	3.19	3	618	72	4.83	96	22.5	157
ST204	120	1060	3.12	3	618	75	4.30	105	21.7	154
AT26	135	1056	3.22	1	606	10	0.43	1086	22.4	159
AT25	135	1057	3.22	2	612	10	1.77	264	22.4	159
AT16	135	1057	3.22	3	618	10	3.94	119	22.4	159
AT27	135	1054	3.22	4	624	10	4.31	108	22.4	159
AT28	135	1057	3.22	5	630	10	3.86	121	22.4	159
AT56	135	1056	3.22	6	636	10	3.52	132	22.4	159
AT64	135	1056	3.22	7	642	10	3.39	137	22.4	159
AT65	135	1055	3.22	8	648	10	3.32	141	22.4	159
AT35	135	950	3.17	3	618	10	3.18	145	22.0	156
AT29	135	1025	3.10	3	618	10	3.56	126	21.5	153
AT41	135	1050	3.02	3	618	10	3.02	145	21.0	149
AT43	135	1080	3.02	3	618	10	4.59	95.4	21.0	149
AT33	135	1100	3.10	3	618	10	4.46	101	21.5	153
AT31	135	1125	3.15	3	618	10	4.02	114	21.9	155
AT16	135	1057	3.22	3	618	5	3.94	119	22.4	159
AT79	135	1132	3.10	3	412	10	3.97	113	21.5	153
AT67	135	1110	3.12	3	618	10	4.50	101	21.7	154
AT74	135	1128	3.12	3	721	10	4.41	103	21.7	154
AT70	135	1133	3.14	3	824	10	5.13	88.8	21.8	155
AT72	135	1132	3.14	3	927	10	5.17	87.8	21.8	155
AT73	135	1114	3.12	3	1030	10	5.24	86.3	21.7	154
AT75	135	1133	3.12	3	1133	10	4.70	96.3	21.7	154
AT82	135	1130	3.12	3	1236	10	5.06	89.4	21.7	154
AT80	135	1140	3.14	3	1339	10	2.37	192	21.8	155
AT81	135	1145	3.14	3	1442	10	2.60	175	21.8	155

Table A.1 (cont'd)

Sample	p (Torr)	T_s (°C)	P_t (kW)	c (%)	f_t (sccm)	t (h)	μm/h	Specific Yield (kW-h/g)	$\langle P_V \rangle$ (W/cm^3)	$\langle P_A \rangle$ (W/cm^2)
AT88	100	745	2.69	4	624	10	1.67	234	11.5	132
ST138	100	1031	3.33	3	721	20	3.42	141	23.1	164
ST138	100	165	3.33	3	824	20	3.27	147	23.1	164
ST140	100	1013	3.19	3	721	20	3.28	141	22.2	157
ST141	100	1018	3.22	3.5	621	20	3.09	151	22.4	159
ST142	100	994	3.19	2.5	615	20	2.86	162	22.2	157
ST126	100	1028	3.26	3	412	20	3.8	124	22.6	160
ST134	100	1042	3.21	3	515	20	3.14	148	22.3	158
ST135	100	1050	3.21	3	412	20	2.99	156	22.3	158
ST137	100	1018	3.19	3	618	20	3.28	141	22.2	157
ST132	110	1088	3.26	3	515	20	3.60	131	22.6	160
ST133	110	1067	3.28	3	515	20	4.04	118	22.8	161
TK15	110	1015	3.29	5	630	5	1.74	274	22.8	161
AT89	90	703	2.69	4	624	10	1.67	234	18.7	132
AT105	90	945	2.48	3	618	8	2.60	138	17.2	122
AT110	90	945	2.48	2	612	8	1.48	242	17.2	122
BC1	80	650	2.37	4	624	19	0.174	1975	16.4	117
AT104	80	887	2.48	3	618	8	1.96	183	17.2	122
AT109	80	845	2.50	2	612	8	1.64	221	17.4	123
BC2	70	601	2.10	4	624	8	0.55	526	14.6	104
AT103	70	803	2.29	3	618	8	1.35	246	15.9	112
AT108	70	801	2.29	2	612	8	1.11	300	15.9	112
JZ1	33	750	1.47	2	204	8	0.32	290	8.65	32
JZ2	45	850	2.05	2	204	8	0.64	203	12.1	45
JZ3	57	950	2.51	2	204	8	0.58	274	14.8	55
JZ4	51	900	2.34	1.5	50.75	8	0.32	463	13.8	51
JZ5	51	900	2.34	1.5	101.5	8	0.50	292	13.8	51
JZ6	51	900	2.34	1.5	203	8	0.61	243	13.8	51
JZ7	51	900	2.34	1.5	304.5	8	0.65	228	13.8	51
JZ8	51	900	2.34	1.5	406	8	0.68	218	13.8	51

Table A.1 (cont'd)

Sample	p (Torr)	T_s (°C)	P_t (kW)	c (%)	f_t (sccm)	t (h)	μm/h	Specific Yield (kW-h/g)	$\langle P_V \rangle$ (W/cm^3)	$\langle P_A \rangle$ (W/cm^2)
JZ9	51	900	2.34	1.5	406	8	0.55	163	13.8	51
JZ10	40	836	2.28	1.5	406	8	0.47	179	13.4	49
JZ11	40	825	2.24	1.5	406	8	0.46	180	13.4	49
JZ12	37	813	2.20	1.5	406	8	0.42	194	13.4	49
JZ13	40	845	2.24	1.25	400	8	0.37	224	4.6	28
JZ14	40	845	2.24	1.38	400	8	0.42	197	4.6	28
JZ15	40	845	2.24	1.5	400	8	0.40	207	4.6	28
JZ16	40	845	2.24	1.63	400	8	0.40	207	4.6	28
JZ17	40	845	2.24	1.75	400	8	0.35	237	4.6	28

LIST OF REFERENCES

LIST OF REFERENCES

[1] M. Kamo, Y. Sato, S. Matsumoto, and N. Setaka, " *Diamond synthesis from gas phase in microwave plasma*," J. Crystal Growth,Vol. **62**, pp.642-644, 1983.

[2] A. R. Badzian, T. Badzian, R. Roy, R. Messier, and K. E. Spear, " *Crystallization of diamond crystals and films by microwave assisted CVD (Part II)*," Mat. Res. Bull.,Vol. **23**, pp.531-548 , 1988.

[3] K. Kobashi, K. Nishimura, Y. Kawate, and T. Horiuchi, " *Synthesis of diamonds by microwave plasma chemical-vapor deposition: morphology and growth of diamond films*," Physical Review B, Vol. **38**, pp4067-4084, 15 August1988.

[4] D. Pickrell, W. Zhu, A. R. Badzian, R. Messier, and R. E. Newnham, " *Downstream plasma-enhanced diamond film deposition*," Appl. Phys. Lett., Vol. **56**, pp.2010-2012, 14 May 1990.

[5] R. A. Bauer, N. M. Sbrockey, and W. E. Brower, Jr., " *Quantitative nucleation and growth studies of PACVD diamond film formation*," J. Mater. Res.,Vol. **8**, pp.2858-2869, November 1993.

[6] N. Lee and A. Badzian, " *Effect of methane concentration on surface morphologies and surface structures of (001) homoepitaxial diamond thin films*," Appl. Phys. Lett., Vol. **67**, pp.2011-2013, 2 October 1995.

[7] H. Kawarada, T. Suesada, and H. Nagasawa, " *Heteroepitaxial growth of smooth and continuous diamond thin films on silicon substrates via high quality silicon carbide buffer layers*," Appl. Phys. Lett., Vol. **66**, pp.583-585, 30 January 1995.

[8] H. C. Barshilia, B. R. Mehta, and V. D. Vankar," *Growth of diamond thin films by microwave plasma chemical vapor deposition process*," J. Mater. Res., Vol. **11**, pp. 1019-1024, April 1996.

[9] J. Zhang, " *Experimental development of microwave cavity plasma*

reactors for large area and high rate diamond film deposition," Ph.D dissertation, Michigan State University(1993).

[10] G.S. Yang, M. Aslam, K. P. Kuo, D. K. Reinhard, and J. Asmussen, " *Effect of ultrahigh nucleation density on diamond growth at different growth rates and temperatures,"* J. Vac. Sci. Tech.,Vol. **13**, pp.1030-1036(May/June 1995).

[11] K. P. Kuo and J. Asmussen, " *An experimental investigation of high pressure synthesis of diamond films using a microave plasma cavity reactor,"* accepted in Diamond and Related Materials, to be published.

[12] K. P. Kuo and J. Asmussen, " *An experimental investigation of high pressure synthesis of diamond films using microwave plasma cavity reactor,"* 23rd IEEE International Conference on Plasma Science, Boston, Massachusetts, June 1996.

[13] K. P. Kuo and J. Asmussen, " *A parametric study of high pressure synthesis of diamond films using microwave plasma cavity reactor,"* 7th European Conference on Diamond, Diamond-like and Related Materials, jointly with 5th International Conference on the New Diamond Science and Technology(ICNDST-5), Tours, France(September, 1996).

[14] K. P. Kuo and J. Asmussen," *A method for uniform diamond coating on the high packaging density drill tools using a CO/H_2 microwave plasma jet discharge,"* U.S. Patent in process.

[15] J. C. Angus and C. C. Hayman, " *Low-pressure, metastable growth of diamond and diamondlike phases,"* Science, Vol. **241**, 19 August 1988.

[16] R. F. Davis, " *Diamond films and coatings,"* Noyes Pubications, pp. 224.

[17] D. S. Dandy, M. E. Coltrin," *Relationship between diamond growth rate and hydrocarbon injector location in direct-current arcjet reactors,"* Appl. Phys. Lett., Vol. **66**, pp.391-393, 16 January 1995.

[18] S. Matsumoto, Y. Sato, M. Kamo, and N. Setaka, " *Vapor deposition of diamond particles from methane,"* Jpn. J. Appl. Phys., Vol. **21**, pp. L183-L185(March 1982).

[19] S. Matsumoto, Y. Sato, M. Tsutsumi, and N. Setaka, " *Growth of diamond particles from methane-hydrogen gas,"* Jpn. J. Appl. Phys.,

Vol. **17**, pp. 3106-3112(1982).

[20] C. J. Chu, R. H. Hauge, J. L. Margrave, and M. P. D'Evelyn, " *Growth kinetics of (100), (110), and (111) homoepitaxial diamond films*," Appl. Phys. Lett., Vol. **61**, pp. 1393-1395, 21 September 1992.

[21] A. Sawabe and T. Inuzuka," *Growth of diamond thin films by electron assisted chemical vapor deposition*," Appl. Phys. Lett., Vol. **46**, pp. 146-147, 15 January 1985.

[22] K. Kukmagai, K. Miyata, K. Nishmura, and K. Kobashi, " *Growth of (110)-oriented diamond films by electron-assisted chemical vapor deposition*," J. Mater. Res., Vol. **8**, pp. 314- 320(Feb 1993).

[23] K. Suzuki, A. Sawabe, H. Yasuda, and T. Inuzuka, " *Growth of diamond thin films by dc plasma chemical vapor deposition*," Appl. Phys. Lett, Vol. **50**, pp. 728-729(March1987).

[24] K. Suzuki, A. Sawabe, and T. Inzuka," *Growth of diamond thin films by dc plasma chemical vapor deposition and characteristics of the plasma*," Jpn. J. Appl. Phys., Vol. **29**, pp. 153-157, January 1990.

[25] K. Kurihara, K. Sasaki, M. Kawarada, and N. Koshino, " *High rate synthesis of diamond by dc plasma jet chemical vapor deposition*," Appl. Phys. Lett, Vol. **52**, pp. 437-438, Feb. 1988.

[26] S. W. Reeve, W. A. Weimer, and D. S. Dandy, " *On the optimization of a dc arcjet diamond chemical vapor deposition reactor*," J. Mater. Res., Vol. 11, pp. 694-702, March 1996.

[27] S. K. Baldwin, T. G. Owano, and C. H. Kruger, " *Increased deposition rate of chemically vapor deposited diamond in a direct-current arcjet with a secondary discharge*," Appl. Phys. Lett, Vol. **67**, pp. 194-196(July 1995).

[28] Y. Matsui, A. Yuuki, M. Sahara, and Y. Hirose, " *Frame structure and diamond growth mechanism of acetylene torch*," Jpn. J. Appl. Phys., Vol. **28**, pp. 1718-1724, September 1989.

[29] R. C. Aldredge and D. G. Goodwin, " *Influences of ambient atmosphere on diamond synthesis using an oxygen-acetylene torch*," J. Mater. Res., Vol. **9**, pp. 80-84, January 1994.

[30] K. Bang, A. J. Ghajar, and R. Komanduri," *The effect of substrate surface temperature on the morphology and quality of diamond films*

produced by the oxyacetylene combustion method," Thih Solid Films, Vol. **238**, pp. 172-183, 1994.

[31] H. S. Shin and D. G. Goodwin," *Diamond growth in premixed propylene-oxygen flames*," Appl. Phys. Lett. Vol. **66**, pp.2909-2911, 22 May 1995.

[32] S. J. Harris, H. S. Shin, and D. G. Goodwin," *Diamond films from combustion of methyl acetylene and propadiene*," Appl. Phys. Lett., Vol. **66**, pp. 891-893, 13 February 1995.

[33] J. S. Kim and M. A. Cappelli, " *An experimental study of the temperature and stoichiometry dependence of diamond growth in a low pressure flat flames*," J. Mater. Res., Vol. **10**, pp. 149-157, January 1995.

[34] J. S. Kim and M. A. Cappelli," *Diamond film synthesis in low-pressure premixed methane-oxygen flames*," Appl. Phys. Lett., Vol. **67**, pp.1081-1083, 21 August 1995.

[35] S. Matusmoto, " *Chemical vapour deposition of diamond in RF glow discharge*," J. Mater. Sci. Lett., Vol. **4**, pp. 600-602, 1985.

[36] S. Matusmoto, M. Hino, and T. Kobayashi, " *Synthesis of diamond films in a rf induction thermal plasma*," Appl. Phys. Lett., Vol. **51**, pp. 737-739(September 1987).

[37] M. Kohzake, K. Uchida, K. Higuchi, and S. Node," Large-area *high-speed diamond deposition by rf induction thermal plasma chemical vapor deposition method*," Jpn. J. Appl. Phys., Vol. **32**, pp. L438-L440, 15 March 1993.

[38] J. J. Chang, T. D. Mantei, R. Vuppuladhadium, and H. E. Jackson, " *Effects of oxygen and pressure on diamond synthesis in a magnetoactive microwave plasma*," J. Appl. Phys.,Vol. **59**, pp.2918, 1992.

[39] Z. Ring, T. D. Matei, S. Tlali, and H. E. Jackson," *Plasma synthesis of diamond at low temperature with a pulse modulated magnetoactive discharge*," Appl. Phys. Lett., Vol. **66**, pp. 3380-3382, 12 June 1995.

[40] Z. Ring and T. Mantei, " *Low-temperature diamond growth in a pulsed microwave plasma*," J. Vac. Sci. Technol. Vol. **A 13**, pp. 1617-1618, May/June 1995.

[41] Y. Mitsuda, T. Yoshida, and K. Akashi, " *Development of a new*

microwave plasma torch and its application," Rev. Sci. Instrum.,Vol. **60**, pp.249-252, February, 1989.

[42] K. Takeuchi and T. Yoshida, " *The effect of oxygen on diamond synthesis is a microwave plasma jet*," J. Appl. Phys.,Vol. **71**, pp.2636-2639, 15 March 1992.

[43] Y. Liou, A. Inspektor, R.Weimer, and R. Messier, " *Low-temperature diamond deposition by microwave plasma-enhanced chemical vapor deposition*," Appl. Phys. Lett., Vol. **55**, pp.631-633, 14 August 1989.

[44] Y. Liou, A. Inspektor, R. Weimer, D. Knight, and R. Messier, " *The effect of oxygen in diamond deposition by microwave plasma enhanced chemical vapor deposition*," J. Mater. Res.,Vol. **5**, pp.2305-2312, November 1990.

[45] P. Bachmann, D. Leers, and H. Lydtin, " *Toward a general concept of diamond chemical vapour deposition*," Diamond and Related Materials, Vol. **1**, pp.1-12, 1991.

[46] Y. K. Kim, K. Y. Lee, J. Y. Lee, " *Texture-controlled diamond films synthesized by microwave plasma enhanced vapour deposition*," Thin Solid Films,Vol. **272**, pp.64-70, 1996.

[47] M. C. Salvadori, J. W. Ager III, I. G. Brown, and K. M. Krishnan, " *Diamond synthesis by microwave plasma chemical vapor deposition using graphite as the carbon source*," Appl. Phys. Lett., Vol. **59**, pp.2386-2388, 4 November 1991.

[48] Z. Feng, K. Komvopoulos, I. G. Brown, D. B. Bogy, " *Effect of graphite carbon films on diamond nucleation by microwave-plasma-enhanced chemical-vapor deposition*," J. Appl. Phys., Vol. **74**, pp.2841-2849, 15 August 1993.

[49] Z. Feng, M. A. Brewer, K. Komvopoulos, I. G. Brown, D. B. Bogy, " *Diamond nucleation on unscratched silicon substrates coated with various non-diamond carbon films by microwave plasma-enhanced chemical vapor deposition*," J. Mater. Res.,Vol. **10**, pp.165-174, January 1995.

[50] M. A. Brewer, I. G. Brown, M. R. Dickinson, J. E. Galvin, R. A. MacGill, and M. C. Salvadori, " *Simple, safe, and economical microwave plasma-assisted chemical vapor deposition facility*," Rev. Sci. Instrum., Vol. **63**, pp3389-3393, June 1992.

[51] S. Khatami, Ph.D Dissertation, Michigan State University, 1997.

[52] C. F. M. Borges, S. Schelz, L. St.-Onge, M. Moisan, L. Martinu, " *Silicon contamination of diamond films deposited on silicon substrates in fused silica based reactors,*' J. Appl. Phys., Vol. **79**, pp.3290-3298, 15 March1996.

[53] C. F. M. Borges, V. T. Airoldi, E. J. Corat, M. Moisan, S. Schelz, and D. Guay, " *Very low-roughness diamond film deposition using a surface-wave sustained plasma,*' J. Appl. Phys., Vol. **80**, pp.6013-6020, 15 November1996.

[54] C. F. M. Borges, L. St.-Onge, M. Moisan, A. Gicquel, " *Influence of process parameters on diamond film CVD in a surface-wave driven microwave plasma reactor,*' Thin Solid Films, Vol. **274**, pp.3-17, 1996.

[55] X. Zhang, T. Shi, J. Wang, X. Ahang," *Oriented growth of a diamond film on Si(100) by hot filament chemical vapor deposition,*" J. Crystal Growth, Vol. **155**, pp. 66-69, 1995.

[56] R. F. Clausing, L. Heatherly, L. L. Horton, E. D. Specht, G. M. Begun and Z. L. Wang, " *Textures and morphologies of chemical vapor deposited (CVD) diamond,*" Diamond and Related Materials, Vol. **1**, pp. 411-415, 1992.

[57] G. Popvici, C. H. Chao, M. A. Prelas, E. J. Charlson and J. M. Meese, " *Smooth diamond films grown by hot filament chemical vapor deposition on positively biased silicon substrates,*" J. Mater. Res., Vol. **10**, pp. 2011-2016, August 1995.

[58] Q. Chen, J. Yang, and Z. Lin, " *Synthesis of oriented textured diamond films on silicon via hot filament chemical vapor deposition,*" Appl. Phys. Lett., Vol. **67**, pp. 1853-1855, 25 September 1995.

[59] J. M. Olson and M. J. Dawes," *Examination of the material properties and performance of thin-diamond film cutting tool inserts produced by arc-jet and hot-filament chemical vapor deposition,*" J. Mater. Res. Vol. **11**, pp.1765-1775 (Jul 1996).

[60] V. J. Trava-Airoldi, E. J. Corat, E. Del Bosco, N. F. Leite, " *Hot filament scaling-up for CVD diamond burr manufacturing,*" Surface and Coating Technology, Vol. **76-77**, pp. 797-802, 1995.

[61] A. Johnson, " *CVD Diamond Inserts Stick,*" Cutting Tool Engineering, pp. 34-39, Feb 1996.

[62] P. K. Bachmann and R. Messier, " *Emerging Technology of diamond*

thin films," C&EN, Vol. **24**, 15 May 1989.

[63] R. B. Jackman, J. Beckman, J. S. Foord, " *Diamond chemicak vapor deposition from a capacitively coupled radio frequency plasma*," Appl. Phys. Lett.,Vol. **66**, pp. 1018-1020, 20 February 1995.

[64] S. P. Bozeman, D. A. Tucker, B. R. Stoner, J. T. Glass, and W. M. Hooke, " *Diamond deposition using a planar radio frequency inductively coupled plasma,*" Appl. Phys. Lett, Vol. **66**, pp. 3579-3581(June 1995).

[65] W. Zhu, B. R. Stoner, B. E. Willams, and J. T. Glass, " *Growth and Characterization of diamond films on nondiamond substrates for electronic applications*," Proceedings of IEEE, Vol. 79, pp. 621-646, May 1991.

[66] A. Masood, M. Aslam, M. A. Tamor and T. J. Potter, J. Electrochem. Soc., Vol. **138**, pp.L67 (1991).

[67] J. Mossbrucker, Ph.D Dissertation, Michigan State University, 1997.

[68] P. Hendra, C. Jones, and G. Warnes, Fourier Transform Raman Spectroscopoy, Horwood, Chichester(1991).

[69] P. W. Morrison, A. Somashekhar, J. T. Glass, and J. T. Prater, " *Growth of diamond films using an enclosed combustion flame,*" J. Appl. Phys.,Vol. **78**, pp.4144-4156(1995).

[70] H. C. Barshilia, B. R. Mehta, and V. D. Vankar, "*Growth of Diamond Thin Films by Microwave Plasma Chemical Vapor Deposition,*" J. Mater. Res., Vol. **11**, pp.1019-1024(April 1996).

[71] S. L. Flegler, Scanning and Transmission Electron Microscopy.

[72] R. F. Clausing, L. Heatherly, L. L. Horton, E. D. Specht, G. M. Begun, and Z. L. Wang, " *Textures and morphologies of chemical vapor deposited(CVD) diamond,*" Diamond and Related Materials, pp.411-415(1992).

[73] H. Maeda, K. Ohtsubo, M. Irie, N. Ohya, K. Kusakabe, and S. Morooga, " *Determination of diamond [100] and [111] growth rate and formation of highly oriented diamond films by microwave plasma assisted chemical vapor deposition,*" J. Mater. Res. Vol. **10**, pp.3115-3123(Dec 1995).

[74] M. J. Ulczynski, D. K. Reinhard, M. Prystajko and J. Asmussen, Advances in New Diamond Science and Technolog, Ed. S. Saito, N. Fujimori, O. Fukunagu and M. Kamo, pp.41(1994).

[75] S. Khatami and J. Asmussen, 23rd IEEE International Conference on Plasma Science, Boston, Massachusetts, June 1996.

[76] A. Gucquel, E. Anger, M. F. Ravet, D. Fabre, G. Scatena, and Z. Z. Wang, " *Diamond deposition in a bell jar reactor: influence of the plasma and substrate temperature on the microstructure and growth rate,*" Diamond and related Materials,Vol. **2**, pp.417-424 (1993.)

[77] W. Zhu, " *Microwave plasma-enhanced chemical vapor deposition and structural characterization of diamond films,*" Ph.D Dissertation, Penn. State University, 1989.

[78] S. J. Harris and A. M. Weiner, " *Pressure and temperature effects on the kinetics and quality of diamond films,*" J. Appl. Phys.,Vol. **75**, pp.5026-5032(May1994).

[79] M. P. Everson and M. A Tamor, " *Investigation of growth rates and morphology for diamond growth by chemical vapor deposition,*" J. Mater. Res., Vol. **7**, pp.1438-1443(June 1992).

[80] N. Setake, " *Low pressure gas phase synthesis of diamond,*" Hyomen (Surface),Vol. **22**, pp.110 (1984).

[81] J. Wei, H. Kawarda, J. Suzuki, and A. Hiraki, " *Growth of diamond films at low pressure using Magneto-microwave plasma CVD,*" Journal of Crystal Growth,Vol. **99**, pp.1201-1205(1990).

[82] A. Gicquel, K. Hassouni, S. Farhat, Y. Breton, C. D. Scott, M. Lefebvre, and M. Pealat, " *Spectroscopic analysis and chemical kinetics modeling of a diamond deposition plasma reactor,*" Diamond and Related Materials, Vol. **3**, pp.581-586(1994).

[83] Y. K. Kim, K. Y. Lee, J. Y. Lee, " *Texture-controlled diamond films synthesized by microwave plasma enhanced vapour deposition,*" Thin Solid Films,Vol. **272**, pp.64-70 (1996).

[84] C. J. Chu, R. H. Hauge, J. L. Margrave, and M. P. D' Evelyn, " *Growth kinetics of (100), (110), and (111) homospitaxial diamond films,*" Appl. Phys. Lett,Vol. **61**, pp.1393-1395 (September 1992).

[85] L. K. Bigelow and N. M. henderon, 2nd Int. Conf. on the Diamond

Sci. and Tech., ICNDST-2, Washiongton, D.C., Sep. 23, 1990.

[86] R. A. Rudder, R. E. Thomas, R. J. Markaunas, 179th Meeting of Electrochemical Society, Washington, D.C., May 5-10, 1991.

[87] R. F. Davis, Diamond Films and Coatings, edited by R. F. Davis, Noyes publications.

[88] P. K. Bachmann," *Emerging Technology of diamond thin films*," Science,pp.24-39 (15 May 1989).

[89] G. Johnson and O. L. Sparkman, " *The future of small hole drilling?*" Drilling Advances, Vol. **19**, No.3, pp.40-44(3 March 1996).

[90] B. Schulte, H. Juergensen, P. Blackborow, and E. Sevillano," *Flexibility of microwave plasma chemical vapour deposition for diamond growth*," Surface and Coatings Technology,Vol. **74-75**, pp.634-636 (1995).

[91] M. Portland, " *Diamonds could be high tech's best friend*," Business Week, pp.90-91(February 12 1990).

[92] J. T. C. Lee, " *A comparison of HDP sources for polysilicon etching*," Solid State Technology, cover article, pp.1-4(August 1996).

[93] K. Takeuchi and T. Yoshida," *The effect of oxygen on diamond synthesis in a microwave plasma jet*," J. Appl. Phys.,Vol. **71**, pp.2636-2639 (March1995).

[94] S. W. Reeve, W. A. Weimer, and D.S. Dandy," *On the optimization of a dc arejet diamond chemical vapor deposition reactor*," J. Mater. Res., Vol. **11**, pp.694 (March 1996).

[95] A. Higa, A. Hatta, T. Ito, T. Maehama," *Homoepitaxial diamond synthesis by dc arc plasma jet chemical vapor deposition*," Jpn. J. Appl. Phys.,Vol. **35**, pp.L577-L580 (May 1996).

[96] A. Higa, A. Hatta, T. Ito, M. Toguchi, and A. Hiraki, " *Effect of CO2 addition on diamond growth by DC arc plasma jet chemical vapour deposition*," Jpn. J. Appl. Phys., Vol. **35**, pp.216-220(1996).

[97] F. Deuerler, M. Pies, H. Van Den Berg, R. Tabersky, " *Production, characterization, and wear behaviour of plasma jet CVD diamond films on hard metal cutting tools*," Phys. Stat. Sol., Vol. **154**, pp.403-423(1996).

[98] M. Nesladek, K. Vandierendonck, C. Quaeyhaegens, M. Kerlchofs, and L. M. Stals, " *Adhesion of diamond coatings on cemented carbides*," Thin Solid Films, Vol. **270**, pp.184-188(1995).

[99] A. K. Mehlmann, A. Fayer, and S. F. Dirnfeld, " *nucleation and growth of diamond on cemented carbises by hot-filament chemical vapor deposition*," Diamond and Related Materials, Vol. **2**, pp.317-322(1993).

[100] J. Ting and M. L. Lake, " *Diamond-coated carbon fiber*," J. Mater. Res., Vol. **9**, pp.636-642(March 1994).

[101] J. Ting, A. G. Lagounov, M. L. Lake, " *Chemical vapour infiltration of diamond into a porous carbon*," J. Mater. Sci. Lett., Vol. **15**(1996).

[102] Y. Saito, I. Isozaki, A. Masuda, K. Fukumoto, M. Chosa, and T. Ito, " *Adhesion strength of diamond film on cemented carbide insert*," Diamond and Related Materials, Vol. **2**, pp.1391-1395(1993).

[103] Y. Muranaka, H. Yamashita, K. Sato, and H. Miyadera, " *The role of hydrogen in diamond synthesis using a microwave plasma in a* CO/H_2 *system*," J. Appl. Phys., Vol. **167**, pp.6247-6254(May 1990).

[104] purchased from Travel Tool Company, CT.

[105] purchased from BFGoodrich Super Temp., Santa Fe Springs, CA.

[106] Macro-Raman Spectroscopic equipment.

[107] Environmental Scanning Electron Microscopy, Model 2020 #101, purchased from ElectroScan, Wilmington, MA.

[108] Any thing related to the graphite signal stronger than diamond in Raman.

[109] J. Zhang and J. Asmussen, U.S. Patent Number 5,311,103.

[110] J. Zhang and J. Asmussen, U.S. Patent Number 5,571,57.

[111] G. L. King, " *Temperature and concentration of ionic and meutral species in resonant microwave cavity plasma discharge*," Ph. D dissertation, Michigan State University (1994).

[112] J. Asmussen and R.Garard, " Precision Microwave Applicators and Systems for Plasma and Material Processing" Microwave Processing of Materials, Ed. W.A. Sutton, M.H.Brooks and I.J.Chabinsky.

[113] J.Asmussen, "Microwave Plasma Disk Processing Machine" in High Density Plasma Sources, Ed. O.A Popov, 251-311 (Noyes Publ., N.J. 1995).

[114] J. Asmussen and J. Root, " Ion generating apparatus and method for the use thereof," U.S. Patent No. 4,507,588 (26 March, 1985).

[115] J. Asmussen and D. K. Reinhard, " Method for treating a surface with a microwave plasma and improved apparatus," U.S. Patent No. 4,585,688 (29 April 1986).

[116] H. M. Relyea, F. Breidenich, J. V. Beck, and J. J. Mcgrath, " Measurement of thermal properties of thin films using infrared thermography," pp. 183-194, Thermal Conductivity, Vol. 23, Edited by K. E. Wilkes, R. B. Dinwiddie, R. S. Graves, Oak Ridge National Laboratory, Oak Ridge, Tennessee. (Technomic Publishing Company, Inc., 1996).